Fusion-Fission Systems Analysis and the Impact of Nuclear Data Uncertainties on Design

M.Z. Youssef

May 1980

UWFDM-358

Ph.D. thesis.

FUSION TECHNOLOGY INSTITUTE

UNIVERSITY OF WISCONSIN

MADISON WISCONSIN

Fusion-Fission Systems Analysis and the Impact of Nuclear Data Uncertainties on Design

M.Z. Youssef

Fusion Technology Institute
University of Wisconsin
1500 Engineering Drive
Madison, WI 53706

http://fti.neep.wisc.edu

May 1980

UWFDM-358

Ph.D. thesis.

FUSION-FISSION SYSTEMS ANALYSIS AND THE IMPACT OF NUCLEAR DATA UNCERTAINTIES ON DESIGN

by

MAHMOUD ZAKY H.M. YOUSSEF

A thesis submitted in partial fulfillment of the
requirements for the degree of

DOCTOR OF PHILOSOPHY
(Nuclear Engineering)

at the

University of Wisconsin-Madison

1980

ABSTRACT

FUSION-FISSION SYSTEMS ANALYSIS
AND THE IMPACT OF NUCLEAR DATA
UNCERTAINTIES ON DESIGN

Mahmoud Zaky H.M. Youssef

Under the Supervision of Professor Robert W. Conn

The research in this thesis aimed at arriving at an optimal blanket design for the fusion-fission hybrid reactor, SOLASE-H. In this design, light water reactor-type ThO_2 fuel assemblies are extracted from the blanket after reaching ~4% enrichment in U-233 and placed directly in fission reactors without reprocessing. Sodium is used as a coolant and lead as a neutron multiplier through the (n,2n') reactions. The neutron spectrum has been tailored to minimize nonuniformity in the spacial distribution of the bred U-233. Starting with 196,350 kg of Th, the amount left after 2.7 years is 187,500 kg. The U-233 produced is 7,560 kg with ~13% burnup. The blanket energy multiplication varies from ~1.59 at the beginning of life to ~4.96 at 4% enrichment time.

A mathematical model has been developed to describe the fissile fuel and tritium flow in a fusion-fission system consisting of a fusion hybrid, a tritium production reactor and several fission reactors. Different possible combinations of systems can be obtained by shifting the tritium breeding function among the various parts.

At steady state, it has been found that the total thermal power of the fission reactors per unit of fusion power depends only on the total conversion ratio of the fission reactors and of the hybrid and an economic analysis is required to determine which combination of systems will produce electricity at the lowest cost.

Because of the substantial computational cost of performing neutronics calculations in a hybrid, a separation technique has been developed that divides the transport equation into two parts. The transport of fusion-produced neutrons (first generation neutrons) is separately calculated and a fission neutron source is generated. The behavior of the second and subsequent generations of neutrons is obtained using fewer energy groups and a low order treatment for scattering. This leads to a computational cost reduction of ~50%. A sensitivity theory consistent with the separation technique has been developed and used to demonstrate that the use of a low-order scattering description when solving the second part of the problem leads to small errors (<1%) in the U-233 breeding.

An extended sensitivity and uncertainty analysis has been performed to investigate the impact of the present neutron cross sections uncertainties on various design parameters (responses) in the SOLASE-H hybrid reactor. The cross sections uncertainty covariance matrices have been generated and folded with the sensitivity coefficients to obtain estimates for the uncertainties in the responses. The analysis showed that the uncertainty in the U-233 breeding ratio, R_U, is ~4% and is mostly due to errors associated with the Pb cross

sections which amounts to a ~56% contribution. Reducing the uncertainty in the Pb(n,2n'), Pb(n,3n') and the Pb(n, nonelastic) cross sections, particularly in the energy range 14-20 MeV, will significantly reduce the uncertainty in the ratio, R_U. Improving the Th(n,γ) cross section values in the energy range 0.35-3.35 KeV can lead to a 40% reduction in the uncertainty in the U-233 breeding ratio. This improvement will also reduct the 3.4% uncertainty in the tritium breeding ratio from ^{6}Li, $R_{^6Li}$. It was found that more accurate evaluation for the Pb(n, nonelastic) cross section in the energy range 0.73-14 MeV can reduce (~25%) the uncertainty in the tritium breeding from ^{6}Li. Uncertainty in the order of ~ 1% in the tritium breeding ratio from ^{7}Li, $R_{^7Li}$, was found which shows that the present nuclear date uncertainties are adequate for predicting tritium breeding from ^{7}Li. Most of the uncertainty (~3%) in the displacements per atom in the Zircaloy-2 cladding, $\overline{R}_D$, is due to the uncertainties in the Pb (n, inelastic) cross section. The uncertainty analysis reveals also the importance of reducing the present uncertainties in the Th(n, fission) cross sections to minimize the uncertainty (~8%) in the heating rate from nuclear reactions, R_H^Q. It has been found that the uncertainties in ^{6}Li cross sections are adequate for predicting the various responses considered.

Date: _____ Signed: _____

Robert W. Conn,
Professor of Nuclear
Engineering

ACKNOWLEDGEMENTS

The opportunity I have had as a graduate student at the University of Wisconsin-Madison under the supervision of Professor R.W. Conn is unique and productive. To my advisor, I express my gratitude and sincere thanks for his inspiring discussions, continuous guidance and support during the different phases of my graduate research.

I am grateful to Professor C. W. Maynard for his valuable comments and advice and with whom any discussion can lead to more perfection.

I am appreciative of the help I recieved from the staff and faculty members of the Nuclear Engineering Department at the University of Wisconsin. I would particularly like to express my appreciation to Professor W. Vogelsang, Professor G. Moses, and Professor S. Abdelkhalik for their constractive discussions and remarks during my work in the Hybrid Reactor research project. Gratitude is also due to Dr. Y. Gohar, Dr. E. Cheng, and my fellow graduate student T. Wu for their cooprative assistance during the early years of my research. I would like to extend my thanks to Dr. M. Ragheb and Dr. R. Perry with whom I have had a mutually rewarding collaboration.

I wish to express my apprectiation to Mrs. N. Jackson and W. Kornacki who typed this manuscript and to Mr. D. Bruggink who put his effort in preparing its figures.

To my wife, Mona, and my beloved son, M. Amr, I dedicate this work. This research was supported by the U.S. Electric Power Research Institute.

TABLE OF CONTENTS

LIST OF TABLES

LIST OF FIGURES

Chapter I

INTRODUCTION

The fusion-fission hybrids, which can represent a long-term energy option, have been widely studied recently. The attractiveness of such reactors is due to the two revenue sources that can be obtained, namely, fissile fuel and electric power. Because of the potential of the fusion-fission system as a fissile fuel breeder by neutron capture in a fertile fuel (Th-232 and/or U-238), this will eliminate the increasing threatening shortage in U-235 which represents the only naturally occuring fissile fuel. In this respect, if the breeding characteristics of the fusion hybrid and the fast breeder reactor (e.g., LMFBR) are compared, the fusion-fission system will out-perform the fast breeder. This is due to utilizing the energetic D-T neutrons produced in the hybrid to breed the fissile fuel (U-233 and/or Pu-239). As a power producer, the bred fissile fuel can be burned in the hybrid blanket and a high power multiplication factor can be achieved. This in turn can relax the physics performance and lower certain technology requirements.

One of the design goals in a hybrid is to be self-sufficient in tritium. However, the possibility of shifting the tritium production function to fission reactors has recently been the subject of several studies. As it has been argued, this can reduce the complexity involved in hybrid designs. In this respect, the hybrid reactor plays the role of a fuel factory providing the

fission reactors with fissile fuel which in turn can provide the tritium fuel needs of the hybrid reactor.

As compared to fission reactors, the hybrid reactors can be made subcritical under all conditions. A hybrid reactor is distinguished by the properties of the energetic D-T neutrons. These external neutrons have a higher value in terms of producing secondary neutrons in the hybrid blanket from (n,2n'),(n,3n') and/or fission than do neutrons resulting from fission or (n,3n') reactions. The contribution of these secondary neutrons to different reactions and energy production is small compared to the corresponding contribution from the external D-T neutrons. While the D-T neutrons are highly anistropic in nature, the neutrons from fission reactions are produced isotropically and can be treated differently.

The design parameters of prime importance in hybrid reactor calculations are; the fissile fuel ratio (defined as the number of fissile atoms produced per D-T neutron) and the tritium breeding ratio (defined as the number of tritium atoms produced per D-T neutron). The radiation damage rate measured in terms of the number of displacements per atom, and the heat deposition rate are among other important design parameters (responses). In a hybrid blanket design, the predicted values of these parameters are uncertain due to the present uncertainties associated with the neutron cross sections data base. Basically, the sensitivity coefficient, defined as the first derivative of the response with respect to the basic neutron cross section, can be used to answer questions

of the relationship between the changes of a design quantity and of the basic data field. This coefficient is an indicator of what cross section data, as a function of nuclide, reaction type, and energy, is important in evaluating a certain design parameter. Analysis of this sort can be implemented with the present nuclear data uncertainties to give predictions of the uncertainties in different responses.

The main objectives of the research presented in this thesis are to

1. Investigate the impact of shifting the tritium production function to fission reactors on the total thermal power produced in a combination of a hybrid reactor and several fission reactors.

2. Investigate the potential of a hybrid reactor to produce U-233 enriched fuel assemblies to be used directly in fission reactors without reprocessing and to develop a fuel management procedure to maximize the bred U-233 fuel uniformity across bundle while minimzing the power swing between the fresh and steady state condition.

3. Reduce the computational cost usually encountered in the neutronics survey study when designing a hybrid blanket.

4. Evaluate the uncertainties in various important design parameters due to the present uncertainties in the neutron cross sections data.

The first objective has been achieved by incorporating a dedicated tritium production reactor (a fission reactor) devoted

mainly to tritium production with a hybrid reactor and several fission reactors. The thermal power is produced mainly in the fission reactors and the hybrid is viewed as a fissile fuel supplier. An approach of this sort allows tritium to be produced in reactors that are currently operational. Different combinations of these systems are found by shifting the tritium breeding function among the various parts. In this respect, a mathematical model has been developed to describe the fissile fuel and tritium flows in these different combinations of systems. The results of this study have been presented in Chapter III.

The second objective has been carried out and the blanket for a laser-driven fusion-fission hybrid reactor, SOLASE-H, has been designed. Light water reactor-type fuel assemblies based on the $^{232}Th/^{233}U$ cycle are enriched to 4% in the hybrid blanket and then the highly radioactive proliferation resistant assemblies are placed directly into an LWR without intermediate reprocessing. Sodium is used as a coolant and lead as a front zone neutron multiplier to enhance neutron production through the (n,2n') reactions. The main consideration in designing the SOLASE-H blanket is to maximize the fissile fuel production rate subject to the constraints that the U-233 fuel distribution in the fuel zone be as uniform as possible. A fuel assembly rotational scheme has been developed to achieve this purpose. The results of the neutronics study for the SOLASE-H hybrid are given in Chapters IV and V.

The third objective is accomplished by treating the D-T neu-

trons and the fission neutrons separately. A separation technique that divides the transport equation into two parts is developed and is described in Chapter VI. In this technique, the transport of the D-T neutrons is separately calculated and a fission neutron source is generated. The behavior of the subsequent neutrons from fissioning is obtained using more simplified approximations (e.g., diffusion theory). A reduction in the computational cost of a factor of 2-3 can be obtained. A sensitivity theory consistent with the separation technique has been developed to evaluate the sensitivity coefficient mentioned earlier and is used to test for the accuracy and the range of applicability of the separation technique.

Finally, the fourth objective has been achieved. The sensitivity coefficients and profiles have been evaluated for five different responses of the SOLASE-H blanket, namely: (a) the U-233 breeding ratio, (b) the tritium breeding ratio from ^{6}Li, (c) the tritium breeding ratio from ^{7}Li, (d) the average displacements per atom per D-T neutron in Zircaloy-2 through the first 3 cm in the fuel zone, and (e) the heat deposition rate in the blanket per neutron due to nuclear reactions. The various cross sections uncertainty information implemented in the Evaluated Neutron Data File, ENDF/B-V, has been processed and the cross section covariance matrices have been generated. The uncertainties in the five responses considered have been estimated by folding the covariance matrices with the results obtained from the sensitivity analysis.

The results of these analyses are presented in Chapters VII to X. Although the sensitivity and uncertainties analysis performed in this research have been carried out for the SOLASE-H blanket design, it may not be appreciably different for other hybrid designs which suppress fissioning in the bred U-233 fuel.

Chapter II

FUSION-FISSION HYBRID SYSTEMS REVIEW

II.1 Introduction

The fusion-fission hybrid, when realized as a commercial power plant, will represent a long-term energy option. Utilizing the properties of the energetic neutrons from the D-T reaction in this system to breed fissile fuel (U-233 or Pu-239) by neutron capture in a fertile fuel (Th-232 or U-238) for subsequent use in fission reactors (LWR, HTGR) will substantially extend the naturally occurring fissile fuel supply (U-235) by the use of essentially non-exhaustible fertile materials.

The fusion-fission system can be designed and the neutron spectrum in the breeding blanket of that system can be tailored to produce two sources of revenue: fissile fuel and electric power. As far as breeding fissile fuel is concerned, the fusion-fission hybrid should far exceed the capability of the fast breeder (LMFBR) as a fuel source. In the following we discuss the role which the fusion-fission hybrid can play in this regard. The different philosophies for designing the blanket of the hybrid to perform different functions is reviewed based on the current fusion-fission designs in the published literature.

II.2 Comparison Between Fast Breeder and Fusion-Fission Systems as Fissile Fuel Breeders

The potential of fast breeders to provide the make-up fissile fuel needs for fission reactor burners and converters has been studied extensively.[1] It has been emphasized that a long-term energy option is

achieved if the matched fission reactors have a high conversion ratio (e.g., tight lattice LWR and HTGR) and if the doubling time is sufficient to match expanding industrial needs. However, if the breeding characteristics of the fusion and fast breeder reactors are compared, the fusion-fission system will out-perform the fast breeder. Such a comparison has been done by Fortescue[2] where he developed expressions to allow ready comparison of a hybrid fusion-fission plant and fast breeder with respect to the number of thermal reactors that their fissile fuel production could support, both for their fissile fuel needs and for the new inventory needs of an expanding industry.

One type of fusion-fission hybrid allows fission to take place in the fusion blanket and utilizes the 200 MeV per fission to multiply the 14.1 MeV D-T neutron energy. Breeding fissile fuel to be transferred to the fission reactors is also possible. If fissioning is not allowed in the fusion blanket and breeding fissile fuel is emphasized, the number of fission reactors that can be supplied will be enhanced and this integrated fusion hybrid-fission reactor symbiote will perform the fissile fuel breeding function primarily in the fusion blanket. Power is produced primarily in the fission reactor which also recycles fissile fuel in its core. Further, it is expected that complexity in the engineering design to retrieve the bred tritium from the fusion blanket may be simplified if the tritium production function is transferred to the fission reactors.[2] In the next chapter, several combinations of fusion-fission symbiotic systems are investigated which may include a tritium producer reactor dedicated mainly to tritium production.

In Fortescue's comparison, the fusion reactor plays the role of fissile fuel factory (no power is produced in the fusion blanket). The relations he derives[2] are expressed in terms of the neutron multiplication factor obtained in the fusion blanket, and the analogous quantities represented by the conversion ratio of the fast and thermal fission reactors included with the comparison.

The annual growth rate, G_A, that matches the industrial expansion, expressed as fraction of fissile inventory in the fission reactors (no fissile inventory is assumed in the fusion reactor), is[19]

$$G_A(\%) = \frac{10.95(C_{FB}-1)-(1+\alpha)(1-C)P}{\frac{(1+Z)P}{0.383\ RL} + 10.95\ \ D} \quad , \qquad \text{(II.1)}$$

where the fusion reactor is the fissile fuel breeder. The corresponding expression in the case where the fast breeder reactor is used instead is

$$G_A(\%) = \frac{0.383\ R_B L(1+\alpha_B)}{f[1+Z_B+\frac{PR_B}{R}(1+Z)]} \times [(C_B-1)-(1-C)\ kP] \quad , \qquad \text{(II.2)}$$

where

$$k = \frac{(1+\alpha)f}{(1+\alpha_B)} \simeq 1$$

f = fast fission factor associated with the fast breeder

α, α_B = capture to fission ratio in the fission reactors and the fast breeder, respectively

C_{FB}, C_B, C = the total atoms (tritium + fissile) produced per DT neutron in the fusion blanket, the conversion ratio

in the fast breeder and the fission reactors, respectively

Z_B, Z = $\frac{\text{out-of-core inventory}}{\text{in-core inventory}}$, in the fast breeder and the fission reactor, respectively

R_B, R = fissile rating per fissile initial inventory, $(\frac{MW_t}{kg})$, in the fast breeder and the fission reactors, respectively

L = load factor

P = $\frac{\text{thermal power of fission reactors}}{\text{breeder (fusion or fast reactor) thermal power}}$

D = delay time in tritium processing (years).

Under steady-state conditions, with no allowance for system growth, we have G_A=0. If there is no delay in tritium processing (continuous extraction and feed), D=0. In Eq. (II.1), it is assumed that one fission produces 11 times the heat from one fusion. Fig. (II.1) gives the ratio of the thermal power of the fission reactors to the fusion and the fast breeder themal power, respectively, for different values of fission reactor conversion ratio and breeding capacity in the fusion reactor (C_{FB}) and the fast breeder C_B. Allowing for industry growth, G_A is represented in Fig. (II.2) for C=0.9 and for both fusion and fast breeders. The range of C_{FB} is typical of a symbiotic fusion-fission system ($C_{FB} \sim 1.4$) as will be shown later. The range of C_B values from 1 to 1.5 represents the potential value in a fast breeder. The range C_B = 0.9 - 0.95 is atypical of a HTGR based on U^{233} inventory and feed. Comparing Fig. (II.1)-a and Fig. (II.1)-b, it is clear that enormously higher numbers of converter reactors can be fed by one

fusion plant of equal fusion power compared to the corresponding value if the fast breeder is used. Some 20 to 50 converter reactors (C=0.9) could be maintained by a fusion plant of equal power while only 2 to 5 could be supported with a fast breeder, a factor of 10 less. Also, notice from Fig. (II.2) the higher growth rate that can be obtained with the fusion breeder for a given value of breeding ratio. An analysis of this sort has been carried by Gordon and Harms[3] for such a symbiotic system where they demonstrated that a doubling time of less than a year is attainable.[3,4]

The potential of utilizing a symbiotic system for fissile fuel production using a molten salt containing ThF_4 for U^{233} breeding for subsequent use in a molten salt fission reactor (MSR) was first introduced by Lidsky[5] early in 1969. Recently, Blinkin and Novikov[6] optimized a fusion blanket similar to Lidsky's blanket to make the fuel handling and reprocessing simpler by devoting the MSR to breed only tritum while consuming the U^{233} supplied from the fusion reactor which carries ThF_4-NaF-BeF_2 molten salt. As they claimed, this will avoid the very difficult problems of generating tritium in a highly complicated fusion machine and will make the reprocessing much simpler. As they reported, reprocessing will consist merely of constantly removing U^{233} from the salt circulating in the fusion reactor blanket by fluorination and removing xenon from the fuel salt of the MSR by purging. Doubling times of ~ 4 years could be obtained compared to ~ 10 yrs evaluated by Lidsky while maintaining the same breeding capacity in the fusion blanket (C_{FB} ~ 1.47) and the same

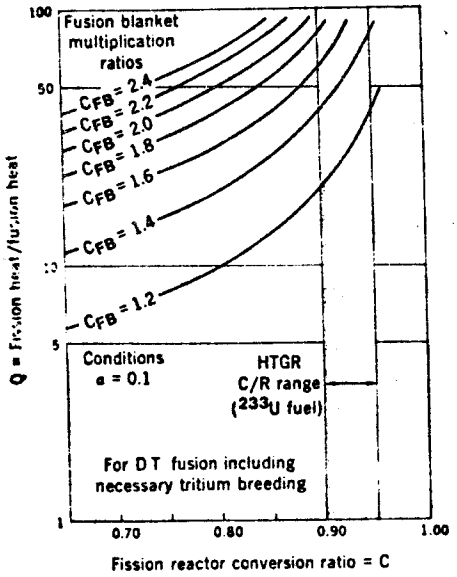

(a) Ratio of the fission heat produced to the fusion heat required to supply the neces sary fuel, under steady-state conditions.
G_A, D=0.0

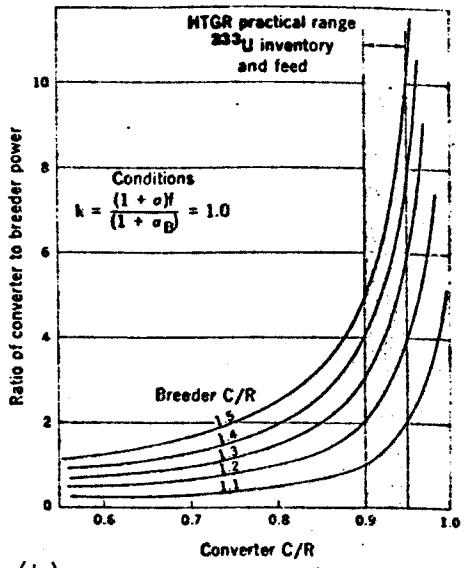

(b) Fast breeder-converter combination under steady-state conditions.
G_A, D=0.0

Fig. (II.1): Comparison Betweed Fast Breeder And Fusion Hybrid Performance At Steady State.

Fig. (II.2): Comparison Between Fast Breeder And Fusion Hybrid Performance With Allowance For Industry Growth.

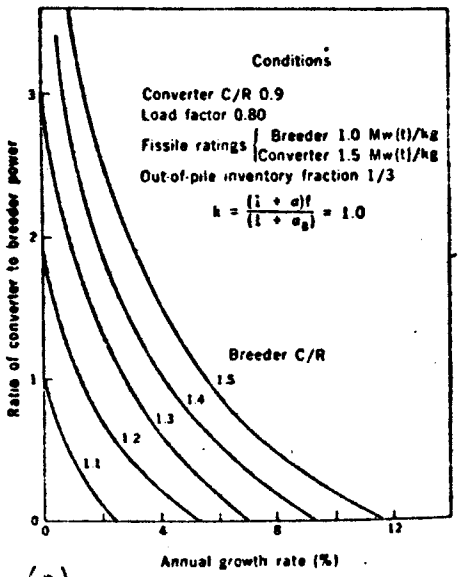

(a) Fast breeder-converter combination with self-sustaining growth.

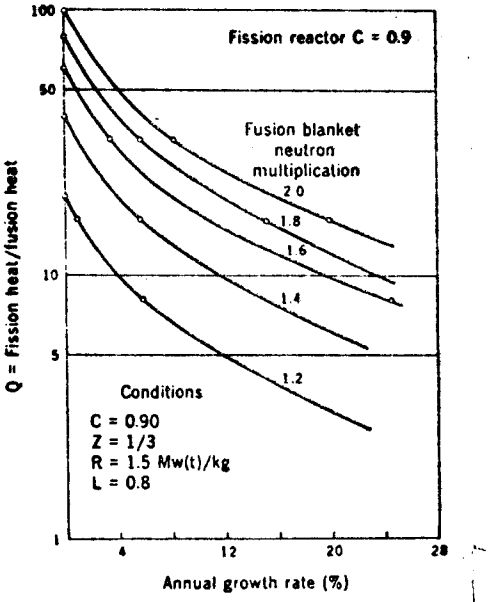

(b) Growth of fusion-fission reactor association (zero tritium processing delay).

support ratio (P ~ 10).

From a safety point of view, the fusion breeder can be made definitely subcritical under all conditions. It is easier to control the flux level in the fusion breeder than in the fast breeder, because the latter is characterized by a short neutron lifetime. The reason is due to the properties of the energetic D-T neutron which has a "higher value" in terms of producing secondary neutrons in the fusion blanket from (n,2n), (n,3n) and/or fission than do neutrons resulting from fission or (n,3n) reactions. The contribution of these secondary neutrons to different reactions and energy production is small compared to the contribution due to the D-T neutrons and the system would shut itself down very quickly if the source neutrons were removed.

The difference in the energetics between the D-T neutrons and the subsequent secondary neutrons has suggested a computational scheme which treats the latter separately. Appreciable reduction in the computation cost is obtained, with high accuracy, when simple approximations are used (e.g., diffusion theory) to treat the secondary neutrons. This point will be elaborated and the results of this computational scheme will be presented in Chapter VI of this study.

The low fissile fuel inventory in the fusion-fission system is another advantage which renders this system a "safe-breeder". Problems associated with reforming critical assemblies upon core meltdown are minimized in a fusion breeder loaded with a fertile fuel.

It should be noted, however, in comparing the fast breeder and

the fusion reactor as a "fissile fuel factory" that the fusion plant will not necessarily be a more economic proposition because there is no clear-cut knowledge about the cost of a fusion plant. Some economic studies have been done by Lawrence Livermore Lab. (LLL) in a joint effort with Bechtel Corp. for designing and estimating the cost of a laser driven fusion-fission system which produces Pu^{239} as well as power. Bechtel estimates the cost of such a system to be 2-3 times higher than a LWR of an equal power.[7] For other fusion drivers, the cost is expected to be within this range. Some other economic considerations can be found elsewhere.[8]

In the following section, the nuclear considerations in designing different fusion blankets to perform different functions are reviewed based on the current designs of fusion-fission systems.

II.3 Important Considerations in Fusion Hybrid Blanket Designs

In its simplest form, the fusion-fission system consists of a fusion component producing and containing a fusion plasma surrounded by a blanket which intercepts the fusion neutrons. The principal approaches to fusion being pursued are the tokamak[10] and mirror[11] magnetic confinement fusion, and laser[12] and electron beam heated inertial confinement fusion.[13] While other neutron producing fusion reactions are possible, namely, D-D, the much higher cross section for D-T at relatively low temperatures makes D-T fusion the practical choice for fusion-fission systems.

The purpose of the blanket is to produce tritium needed for the D-T reaction, produce fissile fuel from neutron capture in fertile

material and/or to produce energy. The role of the blanket can vary from just producing fissile fuel[2],[5-6],[14-16] (symbiotic) to a nearly critical fission assembly[17] ($K_{eff} \simeq 0.94$).

To emphasize the potential of the D-T neutrons to be multiplied in the blanket, we show in Fig. (II.3) the fission cross section for U^{238} and Th^{232} as function of neutron energy. At 14.1 MeV, U^{238}(n, fiss) $\simeq$ 1.15 barns while Th^{232}(n,fiss) $\simeq$ 0.37 barns. Because of the 200 MeV released per fission, the energy of the D-T neutrons is multiplied if fissioning occurs in the blanket. The fissioning in the blanket can be enhanced by noticing that most of the neutrons released per fission are themselves above the fast fission threshold. We give in Fig. (II.4) the average number of neutrons generated per fission vs. incident neutron energy. For 14.1 MeV neutron induced-fission, the number of neutrons generated in U^{238} is 4.5 and in Th^{232} is 3.87. The resultant energy multiplication will reduce fusion technology requirements (e.g., lower the value of $n\tau$, lower the magnetic fields, lower the beam energies, lower the fusion gain, ...). This relaxation in the design parameters may allow earlier commercialization of fusion and thus, an earlier return on investment in fusion research.[18-20]

The potential of using a fertile material for fissile fuel breeding and energy multiplication is shown in Table (II.1) which gives the energy multiplication M (defined as the ratio of the total energy deposited in the blanket per 14.1 MeV D-T neutron) and the breeding reaction (n,γ) per incident D-T neutron (this entry is called the

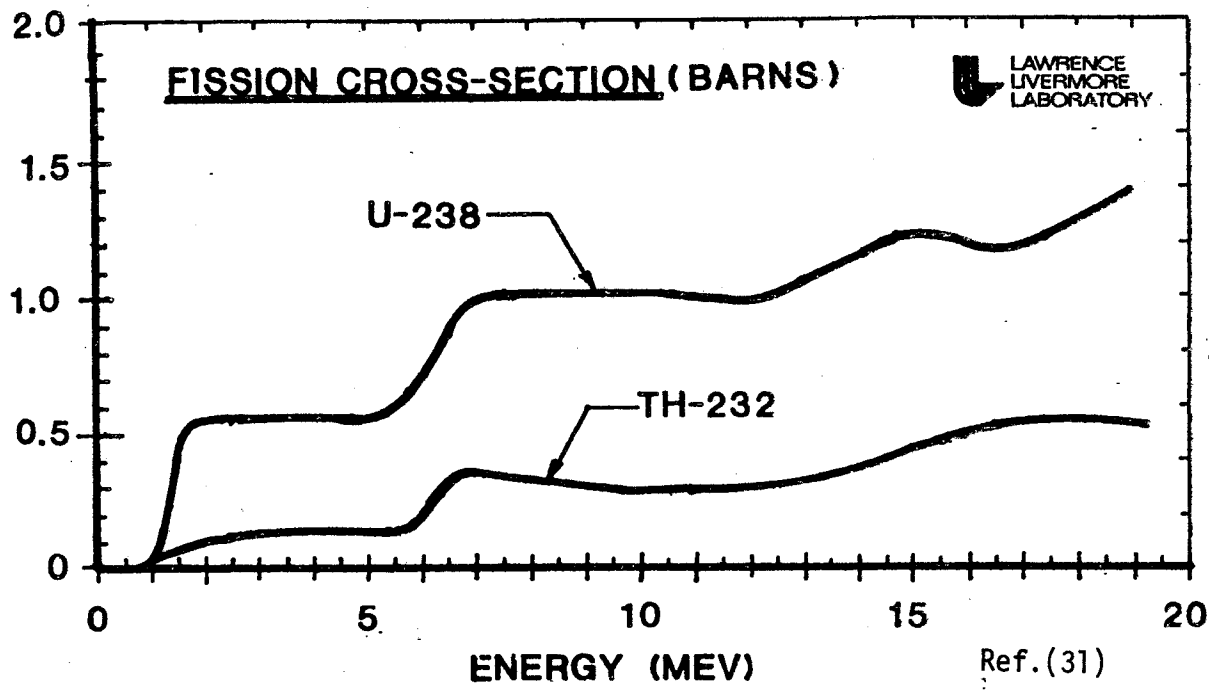

Fig. (II.3): Fission Cross Sections For U-233 and Th-232.

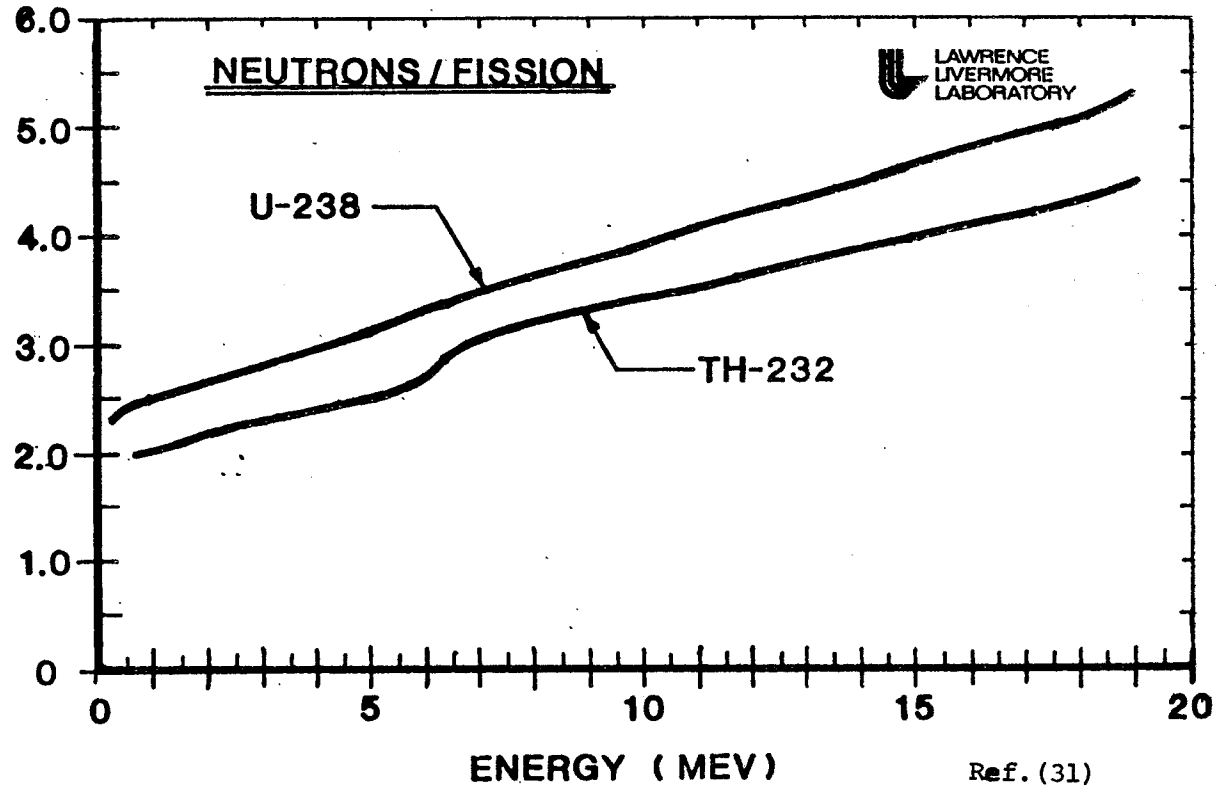

Fig. (II.4): Neutron Yield Per Fission Reaction For U-233 and Th-232.

fissile fuel conversion ratio C) in an infinite medium containing natural uranium, U^{238}, and Th^{232}. An energy multiplication M $\simeq$ 22 can be obtained with a high fissile fuel conversion ratio (C ~ 5). Because of the lower fission cross section for Th^{232}, the capacity to breed U-233 is lower (C $\simeq$ 2.7).

In a realistic blanket design, several considerations must be addressed in order to have a consistent blanket design.[21] Among those considerations are: nuclear performance, blanket geometry, refueling and replacement, tritium handling, heat removal, structural integrity, materials, safety, and environmental issues. Tritium breeding to sustain the D-T reaction and high fissile breeding to supply several fission reactors are two major nuclear considerations. The blanket geometry should conform to the D-T neutron source and allow for penetration, blanket refueling, and replacement. Tritium removal and containment methods are important considerations because choices made affect tritium breeding rates needed. Tritium is provided through $^{6}Li(n,\alpha)t$ and/or $^{7}Li(n,\alpha,n')t$ reactions. Natural or enriched lithium can be used as a coolant for the front zone and/or the fuel zone containing the fissile fuel breeding zone. As a rule, breeding tritium from ^{6}Li is performed in zones which have substantially-moderated neutrons where the $^{6}Li(n,\alpha)T$ reaction is high. The total tritium breeding ratio, T, defined as the number of tritium atoms produced in the blanket per D-T neutron, should be slightly greater than 1.0 to provide the necessary fuel for the D-T reaction and to substitute for tritium losses and decay. As mentioned before, in some designs, the tritium breeding function may be eliminated from

Table (II.1)

Results for Infinite Medium (per D-T neutron)

(Ref. 21, 31)

Material	Energy Deposited MeV	M	Breeding Reaction (n,γ) ; (f/n)
Natural Uranium	309	22	5
Uranium-238	233	16	4.4
Thorium	64	4.5	2.7

Table (II.2)

Blanket* vs. Infinite Medium and Fuel Type
(per 14.1 MeV D-T Neutron)

(Ref. 21, 31)

Infinite Medium (natural uranium)	T / 0.0	f/n / 5.0	(MeV) / 309	M / 22
Blanket* With U	1.1	2.2	200	14
Blanket* With UO_2	1.1	1.1	100	7.1
Blanket*With UC	1.1	1.4	130	9.3

*Blanket:

Zone 1: 69% U + 10% SS + 16% Li

Zone 2: 86% Li + 9% SS

the blanket and be performed in the fission reactors.

High power density, particularly in the front zone of the blanket facing the high 14.1 MeV neutron flux, represents a design challenge and an appropriate heat removal system is needed to remove the excessive heat from this zone and the rest of the blanket. Structural integrity dictates the type of structural material to be used in the blanket. The performance of the blanket is quite sensitive to the ratio of structural material to fuel due to neutron competition. The type of fuel used (metal, carbides, oxides) is both important in nuclear design as well as fuel integrity. For example, uranium metal has swelling problems at burnups and temperatures that are too low to be of much interest for hybrids which emphasize power production.[12,21] It is a suitable fuel material for fusion systems which emphasize fuel production. In Table (II.2), we show how the blanket requirements and design trade-offs may affect the blanket performance. It is clear from this table that requiring a natural uranium blanket to breed tritium containing structure results in a plutonium breeding ratio of ~ 2 compared to 5 in the case of an infinite medium. Also, using ceramic uranium fuel will reduce the nuclear performance of the blanket (e.g., UO_2 performance is 1/2 U-nat. performance and UC performance is 2/3 U-nat. performance). Ceramic fuel may be used in blankets which have high power densities ($> 200 \frac{W}{cm^3}$) with a high flux influence. Due to the buildup of fission products and high radioactivity levels throughout the blanket, remote handling is necessary to replace the first wall (subjected to radiation damage due to long irradiation) and for refueling.

II.4 Classes of Hybrid Blankets

Several different fusion-fission system designs have been investigated and their performance is reported in the literature. These systems have been extensively investigated during the last four years although the early work in this field appeared in 1953.[22] Leonard has recently provided a bibliography of fusion-fission publications listing some 160 entries.[23] Refs. (15) and (24) give a recent review of the fission-fusion systems. Different designs can be extracted from Refs. 25-28.

Based on the different designs, the type of blanket can be classified as: uranium fast fission blanket, thorium fast fission blanket, thermal fission blanket, plutonium and U^{238} enriched fast fission blankets, and the non-fissioning blanket. Some of these blankets have been designed to emphasize fissile fuel production while others emphasize power production. As mentioned before, in the non-fissioning blanket, fissioning in both the fertile and the bred fissile fuel is suppressed. In a thermal fissioning blanket, fissioning is encouraged in the bred fuel and the blanket is devoted to power production. In other types of blankets fissile fuel production is emphasized with power produced as a by-product to improve the economics of the system. Except for the non-fissioning blanket, the fusion-fission system is termed a hybrid.

II.4.A Front Zone Neutron Multiplier

It has been argued that including a front zone to multiply the D-T neutrons will improve the blanket performance.[29-30] For

example, in a hybrid system, including a "fission plate" containing depleted uranium with a concentration 53% U^{238}, 25% sodium, and 12% stainless steel will multiply the fusion neutron energy by a factor of 3-7 and the number of neutrons leaving the fast fission blanket will be 1.6-1.9 times larger than the number of incident fusion neutrons if the thickness of this front zone varies from 3-15 cm.[29] Pu^{239} can be added to this fission plate to enhance the neutron multiplication through fissioning.[17] In general, the material choices for this zone are:[19]

A. Fuels:
   1. Type: metals, oxides, or carbides
   2. Fertile isotopes: Th^{232} or U^{238}
   3. Fissile isotopes: U^{233}, U^{235}, or Pu^{239}
   4. Cladding: stainless steel or refractory metals.

B. Coolants: gas or liquid metal

C. Structure: stainless steel or refractory metals.

If fissioning is suppressed throughout the blanket, the front zone may include materials (Be, Mo, Nb, Pb, ...) to multiply neutrons through (n,2n) reactions. The TZM material can also be used (as in Lidsky's[5] symbiotic system).

The most crucial issues affecting the technical and economic feasibility of fusion-fission hybrid systems occurs in the blanket region closest to the fusion neutron source because of the exposure to the high levels of energetic neutron flux and if fissioning takes place in the neutron multiplier zone, the power density in the front zone may be excessively high.[17] Therefore, important performance

indicators such as first wall flux, blanket power density, and blanket lifetime will be determined by the conditions in the region closest to the fusion source.[29]

II.4.B Different Options Possible After the Front Zone

The different blanket types are named in the literature according to the function performed in the region next to the front zone. Hybrid blankets can be designed to maximize breeding (tritium and/or fissile material) or fusion-neutron energy multiplication. In general, fissile production per source neutron (f/n) is maximized in uranium or thorium fast fissioning blankets. Thus, fissioning in the fertile material is used for enhancing the neutron multiplication for breeding purposes, and fissioning in the bred fuel is minimized. On the other hand, energy multiplication is maximized in thermal-fission blankets containing heterogeneous lattices of fissionable material and moderators by enhancing fissioning in the bred fuel. Substantial portions of the spectrum of different fission reactor technologies can be employed in designing these blankets. Thus, the fusion-fission systems based on these options will minimize the changeover of the present fission reactor technology. As far as material choices are concerned, for thermal-fission blankets we have:[19]

A. Fuels

1. Type: oxides or carbides
2. Fertile isotopes: Th^{232} or U^{238}
3. Fissile isotopes: U^{233}, U^{235}, Pu^{239}

4. Cladding: graphite, zirconium, or stainless steel

B. Moderators: graphite or hydrides

C. Coolant: gas or liquid metal

D. Structure: materials with low thermal-neutron absorption.

The material choices for U- or Th- fast fission blankets may be the same as in the front zone fission plate.

One of the options that can be adopted is to use the fusion-fission system to breed tritium. Although this option has not been studied in the literature, we mention it here for completeness. In this case, lithium behind the front zone neutron multiplier is used to breed excess tritium for the startup of pure fusion reactors.

In the symbiotic system, the zone following the front zone neutron multiplier is used for breeding fissile fuel without allowing fissioning to occur in either the fertile or the bred fuel. An intermediate zone containing a low-Z material may be added between this zone and the front zone to serve as a moderator. The neutrons reaching the fuel zone will be thermalized and neutron capture in the fuel zone is enhanced. Because of the competition between (n,γ) reactions and $^{6}Li(n,\alpha)t$ reactions at low neutron energies, the amount of ^{6}Li present in the fuel zone should be minimized to assure high fissile fuel production rates.

II.4.C Reflector and Tritium Breeding Zone

Most of the neutrons are thermalized when they reach the back edge of the blanket. It is in this region where the $^{6}Li(n,\alpha)t$ reaction rate is high and thus serves for tritium breeding. A

reflector zone is included to lessen neutron leakage. We summarize in Fig. (II.5) the role of the blanket in fusion-fission systems.

II.5 Typical Performance for Different Fusion-Fission Systems

Based on a literature survey, we have summerized in Ref.(36) some of the current conceptual designs of fusion-fission systems with a schematic representation of the blanket used in each design. These designs reflect the different philosophy of designing a hybrid system (e.g. U-fast fission, Th-fast fission, etc. ...). The important parameters of interest are: energy multiplication (M), fissile atoms produced per D-T neutron (f/n), and tritium atoms produced per D-T neutron, T.

We summarize in Fig. (II.6) the performance parameters of fusion-fission systems which breed U-233. One notices the following:

- The energy multiplication, M, is almost a linear function with the fissile breeding ratio f/n for Th-non-fissioning blankets and Th-fast fissioning blankets. Allowing for fissioning in the latter, f/n and M are slightly higher than the corresponding values in the Th non-fissioning blanket. In both cases, the value of the total breeding capture (C_{FB} = f/n + T) $\simeq$ 1.2 - 1.8 while M $\simeq$ 1 - 3.
- In blankets which utilize fast fission in U-238 as a neutron and energy multiplier in the front zone, the values of f/n and M are higher. M is a factor of 3-7 higher than the no-fission-front zone blankets and f/n is a factor of 1.3-1.9 higher. Including Pu in the front zone will enhance neutron

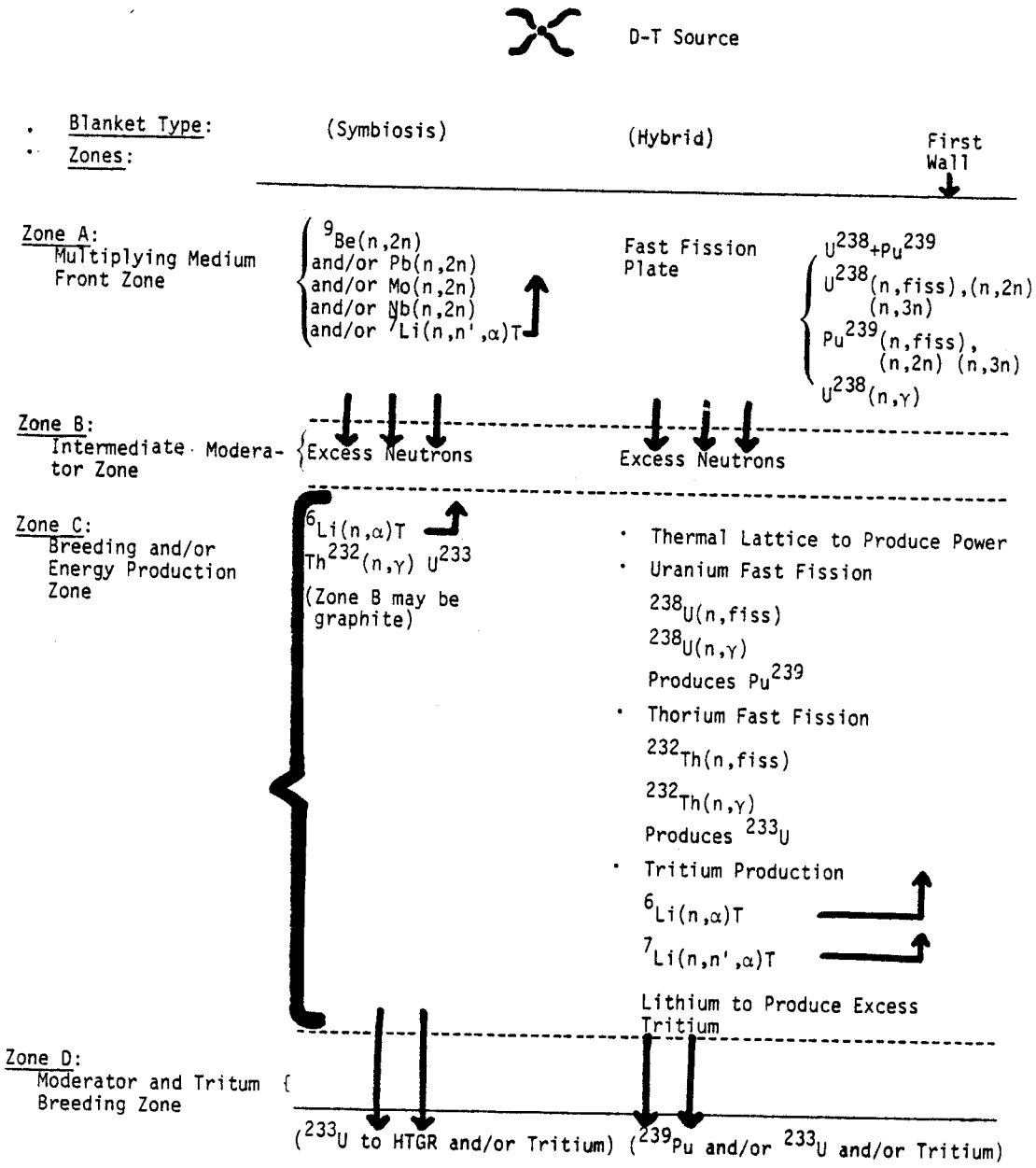

Fig. (II.5): Schematic Diagram of the Blanket for Different Fusion-Fission Systems.

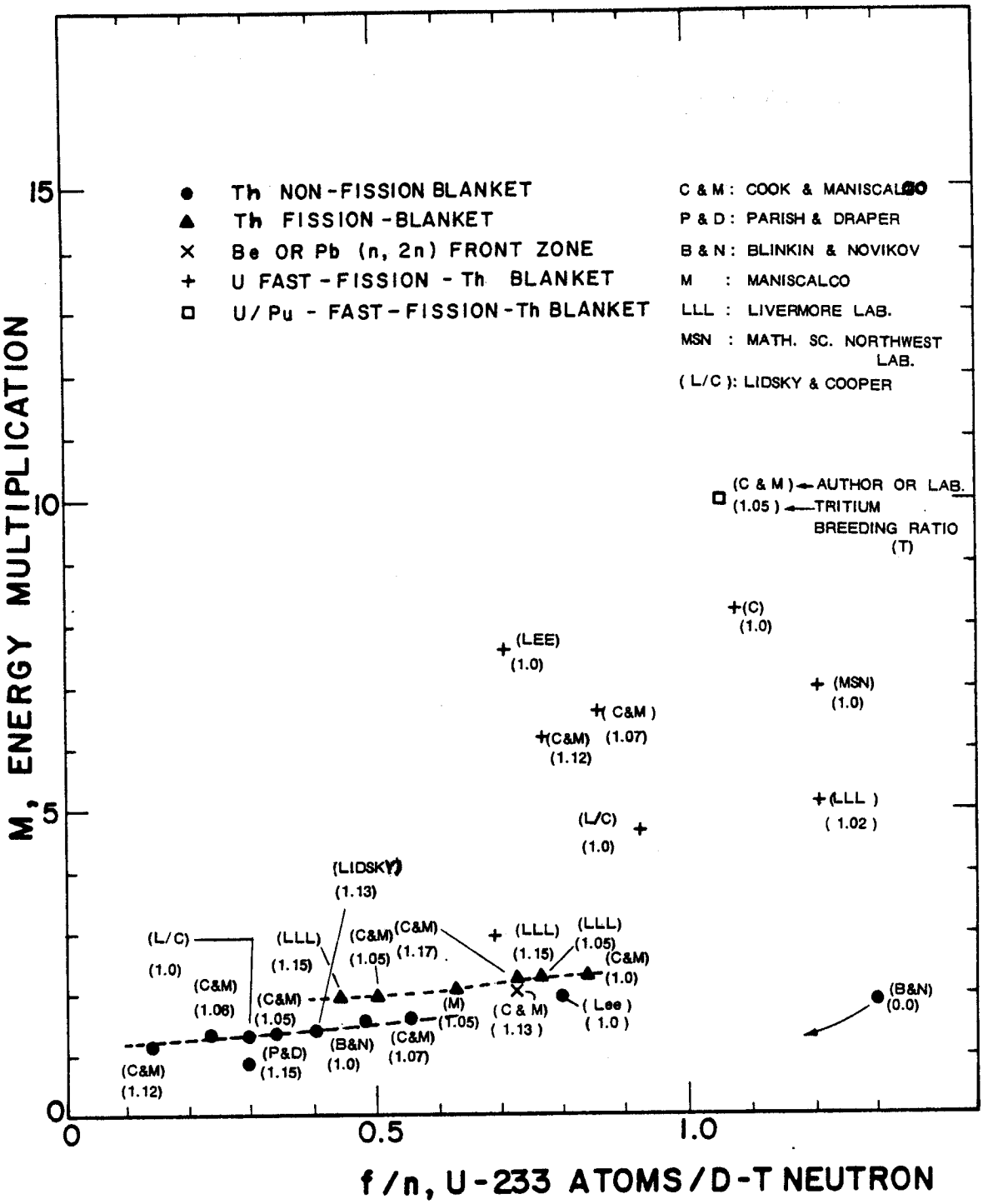

Fig. (II.6): Performance of ^{233}U-Producing Blankets

and energy multiplication throughout the blanket. Values of f/n ~ 4 and M ~ 80 can be obtained in this case as in the Su & McCormick design.[17] This will be at the expense of having higher power density in the front zone and the presence of a fissile inventory in the blanket.

- As the spectrum gets softer in the blanket and fissioning of the bred U-233 is allowed, the energy multiplication (M) does not follow a linear relation with f/n as in the non-fissioning blankets.
- If fissioning is suppressed in the blanket, including a Be (or Pb) front zone multiplier will improve the blanket performance due to neutron multiplication through (n,2n) reactions.

In Fig. (II.7) the performance of blankets which breed Pu^{239} is presented (see Ref(36)). Higher energy multiplication and breeding ratios are obtained in these blankets compared to the U-233 breeding blanket. This is due to the higher fission cross section and neutron yield for U^{238} compared to Th^{232} at 14.1 MeV neutron energy. The dispersion between the values of M and f/n for different designs reflects the deviation from linearity as more fissioning is encountered in the blanket. However, this is less noticeable in the fast fissioning blankets. In fact, having higher multiplication will be at the expense of fissile fuel bred. Table (II.3) summarizes the expected values of energy multiplication and fissile breeding ratio for different types of blankets based on the Th/U and U/Pu fuel cycles.

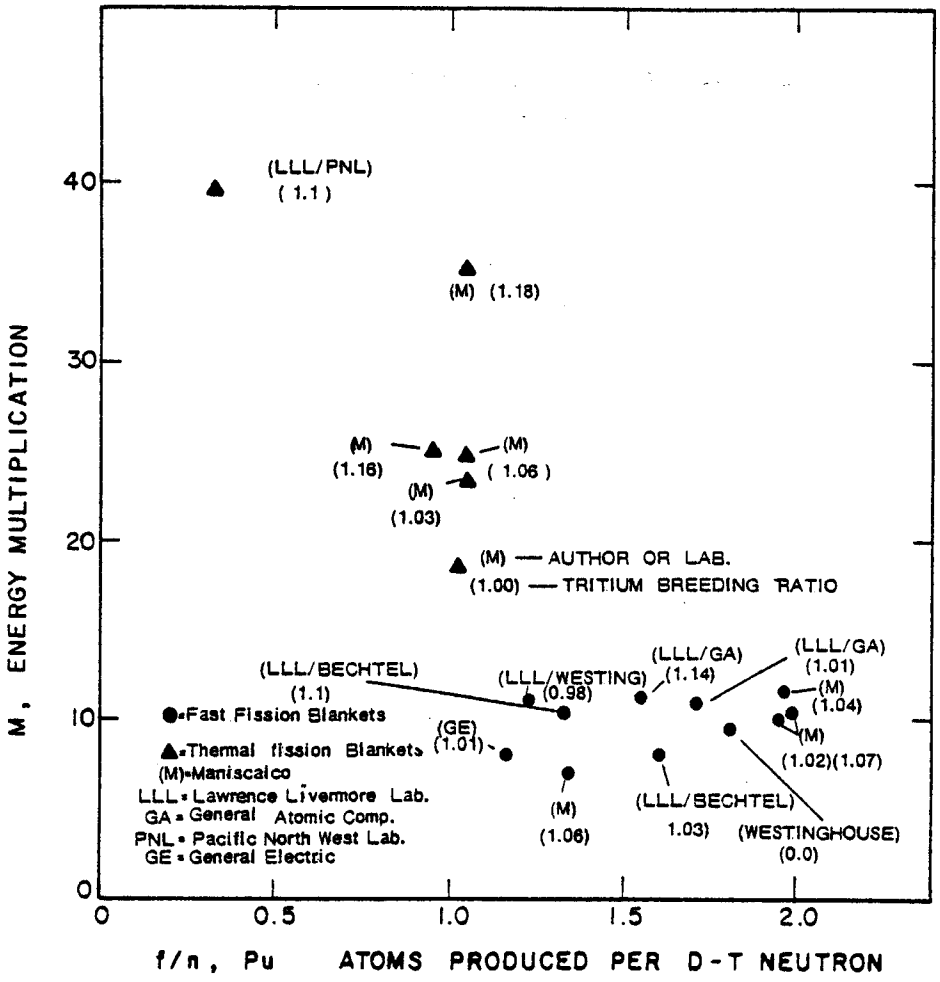

Fig. (II.7): Performance of ^{239}Pu-Producing Blankets.

Table (II.3)

Different Blanket Types and the Expected Performance

Cycle	Type of Blanket	Representation of the Blanket	M	f/n	C_{FB}=f/n+T
Th^{232}/U^{233}	Non-Fissioning	|Li|Th|	1.0-1.2	0.13-0.8	1.2-1.8
	Be Front Zone	|Be+Li+Th|	~ 1.6	~ 0.8	~ 1.8
	Th-Fast Fission	|Th|Li|	1.5-2.5	0.5-0.9	1.5-1.9
	U-Fast Fission	|U|Th+Li|	3-10	0.8-1.5	1.8-2.5
	U/Pu-Fast Fission	|U+Pu|Th+Li|	> 10	> 1.2	> 2.2
	U/Pu-Fast Fission (Thermal Th-Blanket)	|U+Pu|Th+U^{233} +Li|	> 30	-	1.0
U^{238}/Pu^{239}	U-Fast Fission	|U|Li|	7-11	1.1-2	2.2-3
	U/Pu-Thermal Blankets	|U+Pu|U+Li|	> 20	~ 1.0	2.1

II.6 Comparison Between Th/U and U/Pu Fuel Cycles

Because of the higher energy multiplication in U/Pu blankets, the fusion driver requirements are relaxed in designs using these blankets from those using Th/U blankets for the same fraction of recirculating power needed for the fusion driver. This can be seen from Fig. (II.8) where Fig. (II.8)-a describes the energy balance and Fig. (II.8)-b shows the effect of the blanket energy multiplication on the fusion gain (fusion gain = $\frac{\text{thermal fusion power}}{\text{electric input to the fusion driver}}$) for different values of recirculating power fraction. As shown, the fusion gain decreases drastically as M increases. In particular, for a fusion-fission system which operates as a fissile fuel producer (recirculating fraction ~ 100%), the uranium-fueled fast fission blankets can produce fissile fuel in an energy breakeven mode with fusion energy gains that are 2-6 times lower than those required for similar thorium-fueled blankets and 30 times lower than those required for a pure fusion power plant where M=1.[19] For systems which are energy producers (recir. power $\lesssim$ 25%) and in the case of the U/Pu fast fission-thermal blanket ($|U+Pu|Th+U^{233}+Li|$) the fusion gain is 20 times lower than for a thorium-fast fission blanket with the same recirculation fraction.

However, blankets based on Th/U fuel cycles will breed U-233 which is a superior fuel for a near breeder reactor (HTGR, MSR) because of its low capture to fission ratio (~ 0.1 compared to 0.3 in a LWR burner based on a U/Pu cycle). With the fusion-fission reactor as a fissile fuel factory,[32] the supporting ratio (defined

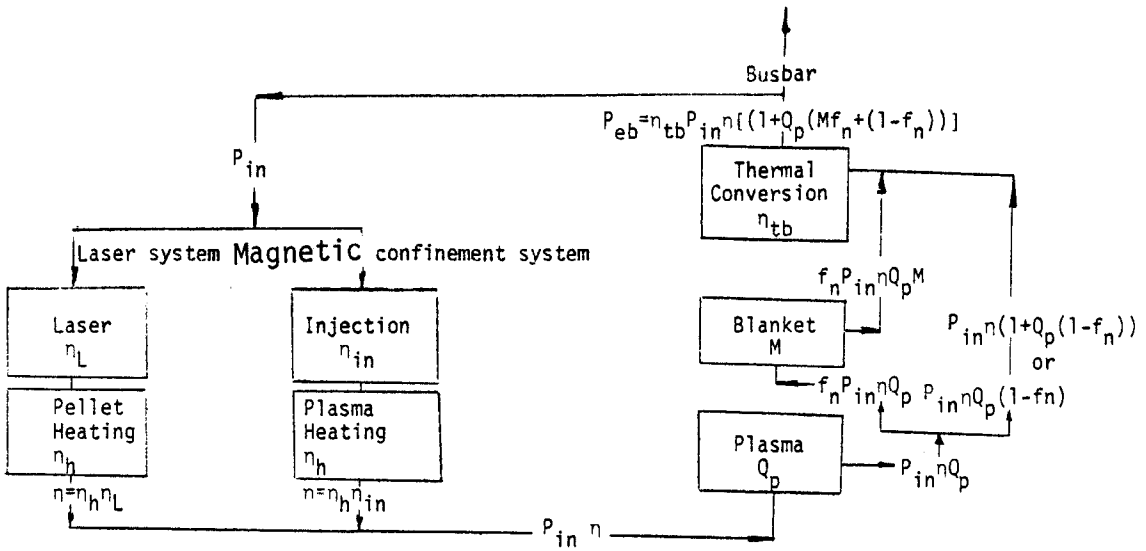

$$\text{Circulating power fraction} = \frac{P_{in}}{P_{eb}} = \frac{1}{\eta_{tb}\eta[1+Q_p(0.8M+0.2)]} \quad \begin{cases}\text{power to heat the plasma is retained,}\\ f_n=0.8\end{cases}$$

$$= \frac{1}{\eta_{tb}\eta Q_p(0.8M+0.2)} \quad \begin{cases}\text{power to heat the plasma is not retained}\\ f_n=0.8\end{cases}$$

η_L = laser system efficiency

η_{in} = injection efficiency

η_h = plasma (or pellet) heating efficiency

P_{in} = electric power input to injectors (or to laser)

η_{tb} = thermal to electrical power conversion of the fusion-fission breeder $\simeq$ 0.35

f_n = fraction of energy carried by the D-T neutrons ($\sim$ 0.8)

Q_p = plasma power multiplication (or pellet gain)

ηQ_p = fusion gain = $\frac{\text{fusion power}}{\text{electric input to the fusion driver}}$

Fig. (II.8)-a: Energy Balance in Fusion Hybrids.

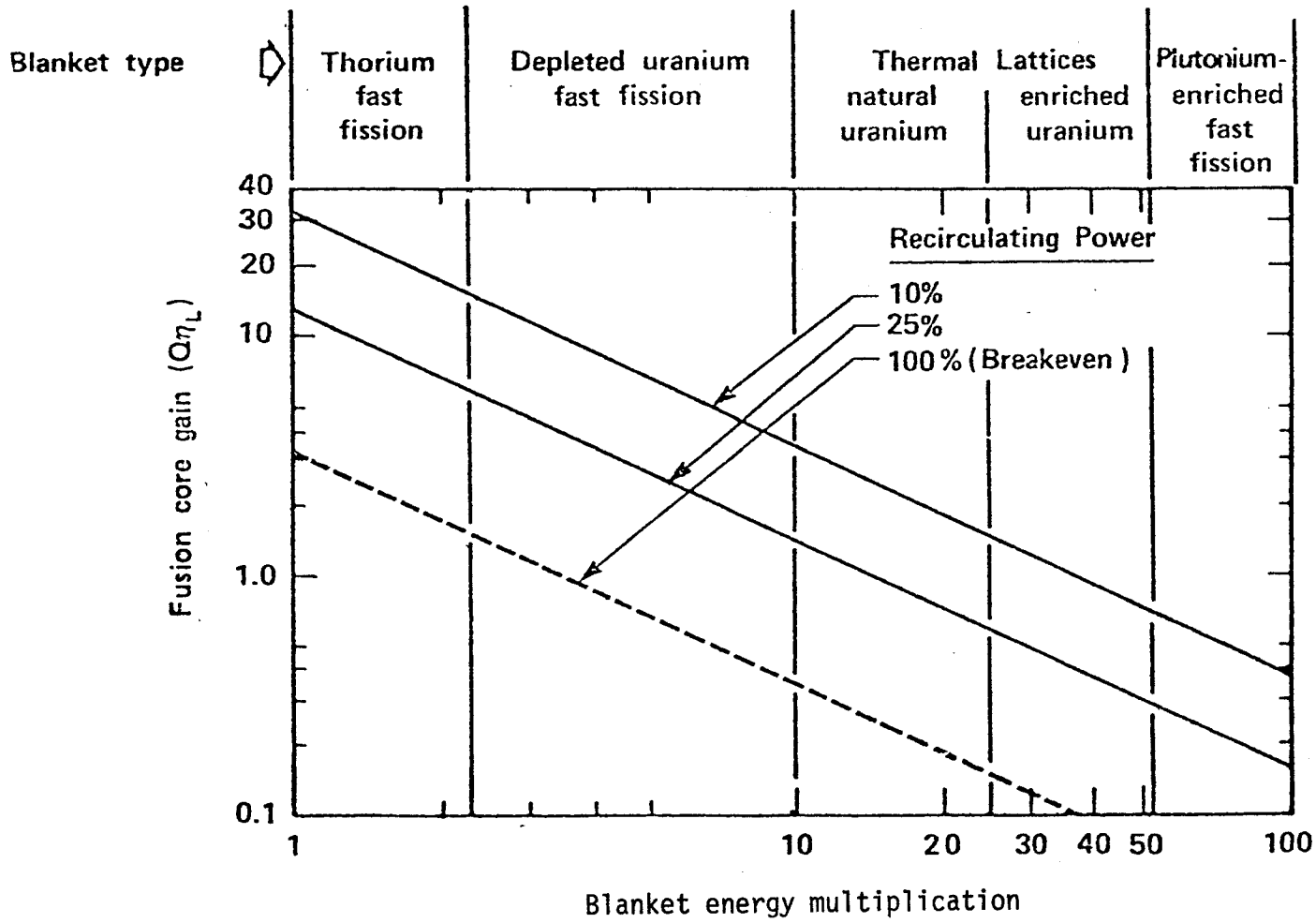

Laser Fusion Core Gain Requirements for Hybrid Fusion/Fission Systems (Ref. 19).

Fig. (II.8-b)

as the number of fission reactors of equal thermal power to the hybrid reactor which are supported by their fissile fuel needs from the hybrid) will be higher with Th/U fuel cycles than with U/Pu fuel cycles due to the higher conversion ratio, C, of the near breeder fission reactors (C ~ 0.95) compared to the burners (C ~ 0.6). Thus, with an internationally-controlled "secure fence" consisting of a fusion-fission fuel factory and a reprocessing plant, most of the power will be produced outside this fence and the integrated system will be a proliferation-controllable one.[33]

A final choice of whether the optimized fusion-fission system will be a power producer (on-line) or a fuel factory (no electricity is generated in the hybrid) and whether it is preferable to use U/Pu or Th/U fuel cycles should be based on an economic evaluation. Bender has studied these options in a mirror-system coupled to fission reactors through fissile fuel and power linkages.[34] He showed that working in an "on-line" mode (i.e., the hybrid produces fissile fuel + electricity) is more favorable economically than working in a fuel factory mode for both fuel cycles although the penalty obtained is less when the Th/U fuel cycle is used. Also, he demonstrated that the relative total system capital cost, R_c (defined as the capital cost of the combined system ($/kWe) relative to the capital cost of the fission reactors only), is insensitive to the hybrid capital cost even if the fusion power amplficiation, Q_p, is low (~ 0.5). With Th/U cycles and fixing R_c to be 1.25 (i.e., 25% increase in the electricity cost when the fusion and

fission reactors are coupled), he demonstrated that the allowable relative unit capital cost K (defined as the ratio of the unit capital cost of the hybrid ($/kWth) to the unit capital cost of the fission reactors) is higher for Th/U cycles than for U/Pu cycles; that is, more expensive Th/U-hybrids can be built without severely affecting the total electricity cost when compared to U/Pu-hybrid. Bender uses his economic model to compare different types of blankets that breed U-233.[35] He shows that system economics are dominated by the value of f/n, i.e. $R_c \sim 1/(f/n)$ while the support ratio, R_t, is dominated by the ratio (f/n)/M. These conclusions apply for $Q_p > 1$. In Bender's model, the electricity cost is considered to be dominated mainly by the capital cost.

II.7 Conclusions and Remarks

It is demonstrated from the survey presented in this chapter that the fusion-fission hybrids can be designed to meet a broad spectrum of fissile fuel and energy requirements. Minimum extension in the present technology encountered in the LWRs and fast breeders is predicted to meet these requirements. Thus, an early introduction of the fusion-fission systems as a long term option is expected.

In the next chapter we present the results of investigating the role the hybrid can play in providing the fissile fuel needs to several fission reactors. In particular, we studied the possibility of shifting the tritium breeding function to the fission reactors and/or to a dedicated tritium producer reactor devoted mainly to that purpose. As pointed out earlier, this may lessen the complexity

encountered in fusion hybrid designs.

Reference

1. Fortescue, P., "Assurance of a Durable Nuclear Industry," Nucl. Eng. International 21 (Oct. 1976), 71-75.

2. Fortescue, P., "Comparative Breeding Characteristics of Fusion and Fast Reactors," Science, Vol. 196 (4296), 1326-1329 (June 1977).

3. Gordon, C.W., Harms, A.A., "Comparative Energetics of Three Fusion-Fission Symbiotic Nuclear Reactor Systems," Nucl. Eng. & Design 34 (1975), 269-280.

4. Harms, A.A., "Nuclear Energy Synergetics," Atomkernenergie, 32 (1978) 3-11.

5. Lidsky, L.M., "Fission-Fusion Symbiosis: General Considerations and a Specific Example," in Proc. British Nuclear Energy Society, Nuclear Fusion Reactor Conference at Culham Lab., 1969, Culham Lab. Report CLM-NFR (1969), 41.

6. Blinkin, V.L., Novikov, V.M., "Symbiotic System of a Fusion and Fission Reactor With Very Simple Fuel Reprocessing," Nucl. Fusion, 18 (1978), 893-900.

7. Maniscalco, A.J., Hansen, L., "Present Status of Laser Driven Fusion-Fission Energy Systems," Proc. of the Second Fusion-Fission Energy Systems Review Meeting, Nov. 2-3 (1977), Vol. I, CONF-77115 (July 1978).

8. Proceedings of the Second Fusion-Fission Energy Systems Review Meeting, Nov. 2-3 (1977), Vol. II, CONF-77115 (1978).

9. Lidsky, L.M., "Fusion-Fission Systematics," Ref. 8, Vol. I (1978), 83-97.

10. Rose, R.P., "Status of Westinghouse Tokamak Hybrid Studies," Ref. 8, Vol. I (1978), 123-143.

11. Bender, D.J., Mirror Hybrid Reactor Studies," Ref. 8, Vol. I (1978), 99-122. Also UCRL-80694.

12. Maniscalco, J.A., Hansen, L.F., Present Status of Laser Driven Fusion-Fission Energy Systems," Ref. 8, Vol. I (1978), 145-182.

13. Oliver, D., Copper, R., Lidsky, L., "Breeding of Fissile Fuel With Linear Fusion Sources," Proc. of the Second Topical Meeting on The Technology of Controlled Nuclear Fusion, Vol. II, Sept. 21-25 (1976), Richland, Washington, CONF-760935-P2 (1976).

14. Fortescue, P., "The Fusion Breeder Concept," Annals of Nuclear Energy, Vol. 2 (1975), 29-32.

15. Lidsky, L.M., "Fission-Fusion Systems: Hybrid, Symbiotic and Augean," Nucl. Fusion 15 (1975), 151.

16. Harms, A.A., Gordon, C.W., "Fissile Fuel Breeding Potential With Paired Fusion-Fission Reactors," Annals of Nucl. Energy, Vol. 3 (1976), 411-420.

17. Su, S.F., Woodruff, G.L., McCormick, N.J., "A High Gain Fusion-Fission Reactor For Producing Uranium-233," Nucl. Technology 29 (1976), 392-405.

18. Lee, J., "Mirror Fusion-Fission Hybrids," Atomkernenergie 32 (1978), 19-29.

19. Maniscalco, J., "Fusion-Fission Hybrid Concepts for Laser-Induced Fusion," Nucl. Technology, 28 (1976), 98-107.

20. Bender, D.J., Lee, J.D., "A Prospective on the Fusion-Fission Hybrid Reactor," Lawrence Livermore Lab., UCID-17622 (Oct. 1977).

21. Lee, J.D., "Nuclear Design of Fast Hybrid Blankets," Ref. 8, Vol. II (1978), 377-396. Also see UCRL-80651.

22. California Research and Development Company, Proposal for a Driven Thermonuclear Reactor, USAEC Report LWS-24920 (Rev.) (1953).

23. Leonard, B.R., Jr., "Bibliography of Fusion-Fission Publications", Battelle Northwest Laboratories, Richland, Washington, U.S.A., PNL-SA-6492 (April 1978).

24. Leonard, B.R., Jr., "A Review of Fusion-Fission (Hybrid) Concepts," Nucl. Technology 20 (1973), 161-178.

25. DCTR Fusion-Fission Energy Systems Review Meeting," Dec. 3-4 (1974), ERDA, Germantown, Maryland, ERDA-4 (1974).

26. Proceedings of the Second Topical Meeting on The Technology of Controlled Nuclear Fusion, Vol. II, Sept. 21-23 (1976), Richland, Washington, CONF-760935-P2 (1976).

27. "Proceedings of the US-USSR Sympsoium on Fusion-Fission Reactors", July 13-16 (1976), CONF-760733 (1976).

28. "Proceedings of the Second Fusion-Fission Energy Systems Review Meeting," Vol. I, II, Nov. 2-3 (1977), CONF-771155 (1978).

29. Maniscalco, J.A., Hansen, L.F., "New Initiatives in Laser Driven Fusion-Fission Energy Systems," UCRL-81509, Lawrence Livermore Lab. (May 1978). Also Ref. 8, Vol. I (1978), 277-296.

30. Cook, A.G., Maniscalco, J.A., "Uranium-233 Breeding and Neutron Multiplying Blankets for Fusion Reactors," Nucl. Technology, 30 (July 1976), 5-11.

31. Lee, J.D., "Subcritical Fast Fission Blanket," Lawrence Livermore Radiation Laboratory, Thermonuclear Reactor Memo TRM-20 (1970).

32. Bethe, H.A., "The Fusion Hybrid", Nuclear News (May 1978).

33. Conn, R.W., Moses, G.A., Abdel-Khalik, S.I., "Notes on Fusion Hybrid Reactors", UWFDM-240, Fusion Research Program, The University of Wisconsin, April (1978).

34. Bender, D.J., "Performance Parameters for Fusion-Fission Power Systems", Lawrence Livermore Lab., UCRL-80589, Rev. 1, May (1978).

35. Bender, D., "The Best U-233 Producing Blanket for the Tandem Mirror Hybrid", Lawrence Livermore Lab., UCID-17823, June (1978).

36. Youssef, M.Z., Conn R.W., "A survey of Fusion-Fission System Designs and Nuclear Analyses", UWFDM-308, Fusion Research Program , The University of Wisconsin, June (1979).

Chapter III

TRITIUM AND FISSILE FUEL EXCHANGE BETWEEN HYBRIDS, FISSION POWER REACTORS, AND TRITIUM PRODUCTION REACTORS*

III.1 Introduction

Utilizing neutrons from fusion reactions to produce fissile fuel in fusion-fission hybrid reactor blankets has recently been the subject of several extended studies.[1-11] For the standard case, both fissile fuel and tritium are produced in the hybrid blanket. In addition, the possibility of breeding tritium in fission power reactors designed for that purpose, and transferring it to the hybrid (which may breed some tritium), has been studied by several authors,[12-24] as mentioned in the previous chapter.

In the study presented in this chapter, an extension to the mathematical model used by Gordon and Harms[14-16] is developed to describe an overall system which may also include a fission reactor devoted mainly to producing tritium. The remaining fission reactors are not necessarily tritium producers. An approach of this sort may be of interest because tritium production reactors are currently operational. The main motivation for dividing functions would be to simplify hybrid design and/or to utilize already existing dedicated tritium production fission reactors.

It is assumed in the models discussed here that all the components of the system are in equilibrium. The time to reach equilibrium is not discussed. In the following sections, the neutron reactions, the mathematical model, and the numerical results for different

fusion-fission models are given. A comparison between different model systems and concluding remarks are presented in Sec. III.5.

III.2 Neutron Reactions and Model Description

Fissile fuel is produced by capture through the reactions

$$^{232}Th(n,\gamma)^{233}Th \xrightarrow[22\ min]{\beta^-} {}^{233}Pa \xrightarrow[27.4\ days]{\beta^-} {}^{233}U \quad , \qquad \text{(III.1)}$$

$$^{238}U(n,\gamma)^{239}U \xrightarrow[23\ min]{\beta^-} {}^{239}Np \xrightarrow[2.3\ days]{\beta^-} {}^{239}Pu \quad , \qquad \text{(III.2)}$$

and in the model developed here, consumption of the fissile fuel is assumed to take place only in the fission reactors. The fusion fuel (tritium) is produced by the reactions

$$n + {}^{6}Li \rightarrow T + \alpha \ , \quad Q = 4.38\ MeV \quad , \qquad \text{(III.3)-a}$$

$$n + {}^{7}Li \rightarrow T + \alpha + n' \quad , \quad Q = -2.7\ MeV \qquad \text{(III.3)-b}$$

where Q is the energy released in the reaction. Tritium is also produced by neutron capture in deuterium when heavy water is used as a moderator in the fusion reactors. The production of tritium in fission reactors can be enhanced by using lithium in the control rods or by locating lithium in the reactor reflector.[13] The latter case is a choice between using the neutrons for fissile fuel or tritium production. Tritium is assumed to be consumed only in the fusion core through the reaction

$$D + T \rightarrow n + {}^{4}He + (17.6\ MeV) \qquad \text{(III.4)}$$

The general model for the entire system is illustrated in Fig. (III.1). A tritium producer reactor and several fission reactors

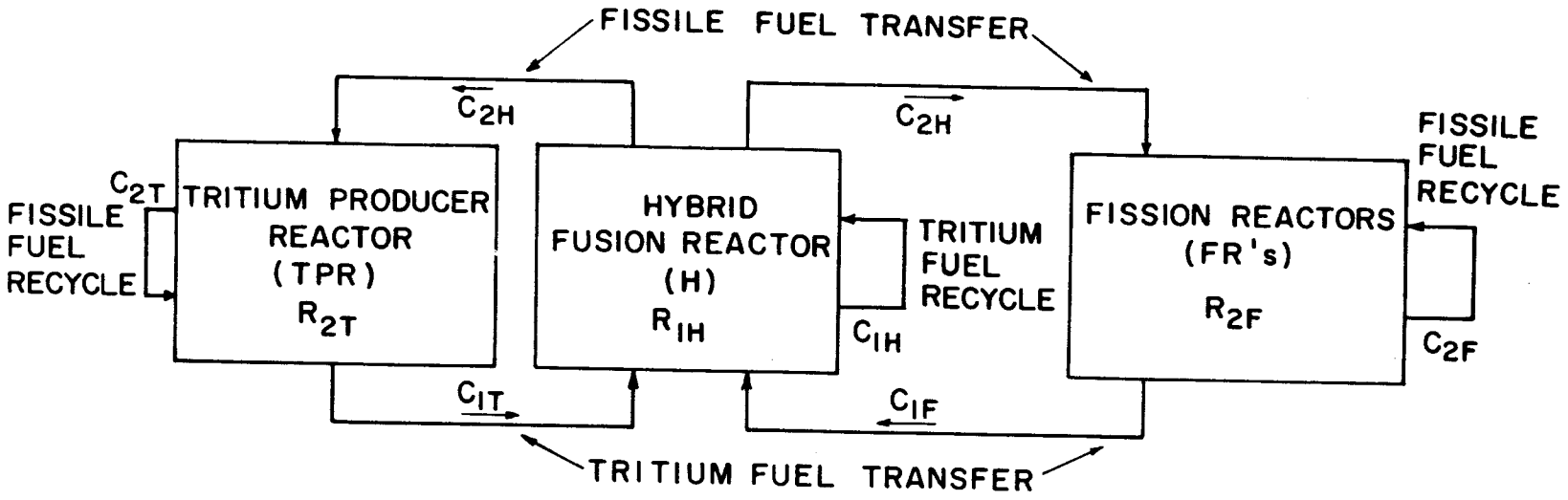

Fig, (III.1)

General material flows, conversion ratios, and reaction rates for an overall energy system consisting of fission reactors, fission-fusion hybrid reactors, and tritium production reactors.

provide tritium to the fusion hybrid. The hybrid in turn supplies fissile fuel to both the tritium production reactor and the fission reactors. The fusion hybrid may breed some tritium, which is recycled to it; the fissile fuel produced in the tritium production reactor and the fission reactors is also recycled. The coupling coefficients, C_{ij}, associated with the recycle and transfer of nuclei are shown in the figure. The first subscript identifies the type of fuel ($i = 1$ for tritium and $i = 2$ for fissile fuel), while the second subscript identifies the reactor type ($j = H$ for the fusion hybrid, $j = F$ for the fission reactors, and $j = T$ for the tritium production reactor). The fissile fuel reaction rates, R_{ij}, are shown on the figure, and the subscripts are as described above.

Two limiting systems have been studied, namely,

1. The sharing system where tritium is produced in the fission reactors. The tritium production reactor may or may not be included in the system.
2. The dedicated system where tritium is produced only in the tritium production reactor. No tritium is produced in the fission reactors.

Schematic diagrams of the sharing and dedicated systems are given in Fig. (III.2). Tritium may or may not be produced in the hybrid reactor.

III.3 Mathematical Model

We are interested in evaluating the effect of including a dedicated reactor for tritium production as part of the overall fusion-

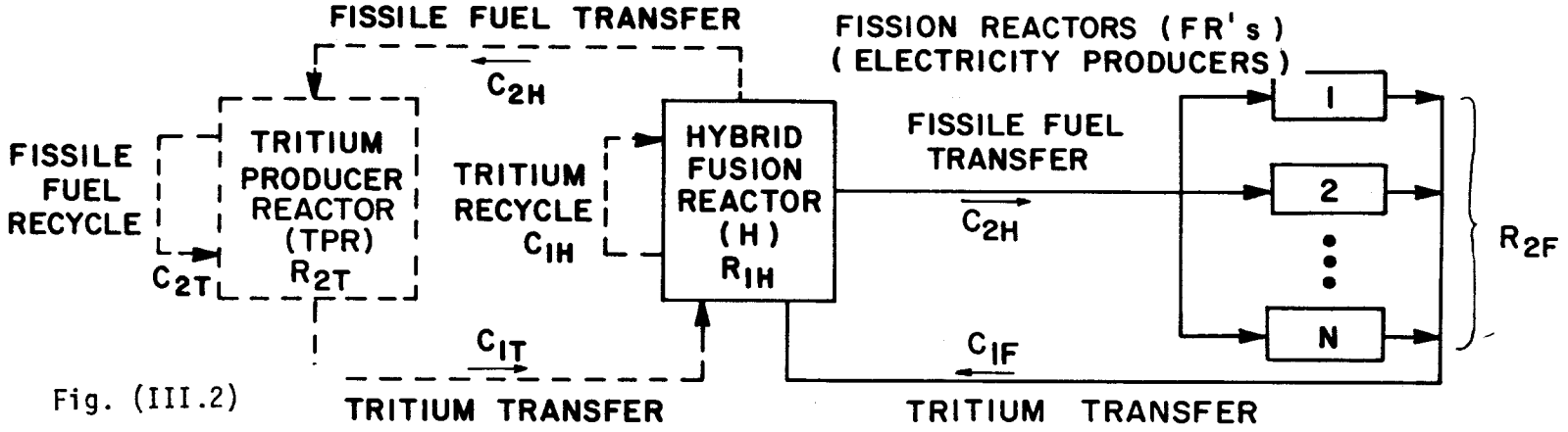

Fig. (III.2)

THE SHARING SYSTEM. THE FR's PROVIDE THE HYBRID WITH TRITIUM WHICH IN TURN PROVIDES THE FR's WITH FISSILE FUEL. THE HYBRID MAY OR MAY NOT PRODUCE TRITIUM. THE TPR MAY BE INCLUDED.

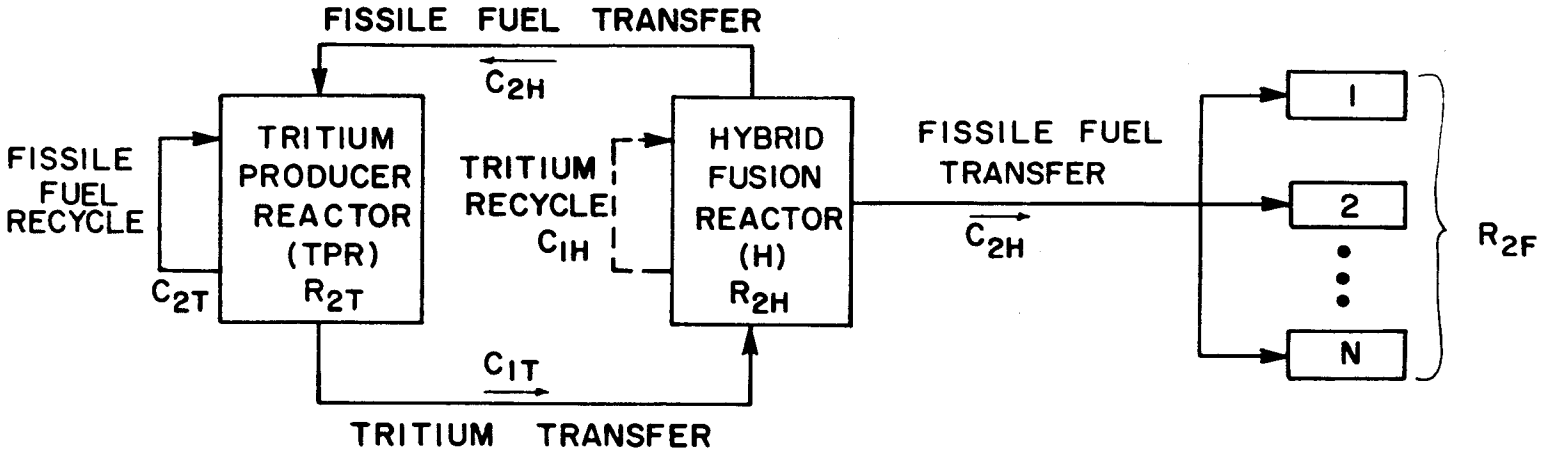

THE DEDICATED SYSTEM. THE TPR PROVIDES THE HYBRID WITH TRITIUM; THE HYBRID PROVIDES THE TPR AND THE FR's WITH FISSILE FUEL; THE HYBRID MAY OR MAY NOT BREED TRITIUM.

fission system. For this exploratory analysis, a simple mathematical model is adopted to describe fuel and power flow. We assume that the transfer and recycling processes are continuous and that losses of either fissile fuel (during reprocessing) or fusion fuel (tritium handling and decay) are negligible. The assumption of continuity of fuel flow among different parts of the overall system can easily be met, for example, if a molten-salt-type fuel is used. Blinkin and Novikov,[21] who confine their analysis to hybrid and fission reactors only, argue that using molten salt in these reactors will lead to simpler and less expensive continuous fuel reprocessing. This, in turn, shortens the delay time between fuel production and transfer and minimizing fuel losses.

In the analysis here, we assume that the coupling coefficients, C_{ij}, are constant. This can be achieved in the hybrid reactor if the blanket is designed to minimize fission events, a typical consideration in a hybrid designed primarily as a fissile fuel producer. It also implies the neglect of fuel burnup. We find that, depending on exposure time, burnup in the fusion hybrid could be 10% of the amount of fuel bred. Nevertheless, we do not find large changes in the coupling coefficients and adopt the constant C_{ij} assumption, as did Gordon and Harms.[14-16] Note that C_{ij} will not be constant in blankets designed for power production.

The time variation in the model of Harms and Gordon[15] of the number of tritium atoms in the system is

$$\frac{dN_1(t)}{dt} = R_{1H}C_{1H}+R_{2F}(1 + \alpha_F)C_{1F}-R_{1H} \quad , \qquad \text{(III.5)}$$

while the number of fissile atoms varies as

$$\frac{dN_2(t)}{dt} = R_{1H}C_{2H} + R_{2F}(1 + \alpha_F)C_{2F} - R_{2F}(1 + \alpha_F) \qquad \text{(III.6)}$$

In these equations, C_{1H} and C_{2H} are, respectively, the number of tritium atoms and the net number of fissile atoms produced in the hybrid blanket per fusion event; C_{1F} is the number of tritium atoms produced in the fission reactors per fissile fuel absorption event. The fissile fuel conversion ratio in the fission reactors is the coefficient C_{2F}; R_{2F} is the fission reaction rate in these reactors, while R_{1H} is the fusion reaction rate in the hybrid; α_F is the capture-to-fission ratio in the fission reactors.

The first term in Eq. (III.5) is the tritium production rate in the hybrid reactor. The second term is the tritium production rate in the fission reactors. The last term is the loss rate in the hybrid core due to fusion reactions. Similar rates for fissile fuel production are given by the first two terms in Eq. (III.6). The last term represents the loss rate due to absorptions in the fission reactors.

If a dedicated tritium production reactor is included as an integral part of the overall fusion-fission system, then Eqs. (III.5) and (III.6) are modified to become

$$\frac{dN_1(t)}{dt} = R_{1H}C_{1H} + R_{2F}(1 + \alpha)C_{1F} + R_{2T}(1 + \alpha_T)C_{1T} - R_{1H} \qquad \text{(III.5)}'$$

and

$$\frac{dN_2(t)}{dt} = R_{1H}C_{2H} + R_{2F}(1 + \alpha_F)C_{2F} + R_{2T}(1 + \alpha_T)C_{2T}$$
$$-R_{2F}(1 + \alpha_F) - R_{2T}(1 + \alpha_T) \qquad \text{(III.6)}'$$

In Eq. (III.5)', C_{1T} and C_{2T} are the number of tritium atoms and fissile fuel atoms produced in the tritium production reactor per fissile fuel absorption event, respectively, and R_{2T} and α_T are the fission reaction rate and the capture-to-fission ratio in this reactor, respectively. Thus, the third term in both Eqs. (III.5)' and (III.6)' are the tritium production rate and the fissile fuel production rate in the tritium production reactor, respectively. The last term in Eq. (III.6)' is the fissile fuel loss rate in the tritium production reactor.

Different modes of operation are possible. As first suggested by Lidsky[20] and discussed later by Gordon and Harms[14] and by Blinkin and Novikov,[21] a constant ratio fuel inventory operating mode is defined by

$$\frac{N_1}{N_2} = \text{constant},$$

and permits us to define the characteristic time constant, τ, for both tritium and fissile fuel, i.e.,

$$\frac{1}{N_1}\frac{dN_1}{dt} = \frac{1}{N_2}\frac{dN_2}{dt} = \frac{1}{\tau} \quad .$$

In a second operating mode, called a mixed mode by Harms[16] one has either

$$\frac{dN_1}{dt} \neq 0 \quad , \quad \frac{dN_2}{dt} = 0$$

or

$$\frac{dN_2}{dt} \neq 0 \quad , \quad \frac{dN_1}{dt} = 0 \quad .$$

When $dN_2/dt = 0$, one can breed more tritium for other fusion reactors. The second operational criterion is adopted if one is interested in eliminating the evnironmental hazard of tritium and allow for producing fissile fuel for an external market of existing fission reactors.[13,23] In the model adopted in our analysis, we concern ourselves only with steady-state operation, which represents an equilibrium where no net gain of fuel of either kind takes place. In this case, the solution of the equation describing the system will not depend on the specific inventory of the fuel (tritium and fissile fuel).

We define P_F, P_T, and P_{fus} as the total thermal power of the fission reactors, the thermal power of the tritium production reactor, and the fusion power, respectively, i.e.,

$$P_F = E_{fiss} R_{2F} \quad ,$$

$$P_T = E_{fiss} R_{2T} \quad , \qquad \text{(III.7)}$$

and

$$P_{fus} = E_{fus} R_{1H} \quad .$$

In these equations, E_{fiss} and E_{fus} are the energies released per fission (~200 MeV) and fusion (~17.6 MeV) event, respectively. At

steady state, Eqs. (III.5)' and (III.6)' become

$$(1-C_{1H})=\varepsilon\left[\frac{P_F}{P_{fus}}(1+\alpha_F)C_{1F}+\frac{P_T}{P_{fus}}(1+\alpha_T)C_{1T}\right] \tag{III.8}$$

and

$$C_{2H}=\varepsilon\left[\frac{P_F}{P_{fus}}(1+\alpha_F)(1-C_{2F})+\frac{P_T}{P_{fus}}(1+\alpha_T)(1-C_{2T})\right] \tag{III.9}$$

where $\varepsilon=E_{fus}/E_{fiss}$. The two power parameters of interest are $P_F/P_{fus}\equiv p_F$, the total thermal power of the fission reactors per unit of fusion power, and $P_T/P_{fus}\equiv p_T$, the thermal power of the tritium production reactor per unit of fusion power. Equations (III.8) and (III.9) are two linear equations relating the specific power ratios, p_F and p_T, to the coefficients C_{ij}. Taking these ratios as the dependent variables, we find

$$p_F=\frac{(1-C_{2T})(1-C_{1H})-C_{1T}C_{2H}}{\varepsilon(1+\alpha_F)[C_{1F}(1-C_{2T})-C_{1T}(1-C_{2F})]} \tag{III.10}$$

$$p_T=\frac{(1-C_{2F})(1-C_{1H})-C_{1F}C_{2H}}{\varepsilon(1+\alpha_T)[C_{1T}(1-C_{2F})-C_{1F}(1-C_{2T})]} \tag{III.11}$$

The values of C_{ij} can be estimated based on the large number of hybrid blanket neutronics studies that have been performed. As shown in Chapter II, in a hybrid blanket using thorium to breed ^{233}U, the total breeding capacity, C_H, defined as the summation of C_{1H} and C_{2H}, is typically ~1.5. For a blanket that breeds ^{239}Pu from ^{238}U, C_H is ~2.5. Similarly, the total breeding capacity in the fission reactors,

C_F, is $C_{1F}+C_{2F}$, while that in the tritium production reactor is $C_T=C_{1T}+C_{2T}$. The values of C_F and C_T are determined by the neutron economy in the fission reactors and the tritium production reactor. The maximum value in either case is $(\eta-1)$, where η is the number of neutrons emitted per absorption event in the fuel. The value of η depends on the fuel utilized (^{232}Th-^{233}U or ^{238}U-^{239}Pu) and the nature of the neutron spectrum (fast or thermal).

The final thermal power of interest is the total thermal power of the hybrid reactor, P_H, which is given by[25] (see Fig. (II.8)-a)

$$P_H=P_{fus}\left[\frac{1}{\gamma_{in}Q}+1+f_n(M-1)\right] \quad , \qquad \text{(III.12)}$$

where

Q = ratio of the fusion power to the net power injected to maintain the plasma

f_n = fraction of fusion energy released in neutrons

M = hybrid blanket energy multiplication defined as the ratio of energy deposited in the blanket per 14.1-MeV deuterium-tritium neutron

γ_{in} = efficiency of energy injection in the plasma.

Note that M is a function of C_{2H}, i.e., a blanket designed to have a high value of C_{2H} may well have a high value of M and P_H. This is found to be true[22] for the ^{232}Th-^{233}U fuel cycle in hybrids designed primarily for fissile fuel production. Examples include thorium nonfissioning blankets and blankets with significant thorium fast fission. In these cases (presented in Chapter II), it is found that

M increases linearly with C_{2H}. When fission in the fissile fuel is enhanced in the hybrid blanket, M increases at the expense of C_{2H}, and the linearity just described does not hold. What concerns us here is the adequacy of the assumption that C_{2H} (and C_{1H}) is constant. The assumption is usually true in thorium nonfissioning blankets. Its applicability in U-Pu systems is adequate when $C_{2H} \simeq 2.5$ and $M \simeq 5$ at beginning-of-life. If $C_{2H} \simeq 2.5$ and $M \simeq 10$ (implying significant ^{239}Pu fissions at beginning-of-life), the constancy of C_{2H} is more questionable.

Formally, Eqs. (III.10), (III.11), and (III.12) and the constraints given by the values of C_H, C_F, and C_T describe the entire system. In Sec. III.4, two special cases-the sharing system and the system with dedicated tritium production reactor-are analyzed.

Before proceeding to look at these special cases, some remarks about the general system can be made. Since Eqs. (III.8) and (III.9) are sufficient to describe the system, any linear combination of the equations will suffice equally well. One such linear combination arises if Eq. (III.8) is subtracted from Eq. (III.9), yielding

$$C_H - 1 = \varepsilon[p_F(1+\alpha_F)(1-C_F) + p_T(1+\alpha_T)(1-C_T)] \quad . \tag{III.13}$$

If the breeding capacity of the hybrid, C_H, is fixed, Eq. (III.13) shows that the power ratio in the fission reactors is bounded. Furthermore, if the breeding capacity in the fission reactors is also fixed, the largest value of p_F is obtained when the second term

is zero, i.e., when $p_T=0$ (implying no tritium production reactor) or when the design of the tritium production reactor has been optimized to the point that it has a breeding capacity, C_T, of unity. Only if the tritium production reactor were a true breeder ($C_T>1$) would the addition of a tritium production reactor result in an increase in the power available from the fission reactors, because in this case the tritium production reactor is able to produce tritium for the hybrid and also produce some fissile fuel for the fission reactors. Thus, any realistic system ($C_T<1$) with a tritium production reactor leads to lower values of p_F relative to a non-tritium-production-reactor system.

III.4 Special Combinations of Systems

III.4.A The Sharing System

In the sharing system, tritium is assumed to be produced in the fission reactors. The tritium production reactor may be included in the system.

III.4.A.1 The System Without a Tritium Production Reactor

If there is no dedicated tritium producing fission reactor, p_T is zero, and from Eqs. (III.10) and (III.11), we find

$$p_F = \frac{1}{\varepsilon(1+\alpha_F)} \frac{C_H-1}{1-C_F} \quad , \tag{III.14}$$

with

$$C_{1F}C_{2H}=(1-C_{2F})(1-C_{1H}) \quad . \tag{III.15}$$

Equation (III.15) relates the coefficients C_{ij} at steady state. These

equations thus describe a system of fission reactors and hybrids in which tritium for the hybrid is produced using the fission power reactors.

From Eq. (III.14), we see that when the breeding capacities, C_H and C_F, are conserved in the hybrid and the fission reactors, respectively, the value of the thermal power of the fission reactors per unit fusion power, p_F, will not change regardless of whether tritium is produced in the hybrid reactor or in the fusion reactors. The same conclusion is true regarding fissile fuel production in either the hybrid or the fission reactors. In Table (III.1), we give the breeding coefficients, C_{ij}, for four special cases. In all these cases, p_F is the same if C_H and C_F are fixed. In Fig. (III.3), we show the dependence of p_F on the total breeding capacity, C_F, in the fission reactors. Two breeding capacity values in the hybrid reactor are considered, namely, C_H=1.5 and C_H=2.5. As mentioned before, the former value is typical of a hybrid reactor based on the ^{232}Th-^{233}U fuel cycle, and so we have used a value for α_F=0.1. For the ^{238}U-^{239}Pu fuel cycle, C_H is usually about 2.5, and we have used α_F equal to 0.35. Clearly, increasing the breeding capacity in the fission reactors gives higher thermal power in these reactors per unit of fusion power because of the better neutron economy in the fission reactors. The same effect is obtained if the hybrid blanket is designed to have a high value of C_H. Note that the rate of change dp_F/dC_H is $\sim 1/(1-C_F)$, while the rate of change, dp_F/dC_F, is $\sim 1/(1-C_F)^2$. Thus, better coupling between the hybrid and the fission reactors is obtained if the

Table (III.1) The Value of Breeding Coefficients C_{ij} for Four Special Cases of the Sharing System. The TPR is Not Included.

	All Tritium is Bred in:		All Fissile Fuel is Bred in:	
	The FR's	The Hybrid	The FR's	The Hybrid
The Hybrid (H) Tritium Breeding Coefficient, C_{1H}	0	1	C_H	$\frac{C_F C_H - 1}{C_F - 1}$
Fissile Breeding Coefficient, C_{2H}	C_H	C_{H-1}	0	$\frac{1-C_H}{C_{F-1}}$
The Fission Reactors (FR's) Tritium Breeding Coefficient, C_{1F}	$\frac{1-C_F}{C_H-1}$	0	C_{F-1}	C_F
Fissile Fuel Breeding Coefficient, C_{2F}	$\frac{C_H C_F - 1}{C_H - 1}$	C_F	1	0

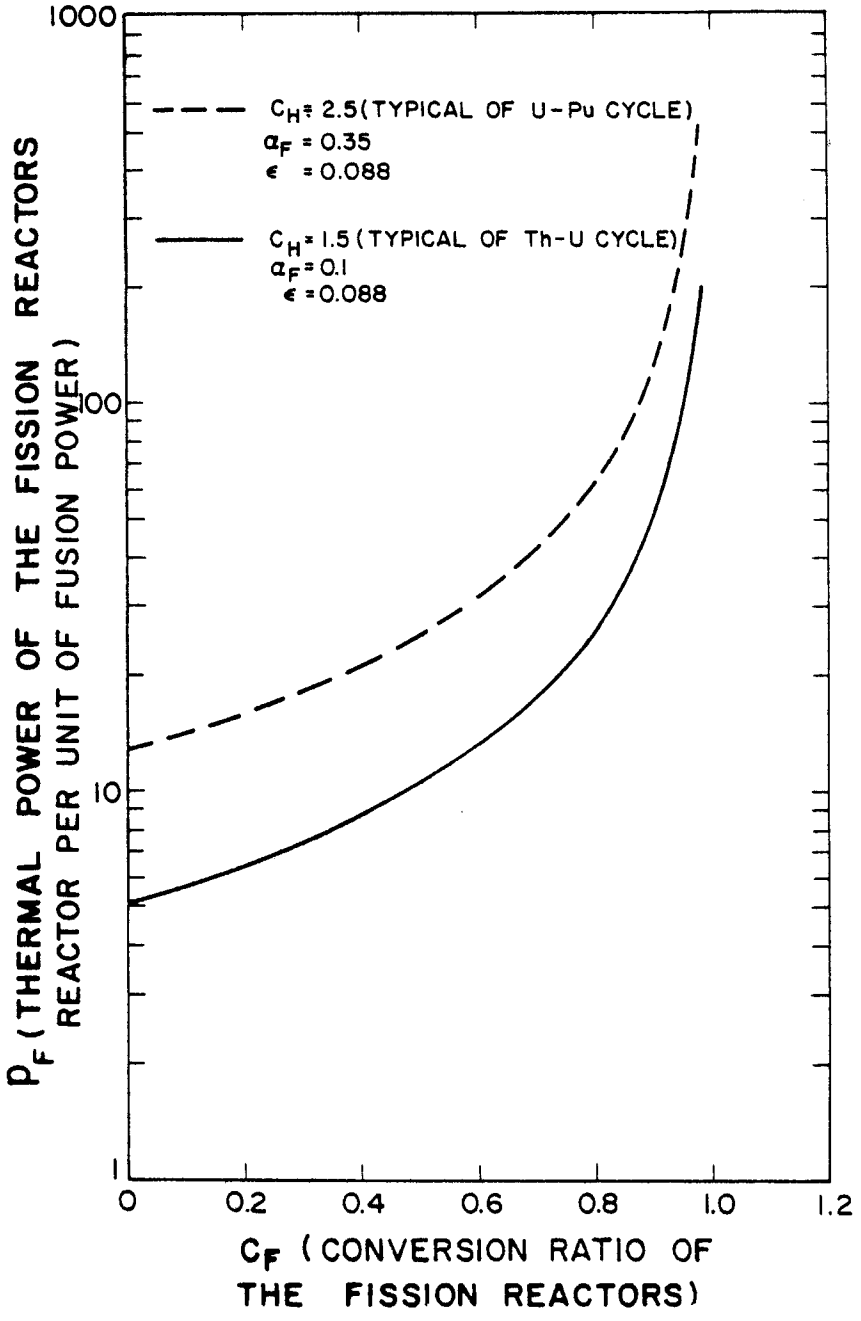

Fig (III.3): The Variation of the Thermal Power of Fission Reactors Per Unit of Fusion Power Which Can Be Supported By a Hybrid as a Function of the Conversion Ratio of the Fission Reactors. ε is the Ratio of the Energy per Fusion Event to the Energy per Fission Event. The Two Curves Characterize U-Pu Cycle Systems or Th-^{233}U Systems.

breeding capacity of the fission reactors, C_F, is near unity.

III.4.A.2 Systems with a Tritium Production Reactor

If the tritium production reactor is included in the system, and if its breeding capacity, $C_T=C_{1T}+C_{2T}$, is unity, then upon examining Eq. (III.13), we find that p_F is again given by Eq. (III.14). Thus, the value of p_F is the same for the same C_H and C_F values. However, the thermal power of the tritium production reactor per unit of fusion power, p_T, will depend on the values of the tritium breeding coefficients C_{1H} and C_{1F}(or C_{2H} and C_{2F}), even if C_H, C_F, and C_T are conserved. For example, in the special case where tritium is produced in the tritium production reactor and the fission reactors but the tritium production reactor does not breed fissile fuel ($C_{1T}=1$, $C_{2T}=0$), we find

$$p_T=\frac{1-C_F-C_{1F}(C_H-1)}{\varepsilon(1+\alpha_T)(1-C_F)} \quad , \quad (C_{1H}=0) \qquad \text{(III.16)}$$

which depends on the tritium breeding coefficient in the fission reactors, C_{1F}. Results for p_T as function C_{1F} are shown in Fig. (III.4) for two values of the total fission reactor conversion ratio, $C_F=0.6$, typical of a light water reactor, and $C_F=0.9$, typical of an advanced convertor reactor. Clearly, p_T varies linearly with C_{1F} and the value of C_{1F} in the limiting case where $p_T=0$ is

$$C_{1F}=\frac{1-C_F}{C_H-1} \quad , \quad (C_{1H}=0) \quad , \qquad \text{(III.17)}$$

as shown in the first column in Table (III.1).

If all the tritium is produced in the tritum production reactor

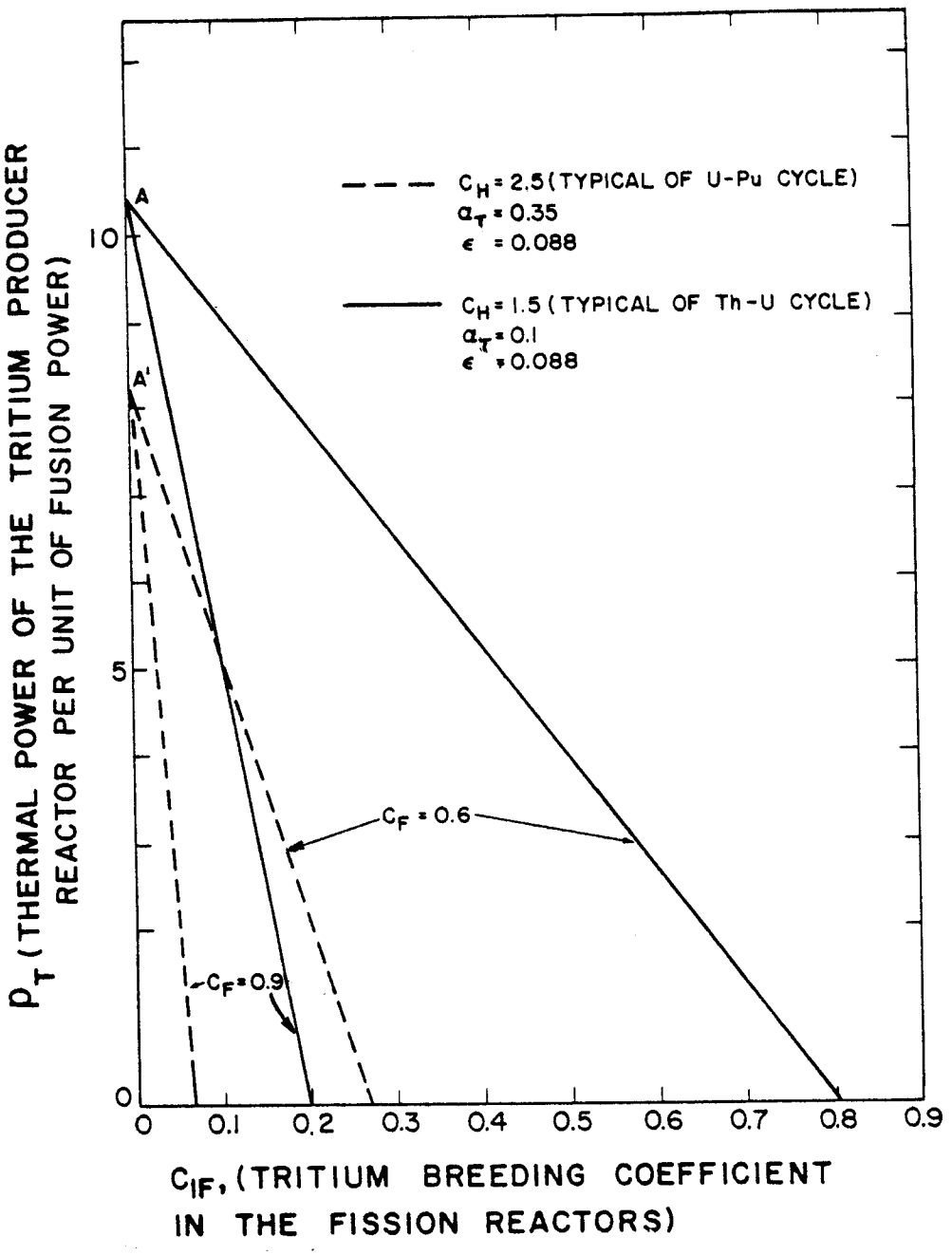

Fig. (III.4): The Thermal Ratio p_T as a Function of the Tritium Breeding Coefficient in the Fission Reactors. At $C_{IF} = 0$, All Tritium is Produced in the Tritium Production Reactor.

(C_{1H}=0, C_{1F}=0), the value of the thermal power of the tritium production reactor per unit of fusion power does not depend on the breeding capacities, C_H and C_F. In this case, p_T assumes the value

$$p_T = \frac{1}{\varepsilon(1+\alpha_T)} \quad , \quad (C_{1H}=C_{1F}=0) \quad . \tag{III.18}$$

This value is given by points A and A' in Fig. (III.4).

III.4.B The Dedicated System

In this system, tritium is not produced in the fission reactors, while the tritium production reactor is devoted solely to tritium production. We have already discussed the case where all tritium is produced in the tritium production reactor. Here we discuss the effect of breeding some tritium in the hybrid blanket. With no tritium bred in the fission reactors (C_{1F}=0, $C_{2F}=C_F$), p_T varies linearly with C_{1H} in the simple form

$$p_T = \frac{(1-C_{1H})}{\varepsilon(1+\alpha_T)} \tag{III.19}$$

We assume that the tritium production reactor has breeding coefficients, C_{1T}=1 and C_{2T}=0. The value of p_F is again given by Eq. (III.14) and is constant for given values of C_H and C_F regardless of whether tritium is produced in the hybrid or the tritium production reactor. As given by Eq. (III.19), p_T is independent of the breeding capacity in either the fission reactors or the hybrid. The limiting but standard case of all tritium breeding in the hybrid (p_T=0, C_{1F}=0, $C_{2F}=C_F$) is obtained when C_{1H}=1, i.e., when the hybrid reactor is self sufficient in tritium production. This case is given in the second column in

Table (III.1.)

III.5 Summary

It is found that for given values of breeding capacity in the hybrid and the fission reactors, C_H and C_F, the thermal power of the fission reactors per unit fusion power is the same for the following types of overall system combinations:

1. All tritium is produced in the hybrid reactor and the tritium production reactor is excluded from the system. The parameters for this system are $P_T=C_{1F}=0$, $C_{2F}=C_F$, and $C_{1H}=1$.

2. All tritium is produced in the fission reactors, and the tritium production reactor is excluded from the system. This system has parameters $P_T=C_{1H}=0$, and $C_{2H}=C_H$.

3. Tritium is produced in the fission reactors and the hybrid reactor. The tritium production reactor is excluded from the system. The system has parameters $P_T=0$, $C_{1H}\neq 0$, and $C_{1F}\neq 0$.

4. Tritium is produced in the fission reactors and the tritium production reactor. This system has parameters $C_{1H}=0$, $C_{1T}=1$, $C_{2T}=0$, and $C_{1F}\neq 0$.

5. All tritium is produced in the tritium production reactor. This system has parameters $C_{1T}=1$ and $C_{2T}=C_{1H}=C_{1F}=0$.

6. Tritium is produced in the tritium production reactor. This system has parameters $C_{1T}=1$, $C_{2T}=C_{1F}=0$, and $C_{1H}\neq 0$.

The performance of the overall systems discussed in this chapter has been characterized by the power ratios p_F and p_T, the power of the fission reactors and the tritium producing reactor per unit of fusion

power. These, however, are not the only nor necessarily the correct figures-of-merit for a system, even though they may be adequate for determining the basic merit of a particular combination of reactor types. For example, rather than using the fusion power of the hybrid as a basis, the thermal power of the hybrid could be used. In this case, one can evaluate the thermal power of the hybrid, P_H, using Eq. (III.12) and the power multiplication factor M inherent to the particular hybrid blanket design under consideration. The figures-of-merit would then be P_F/P_H and P_T/P_H. The first is known as the support ratio,[25] R_t, and is a measure of the fraction of power produced outside the hybrid site.

If the hybrid and the tritium production reactor are viewed as a fuel factory, then a figure-of-merit defined as $P_F/(P_H+P_T)$ might be considered as more appropriate, especially if neither the hybrid nor the tritium production reactor produces electricity. If either one or both produced electricity, one might consider adding terms to the numerator of a figure-of-merit to reflect their role as revenue producers as well as fuel producers.

None of these figures-of-merit is truly satisfactory because they do not reflect which system supplies electricity at the lowest cost or the engineering feasibility of producing tritium in fission reactors that produce power. An economic analysis is required that would account for changes in costs as the various parts of the system take on different roles (for example, breeding only fissile fuels as opposed to breeding fissile fuel and tritium) and changes in revenue

patterns (for example, whether a component produces electricity). Krakowski and Tai[26] have made such an analysis for one particular combination where all fuel is produced in the hybrid, i.e., $P_T=0$, $C_{1F}=0$. An extension of such a technique to a complete economic model covering all combinations is necessary for ultimate comparisons.

There is another possible fusion-fission system combination which has not been discussed in this chapter. In this combination, a dedicated fusion reactor, devoted mainly to tritium production, is coupled with a fusion reactor which only produces fissile fuel. As it has been shown,[27] and as far as the neutronics is concerned, this system is equivalent to a fusion reactor which produces both tritium and fissile fuel. In the next two chapters, we give the results of a neutronics study aimed at optimizing a blanket for U-233 production in a fusion-fission hybrid, SOLASE-H. This blanket also produces tritium and enriches the fertile ThO_2-fuel assemblies to a certain percentage. After reaching the required enrichment, the fuel assemblies are placed directly in the fission reactors without reprocessing.

References

1. Moir, R.W., "Mirror Hybrid Reactors", UCRL-81611, Lawrence Livermore Laboroary (Sept. 1978).

2. Lee, J.D., Bender, D.J., Moir, R.W., "Mirror Hybrids-A Status Report", Lawrence Livermore Laboratory (Sept. 1976).

3. Schultz, K.R., et. al., "A U-233 Fusion-Fission Power System Without Reprocessing-A Preliminary Report", GA-A14635, General Atomic Company (1978).

4. Conn, R.W., Abdel-Khalik, S.I., Moses, G, Youssef, M.Z., "The SOLASE-H Laser Fusion Hybrid", Trans. Am. Nucl. Soc. 30, 58 (1978).

5. Youssef, M.Z., Conn, R.W., Moses, G.A., "Blanket Neutronics Studies for the SOLASE-H Hybrid Reactor", UWFDM-263, University of Wisconsin (Dec., 1978); see also, M. Youssef, et. al., Trans. Am. Nucl. Soc., 32, 35 (1979).

6. Ragheb, M.H., Youssef, M.Z., Abdel-Khalik, S., Maynard, C.W., "Three-Dimensional Lattice Calculations for a Laser Fusion Fissile-Enrichment Fuel Factor", Trans. Am. Nucl. Soc., 30, 59 (1978); see also, Nucl. Technol., 45, 140 (1979).

7. Maniscalco, J.A., Hansen, L.F. Allen, W.O., "Scoping Studies of U-233 Breeding Fusion-Fission Hybrid", UCRL-80585, Lawrence Livermore Laboratory (May, 1978).

8. Maniscalco, J.A., Hansen, L.F., "Present Status of Laser Driven Fusion-Fission Energy Systems", UCRL-81510, Lawrence Livermore Laboratory (May, 1978).

9. Proc. Second Fusion-Fission Energy Systems Review Mtg., Vols. I and II, Washington, D.C. (July, 1978).

10. Proc. U.S.-USSR Symp. Fusion-Fission Reactors, CONF-760733, U.S. Energy Research and Development Administration (July, 1976).

11. Conn, R.W., Moses, G.A., Abdel-Khalik, S.I., "Notes on Fusion Hybrid Reactors", UWFDM-240, Nuclear Engineering Department, University of Wisconsin (Feb. 1978).

12. Harms, A.A., "Upper Bounds of Fissile Fuel Yield with Fusion Breeders", Can J. Phys., 54, 16 (1976).

13. Gordon, C.W., Harms, A.A., "The Basic Characteristics of an Efficient Fusion Breeder", Atomekernenergie (ATKE), 29 (1977).

14. Gordon, C.W., Harms, A.A., "Comparative Energetics of Three Fusion-Fission Symbiotic Nuclear Reactor Systems", Nucl. Eng. Des., 34, 269 (1975).

15. Harms, A.A., Gordon, C.W., "Fissile Fuel Breeding Potential with Paired Fusion-Fission Reactors", Ann. Nucl. Energy, 3, 411 (1976).

16. Harms, A.A., "Hierachical Systematics of Fusion-Fission Energy Systems", Nucl. Fusion, 15, 5, 939 (1975).

17. Lidsky, L.M., "Fission-Fusion Systems: Hybrid, Symbiotic and Augean", Nucl. Fusion, 15, 151 (1975).

18. Lidsky, L.M., "Symbiotics: Optimization of Nuclear Fuel Cycle", Trans. Am. Nucl. Soc., 21, 60 (1975).

19. Lidsky, L.M., "Fusion-Fission Systematics", Proc. Second Fusion Fission Energy Systems Review Mtg., Vol. I, Washington, D.C. (July, 1978).

20. Lidsky, L.M., "Fission-Fusion Symbiosis: General Considerations and a Specific Example", in Proc. BNES Nuclear Fusion Reactor Conf., Culham Laboratory (1969); also, CLM-NFR, p. 41 Culham Laboratory (1969).

21. Blinkin, V.L., Novikov, V.M., "Symbiotic System of a Fusion and a Fission Reactor with Very Simple Fuel Reprocessing", Nucl. Fusion, 18, 893 (1978).

22. Youssef, M.Z., Conn, R.W., "A Survey of Fusion Fission System Designs and Nuclear Analyses", UWFDM-308, Fusion Research Program, Nuclear Engineering Department, University of Wisconsin (June, 1979).

23. Fortescue, P., "Comparative Breeding Characteristics of Fusion and Fast Reactors", Science, 196, 1326 (June 17, 1977).

24. Youssef, M.Z., Conn, R.W., Vogelsang, W.F., "Fissile and Fusion Fuel Exchange Between Fusion Hybrid Reactor, Tritium Producer Reactor, and Fission Reactors", Trans. Am. Nucl. Soc., 32, 45 (1979).

25. Bender, D.J., "Performance Parameters for Fusion-Fission Power Systems", UCRL-80589, Lawrence Livermore Laboratory (May, 1978); see also, D.J. Bender, Nucl. Technol., 44, 381 (1979).

26. Krakowski, R.A., Tai, A.S., "A Simple Economics Parametric Analysis of Fissile Fuel Production by Fusion-Fission Reactors", Proc. Second Fusion-Fission Energy Systems Review Mtg., Vol. II, Washington, D.C. (July, 1978).

27. Vogelsang, W., private communication, Nuclear Engineering Department, The University of Wisconsin.

CHAPTER IV

NEUTRONICS STUDY OF THE SOLASE-H HYBRID REACTOR

IV.1 Introduction

Utilizing the energetic D-T neutrons produced in a fusion-fission hybrid reactor to breed fissile fuel (U-233 or Pu-239) by neutron capture in a fertile fuel (Th-232 or U-238) for subsequent use in fission reactors has recently been addressed by several researchers in a variety of fusion systems (i.e., tokomak,[1-3] electron beam fusion,[4] mirror fusion,[5-6] laser fusion[7]). The artificially produced fuel will substantially extend the world's fissile fuel reserves.[8] This will eliminate the increasing threatening shortage in U-235, which represents the only naturally occurring fissile isotope.

The attractiveness of such reactors is due to the two revenue sources that can be obtained, namely, fissile fuel and electric power. As discussed in Chapter II, in hybrid designs which emphasize a high fissile fuel production rate, fissioning of the bred fuel is minimized in the hybrid blanket and an energy multiplication factor of the order 5 to 20 is attainable.[9] As an electricity producer, the fissile fuel is burned "in situ" in the hybrid blanket resulting in a high energy multiplication factor, typically 10-40.[9] Due to energy multiplication, a relaxation in the fusion energy requirements is possible and may lead to early introduction.

IV.2 Proliferation Considerations

The linkage between a hybrid reactor as a fissile fuel factory and the fission reactors as fuel burners should meet the safeguard require-

ment to prevent the diversion and theft of weapon-grade materials and to offer tight proliferation control. Eliminating the reprocessing as an intermediate stage in the coupling between fission reactors and hybrid reactors can render the bred fuel proliferation resistant. However, this will be at the expense of the full utilization of the fertile fuel. Typical fission reactor fuel assemblies can be placed in a hybrid blanket to enrich the fuel to the proper fissile concentration and render it proliferation resistant by making the fuel cladding highly radioactive. These fuel assemblies, after reaching 3-4% enrichment, are extracted from the hybrid blanket and shipped to the fission reactors for direct use. The spent fuel assemblies from the fission burners are either stored or, if feasible, reinserted in the hybrid blanket for further enrichment. As argued by Feiveson and Taylor,[10-11] and discussed by Bethe,[12] spent or highly radioactive fuel bundles should be self-protecting. Should the reprocessing of the spent fuel extracted from the fission reactors be allowed, the fission products and actinides can be separated from the fissile and fertile fuel and fresh or partially enriched fuel assemblies can be refabricated and reinserted into the hybrid blanket to close the fuel cycle. The reprocessing plant and the hybrid reactor can be an integrated part of an internationally controlled, physically secure fuel production and reprocessing site which can provide fissile fuel needs to many national convertor reactors.[8,13]

IV.3 SOLASE-H as a Fissile Fuel Factory

In this chapter we present the results of one-dimensional optimization studies of the laser-driven fusion-fission hybrid reactor,

SOLASE-H. These studies are aimed at searching for a blanket configuration which results in minimum nonuniformity in the spacial distribution of the bred U-233 from neutron capture in Th-232. A figure-of-merit that maximizes the bred fissile fuel subject to minimizing the peak-to-average enrichment determines the optimum blanket design.

Fig. (IV.1) shows the final design of the SOLASE-H hybrid reactor. This design is based on the optimum blanket obtained in the present study. Th-232 in the form of oxide fuel is used to breed U-233. The reactor cavity is a right circular cylinder surrounding the point fusion source located at the center. The top and bottom blankets are devoted to breeding tritium and comprise 30% of the solid angle subtended at the cavity center. The radius of the cavity is 6 m and the height is 12 m. The ThO_2 fuel assemblies are located only in the radial blanket which allows for 3 assemblies to be stacked on the top of one another. The blanket structure is Zircaloy-2 to be compatible with the cladding of the fuel elements. Sodium is used as a coolant. The front zone of the blanket are pins of lead clad in zircaloy. It has been established in the present study that a Pb front zone leads to a more uniform fissile fuel profile across the fuel assemblies and comparable neutron multiplication when compared to using a Be multiplier. The operating parameters of SOLASE-H are summarized in Ref. (13, 14).

The performance with time of the optimized blanket has been evaluated to establish a rotation scheme for the fuel assemblies which

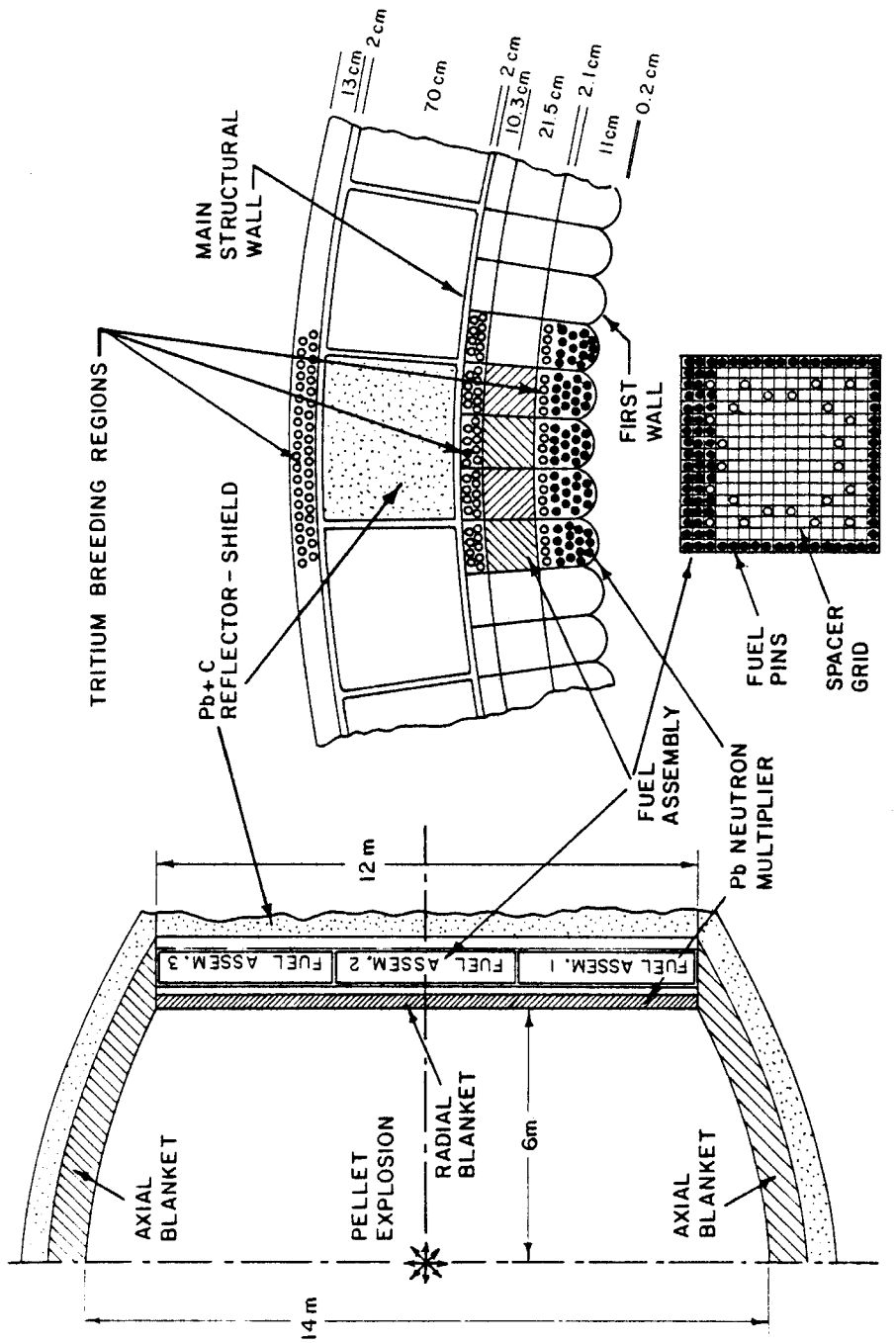

Fig. (IV.1): Schematic Diagram for the SOLASE-H Design.

will result in a symmetric fissile fuel distribution across the fuel assemblies when 4% enrichment is reached. The results of these calculations are presented in Chapter V.

IV.4 Neutronics Optimization Studies

The primary objective of the neutronics study presented here has been to maximize the fissile fuel production rate in a hybrid reactor subject to the constraints that the fissile fuel distribution in the fuel zone be as uniform as possible and that the tritium breeding ratio (TBR) be at least 1. We have primarily considered hybrids which produce uranium-233 from thorium because U-233 is a better performing fuel in LWR's, particularly PWR's. However, similar studies can be done on the production of plutonium-239. The constraint of a uniform U-233 distribution throughout the fuel assembly used in the fuel zone is aimed primarily at minimizing the hot spot factor one would calculate for the enriched fuel assembly loaded into a LWR.

IV.4.A The Blanket Configuration and Calculational Method

Spherical geometry, one-dimensional calculations have been performed to assess the effects of parameter and design variations and to search for optimum blanket performance. In this regard, two main blanket configurations shown in Fig. (IV. 2) have been studied. The first blanket series utilizes beryllium as a neutron multiplier front zone while lead is used in the second series. Lead and beryllium enhance the neutron generation throughout the blanket and replace a U-238 fast fission plate utilized in other studies.[15-19] In addition to introducing plutonium into a U-233 fuel cycle, the fission plate

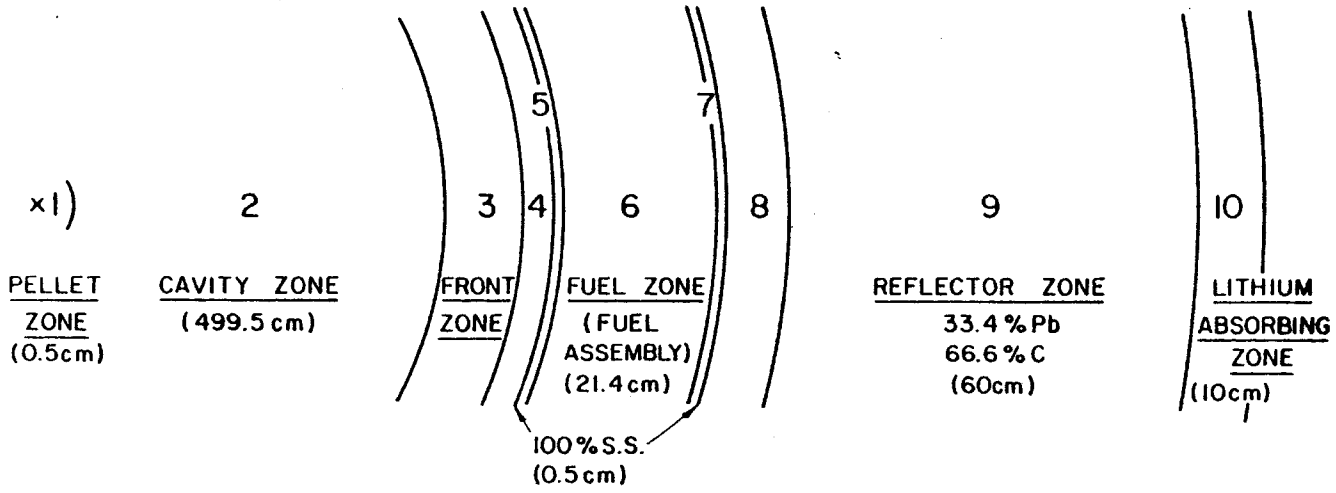

Fig. (Iv.2): Schematic Representation in Spherical Geometry of the Hybrid Blanket (Zones 4 and 8 are not included in the series of blankets using Be as a Front Zone Multiplier).

would also increase the thermal power generated in the blanket. This would yield excess electricity which could be sold to reduce the overall plant running cost. However, the power increase with time makes the design of the cooling system more difficult. In our design, the main concern has been to maximize U-233 production subject to the constraints on fuel production and tritium breeding already mentioned and to ensure sufficient power to make the plant at least self-sufficient in power.

For both classes of reactor blankets (beryllium or lead as a neutron multiplier), the U-233 breeding zone (fuel zone) consists of just one fuel assembly row located behind the neutron multiplier zone. A reflector is positioned behind the fuel zone and consists of 1/3 Pb and 2/3 graphite by volume. The thickness of this reflector is held at 60 cm in all cases. A final liquid lithium neutron absorbing region is located at the outer portion of the blanket.

The fuel zone is thus located in a flux trap between the reflector and the neutron multiplying zone. For this reason, two relatively thin neutron absorbing lithium zones are located immediately in front of and behind the fuel assembly zone in the series of blankets utilizing lead as front zone neutron multiplier. This achieves two ends: 1. Thermal neutrons which would be absorbed at the edge of the fuel assembly are filtered out. Thus, only harder neutrons penetrate and this produces a more uniform U-233 production rate. 2. The neutrons absorbed in the lithium help to meet the constraint that the tritium breeding ratio be 1.

A square single PWR assembly has 264 fuel elements arranged in a 17 X 17 array and is 21.4 cm on a side. The fuel pins have an outer diameter of 0.9498 cm and a square pitch of 1.25 cm. Zircaloy-2 is utilized as the cladding material with a thickness of 0.0572 cm. The ThO_2 fuel pellet diameter is 0.819 cm. Each fuel assembly contains 25 empty locations of outer diameter 0.9498 cm and are reserved for the control rods when the fuel assembly is extracted from the blanket and used in LWR's. The dimensions of the fuel assembly and the fuel pins are shown in Fig. (IV.3). The fuel assembly used in this study is typical of those used in a PWR.[23] The volume percentages corresponding to the dimensions shown in Fig. (IV.3) are: 30.3% ThO_2, 9.2% Zircaloy-2, 1.3% void and 59.2% coolant. When the fuel assembly is placed in the blanket, the fuel zone will occupy a region 21.4 thick. This is held constant for the blankets studied.

To simulate a laser fusion hybrid, the neutron source is localized in a zone 0.5 cm radius at the center of the reactor. The first wall is at a radius of 5 m in the survey calculations. However, in the final design, the optimized blanket is reconfigured to closely approximate the engineering features and the cylindrical geometry of the actual hybrid concept shown in Fig. (IV.1). As mentioned before, the pellet in that design is centered at 6 m from the first wall and the cylindrical radial blanket section is 12 m high. The top and bottom axial caps are designed to produce tritium. Since the caps are devoted solely to tritium production, one requires less tritium breeding in the radial section. As such, we have used a value of 0.6 as the constraint

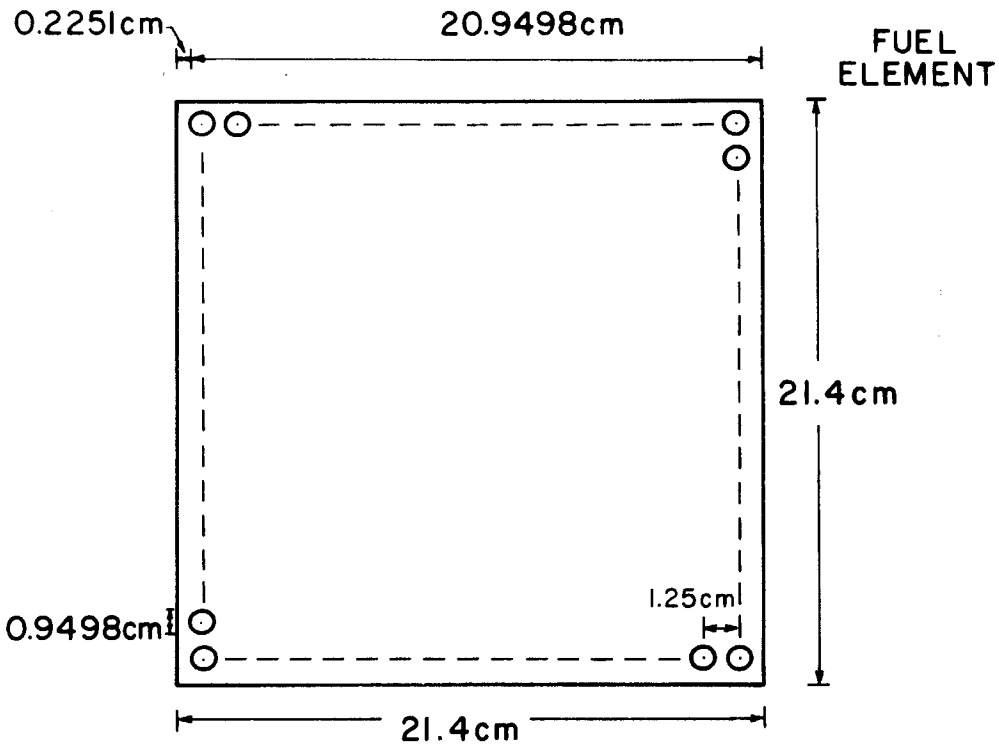

(a) THE 17X17 FUEL ASSEMBLY ;
264 FUEL ELEMENTS AND 25
LOCATIONS FOR CONTROL ROD (TOTAL 289)

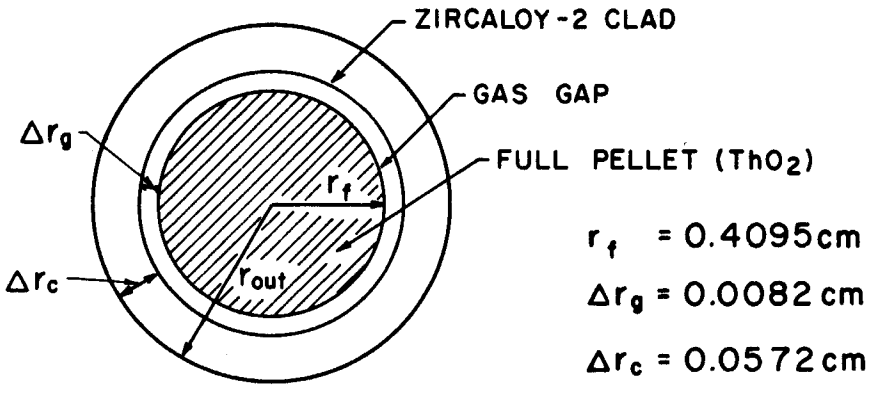

(b) FUEL ELEMENT PIN

Fig. (IV.3): The Fuel Assembly and the Fuel Pin.

on the TBR in these spherical geometry parametric calculations. This corresponds to a value of ~0.4 if 70% of the solid angle subtended by the radial blanket, is considered.

All the neutronic calculations were carried out using the one-dimensional discrete ordinate neutron transport code ANISN.[20] A 25 neutron energy group cross section library has been used based on the DLC-2D[21] library which was generated from ENDF/B III with the SUPERTOG[22] code using a 1/E weighting spectrum for the GAM-II 100-group structure. The energy boundaries for the 25 groups are given in Table (IV.1).

Fig. (IV.2) shows the different zones of the blanket for both series mentioned earlier. Zones 4 and 8 are not included in the Be front zone series. The constituents and the volume percentages in the different zones of the large number of cases studied are summarized on Table (IV.2). We also give the results for the U-233 breeding ratio UBR (U-233 atoms produced per D-T neutron) and the tritium breeding ratio TBR. Note that cases with Li cooling and Na cooling have been also considered in this parametric study.

IV.4.B Beryllium as the Neutron Multiplier

Several different blankets utilizing Be as front zone material were studied. Zircaloy-2 is chosen as the structural material for this zone. The volume percentages are 82.2%-Be, 9.3% coolant and 8.5% Zircaloy-2. The type of coolant in this study is either natural Li or Na.

In blanket #1, natural Li is used as coolant in the front zone (10 cm) and in the fuel zone. Enriched lithium (50% Li-6) is used

Table (IV.1) Energy Boundaries for the 25-Neutron Energy Groups

Group	Energy End Boundaries (eV)	Group	Energy End Boundaries (eV)
1	1.4918 + 07→1.3499 + 07	14	2.4660 + 06
2	1.2214 + 07	15	1.3534 + 06
3	1.1052 + 07	16	7.4274 + 05
4	1.0000 + 07	17	4.0762 + 05
5	9.0494 + 06	18	1.6573 + 05
6	8.1873 + 06	19	3.1878 + 04
7	7.4082 + 06	20	3.3546 + 03
8	6.7032 + 06	21	3.5358 + 02
9	6.0653 + 06	22	3.7267 + 01
10	5.4881 + 06	23	3.9279 + 00
11	4.4933 + 06	24	4.1399 - 01
12	3.6788 + 06	25	2.2200 - 02
13	3.0119 + 06		

CASE NUMBER													
Blanket	#1	#2	#3	#4	#5	#6	#7	#8	#9	#10	#11	#12	#13
Zone 1, 2	Zone 1 Point Source Within 0.5 cm Radius Zone 2 Void 499.5 cm Thickness												
Zone 3	82.2% Be 9.3% Nat. Li Coolant 8.5% Zirc-2 (10 cm)	As #1 but with Na Coolant			As #2 (0 cm)	As #2 (5 cm)	As #2 (15 cm)	100% Pb4-Li Nat. Li (10 cm)	As #2 Pb Replaces Be (5 cm)	As #9 (10 cm)	As #9 (15 cm)	As #9 (20 cm)	As #10
Zone 4	(0 cm)								95% Nat. Li 5% SS (1.5 cm)				
Zone 5, 7	100 % SS (0.5 cm)												
Zone 6	30.3% ThO_2 9.2% Zirc-2 59.2% Nat. Li Coolant 1.3% Void (21.4 cm)	As #1 but with Na Coolant	30.3% ThO_2 3.8% Nat. ^2Li 55.4% Na Coolant 9.2% Zirc-2 7.3% Void 21.4 cm	As #3 but Li is 50% Li^6				As #1 but with Pb4Li Coolant. Nat. Li is Used	As #2				
Zone 8	(0 cm)								95% Nat. Li 5% SS (6 cm)				As #10 (8 cm)
Zone 9	Pb+C Mixture 66.6% C 33.4% Pb (60 cm)												
Zone 10	95% Li (50% Li^6) 5% SS (10 cm)								As #1 but Li is Natural				
Th(n,γX)UBR	0.7132	1.3357	1.1364	0.8970	0.7492	0.9040	0.8230	1.1259	0.8589	0.9567	1.0116	1.0392	0.9338
TBR	0.0998	0.0968	0.3797	0.6703	0.5226	0.5353	0.8003	0.5029	0.6152	0.5946	0.5734	0.5487	0.6254
Th($\nu\sigma_f$)	0.1158	0.1185	0.1184	0.1183	0.1909	0.1527	0.0899	0.0704	0.1218	0.0799	0.0520	0.0338	0.0799
	0.1159	1.9818											

Table (IV.2): Neutronics Results for Different Blankets.

in the lithium absorbing zone (zone 10). The UBR and TBR are 0.71 and 1.1, respectively; when using Na as the coolant in the front and fuel zones (blanket #2), the UBR increases to 1.34 and the TBR dropped to 0.097. Although the utilization of the D-T neutron in fuel and tritium production is higher in blanket #1 (0.71 + 1.1 = 1.81) than in blanket #2 (1.43), the UBR is noticeably higher in blanket #2.

The 25 locations reserved for control rods were filled with natural lithium in blanket case #3, then 50% enriched lithium and Na as the coolant (blanket #4). The competition between Li and Th to absorb neutrons in the fuel zone tends to decrease the UBR (to 1.14) and to increase the TBR (to 0.38) in blanket #3. The corresponding values in blanket #4 are UBR = 0.9 and TBR = 0.67. One should notice that TBR + UBR is almost the same for blanket #3 and 4. This shows that increasing TBR is at the expense of decreasing UBR.

The effect of the Be front zone thickness was studied via the cases, blanket #5 (0 cm front zone), blanket #6 (5 cm), blanket #4 (10 cm) and blanket #7 (15 cm). In these blankets the coolant in the front zone and fuel zone is Na and the 25 locations reserved for control rods were filled with 50% Li-6 enriched lithium. The back lithium zone was kept at 10 cm with 50% enriched lithium. Table (IV.3) gives the reaction rates for blanket cases #6, #4 and #7, respectively. The first 7 rows of this table show the reaction rates which lead to neutron multiplication, in particular the (n,2n) reaction for the structural materials and (n,2n), (n,3n) and $(n,\nu\sigma_f)$ reactions for Th. Rows 8 to 17 give the absorption rate in the entire blanket while rows

Table (IV.3)

Reaction Rates of Blanket #6, #4 and #7 per D-T Neutron

Type	Reaction	Blanket #6 (5 cm)	Blanket #4 (10 cm)	Blanket #7 (15 cm)
Source	Th (n,2n) + (n,3n) + (n, $\nu\sigma_f$)	0.3645	0.2775	0.2077
	Be (n,2n)	0.2848	0.5585	0.7876
	Structure (n,2n)	0.0957	0.0958	0.0961
	Na (n,2n)	0.0035	0.0027	0.0022
	Pb (n,2n)	0.0643	0.0471	0.0344
	D-T neutron	1.0	1.0	1.0
	SUM	1.8129	1.9815	2.1279
Sink	Th (n,abs)	0.9481	0.9319	0.8501
	Be (n,abs)	0.0347	0.0732	0.1175
	Structure (n,abs)	0.0918	0.1399	0.2032
	Na (n,abs)	0.0519	0.0612	0.0928
	^{6}Li (n,abs)	0.5202	0.6477	0.7677
	^{7}Li (n,abs)	0.0001	0.0001	0.0001
	Pb + C (n,abs)	0.1251	0.0957	0.0723
	O	0.0337	0.0262	0.0199
	Leakage	0.0084	0.0064	0.0049
	SUM	1.8138	1.9825	2.1284
Breeding	Th (n,γ)	0.9040	0.8970	0.8230
	^{6}Li (n,t)α	0.5308	0.6667	0.7974
	^{7}Li (n,t)nα	0.0045	0.0036	0.0078
	Li (n,t)	0.5353	0.6703	0.8003

18 to 21 give the reaction rates for breeding U-233 and tritium. The neutron multiplication and absorption rates in the fuel and structural materials as a function of the Be zone thickness are shown in Figure (IV.4). The tritium production rate and the U-233 breeding rate are shown in Figure(IV.5). For a 5 cm Be front zone, the main source of neutron multiplication comes from the (n,2n), (n,3n) and fast fission reactions in Th. However, there is noticeable neutron multiplication from (n,2n) in Be. As the thickness of the Be zone increases, the (n,2n) reaction rate in Be increases and overrides the neutron multiplication due to Th at about a 6 cm Be zone thickness. Further increase of this thickness results in larger neutron multiplication in Be. However, an increase in the Be zone thickness leads to a softer neutron spectrum throughout the blanket. This leads to a decreased rate of fission, (n,2n), and (n,3n) reactions in Th.

The main source of neutron absorption is due to Th (n,abs) and Li^6(n,abs) as shown in Fig. (IV.4), Fig. (IV.5) and Table (IV.3). The percentage of neutrons absorbed in Th compared to the total number of neutrons available is 52.3%, 47%, and 40% for the 5 cm, 10 cm and 15 cm Be zone thickness cases, respectively. For Li^6, the corresponding values are 28.6%, 32.7% and 36%, respectively. The main sources of neutron production are the Th(n,2n), Th(n,3n), Th(n,$\nu\sigma_f$) and Be(n,2n) reactions. The percentage of neutrons from Th compared to the total neutrons available in the blanket are 20%, 14% and 9.8% for 5, 10 and 15 cm Be front zone cases, respectively. The corresponding values for the Be(n,2n) reaction are 15.7%, 28.2% and 37% respectively. This

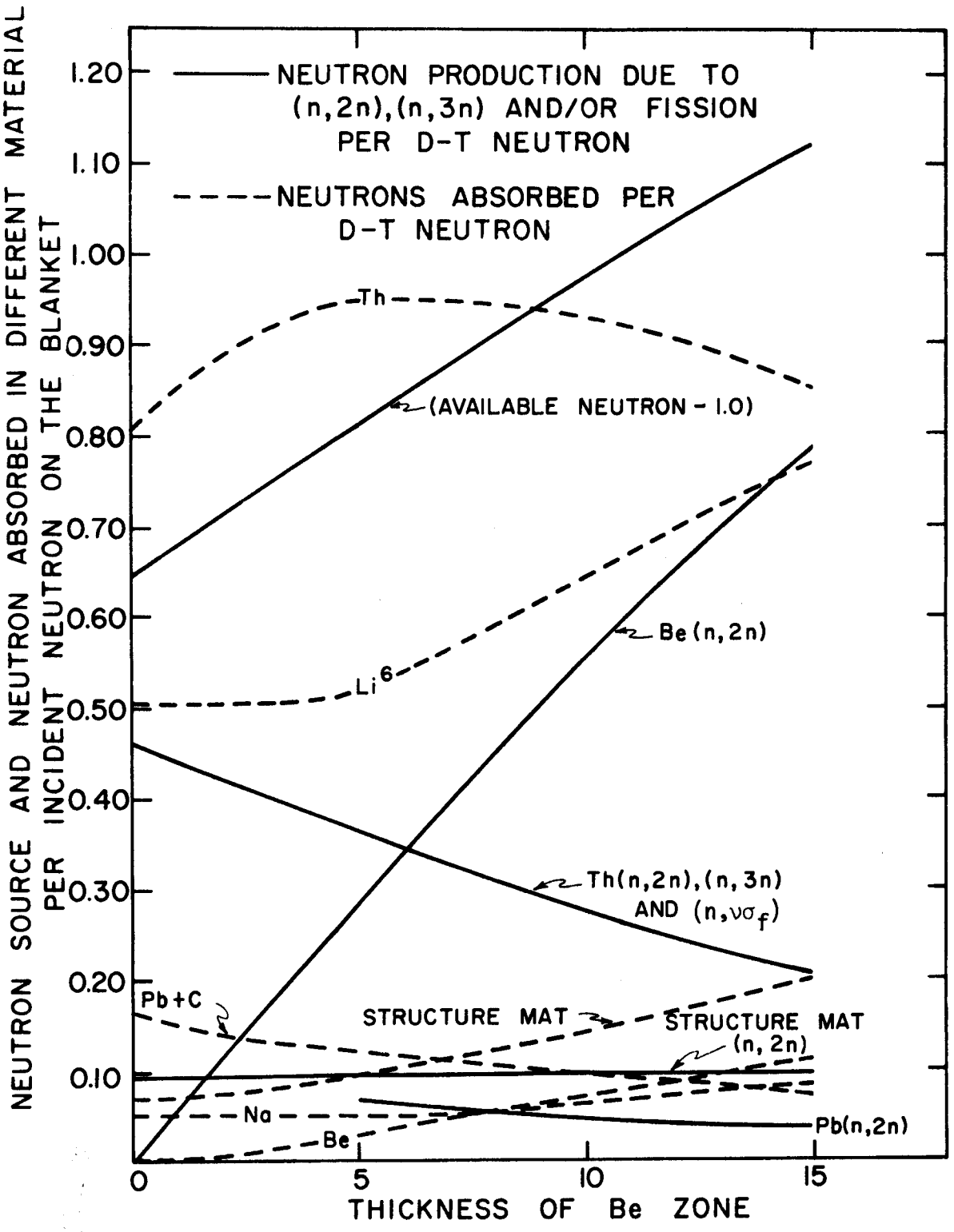

Fig. (IV.4): Neutron Sourses and Sinks as a Function of the Be Front Zone Thickness.

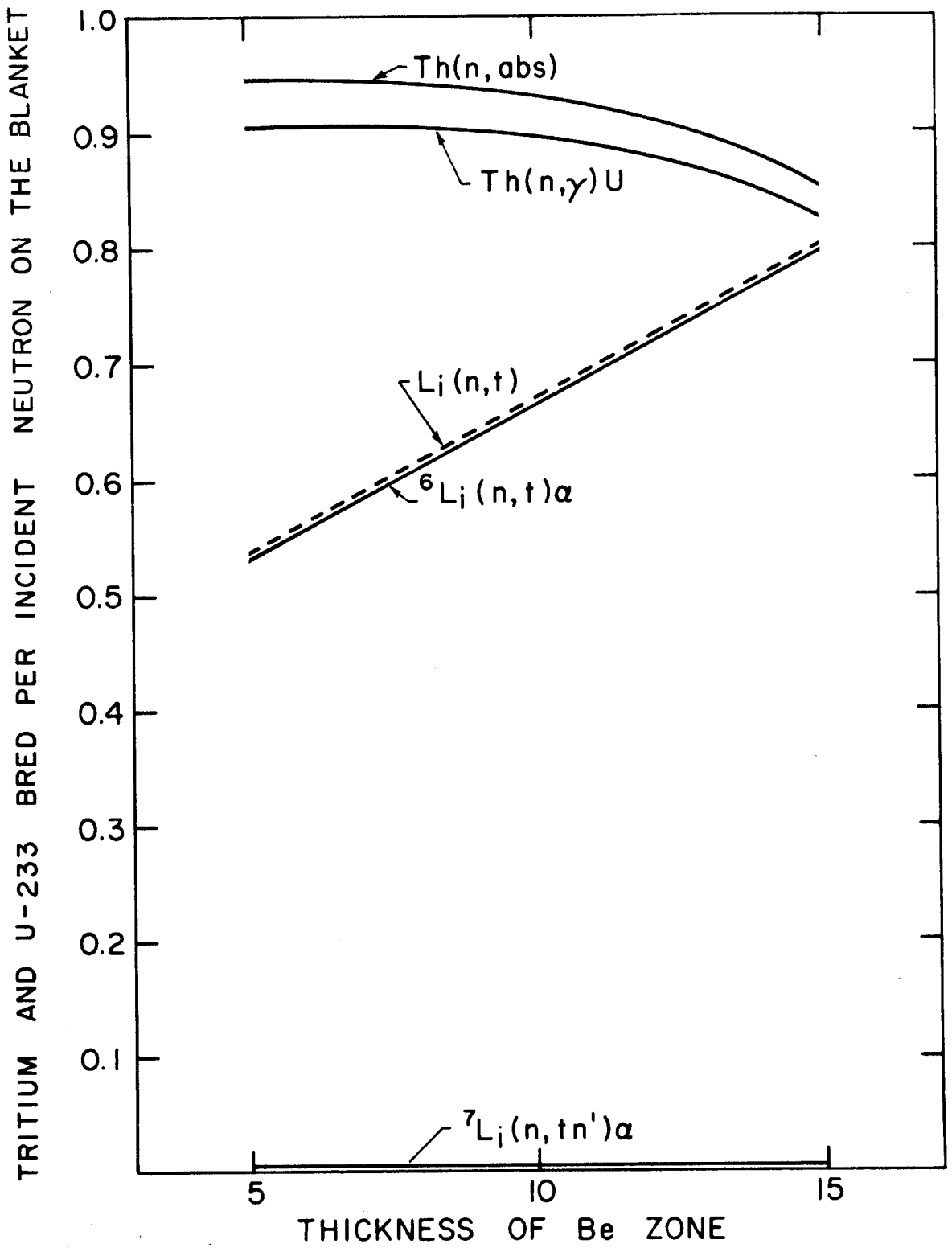

Fig. (IV.5) Tritium and U-233 Breeding Rates as Function of Be Front Zone Thickness per D-T Neutron

shows the effectiveness of Be as a front zone neutron multiplying material. In going from 0 cm to 5 cm Be front zone thickness, the UBR increases from 0.75 to 0.9. It then slightly decreases as the Be zone thickness increases further. In contrast, TBR increases monotonically as the front zone thickness increases. This again is due to the increasingly softer spectrum produced by neutron moderation in Be which permits the $Li^6(n,t)\alpha$ reaction to dominate capture in thorium. The optimum thickness for the Be front zone is about 10 cm. In this case, UBR is 0.9 and TBR is 0.67. The latter value meets the requirement that TBR in the spherical mock-up calculations be ~0.6. The end caps in the final design make up the remainder.

The constraint of uniform U-233 distribution throughout the fuel assembly is not met in this series of blankets. The $Th(n,\gamma)$ reaction rate per D-T neutron throughout the fuel zone is shown in Fig. (IV.6) for blankets #4, #5, #6 and #7, respectively. The reaction rate first decreases and then increases again due to the neutrons from the reflector zone. As the thickness of the Be zone increases, the curves tend to increase in front and decrease in the back. The minimum occurs even closer to the back edge. In general, the fuel zone in this series is self-shielded to fissile fuel production.

When Pb_4Li eutectic replaced the Na coolant of blanket #1, the UBR and TBR become 1.1 and 0.68, respectively. However, the $Th(n,\gamma)$ curve is still steep both in the front and the back edges of the fuel zone (see Fig.(IV.6), curve 5). When 100% Pb_4Li is used as a front zone neutron multiplier (blanket #8) and Pb_4Li is the coolant in the fuel

zone, the steepness of the U-233 production rate near the front edge of the fuel zone decreases noticeably (again see Fig. (IV.6), curve 6).

The adequate performance of blankets using Pb and Li in front of the fuel zone leads us to the second series of blankets that utilizes the Pb as a base for the front zone.

IV.4.C Lead as the Neutron Multiplier

Cases 9 through 13 are blanket models with varying thicknesses of the Pb containing neutron multiplier zone (zone #3). Further, the multiplier zone is followed by 1.5 cm of nat. liquid lithium (with volume percentage of 95% Li and 5% S.S.) and the fuel zone is followed by a 6 cm zone of 95% natural Li and 5% S.S. The purpose of these zones as thermal neutron filters and tritium breeders was discussed earlier. For blanket #10, with a 10 cm Pb multiplier zone, the UBR and TBR are 0.96 and 0.6, respectively. The competition between the $Th(n,\gamma)$ and the $Li^6(n,t)\alpha$ reactions for neutron absorption does serve to flatten the $Th(n,\gamma)$ reaction rate profile in the fuel assembly.

Various reaction rates per D-T neutron for cases of 5 cm, 10 cm, 15 cm and 20 cm Pb front zone thickness are given in Table (IV.4) and shown on Fig. (IV.7). These cases are for blankets #9, #10, #11 and #12, respectively. Blanket #10' is the same as blanket #10 with 50% Li-6 enriched Li in zone 4. Increasing the Pb zone thickness increases the $Th(n,\gamma)$ reaction rate but the increase is slowed when the zone thickness exceeds about 15 cm. The $Li^6(n,t)\alpha$ reaction rate steadily decreases as the front zone thickness increases. Almost all the tri-

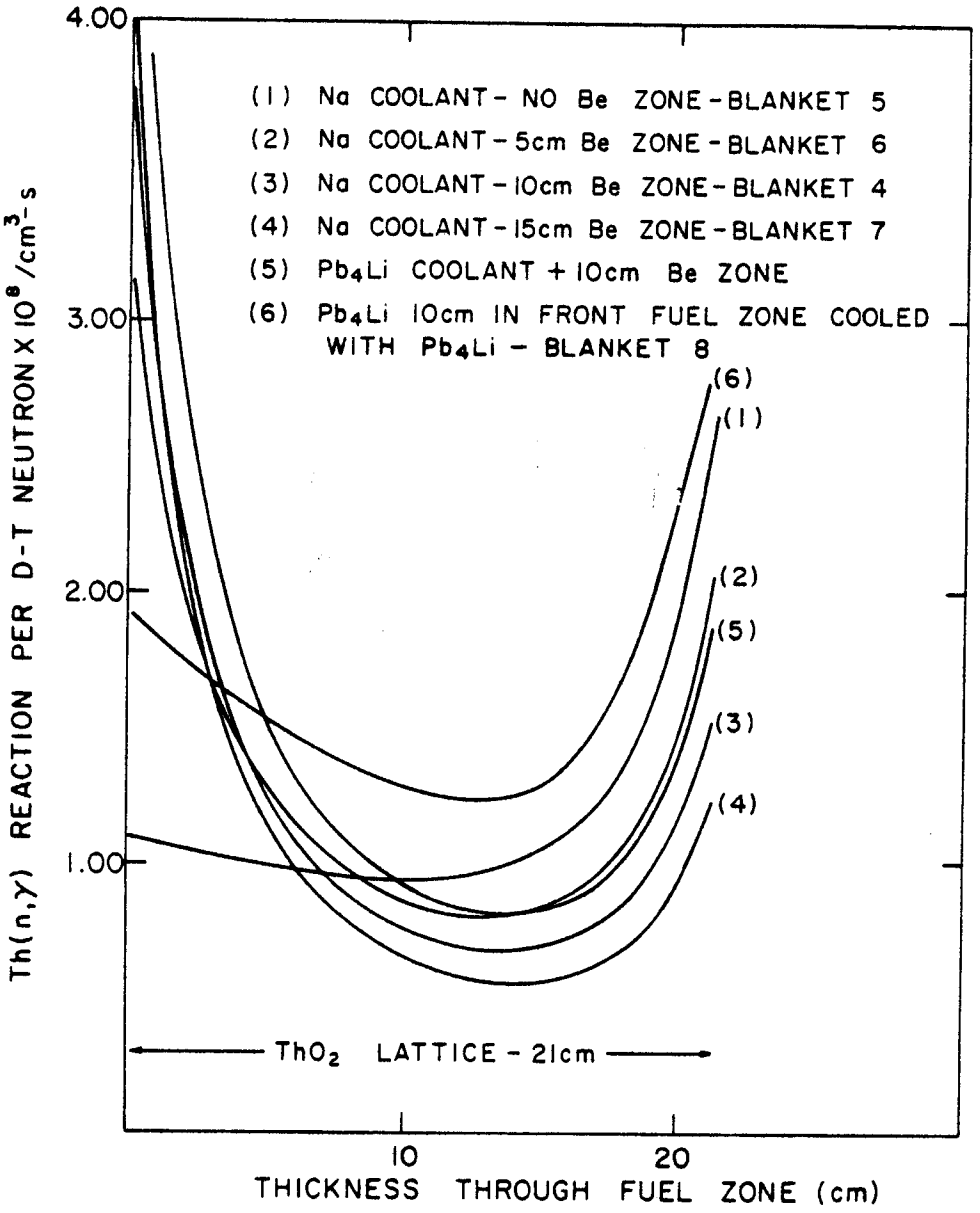

Fig. (IV.6): The U-233 Breeding Distribution in the Fuel Zone per D-T Neutron with Be as the Front Zone.

Table (IV.4) Reaction Rates of Blanket #9, #10, #10', #11, #12, and #13 Per D-T Neutron

Blanket / Parameter	#10' (10 cm)	#9 (5 cm)	#10 (10 cm)	#11 (15 cm)	#12 (20 cm)	#13 (10 cm)
Th(n,γ)	0.7886	0.8589	0.9567	1.0116	1.0392	0.9339
max/min after rotation	1.0739	1.2114	1.2694	1.3412	1.4318	1.2185
TBR(Li-6)	0.7722	0.5774	0.5707	0.5585	0.5395	0.5983
TBR(Li-7)	0.0189	0.0378	0.0239	0.0149	0.0092	0.0271
TBR (total)	0.7910	0.6152	0.5946	0.5734	0.5487	0.6254
Fraction of TBR from Zone 4	0.1434	0.1664	0.1979	0.2294	0.2674	0.1874
Fraction of TBR from Zone 8	0.7812	0.6779	0.6609	0.6392	0.6116	0.6876
Fraction of TBR from Zone 10	0.0754	0.1557	0.1412	0.1313	0.1211	0.1250
Th (n,$\nu\sigma_f$)	0.0798	0.1218	0.0799	0.0520	0.0338	0.0799
Th (n,2n)	0.0633	0.1020	0.0634	0.0390	0.0239	0.0634
Th (n,3n)x2	0.0379	0.0619	0.0379	0.0230	0.0138	0.0379
Sum Th	0.1810	0.2857	0.1812	0.1140	0.0715	0.1812
Pb(n,2n)	0.4937	0.3239	0.4938	0.6008	0.6668	0.4919
Fraction Pb(n,2n) from Zone 3	0.9514	0.8776	0.9513	0.9757	0.9868	0.9551
Fraction Pb(n,2n) from Zone 9	0.0486	0.1224	0.0487	0.0243	0.0132	0.0449
Pb(n,abs)	0.0692	0.0967	0.0976	0.1024	0.1095	0.0918
$\frac{Pb(n,abs)}{Pb(n,2n)}$	0.1401	0.2987	0.1977	0.1705	0.1642	0.1867

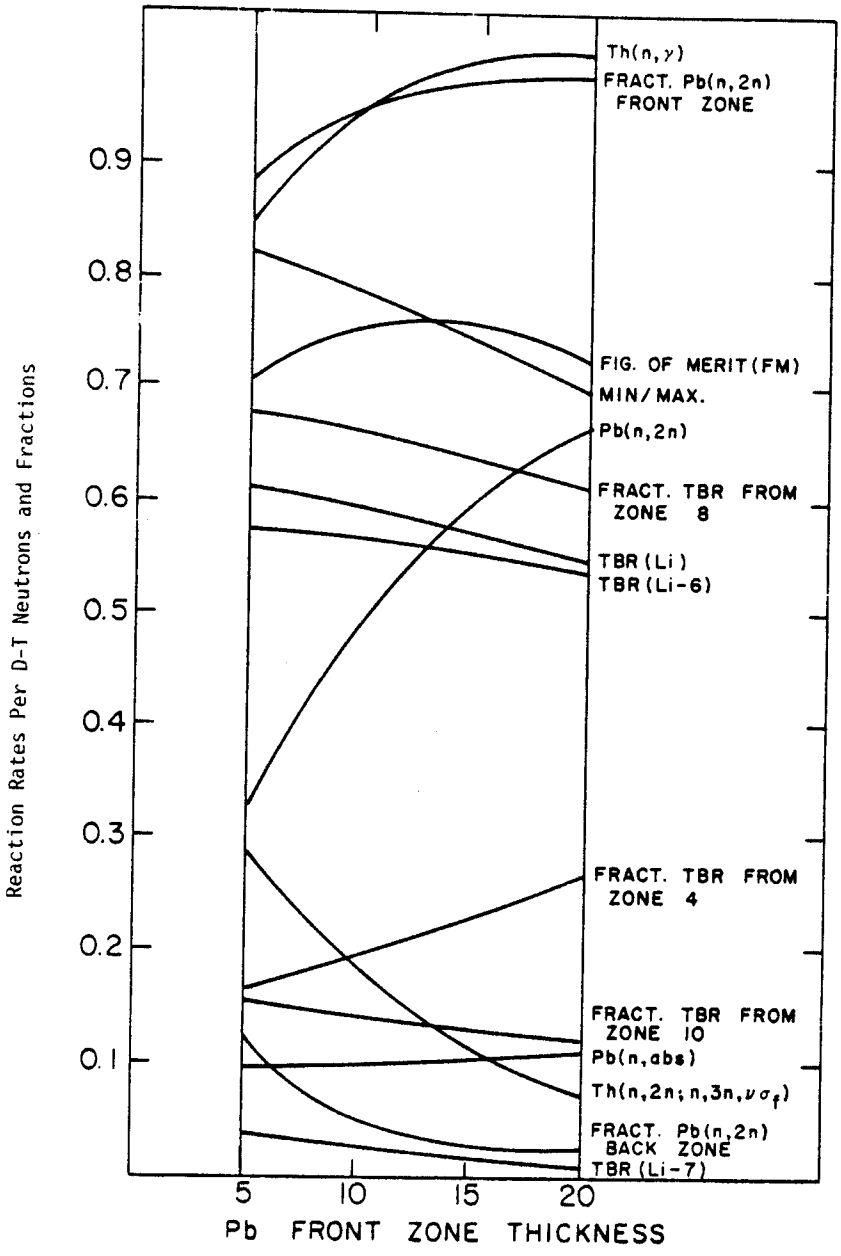

Fig. (IV.7): The Reaction Rates Per D-T Neutron Vs. the Pb Front Zone Thickness.

tium produced comes from the $Li^6(n,t)\alpha$ reaction. The fraction of tritium produced in zone 4 increases from 17% to 27% as the front thickness increases from 5 cm to 20 cm because the spectrum becomes softer. The highest fraction of tritium produced is in zone 8 (~65% for blanket #10). This fraction decreases as the front zone thickness increases. The Li back zone contributes ~14% to the total tritium produced. This fraction decreases steadily as the front zone thickness increases.

The main source of neutron multiplication is the Pb(n,2n) reaction. It increases from ~0.32 to ~0.67 per D-T neutron as the front zone thickness increases from 5 cm to 20 cm. This shows the effectiveness of Pb as a front zone neutron multiplier. As expected, the fraction of Pb(n,2n) reactions from the front zone is much higher than the corresponding value in the reflector zone (~95% for blanket #10) and increases as the front zone thickness increases. The absorption rate in Pb is small (0.098 for blanket #10). The value of Pb(n,abs)/Pb(n,2n) decreases as the front Pb zone thickness increases.

The radial profiles for the $Th(n,\gamma)$ reaction rate through the fuel zone are shown on Fig. (IV.8). These curves are much less steep than the corresponding ones shown in Fig. (IV.6) where Be is the neutron multiplier. To flatten the $Th(n,\gamma)$ reaction rate profile at the back edge of the fuel zone and to gain a higher value of TBR, blanket #10 is modified by increasing the Li zone thickness behind the fuel zone from 6 cm to 8 cm. The UBR and TBR for this modified blanket (blanket #13) are 0.94 and 0.63, respectively. The reaction rates

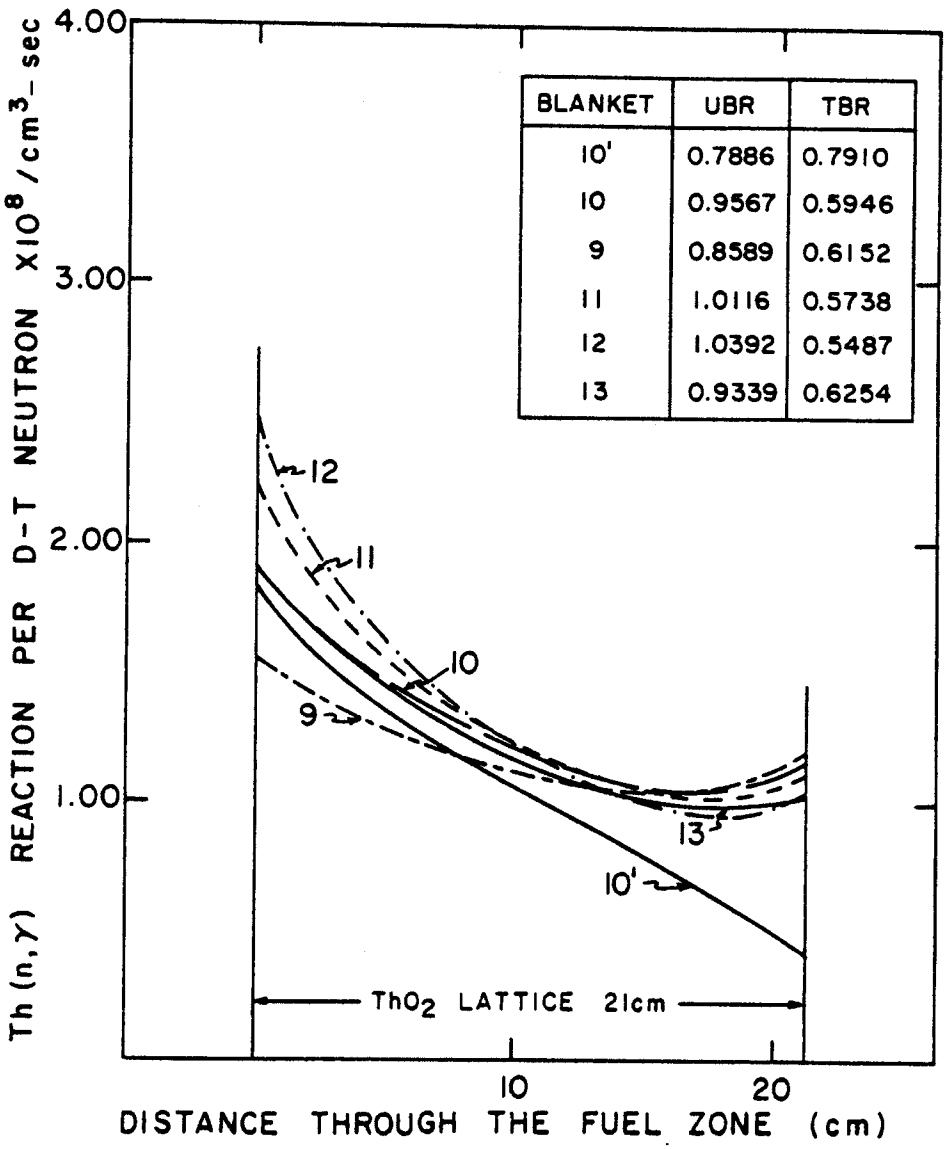

Fig. (IV.8): The U-233 Breeding Rate Distribution in the Fuel Zone Per D-T Neutron With Pb as the Front Zone Neutron Multiplier.

for this blanket are given in Table (IV.4) and the Th(n,γ) reaction rate across the fuel zone is shown in Fig. (IV.8).

IV.4.D Optimization Criteria

From the analysis just discussed, one is motivated to use lead as the neutron multiplier in the blanket front zone since the Th(n,γ) reaction rate profile in the fuel zone is more uniform. The spectrum in the fuel zone is harder. In addition, lead, unlike beryllium does not pose a resource availability problem. Further, for the lead based blankets, the optimized one should meet the following requirements:

. Maximum U-233 production rate with as flat a U-233 distribution across the fuel assembly as possible.

. TBR ~0.6. Overall TBR $\geq$ 1.0.

The first requirement shortens the residence time of the fuel to reach a specified enrichment. The constraint of a flat U-233 profile minimizes hot spot problems when the fuel assembly is placed directly in an LWR without an intermediate reprocessing step.

To begin the optimization search, it is assumed that the Th(n,γ) reaction rate profile across the fuel zone does not change when the fuel assembly is rotated 180° at any time which is short enough before the bred U-233 changes the neutronics of the blanket. This assumption has been verified and is discussed in the next chapter which is devoted to the time behavior of the blankets studied in this chapter. The resultant curve, obtained by the addition of the Th(n,γ) profile to its spacially reversed value to account for the 180° rota-

tion, is symmetric. The resultant curve based on the blanket clean condition composition (i.e., at the beginning of life of the blanket) is taken as the base for choosing the optimized blanket in our design.

The resultant curves obtained for blankets #9, #10, #10', #11, #12 and #13 are shown in Fig. (IV.9). The maximum-to-minimum value of these curves is given in Table (IV.4).

According to our criteria and constraints, the optimized blanket will be the one having the smallest maximum-to-average $Th(n,\gamma)$ reaction rate, denoted by R, for its resultant curve while having a high value of UBR. Thus, the figure-of-merit, FM, is UBR/R and this should be a maximum. However, FM is proportional to $(UBR)^2/Th(n,\gamma)_{max}$ since the average $Th(n,\gamma)$ reaction rate value is proportional to UBR. The FM values $x10^{-8}$ are given in Fig.(IV.9).

Although blanket #12 has the highest value of FM, blanket #13 is chosen as the optimized one to gain the economic benefit of a 10 cm front zone rather than 20 cm (this is a thinner and cheaper blanket). The FM values are nearly equal in both cases. The optimized blanket #13 has TBR = 0.625 which meets the second constraint cited earlier.

IV.5 Conclusions

An optimized blanket utilizing lead as a front zone neutron multiplier has been chosen. It has UBR and TBR of 0.94 and 0.625, respectively. This blanket has a high figure-of-merit value and a nearly flat U-233 production rate across the fuel zone. Carrying out a 180° fuel assembly rotation after half the residence time to reach a specified enrichment will give a symmetric U-233 distribution in the

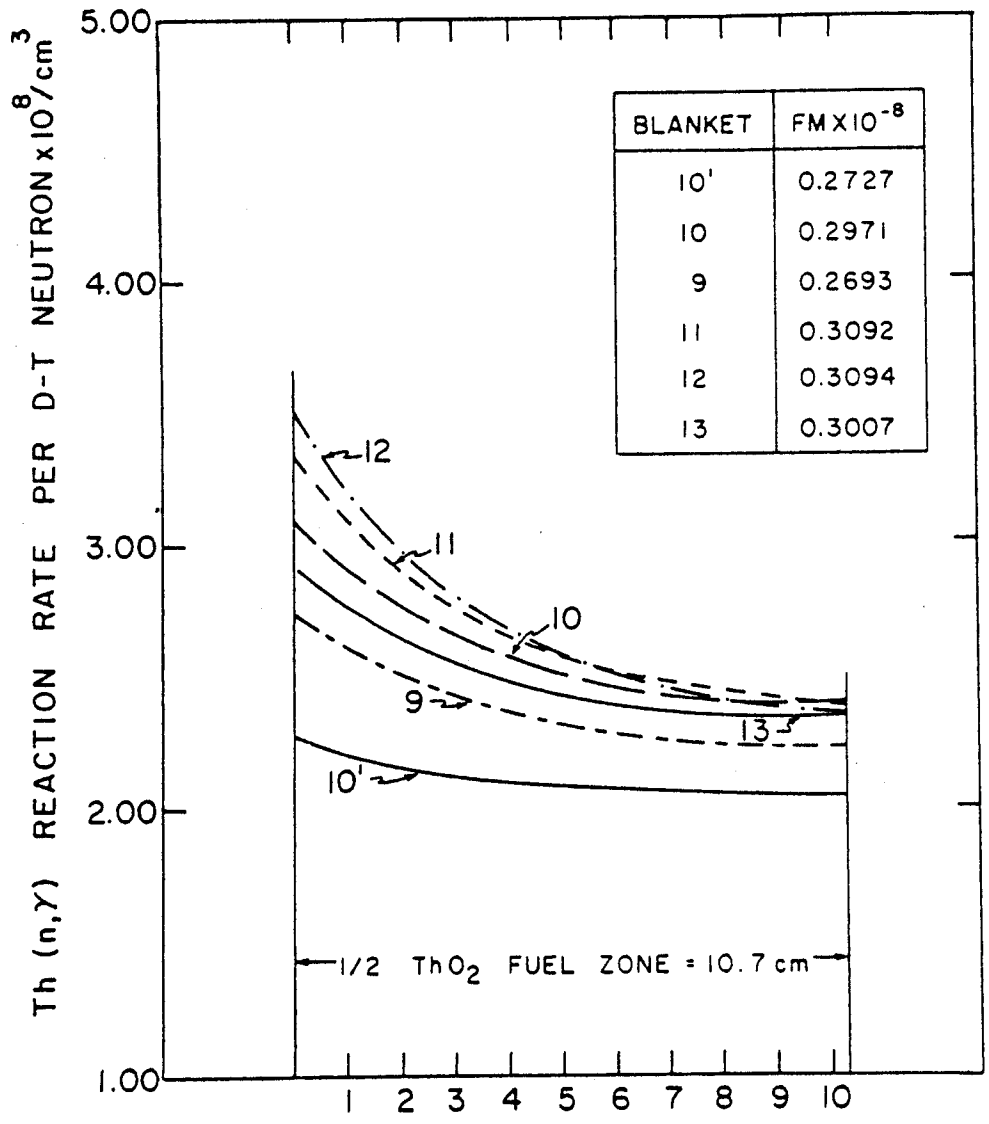

Fig. (IV.9): The U-233 Breeding Rate Distribution Through 1/2 of the Fuel Zone After Rotation.

fuel assembly.

The final SOLASE-H fission-fusion laser driven hybrid reactor is based on the optimized blanket obtained from this study. This final design is given in Fig. (IV.1).

In the next chapter, the behavior of the SOLASE-H blanket with time is investigated. A rotational scheme aimed at assuring a uniform fissile fuel distribution throughout the fuel zone will be discussed and presented next.

REFERENCES

1. Rose, R.P., "Status of Westinghouse Tokamak Hybrid Studies", Proceedings of the Second Fusion-Fission Energy Systems Review Meeting, Washington, D.C., Nov. 2-3 (1977), CONF-771155, Vol.I, 123 (July 1978).

2. Varljen, T.C., "New Initiatives in Tokamak Hybrid Studies", Ref. 1, 251, July (1978).

3. Tenney, F.H., "Reactor Studies of Tokamak Hybrids", Proceedings of the Second Fusion-Fission Energy Systems Review Meeting, Washington, D.C., Nov. 2-3 (1977), CONF-77115, Vol. II, 523, July (1978).

4. Allen, W.O. and Thomson, S.L., "Electron Beam Fusion-Fission Reactor Studies", Third ANS Topical Meeting on the Technology of Controlled Nuclear Fusion, May 9-11, 1978, Santa Fe, NM.

5. Bender, D.J., "Mirror Hybrid Studies", Ref. 1, 99, July (1978).

6. Lee, J.D., Bender, D.J., Moir, R.W., and Schultz, K.K., "Mirror Hybrids - A Status Report", Proc. Second Topical Meeting on the Technology of Controlled Nuclear Fusion, Washington 1976, CONF-760935-P2, pg. 689.

7. Maniscalco, J.A. and Hansen, L.F., "Present Status of Laser Driven Fusion-Fission Energy Systems", Ref. 1, Pg. 145, July (1978). Also, "New Initiatives in Laser Driven Fusion-Fission Energy Systems", Ref. 1, pg. 277, July (1978).

8. Conn, R.W., Moses, G.A., and Abdel-Khalik, S.I., "Notes on Fusion Hybrid Reactors", UWFDM-240, Fusion Research Program, The University of Wisconsin, April (1978).

9. "Proceedings US-USSR Symposium on Fusion-Fission Reactors", CONF-760733, July (1976). This reference includes different hybrid designs. Also see CONF-771155, Vol. I & II, July (1978).

10. Feiveson, H.A. and Taylor, T.B., "Alternative Strategies for International Control of Nuclear Power", Report Prepared for the 1980's Project of Council on Foreign Relations, Oct. (1976).

11. Feiveson, H.A. and Taylor, T.B. Bull. of Atomic Sci. 32, 14 (1976).

12. Bethe, H.A., "The Fusion Hybrid", Nuclear News, pg. 41-44, May(1978).

13. Moses, G.A., Conn, R.W., and Abdel-Khalik, S.I. "Laser Fusion Hybrids-Technical, Economic and Proliferation Considerations", UWFDM-272, Fusion Research Program, The University of Wisconsin, Nov. (1978).

14. Conn, R.W., et.al., "SOLASE-H, A Laser Fusion Hybrid Reactor Study", UWFDM-274, Nuclear Engineering Department, The University of Wisconsin (1978). Also, Trans. Amer. Nucl. Soc., 27, 58 (1978).

15. K.R. Schultz, R.H. Brogli, G.R. Hopkins, M. Jonzen, and G.W. Shirley, "A U-233 Fusion-Fission Power System Without Reprocessing", A preliminary report, General Atomic GA-A14635, UC-code, Sept. (1977).

16. S.F. Su, G.L. Woodruff, N.J. McCormick, "A High-Gain Fusion-Fission Reactor for Producing U-233", University of Washington, Nuc. Technology, Vol. 29, p. 392, June (1976).

17. A.C. Cook and J.A. Maniscalco, "U-233 Breeding and Neutron Multiplying Blankets for Fusion Reactors", Lawrence Livermore Laboratories (LLL), Repring UCRL-77284, Sept. (1975).

18. J.A. Maniscalco, "A Conceptual Design Study for Laser Fusion Hybrid", Reprint UCRL-78682, Sept. (1976).

19. J.A. Maniscalco, L.F. Hansen, and W.O. Allen, "Scoping Studies of U-233 Breeding Fusion Fission Hybrid", (LLL) Reprint UCRL-80585, May (1978).

20. W.W. Engle, Jr., "A User's Manual for ANISN", RISC-CCC-82, Oak Ridge National Lab. (1967).

21. R.Q. Wright and R.W. Rossin, "DLC-2D/100G Neutron Transport Cross Section Data Generated by SUPERTOG from ENDF/B3", RISC data package DLC-2, July (1973).

22. R.Q. Wright, el.al., "SUPERTOG: A Program to Calculate Fine Group Constants and Pn Scattering Matrices from ENDF/B", ORNL-TM-2679 (1969).

23. Duderstadt, J.J., "Nuclear Reactor Analysis", John Wiley & Sons, Inc., pg. 635 (1976).

CHAPTER V

BURN-UP CALCULATIONS FOR THE SOLASE-H BLANKET

V.1 Introduction

The blanket design of the laser driven fusion-fission hybrid, SOLASE-H presented in Chapter IV, is based on an optimization study to search for a blanket configuration that gives a nearly uniform fissile fuel distribution across the fuel assemblies.[1-3] This distribution will minimize the problems related to hot spots when the enriched fuel assemblies are placed directly in a LWR. In the SOLASE-H design, the ThO_2 fuel elements are LWR fuel assemblies. The bundles are extracted from the blanket when 3-4% enrichment in U-233 is reached.

To set a rotational scheme which results in a symmetric fissile fuel distribution across the fuel assemblies, the variation of the enrichment, both in space and time, must be evaluated. The objective of the study presented in this chapter is to assess this problem.

The residence time to reach 4% enrichment has been estimated to be 2.7 yr in the optimized blanket which approximates the SOLASE-H final design. It turns out that the variation of the overall enrichment is nearly linear with time and carrying out a 180° rotation of the bundles after half the residence time (~1.4 yr) will result in a symmetric enrichment profile across the fuel assembly. The maximum to minimum value is 1.26. In the spherical calculational model adopted in this study, the annual fissile fuel production is estimated to be 1.95 tonnes/yr, assuming only 70% of the solid angle is covered

by the fuel-producing radial blanket. This fuel can provide makeup to eight 1000 MW_e LWRs, each with a conversion ratio of 0.75.

V.2 Burnup Model

V.2.A Calculational Procedures and Assumptions

The performance of the blankets studied in Chapter IV will undergo noticeable changes during operation. The fissile nuclide U-233 bred throughout the fuel zone, the depletion of Th-232 and the tritium production rates will vary with time. Detailed time-dependent calculations are necessary to follow changes in both the blanket's composition and performance. Such analysis is also required to accurately assess the fuel production rate and its spacial distribution across the fuel assembly (fuel zone).

The important parameters are: the depletion of Th-232 atoms; the build-up of U-233 atoms, and its effect on the neutron population and energy multiplication, M (defined as the total energy deposited throughout the blanket per 14.1 MeV D-T neutron); and the buildup of actinides and fission products.

There are several burnup codes[4-5] which evaluate the nuclide densities and the buildup of fissionable nuclides as a function of the operating time. These codes have the following characteristics:

- One point depletion codes, i.e., ones which evaluate the depletion at one spatial point only.
- The number of neutron energy groups used are few (4 energy groups in the CINDER[4] code and 3 energy groups in ORIGIN[5]).
- The neutron cross sections used in these codes are based essen-

tially on the spectra encountered in fast reactors.

First, based on unit-source neutron intensity, the ANISN[6] code can be used to calculate a 25-group neutron flux throughout the blanket. This flux, when combined with the actual D-T neutron source intensity, determines the neutron absolute flux level in the blanket. The flux, along with the nuclide densities at the beginning of a particular time step is then used with the burnup code to evaluate new nuclide densities at the end of this time step. These are used in a new ANISN calculation for the next time step and the process is repeated.

For preliminary survey calculations, more simplified burnup procedures have been used in this study to evaluate the net fissile fuel production (U-233) and its spatial distribution across the fuel zone. The effect of fission product poisoning is not taken into consideration nor is the production of other daughter nuclides such as Pa-233 ($Th^{232}(n,2n)Pa^{233}$). This simplifying assumption is reasonable here since the blankets studied were optimized for maximum fuel production without the use of a fission plate of fissile isotopes intended to enhance neutron production.[7-12] Accordingly, the number of fissions per D-T neutron is small and the effect of fission product poisoning should be less harmful neutronically. In our study, the neutron population is enhanced by the (n,2n) reaction in lead (or Be) as mentioned in Chapter IV.

In the burnup model adopted, the time variation in atomic density at each point throughout the fuel zone is calculated using the neutron flux (25-group) at that point. We do not use an average value through

a certain subregion with a fewer number of energy groups (3-4) as in the case when using burnup codes like CINDER and ORIGIN.

The neutron source is obviously localized outside the fuel zone. As such, fissile fuel production across the fuel zone decreases far from the source. A scheme to rotate the fuel assembly after a given operating time is necessary to obtain a flatter fissile fuel distribution.

In the burnup model adopted in this chapter, the important parameters to be evaluated are:

(1) Th-232 and U-233 atomic densities as a function of time.

(2) The percent burnup of the bred U-233 as a function of time.

(3) U-233 and tritium production rate before and just after fuel assembly rotation at any particular time.

Based on these parameters, the time at which rotation of the fuel assembly takes place and the extra time needed to reach a specified U-233 enrichment are evaluated subject to the constraint of as even a fissile fuel distribution as possible. The parameters in (1) and (2) above are evaluated for the different blankets utilizing lead as front zone neutron multiplier (see Chapter IV), while parameters in (3) and the rotation scheme are evaluated for the optimized blanket. The configuration of these blankets are given in Fig. (V.1) and Table (V.1.a) and (V.1.b).

In the following, the burnup model and the results in (1), (2) and (3) above are given.

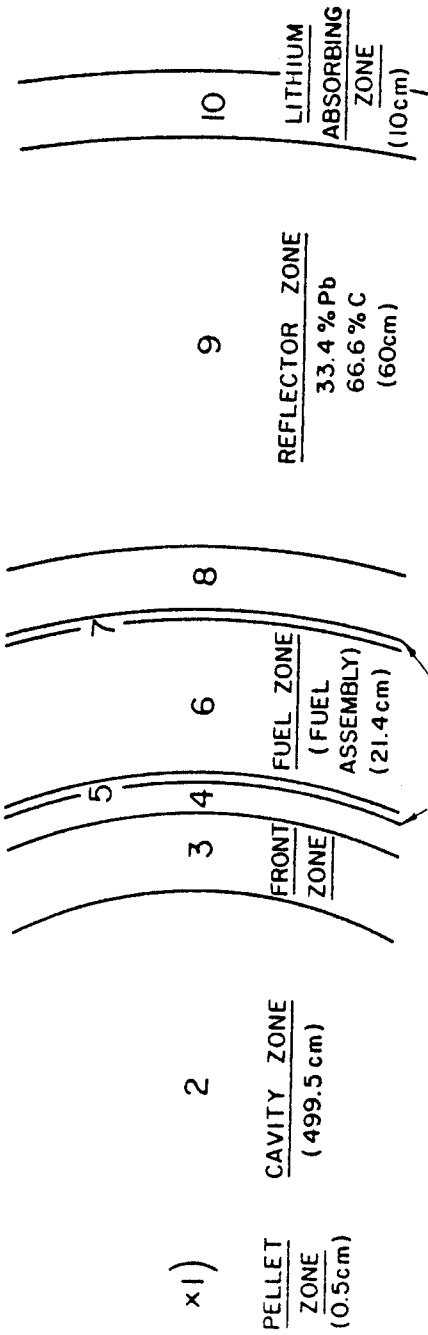

Fig. (V.1): Configuration of the Different Blankets Utilizing Pb as the Front Zone Neutron Multiplier.

Table (V.1a) Zone Composition and Thickness

Zone	Thickness	Composition
1	0.5 cm	Laser Pellet
2	499.5 cm	Vacuum
3	X [see Table(V.1b)]	82.2% Pb 9.3% Na 8.5% Zirc-2
4	1.5 cm	95% Li 5% S.S.
5	0.5 cm	100% S.S.
6	21.4 cm	30.3% ThO_2 9.2% Zirc-2 1.3% Void 59.2% Na
7	0.5 cm	100% S.S.
8	Y [see Table(V.1b)]	95% Li 5% S.S.
9	60 cm	33% Pb 67% C
10	10 cm	95% Li 5% S.S.

Table (V.1b)

Different Blankets Studied for Burnup Calculations

Zones / (a) Blanket #	Zone 3 (X) cm	Zone 4 cm	Zone 8 (Y) cm	U-233 Breeding Ratio UBR(b)	Tritium Breeding Ratio TBR(c)
10'	10 cm	1.5cm-nat Li	6cm-50% Li^6	0.7886	0.791036
9	5 cm	"	6cm-nat Li	0.8589	0.6152
10	10 cm	"	"	0.9567	0.5946
11	15 cm	"	"	0.0116	0.5734
12	20 cm	"	"	1.0392	0.5487
13(d)	10 cm	"	8cm	0.9339	0.6254

(a) See Section IV.4.C
(b) U-233 atoms produced in the fuel zone/D-T neutron
(c) Tritium atoms produced in the blanket/D-T neutron
(d) The optimized blanket

V.2.B Th-232 and U-233 Atomic Densities as Function of the Operating Time

Only the density of Th-232 and U-233 were considered to vary with time. In this case, the rate of change of these nuclide densities is given by

$$\frac{dN^{(2)}(x,t)}{dt} = \sum_i N^{(1)}(x,t)\phi_i(x,t)\sigma_\gamma^{(i,1)} - \sum_i N^{(2)}(x,t)\phi_i(x,t) \cdot \sigma_a^{(i,2)} \qquad (V.1)$$

$$\frac{dN^{(1)}(x,t)}{dt} = -\sum_i N^{(1)}(x,t)\sigma_a^{(i,1)}\phi_i(x,t) \qquad (V.2)$$

where $N^{(2)}(x,t)$ = U-233 atomic density at position x at time t

$N^{(1)}(x,t)$ = Th-232 atomic density at position x at time t

$\phi_i(x,t)$ = Neutron flux of energy group i at position x and time t

$\sigma_\gamma^{(i,1)}, \sigma_a^{(i,1)}$ = Microscopic capture and absorption cross section of Th-232 of energy group i, respectively.

$\sigma_a^{(i,2)}$ = Microscopic absorption cross section of U-233 of energy group i.

The fission yield of Th-232 and U-233 and their radioactive decay were ignored in Eqs. (V.1) and (V.2) [$t_{1/2}$ (Th-232) = 1.41 x 10^{10}yr and $t_{1/2}$ (U-233) = 1.65 x 10^{5}yr].

Upon solving Eqs. (V.1) and (V.2) we get

$$N^{(1)}(x,t) = N^{(1)}(x,t_o)e^{-b(t-t_o)} \qquad (V.3)$$

$$N^{(2)}(x,t) = \frac{c}{a-b} N^{(1)}(x,t_o)[e^{-b(t-t_o)} - e^{-a(t-t_o)}] + N^{(2)}(x,t_o)e^{-a(t-t_o)} , \quad (V.4)$$

where

$$a \equiv a(x) = \sum_i \phi_i \sigma_a^{(i,2)}$$
$$b \equiv b(x) = \sum_i \phi_i \sigma_a^{(i,1)}$$
$$c \equiv c(x) \quad \sum_i \phi_i \sigma_\gamma^{(i,1)} ,$$

with the assumption that the neutron flux does not change with time. $N^{(2)}(x,t_o)$ and $N^{(1)}(x,t_o)$ are the atomic densities of U-233 and Th-232, respectively, at position x and initial time $t = t_o$. The amount of U-233 generated $G(x,t_1 \to t_2)$ in a time interval $t_1 \to t_2$ at position x is

$$G(x,t_1 \to t_2) = -\frac{c}{b} N^{(1)}(x,t_o)[e^{-b(t_2-t_o)} - e^{-b(t_1-t_o)}] = -\frac{c}{b} N^{(1)}(x,t_1)[e^{-b(t_2-t_1)} - 1] \quad (V.5)$$

The amount of U-233 consumed between t_1 and t_2 is

$$C(x,t_1 \to t_2) = \int_{t_1}^{t_2} a\, N^{(2)}(x,t)dt. \quad (V.6)$$

With $N^{(2)}(x,t)$ given by Eq. (V.4) and expressed in terms of t, we find

$$N^{(2)}(x,t) = \frac{c}{a-b} N^{(1)}(x,t_1)[e^{-b(t-t_1)} - e^{-a(t-t_1)}] + N^{(2)}(x,t_1)e^{-a(t-t_1)}).$$

From Eq. (V.6), we find also

$$C(x,t_1 \to t_2) = \frac{ac}{a-b} N^{(1)}(x,t_1) \left[\frac{e^{-b(t_2-t_1)} - 1}{(-b)} - \frac{e^{-a(t_2-t_1)} - 1}{(-a)}\right]$$

$$- N^{(2)}(x,t_1)[e^{-a(t_2-t_1)} - 1] \qquad (V.7)$$

where,

$$N^{(1)}(x,t_1) = N^{(1)}(x,t_o)e^{-b(t_1-t_o)} \qquad (V.8)$$

$$N^{(2)}(x,t_1) = \frac{c}{a-b} N^{(1)}(x,t_o)[e^{-b(t_1-t_o)} - e^{-a(t_1-t_o)}]$$

$$+ N^{(2)}(x,t_o)e^{-a(t_1-t_o)} \qquad (V.9)$$

In terms of $N^{(1)}(x,t_o)$ and $N^{(2)}(x,t_o)$, Eq. (V.7) can be expressed as:

$$C(x,t_1\rightarrow t_2) = \frac{ac}{a-b} N^{(1)}(x,t_o)[\frac{e^{-b(t_2-t_o)} - e^{-b(t_1-t_o)}}{(-b)}$$

$$- \frac{e^{-a(t_2-t_o)} - e^{-a(t_1-t_o)}}{(-a)}]$$

$$- N^{(2)}(x,t_o)[e^{-a(t_2-t_o)} - e^{-a(t_1-t_o)}] \qquad (V.10)$$

The enrichment at a certain position x and time t is define as

$$E(x,t) = \frac{N^{(2)}(x,t)}{N^{(1)}(x,t)} = \frac{\text{Net U-233 atoms/cm}^3}{\text{Th-232 atoms/cm}^3} \qquad (V.11)$$

The fraction of fissile nuclide burned, $Bu(x,t_o\rightarrow t)$ is defined as

$$Bu(x,t_o \to t) = \frac{C(x,t_o \to t)}{G(x,t_o \to t)}$$

$$= \frac{\text{U-233 atoms consumed/cm}^3 \text{ in the interval } t_o \to t}{\text{U-233 atoms generated/cm}^3 \text{ in the interval } t_o \to t}$$

and the initial conditions are

$$\left.\begin{aligned} &t = t_o = 0 \\ &N^{(2)}(x,t_o) = 0 \\ &N^{(1)}(x,t_o) = N^{(1)} = \text{initial Th-232 atomic density} \\ &\qquad\qquad\qquad\qquad \text{throughout the fuel zone.} \end{aligned}\right\} \qquad (V.12)$$

If the variation of Th-232 atomic density with time is slight, as turns out to be the case in the blankets studied, we can consider

$$N^{(1)}(x,t) \simeq N^{(1)}$$

This is equivalent to considering $b \to 0$ in Eq. (V.3). In this case, we have from Eq. (V.5)

$$G(x,t_1 \to t_2) \simeq -\frac{c}{b} N^{(1)}[e^{-bt_2} - e^{-bt_1}] \qquad (V.13)$$

and

$$G(x,0\to t) \simeq -\frac{c}{b} N^{(1)}[e^{-bt} - 1] \qquad \text{(V.14)-a}$$

$$\simeq c N^{(1)} t \qquad , c \equiv c(x) \qquad \text{(V.14)-b}$$

i.e., the U-233 generation is linear with time. Also from Eq. (V.10)

$$C(x,t_1\to t_2) \simeq \frac{ac}{a-b} N^{(1)}[-\frac{e^{-bt_2} - e^{-bt_1}}{b} + \frac{e^{-at_2} - e^{-at_1}}{a}] \ , \qquad \text{(V.15)}$$

and

$$C(x,0\to t) \simeq \frac{ac}{a-b} N^{(1)}[-\frac{e^{-bt} - 1}{b} + \frac{e^{-at} - 1}{a}] \qquad \text{(V.16)}$$

For $b \to 0$, this reduces to

$$C(x,0\to t) = cN^{(1)}[t - \frac{1-e^{-at}}{a}] \ , \qquad \text{(V.17)}$$

and for small values of a, we finally find,

$$C(x,0\to t) \simeq \frac{ac\ N^{(1)} t^2}{2} \qquad \text{(V.18)}$$

Thus the consumption of U-233 up to time t is quadratic in time for small a and $b\to 0$. In this case, the fraction of U-233 burned is

$$Bu(x,0\to t) = \frac{C(x,0\to t)}{G(x,0\to t)} \simeq \frac{at}{2} \ . \qquad \text{(V.19)}$$

which is linear in time. The net U-233 generated at point x and time t under these assumptions is

$$\begin{aligned} N^{(2)}(x,0\to t) &= G(x,0\to t) - C(x,0\to t) \\ &= c\, N^{(1)}{}_t - acN^{(1)}{}_t{}^2/2 \\ &= c\, N^{(1)}{}_t \text{ for small } at^2 \end{aligned} \tag{V.20}$$

One should notice that a, b and c are functions of position.

V.3 Effect of Varying the Pb Neutron Multiplier Front Zone Thickness on the U-233 Bred After Operating Time t

The amount of U-233 produced, consumed and the fraction burned throughout the fuel zone as functions of the operating time has been calculated for the blankets utilizing Pb as a front zone multiplier and shown in Fig. (V.1) and Table (V.1). The total U-233 generated in the fuel zone, $G_t(t)$, is

$$G_t(t) = \int G(\vec{x},0\to t)d\vec{x} \tag{V.21}$$

The amount of U-233 consumed up to time t in the fuel zone, $C_t(t)$, is

$$C_t(t) = \int C(\vec{x},0\to t)d\vec{x} \ . \tag{V.22}$$

The fraction burned, $BU_t(t)$, is

$$BU_t(t) = \frac{C_t(t)}{G_t(t)} \ , \tag{V.23}$$

the net U-233 produced in the fuel zone, $U_t(t)$, is

$$U_t(t) = G_t(t) - C_t(t), \tag{V.24}$$

and the enrichment at that time, $E_t(t)$, is

$$E_t(t) = \frac{U_t(t)}{TH(t)} \simeq \frac{U_t(t)}{TH_o} \tag{V.25}$$

where $$TH(t) = \int N^{(1)}(\vec{x},0\rightarrow t)d\vec{x},$$

the total Th-232 atoms in the blanket at time t and TH_o is its atoms inventory at t=0.

The values of $G_t(t)$ and $C_t(t)$, expressed in kg of U-233 and the percentage of burnup are shown in Fig. (V.2) and Fig. (V.3) for a wall loading of 1.92 MW/m^2. The 25-group fluxes at each spatial point within the fuel zone determined at t=0 (clean condition) were used to evaluate the space dependent coefficients a, b and c. More accurate results necessitate the use of the neutron flux after each step with the new atomic densities, as mentioned in the introduction. This, however, has been done for the optimized blanket (blanket #13) as will be discussed later.

As shown in Fig. (V.2) the U-233 generated, $G_t(t)$, varies linearly in time for each blanket and the U-233 consumed up to time t, $C_t(t)$, is quadratic in t. The percentage of U-233 burned, $BU_t(t)$, is almost linear as shown on Fig. (V.2) and deviates from linearity only after

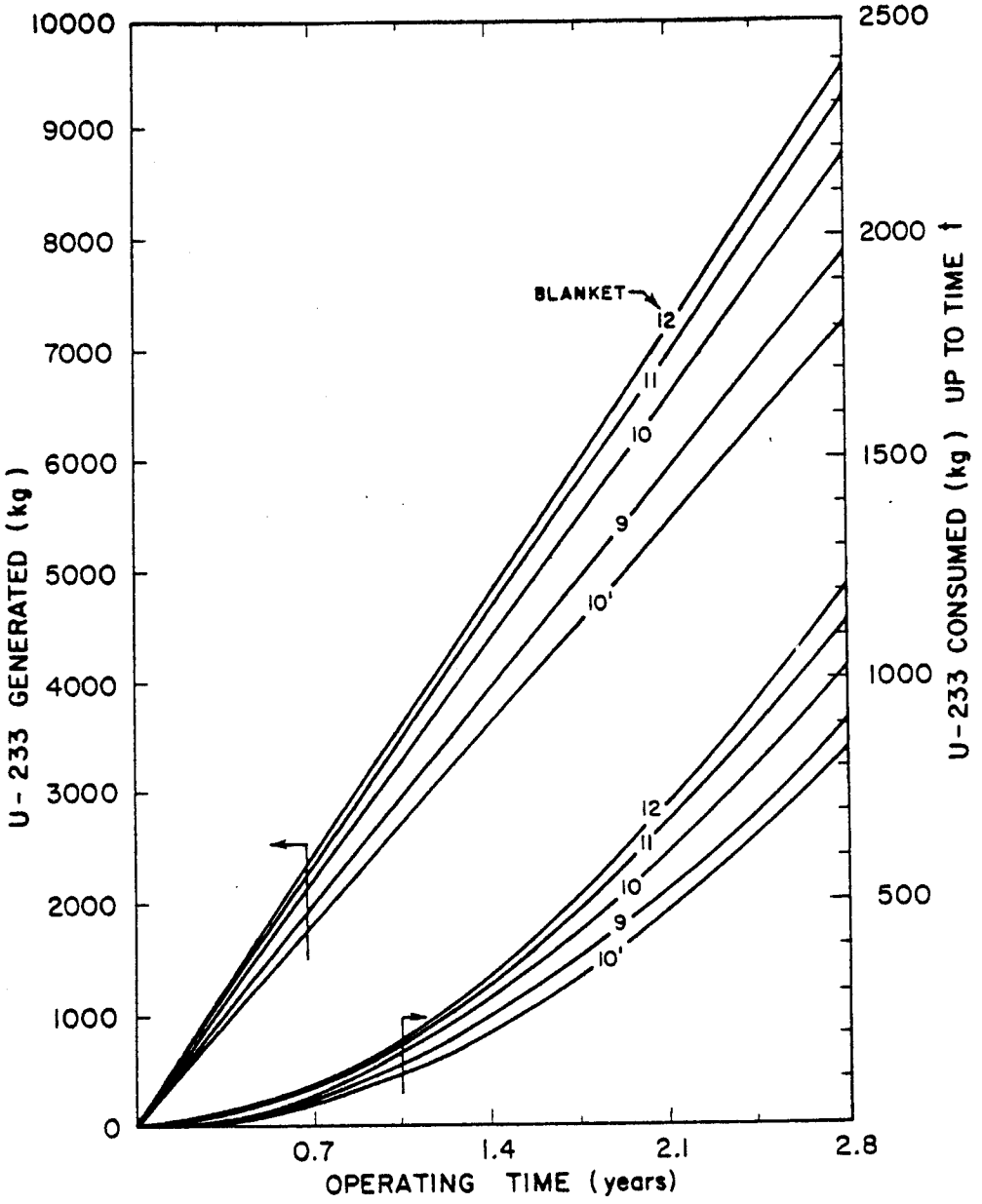

Fig. (V.2): The U-233 Generated and the Amount Consumed Vs. Operating Time (wall Load 1.92 MW/m^2)

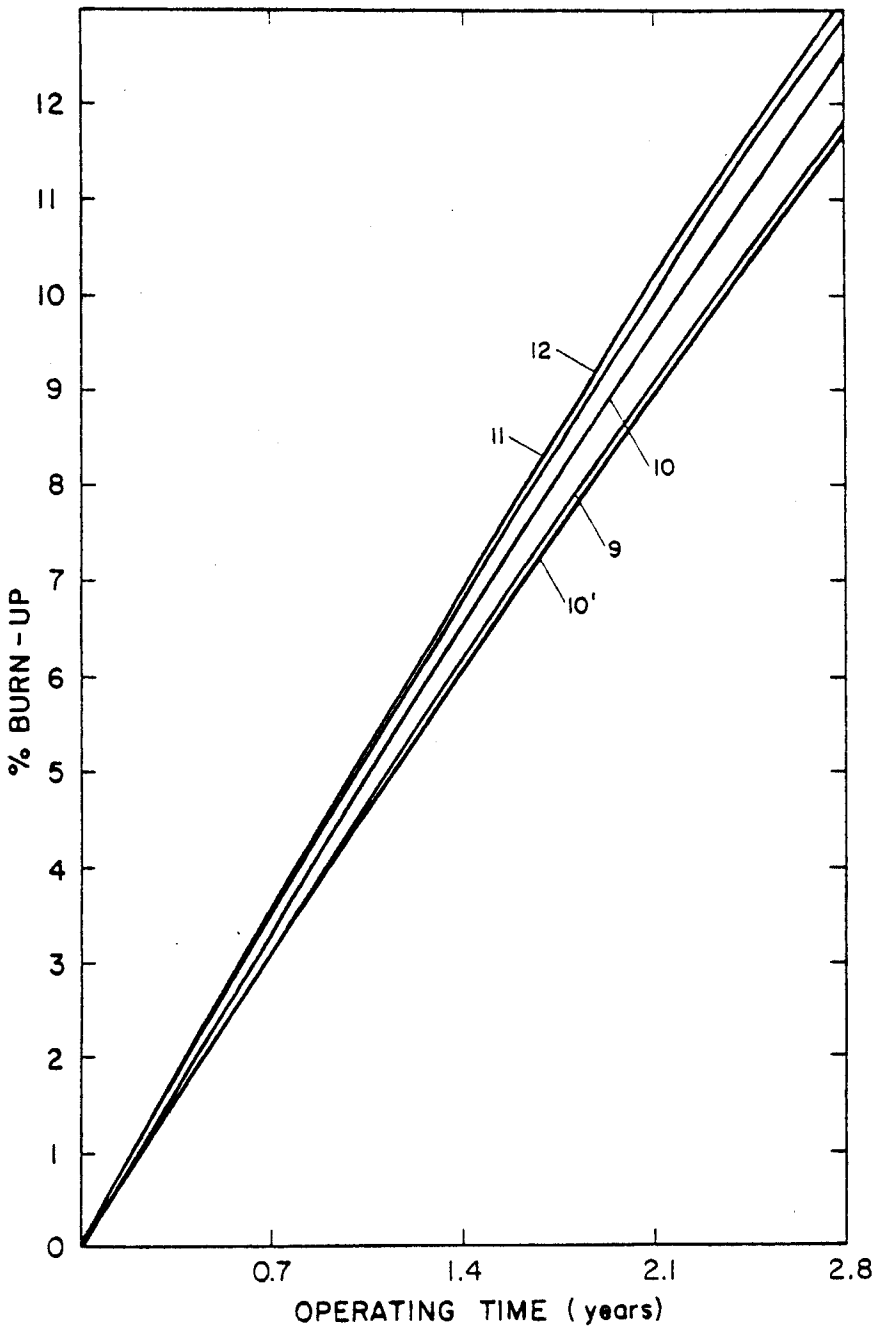

Fig. (V.3): The Percent (%) Burn-Up of U-233 Vs. Operating Time for a Wall Load 1.92 MW/m^2.

~ 2.1 years. This can be shown by considering the fraction of U-233 burned at point x after time t [see Eqs. (V.14)-a and (V.16)]:

$$BU(x,0\to t) \simeq \frac{C(x,0\to t)}{G(x,0\to t)}$$

$$= \frac{\frac{ac}{a-b} N^{(1)}\left[-\frac{e^{-bt}-1}{b} + \frac{e^{-at}-1}{a}\right]}{\frac{c}{b} N^{(1)}\left[e^{-bt}-1\right]} \qquad (V.26)$$

where $N^{(1)}(x,t)$ is considered constant at $t_o=0$. With $b\to 0$, it reduces to

$$BU(x,0\to t) \simeq 1 + \frac{e^{-at}-1}{at} \quad , \qquad (V.27)$$

which has an exponential term. For a non-negligible value of the exponent (large t), the integrated $BU_t(t)$ is non-linear in time.

Blanket #12 has the highest fuel production rate [see Table (V.1)] while blanket #9 has the lowest value among blankets #9, #10, #11, and #12. As mentioned before, increasing the Pb front zone thickness increases the fuel production rate and decreases the tritium production rate. However, the change in these rates is less pronounced when the Pb front zone thickness exceeds 10 cm.

The differences in the values of $G_t(t)$, $C_t(t)$ and $BU_t(t)$ for blankets #9, #10, #11, and #12 are less pronounced for shorter operating times. This is shown in Fig. (V.4) where these values are

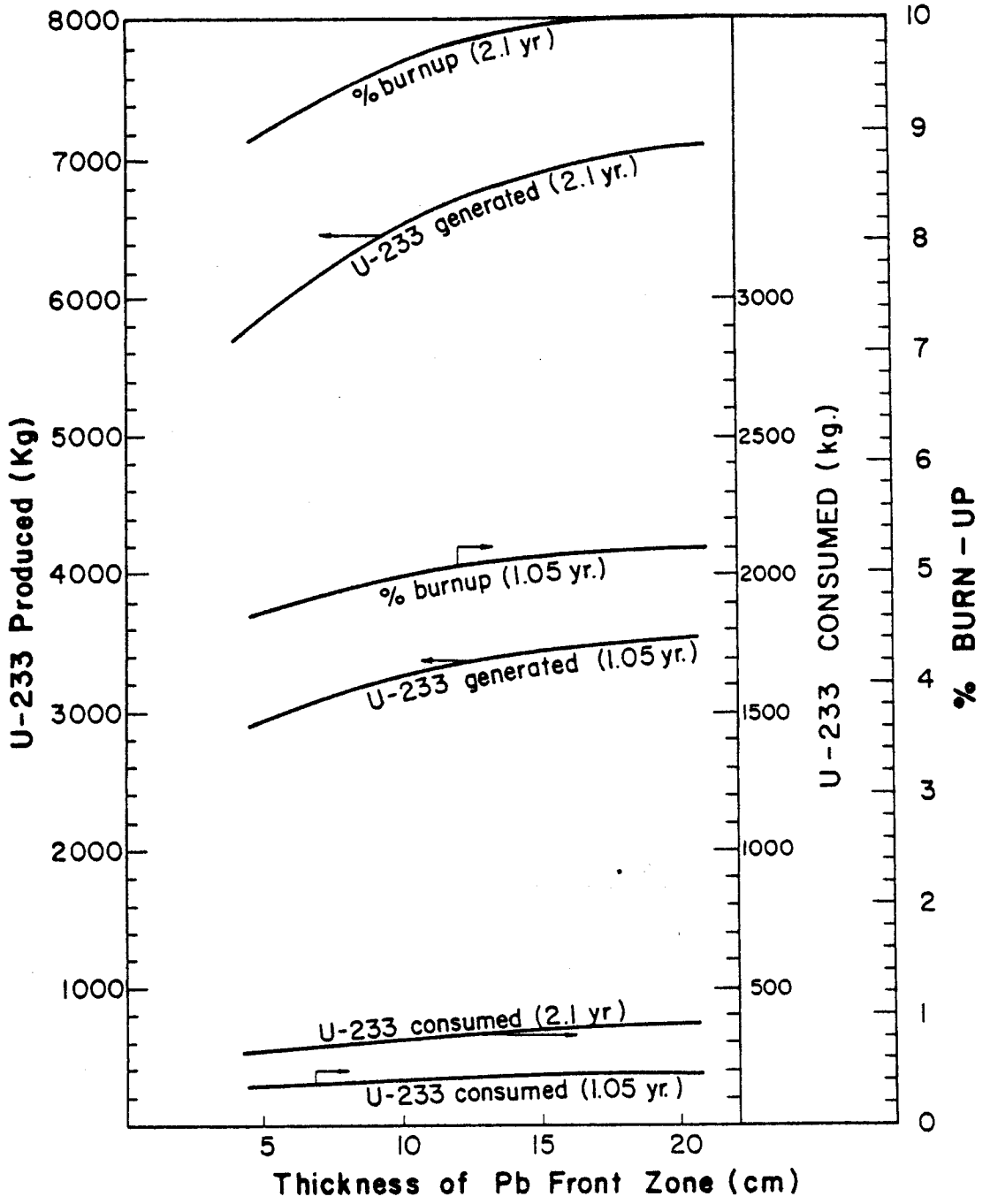

Fig. (V.4): The Effect of Varying the Front Pb-Neutron Multiplier Zone on the Blanket Fuel Production After 1.05 and 2.1 Years.

plotted after 1.05 yr and 2.1 yr for these different blankets. The slope in the curves of $G_t(t)$, $C_t(t)$ and $BU_t(t)$ shown in Fig. (V.4) is larger when the front zone thickness is small. One should notice that at any operating time, although the amount of U-233 produced increases as the front zone increases, the amount of U-233 consumed also increases and curves for $C_t(t)$ do not cross one another.

V.4 Time to Reach a Given Enrichment

To study the effect of non-uniform fissile fuel production rates across the fuel, the time needed to reach a specific enrichment (~ 4%) at each point and for each blanket is calculated. This is shown in Fig. (V.5) for a wall loading of 1.92 MW/m^2. This time is higher for regions further from the D-T neutron source. For blanket #10', [see Table (V.1), the time to enrichment increases as we reach the outer edge since the fissile fuel production rate decreases across the fuel zone. The results in Fig. (V.5) are inversely proportional to the fuel production rate discussed previously in section IV.4.C. The results for the optimized blanket (blanket #13) are also shown on Fig. (V.7). The points near the inner edge of the fuel zone (close to the source) reach 4% enrichment faster than the points near the outer edge. The curves for blanket #12 and the optimized blanket #13 are shown separately in Fig. (V.6) and Fig. (V.7), respectively. Also shown are curves for the time needed to reach 4% enrichment without considering the burning of bred U-233. From these figures, one observes the following:

- The time to enrichment is inversely proportional to $Th(n,\gamma)$

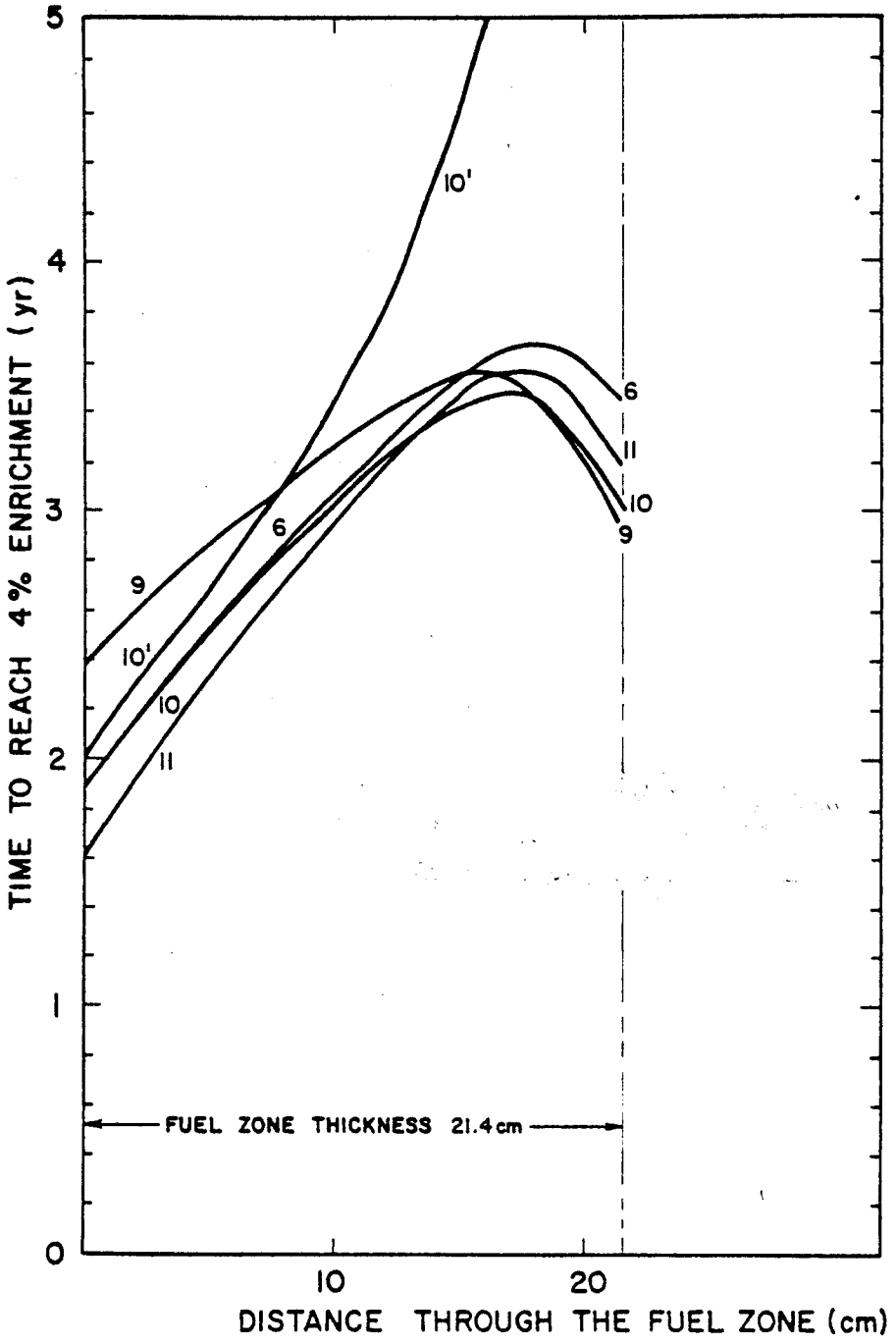

Fig. (V.5): Time to Reach 4% Fuel Enrichment at Each Spacial Point (Wall Load = 1.92 MW/m^2).

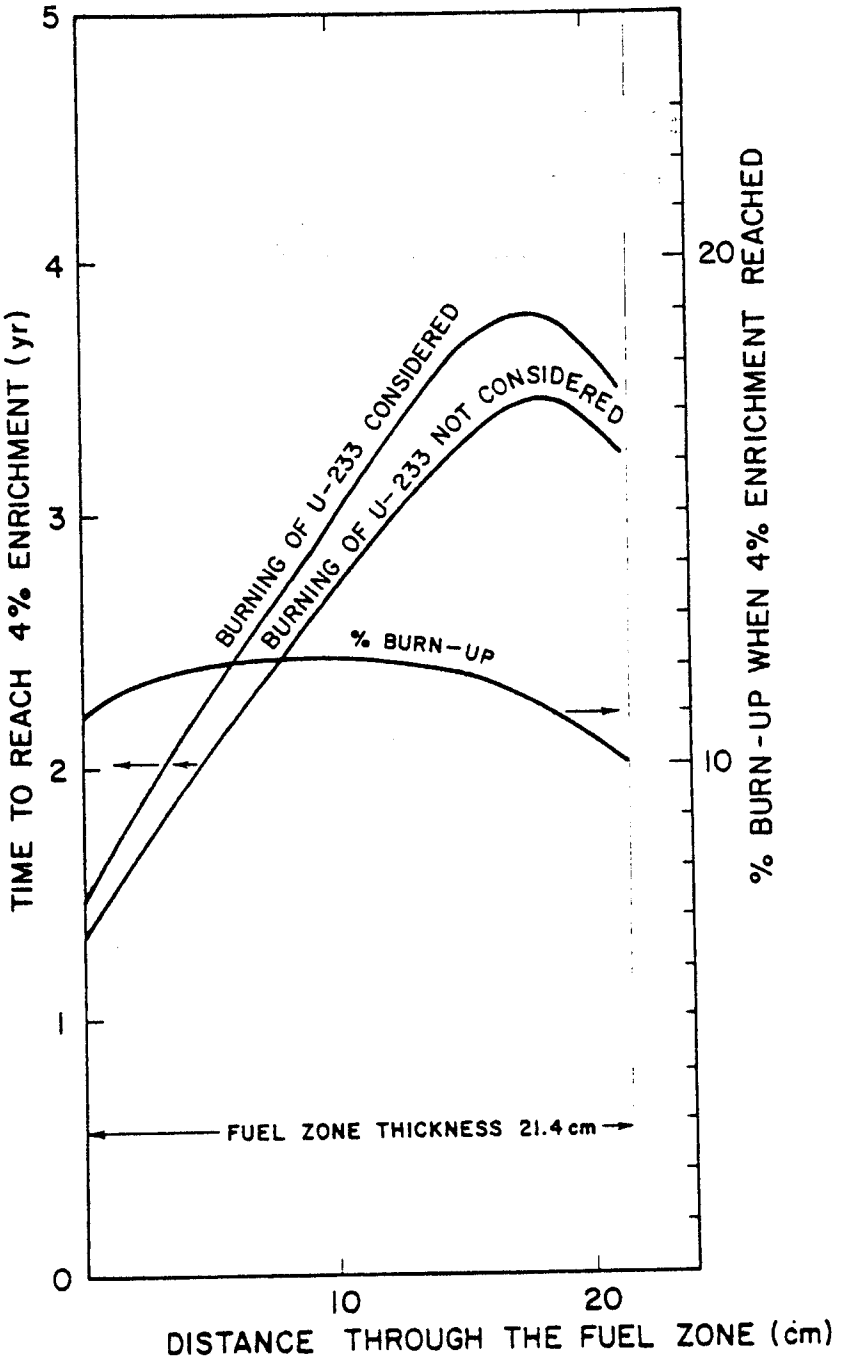

Fig. (V.6): Time to Reach 4% Enrichment Throughout the Fuel Zone With and Without Burning the Bred U-233 Fuel (Blanket # 12 - Wall Load = 1.92 MW/m^2).

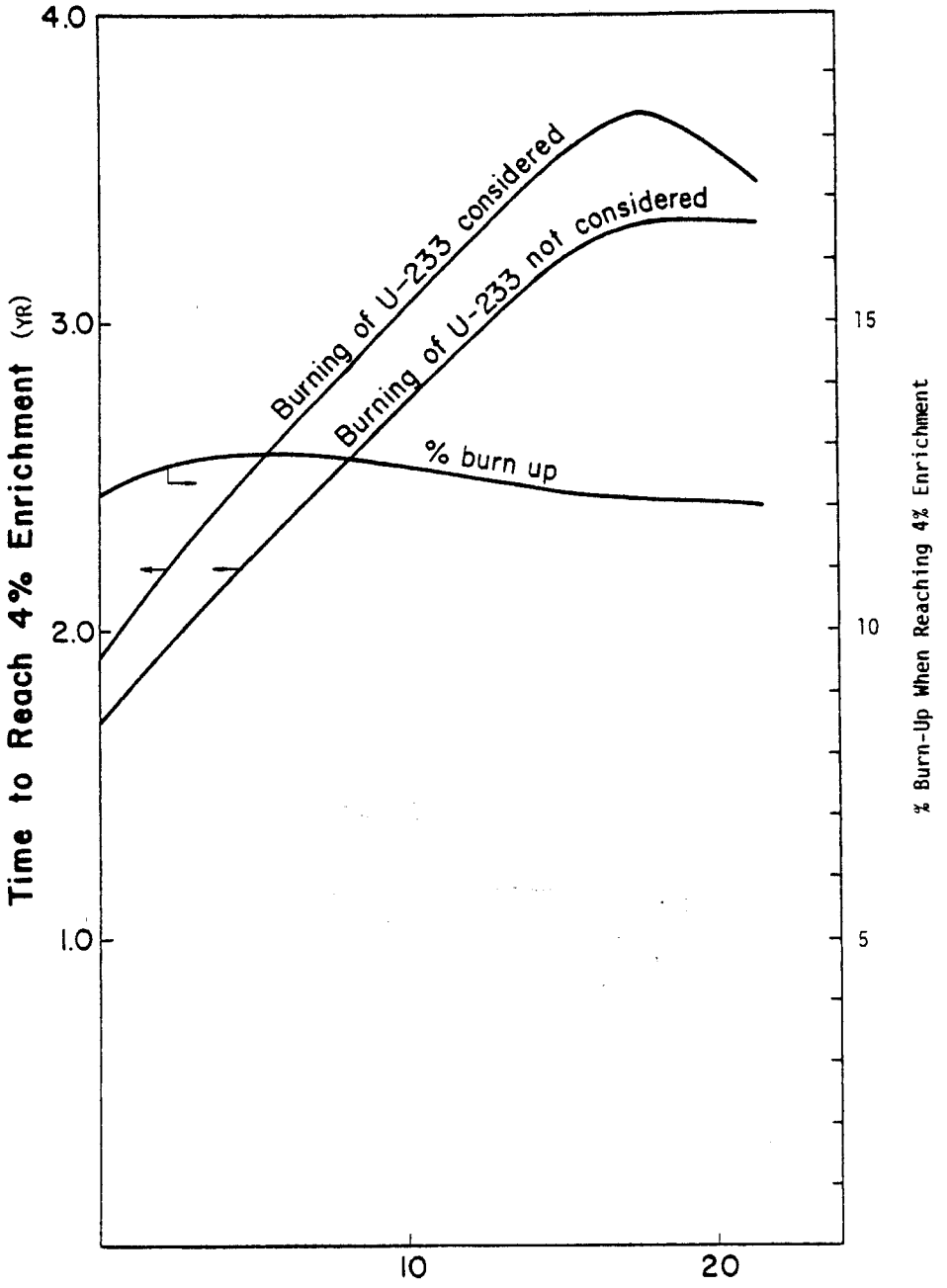

Fig. (V.7): Time for Each Point Throughout the Fuel Zone to Reach 4% Enrichment With and Without Burning the Bred U-233 Fuel (The Optimized Blanket # 13, Wall Load = 1.92 MW/m^2).

reaction rate per D-T neutron.

- Including U-233 burning implies each point requires a longer time to reach the specified enrichment.
- About 12% of U-233 generated is consumed during the enrichment process.

The results shown in Figs. (V.5), (V.6) and (V.7) are useful if there is a shifting scheme to move one fuel element in the fuel assembly from one position to another or to retrieve certain fuel elements after reaching a specified enrichment. In the SOLASE-H design, however, the fuel assembly is extracted from the blanket after reaching a specific overall enrichment. It is rotated 180° after approximately half of the residence time in the blanket to assure a flatter fissile fuel distribution across the assembly. This rotation scheme will be discussed in section V.6 for the optimized blanket #13.

The time needed to reach a specific overall enrichment, $E_t(t)$, defined as the ratio of the total U-233 atoms produced in the fuel zone to the total Th-232 atoms present at time t, is shown in Table (V.2). In this table, we summarize the results of fuel production and consumption in blankets #10', #9, #10, #11, #12 and the optimized blanket #13 after reaching 4% enrichment. The corresponding values without allowing for the depletion of Th-232 and U-233, denoted by fresh condition, are also given for comparison. One should notice that the parameter RT = $(UBR)_0$ T(4%)/Th(Kg) is almost identical for all the blankets. $(UBR)_0$ is the uranium breeding ratio at the beginning of life of the blanket and T(4%) is the time to reach an

Table (V.2) The Blanket Parameters After Reaching 4% Fuel Enrichment Using ϕ_o and Wall Loading of 1.92 MW/m^2

Parameter \ Blanket		#10' (10 cm)(a)	#9 (5 cm)	#10 (10 cm)	#11 (15 cm)	#12 (20 cm)	#13(b) (10 cm)
Time to Reach 4% Enrichment T(4%)yrs	Actual	3.514	3.108	2.840	2.737	2.719	2.914
	Fresh Cond.	3.070	2.765	2.531	2.440	2.420	2.593
U-233 Generated (kg) x 10^{-3}		8.793	8.493	8.643	8.805	8.981	8.654
U-233 Consumed (kg) x 10^{-3}		1.267	1.108	1.109	1.123	1.152	1.121
Net U-233 (kg) x 10^{-3}		7.526	7.385	7.534	7.682	7.829	7.533
Th-232 (kg) x 10^{-4}	Actual	18.733	18.381	18.753	19.122	19.489	18.751
	Fresh Cond.	19.635	19.261	19.635	20.013	20.394	19.635
% Burn Up		14.413	13.053	12.837	12.756	12.824	12.957
RT(c) x 10^5	Actual	1.479	1.450	1.450	1.450	1.450	1.450
	Fresh Cond.	1.233	1.233	1.233	1.233	1.233	1.233

(a) Pb front zone thickness
(b) The optimized blanket
(c) RT = $(UBR)_o$ T(4%)/Th(kg)

overall enrichment of 4%. The value of RT is nearly constant because as $(UBR)_0$ increases, T(4%) decreases. Thus, lesser amounts of Th-232 (although small) are depleted.

The results tabulated in Table (V.2) are evaluated using the 25-neutron group flux at clean condition, ϕ_0. More accurate results are obtained if the variation of the flux due to U-233 build up and Th-232 depletion are taken into consideration. This has been done for the optimized blanket #13 and it is described below.

V.5 The Burnup Calculation for the Optimized Blanket

The atomic density of Th-232 and U-233 after 0.7 yr are evaluated at each spatial point in the fuel zone of blanket #13 with a wall load of 1.92 MW/m^2. The fuel zone is divided into 3 subzones and the average density of Th-232 and U-233 in these subzones is evaluated. Using these densities, the flux ϕ_1 after 0.7 years of operation is evaluated using the ANISN code. The flux ϕ_1 is then used to evaluate the Th-232 and U-233 densities at the end of the next time step Δt of 0.7 years. These densities, along with the ANISN code, are then used to evaluate a new flux, ϕ_2, after 1.4 years of operation.

The parameters of interest at the beginning of life, after 0.7 years and 1.4 years of operation are tabulated in Table (V.3). The values of UBR and TBR increase with time due to the enhanced number of neutrons in the blanket from U-233 fissioning. The number of neutrons produced by U-233 fission is larger by a factor of 1.8 than those from Th-232 fission after 0.7 yr. This factor is 3.6 after 1.4 years of operation. The UBR increases by 3.5% after 0.7 yr and

Table (V.3)

Parameters v s. Operating Time for Blanket #13 per D-T Neutron

Parameter	Fresh Cond.	After 0.7 Year	After 1.4 Years
UBR $\equiv Th(n,\gamma)$	0.9338	0.9673	1.0026
$Li^6(n,T)\alpha$	0.5983	0.6379	0.6805
$Li^7(n,tn')\alpha$	0.0271	0.0274	0.0277
TBR (total)	0.6254	0.6652	0.7082
$Th(n,\nu\sigma_f)$	0.0799	0.0822	0.0848
Th(n,2n)	0.0634	0.0628	0.0622
Th(n,3n)x2	0.0379	0.0374	0.0370
Pb(n,2n)	0.4919	0.4920	0.4921
$U^{233}(n,\nu\sigma_f)$	0	0.1474	0.3048

nearly twice as much (7.4%) after 1.4 years. The TBR increases by 6.4% after 0.7 yr and by 13.2% after 1.4 years. The variation of UBR and TBR is nearly linear with time. The U-233 production rate across the fuel zone is shown in Fig. (V.8) at fresh condition, after 0.7 yr and after 1.4 yr along with their percentage increase. The percentage increase in Th(n,γ) reaction rate is nearly linear with time. This is shown in Fig. (V.8) where the percentage increase of U-233 production rate after 1.4 years compared to the corresponding value after 0.7 yr is slightly larger than the percentage increase after 0.7 yr compared to the corresponding value at the beginning of life (clean condition). The largest percentage increase in U-233 production rate occurs at the outer edge of the fuel zone (~ 5.3% after 0.7 yr and ~ 11% after 1.4 yr). The corresponding lowest value occurs at ~ 4 cm through the fuel zone (~ 2.9% after 0.7 yr and 5.8% after 1.4 yr). The net U-233 atoms/cm^3 and the fuel enrichment across the fuel zone after 1.4 yr are shown on Fig. (V.9) and Fig. (V.10), respectively. These curves are evaluated with ϕ_0 only and with ϕ_0 and ϕ_1.

An estimate of the errors in the important integrated design parameters after 1.4 years of operation evaluated by using the fresh condition flux, ϕ_0, is given in Table (V.4) where these parameters are evaluated with ϕ_0 only, then with ϕ_0 and ϕ_1 (the flux after 0.7 yr). From this table one can see that the error obtained, when we use only ϕ_0, is small (~ 2%).

Since the production of tritium increases with time, procedures

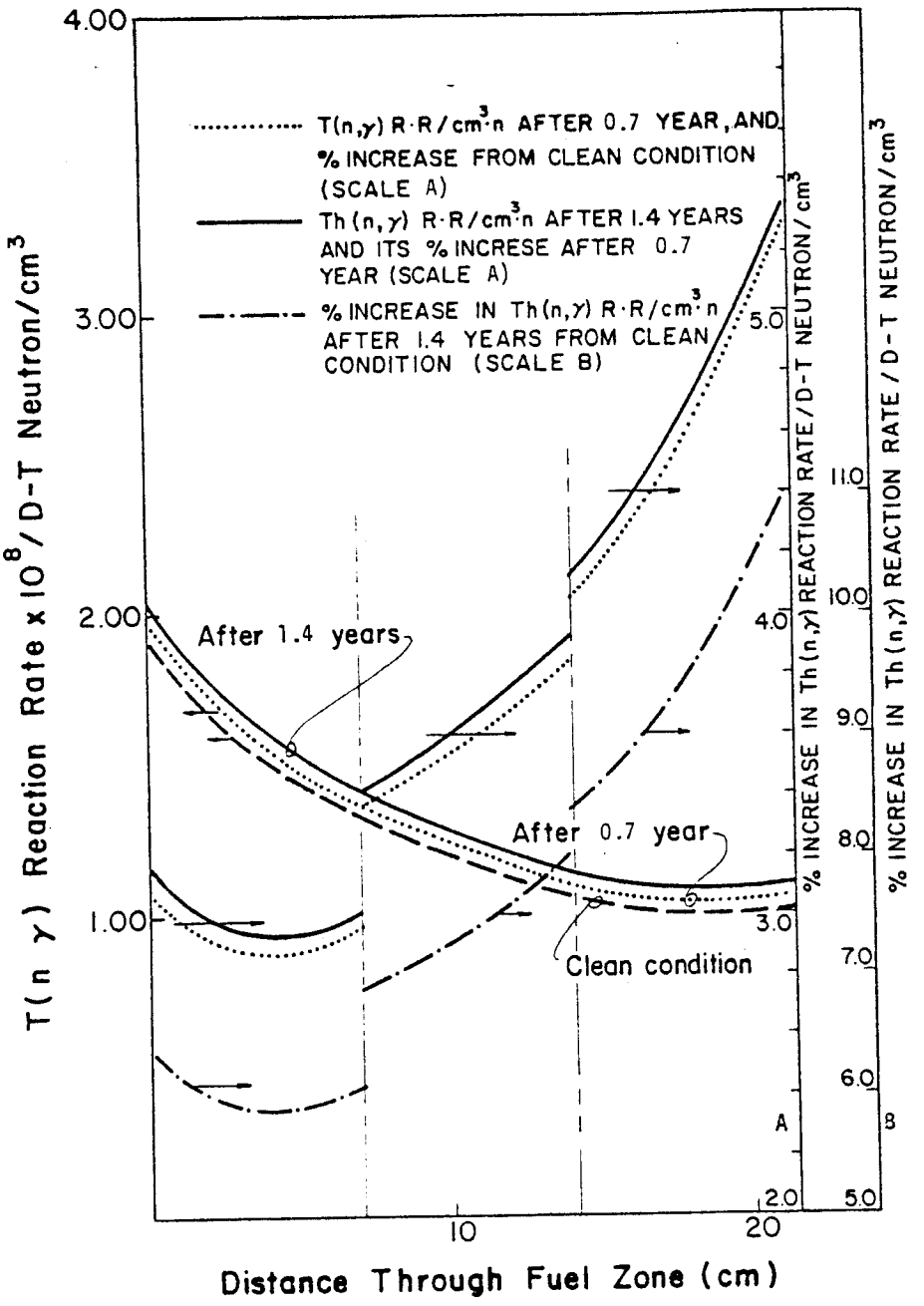

Fig. (V.8): The Th(n,γ) Reaction Rate Vs. Operating Time.

Fig. (V.9): The Net U-233 Atoms/cm^3 After 1.4 year (Wall Load = 1.92 MW/m^2 - Blanket # 13).

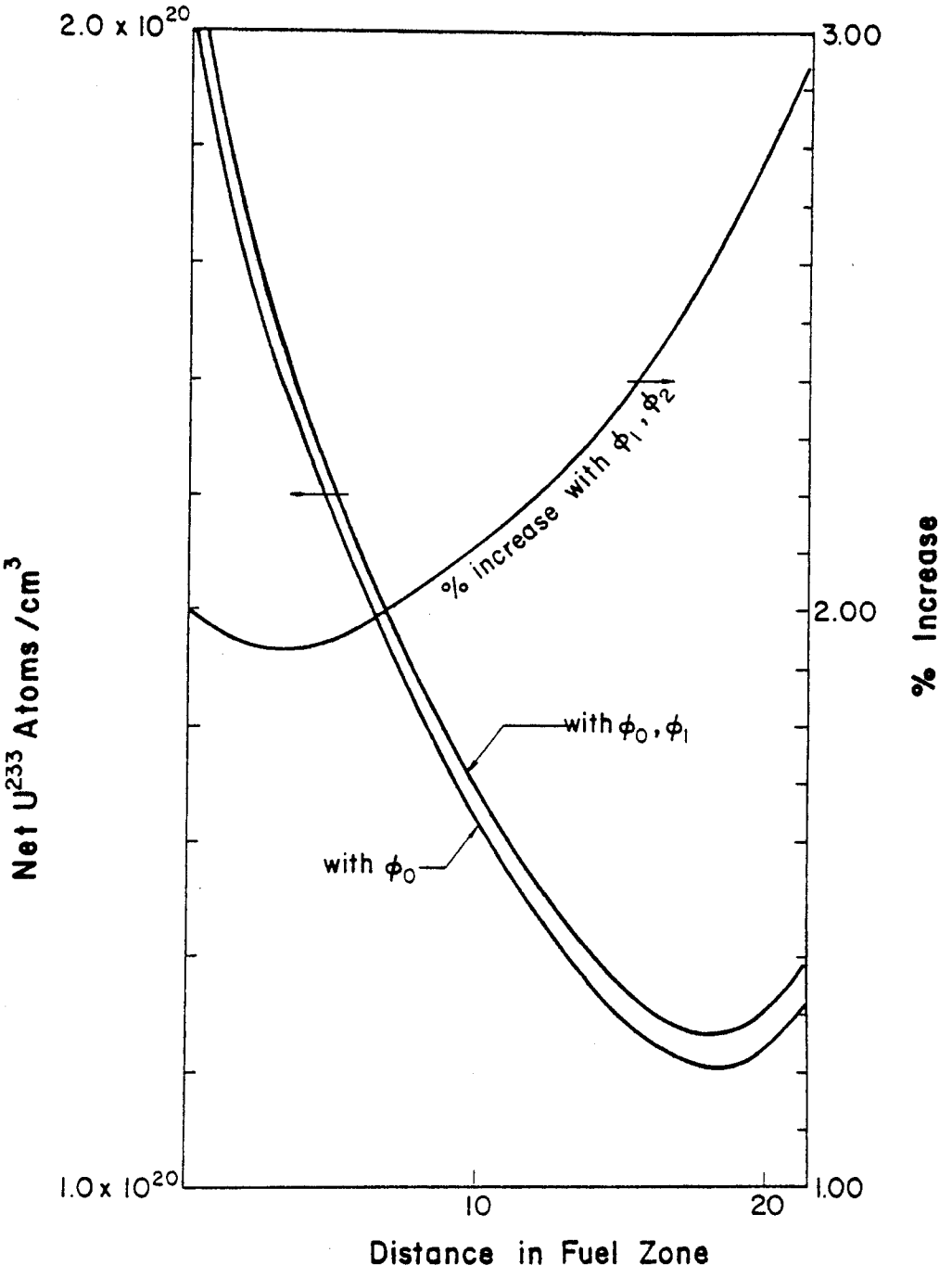

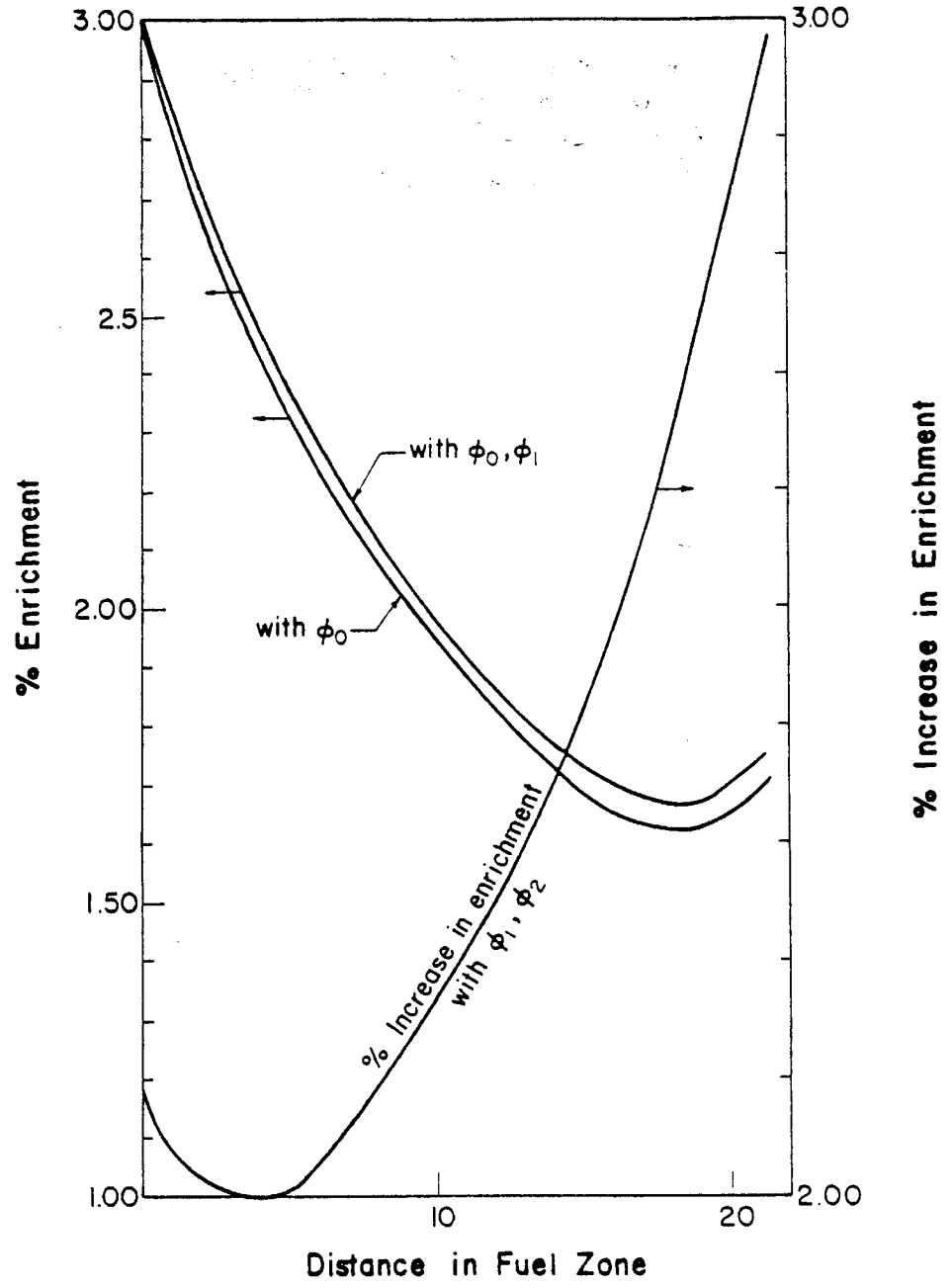

Fig. (V.10): Enrichment in the Fuel Zone After 1.4 year (Wall Load = 1.92 MW/m^2 - Blanket # 13).

Table (V.4)

The Integrated Parameters for Blanket #13 After 1.4 yrs

Parameter	With ϕ_o	With ϕ_o & ϕ_1
Th (kg) x 10^{-5}	1.921	1.920
U-233 Net (kg) x 10^{-3}	3.936	4.022
Enrichment (%)	2.049	2.086
% Change in Th(kg)		-0.05%
% Change in U-233		+2.18%
% Change in Enrichment		+2.2%

for retrieving the non-constant production rate of tritium should be taken. Also, a reliable cooling system to remove the increasing heat that is deposited in the blanket, particularly in the fuel zone, should be designed.

V.6 Effect of Fuel Assembly Rotation on the Fissile Fuel and Tritium Production

The effect of mid-life 180° fuel assembly rotation on the blanket performance (UBR, TBR, etc.) has been studied for the optimized blanket #13.

First, the fuel zone is divided into 3 subzones and the average value of Th-232 and U-233 atomic densities after 1.4 years was evaluated in these subzones using ϕ_0 and ϕ_1. The flux, ϕ_2, in the blanket (before rotation) is then evaluated using the ANISN code along with the other blanket parameters. These parameters are then re-evaluated but with the fuel assembly rotated. In the input to ANISN that is equivalent to replacing the back subzone by the front subzone keeping the middle subzone unchanged. The results are given in Table (V.5) and the fissile fuel production rates are plotted in Fig. (V.11) after 1.4 yrs of operation with and without rotation.

As tabulated in Table (V.5), there is a slight decrease in the fissile fuel and tritium production rates when the fuel assembly is rotated (~ 0.5% for UBR and ~ 0.8% for TBR). The conclusion is that these rates will not significantly change upon rotation. Since this is true for operating times of 1.4 yr, it should be true for shorter operating times.

Table (V.5)

The Parameters of Blanket #13 After 1.4 Yr of Operation With and Without Rotating the Fuel Assembly.*

Parameter	Fuel Assembly Not Rotated	Fuel Assembly Rotated
UBR $\equiv Th(n,\gamma)$	1.0026	0.9980
$Li^6(n,t)\alpha$	0.6805	0.6750
$Li^7(n,Tn')\alpha$	0.0277	0.0277
TBR (total)	0.7087	0.7027
$Th(n,\nu\sigma_f)$	0.0848	0.0845
Th(n,2n)	0.0622	0.0624
Th(n,3n)x2	0.0370	0.0371
Pb(n,2n)	0.4971	0.4921
$U^{233}(n,\nu\sigma_f)$	0.3048	0.2845

* Values given are per D-T neutron

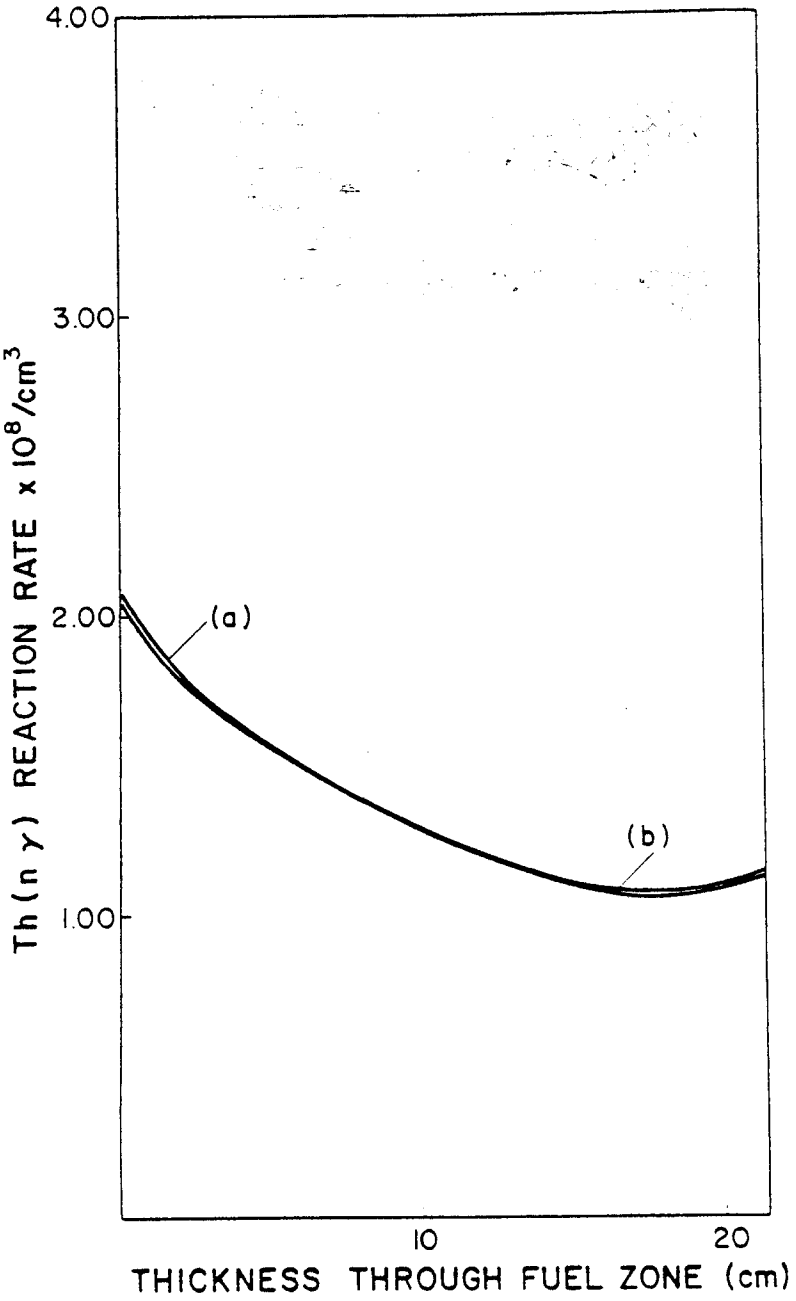

Fig. (V.11): The U-233 Breeding Rate/cm^3 After 1.4 year of Operation Per D-T Neutron;(a) Fuel Assembly Rotated,(b) Fuel Assembly Not Rotated.

This test analysis enables us to rotate the fuel assembly half-way to the time required to reach a specific overall fuel enrichment (~4%). The fuel assembly is then left in the blanket to reach this enrichment. The resulting fissile fuel distribution will be symmetric.

V.7 The Time Needed to Reach 4% Enrichment for the Optimized Blanket

An accurate estimate of the time needed for blanket #13 to reach 4% fuel enrichment, T(4%), is obtained by using the flux in the fresh condition, ϕ_0, the flux after 0.7 yr, ϕ_1, and the flux after 1.4 yr, ϕ_2. The 0.7 yr time step used is large but sufficient since the fission rate and the buildup of U-233 in the blanket is comparatively low. It should be mentioned that although the neutron flux is re-calculated only at the end of each time step (0.7 yr), the Th-232 and U-233 densities are evaluated sequentially at the end of smaller sub-timesteps (1 month).

Two types of approximation were used to evaluate T(4%), the forward difference, F.D. and central difference, C.D., approximation. These approximations are shown schematically on Fig. (V.12) along with the timestep at which each ϕ_0, ϕ_1, and ϕ_2 are assumed to be used in the calculation. The parameters of interest, T(4%), $G_t(T)$, $C_t(T)$, Th(T) and $BU_t(T)$ when blanket #13 reaches 4% enrichment are given in Table (V.6). Determination of T(4%) used in our rotation scheme was based on using ϕ_0, ϕ_1, and ϕ_2 in the C.D. scheme. This is denoted "approximation #4" in Table (V.6). The values of the parameters of

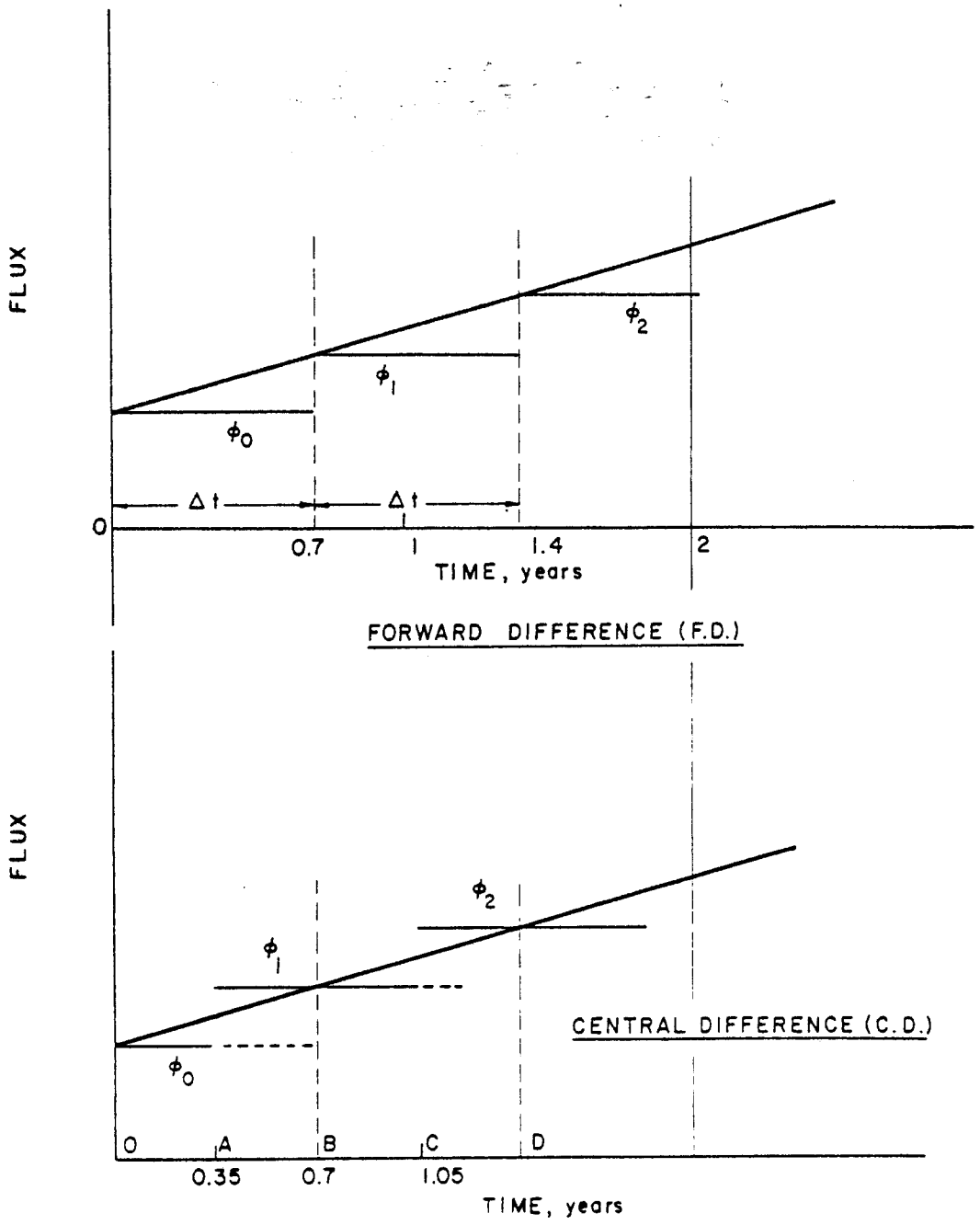

Fig. (V.12): A Schematic Diagram for the Forward (F.D.) and the Central (C.D.) Difference Approximation and the Time Interval.

Table (V6) Parameters of Blanket #13 When Reaching 4% Enrichment (Using Different Approximations)
Wall Load 1.92 MW/m^2

Parameter \ Approx. #	Th & U Depletion is not Considered	Th & U Depletion is Considered			
	Appr. 1	Appr. 2	Appr. 3	Appr. 4	Type of Approx.
T(4%) (yr)	2.593	2.9136	2.7977	2.7175	C.D.
		2.9136	2.8137	2.7490	F.D.
U-233 Generated (kg) x 10^{-3} $G_t(T)$	7.887	8.654	8.6579	8.6629	C.D.
		"	"	8.6626	F.D.
U-233 Consumed (kg) x 10^{-3} $C_t(T)$	0	1.121	1.1251	1.1052	C.D.
		"	1.1252	1.1302	F.D.
Net U-233 (kg) x 10^{-3}	7.887	7.5331	7.5327	7.5578	C.D.
		7.5331	7.5327	7.5323	F.D.
Th-232 (kg) x 10^{-5} Th(kg)	1.964	1.8751	1.8751	1.8749	C.D.
		"	"	1.8750	F.D.
% Burn-Up $BU_t(T)$	0	12.96	12.99	12.76	C.D.
		"	"	13.05	F.D.
Enrichment %	4	4	4	4	Both

interest using other approximations are introduced in Table (V.6) comparison. These approximations are:

Approximation 1: ϕ_0 is used only; Th-232 and U-233 depletion is not considered.

Approximation 2: ϕ_0 is used only; Th-232 and U-233 depletion is considered.

Approximation 3: ϕ_0 and ϕ_1 are used; Th-232 and U-233 depletion is considered.

Approximation 4: ϕ_0, ϕ_1, and ϕ_2 are used; Th-232 and U-233 depletion is considered.

The values in Table (V.6) are given for both F.D. and C.D. approximations. From this table we note that allowing for U-233 and Th-232 depletion increases the value of T(4%). Also, the F.D. approximation overestimates this time.

From Table (V.6), the time needed to reach 4% enrichment for the optimized blanket is 2.72 yr. The U-233 generated is ~8.66×10^3 kg, the U-233 consumed is ~1.11×10^3 kg, the net U-233 is ~7.56×10^3kg and the Th-232 left in the blanket is ~1.87×10^5 kg.

The time needed to reach other values of enrichment (using different approximations in the C.D. case) can be obtained from Fig. (V.13) which illustrates the variation of the enrichment with time. One notices that this variation is nearly linear.

As expected, approximation 4 gives shorter time to reach a given enrichment compared to other approximations.

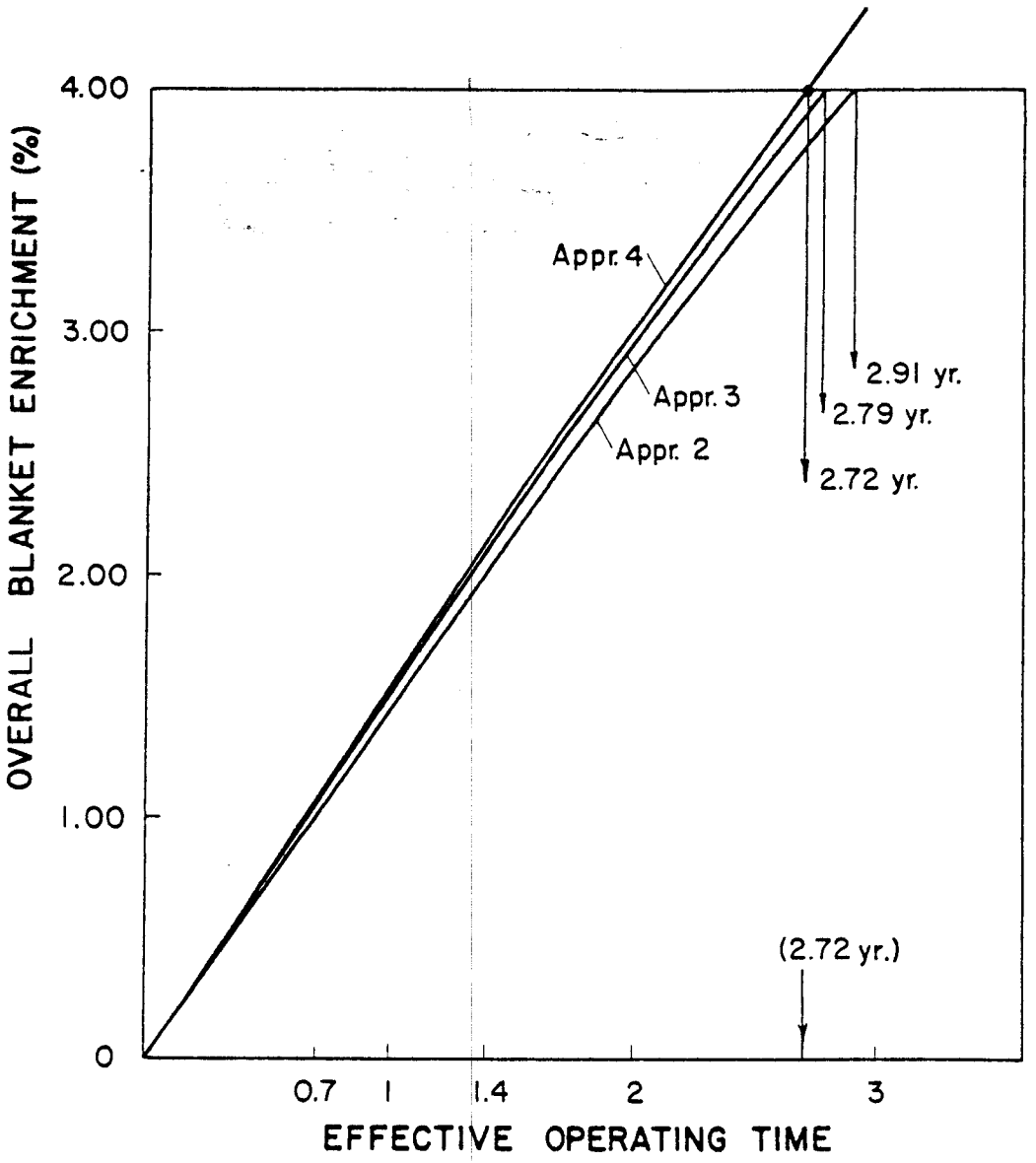

Fig. (V.13): The Overall Blanket Enrichment Vs. Operating Time (Wall Load = 1.92 MW/m^2).

V.8 Conclusion

The time for the optimized blanket to reach 4% enrichment is calculated to be ~2.72 yr. Accordingly, the 180° rotation is done after ~1.4 yr. When the fuel assembly is left in the blanket to complete the 2.72 yr, the distribution of the net U-233 atoms across the fuel assembly will be symmetric. This distribution is shown in Fig. (V.14) where the net U-233 atoms distribution after 2.72 yr without rotation is also shown for comparison. The total Th-232 used in the spherical model of this blanket is ~1.96 x 10^5 kg at fresh condition. After 2.72 yr of continuous operation, the Th-232 present is 1.87 x 10^5 kg. The net U-233 produced is 7.56 x 10^3 kg. Just 12.7% of the fuel produced is burned up in the hybrid and the overall enrichment is then ~4%. As shown in Fig (V.14), the maximum value of U-233 atomic density across the fuel assembly is 3.1 x 10^{20} atoms/cm^3 and occurs at the fuel assembly's edges. The minimum value, which is at the assembly's center, is 2.47 x 10^{20} atoms/cm^3. The corresponding values of the enrichment are 4.69% and 3.75%, respectively. The maximum to minimum value is 1.26 for both. Further study of the performance of this fuel assembly in a LWR is needed to provide information regarding the heat transfer and the radiation damage level with such an enrichment distribution across the fuel assembly.

As a general notice, it has been found that the computational time devoted to performing the neutronics study in the fusion-fission systems, such as the SOLASE-H, is larger compared to a pure fusion

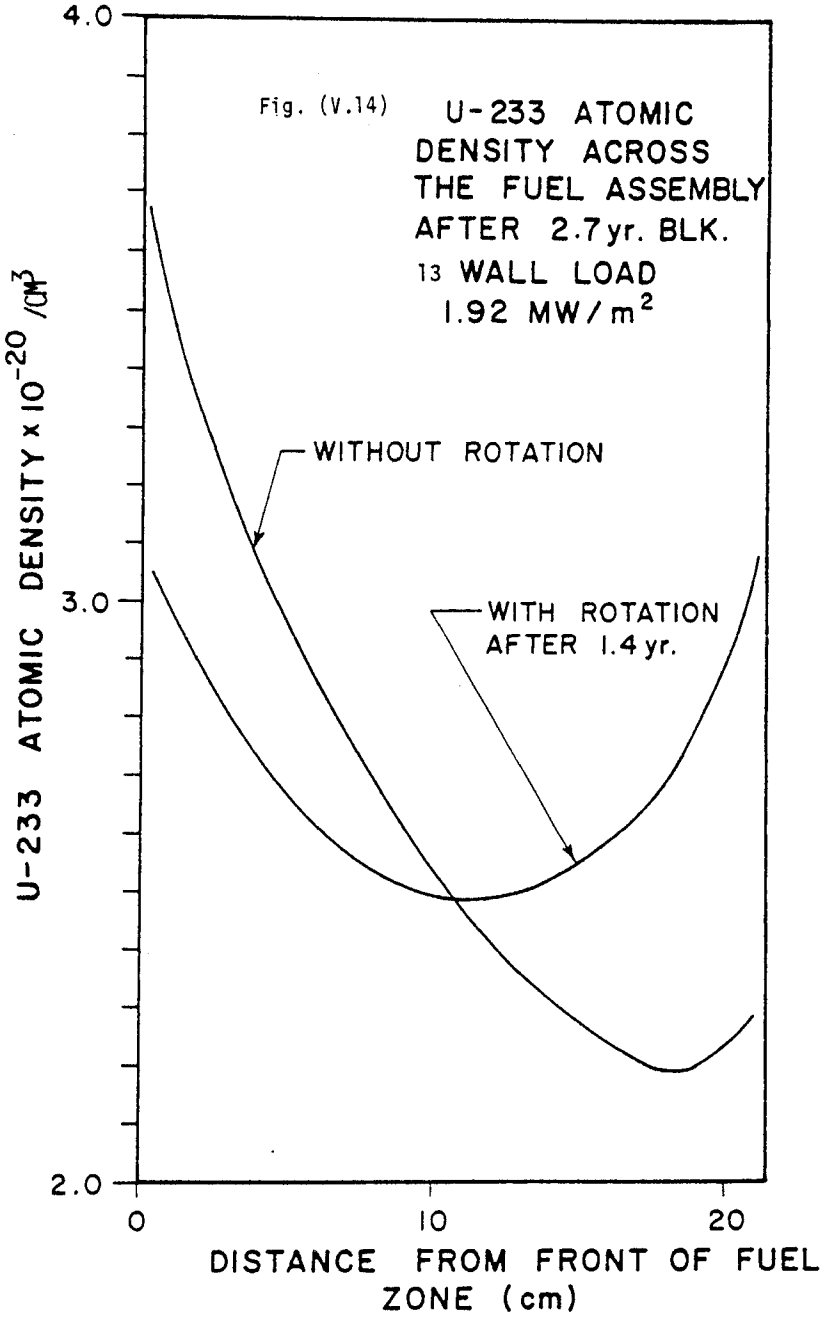

Fig. (V.14): The U-233 Atomic Density Across the Fuel Assembly After 2.7 years (Blanket # 13 - Wall Load = 1.92 MW/m^2).

system. This is due to fissioning in the fertile nuclides present in the blanket. Because of the nature of the 14.1 MeV neutrons and fission neutrons, a mathematical model is developed to separate the transport equation used to solve for the neutron flux, into two parts. The first part is used to solve for the energetic neutron source while the second part is used to solve for the subsequent neutrons generations from fissioning in the fertile materials present in the blanket. Due to using more simplifications when treating the second part, a substantial reduction in the computational cost is obtained (50%). In the next chapter we present this study along with a sensitivity theory to test for the applicability of the separation scheme. An elaborated sensitivity analysis applied for the SOLASE-H, will be given in later chapters.

REFERENCES

1. Youssef, M.Z, Conn, R.W. and Moses, G., "Neutronics Optimization Studies for a Proliferation Resistant Fuel Assembly From a Fusion-Fission Fuel Factory, SOLASE-H", UWFDM-263, Fusion Research Program, The University of Wisconsin, (Oct. 1978).

2. Conn, R.W., et. al., "SOLASE-H, A Laser Fusion Hybrid Reactor Study", U FDM-274, Fusion Research Program, The University of Wisconsin, 1978. Also, Trans. Am. Nuc. Soc., 27, 58 (1978).

3. Youssef, M.Z., Conn, R.W., and Moses, G., "Blanket Neutronics Studies for the SOLASE-H Hybrid Reactor", Trans. Am. Nucl.Soc., 32,35-38 (1979)

4. T.R. England, "CINDER - A One Point Depletion and Fission Product Program", WAPD-TM-344, Westinghouse Electric Corp., Pittsburgh, Penn. (1964).

5. M.J. Bell, "ORIGIN - Isotope Generation and Depletion Code", ORNL-4628, Oak Ridge National Lab., May (1973).

6. W.W. Engle, Jr., "A User's Manual for ANISN", RISC-CC-82, Oak Ridge National Lab. (1967).

7. K.R. Schultz, R.H. Brogli, G.R. Hopkins, M. Jonzen, and G.W. Shirley, "A U-233 Fusion-Fission Power System Without Reprocessing", A Preliminary Report, General Atomic GA-A-14635 - UC-Code, Sept. (1977).

8. S.F. Su, G.L. Woodruff, N.J. McCormick, "A High-Gain Fusion-Fission Reactor for Producing U-233", University of Washington, Nucl. Tech., Vol. 29, pg. 392, June (1976).

9. A.C. Cook and J.A. Maniscalco, "U-233 Breeding and Neutron Multiplying Blankets for Fusion Reactors", Lawrence Livermore Lab. (LLL), Reprint UCRL-77284, Sept. (1975).

10. J.A. Maniscalo, "A Conceptual Design Study for Laser Fusion Hybrid", LLL Reprint UCRL-78682, Sept. (1976).

11. See the Proceedings US-USSR Symposium on Fusion-Fission Reactors, July (1976).

12. See the Third ANS Topical Meeting on the Technology of Controlled Nuclear Fusion, May 9-11, (1978).

Chapter VI

A SEPARATION METHOD FOR THE TRANSPORT EQUATION AND SENSITIVITY THEORY FOR FUSION-FISSION HYBRID ANALYSIS

VI.1 Introduction

A computational technique which can be used to solve the transport equation in a fusion-fission hybrid system is described in this chapter. Such a system is characterized by a highly energetic external neutron source and fissionable materials in the blanket.

Conventionally, the distribution of neutrons can be obtained by solving the transport equation which is basic in the neutronic analysis of fission,[1-3] fusion,[4-6] and fusion-fission hybrid reactors. The Monte Carlo,[11-13] the multi-group P_L[14] and multi-group discrete ordinate S_N[1] are examples of solution techniques. The linearity of the transport equation permits the separation of the equation into two parts. Different methods or approximations can thus be employed. Related work in this connection has been carried out by V. Kotov et. al.[15] who analyzed the sensitivity of hybrid system parameters to nuclear data uncertainties using a Monte Carlo technique to describe neutrons in the high energy range. In our analysis presented in this chapter, the transport equation is separated into two parts and a large number of energy groups and high order angular scattering are included in a discrete ordinate S_N method to describe accurately the first generation neutrons produced by the fusion source. Fission is treated only as a part of the total capture cross section. A fission source for the

second part is generated and the subsequent neutron spectrum associated with fission-produced neutrons is described using a few group method with low order scattering. The total integrated parameters of interest are the summation of contributions from both parts.

The sensitivity theory, which is based on the perturbation technique, is used to test the applicability of the separation method. In particular, it is used to demonstrate that the use of a low order scattering description when solving the second part of the problem will result in an insignificant error in the response of interest. In the subsequent chapters, detailed sensitivity and uncertainty analyses are carried out to investigate the impact of nuclear data uncertainties on different design parameters of the SOLASE-H blanket. In the study presented in this chapter, an expression for the sensitivity coefficient, S, defined as the change in a design parameter, R, to a unit alteration in a system parameter (i.e., cross section) is developed and is used in the context of the separation method.

VI.2 The Theory

VI.2.A Separation of the Transport Equation Into Two Parts

The time-independent neutron transport equation and its adjoint equation are

$$\hat{L}\,\Phi = S(\bar{r},E,\bar{\Omega}) \qquad \text{(VI.1)}$$

$$\hat{L}^{*}\,\Phi^{*} = \Sigma_{r}(\bar{r},E)\ . \qquad \text{(VI.2)}$$

The operators $\hat{L}$ and $\hat{L}^{*}$ are

$$\hat{L}\,\Phi = \bar{\Omega}\cdot\nabla\,\Phi\,(\bar{r},E,\bar{\Omega}) + \Sigma\,(\bar{r},E)\,\Phi\,(\bar{r},E,\bar{\Omega})$$

$$- \int_{E'} dE' \int_{\bar{\Omega}} d\bar{\Omega}'\ \Sigma\, p(\bar{r},E',\bar{\Omega}'\rightarrow E,\bar{\Omega})\,\Phi\,(\bar{r},E',\bar{\Omega}') \qquad \text{(VI.3)}$$

$$\hat{L}^{*}\,\Phi^{*} = -\,\bar{\Omega}\cdot\nabla\,\Phi^{*}\,(\bar{r},E,\bar{\Omega}) + \Sigma(\bar{r},E)\,\Phi^{*}(\bar{r},E,\bar{\Omega})$$

$$- \int_{E'} dE' \int_{\bar{\Omega}'} d\bar{\Omega}'\ \Sigma\, p(\bar{r}\ ,E\ ,\bar{\Omega}\rightarrow E',\bar{\Omega}')\Phi^{*}(\bar{r},E',\bar{\Omega}') \qquad \text{(VI.4)}$$

where $\Sigma(\bar{r},E)$=total macroscopic cross-section at position $\bar{r}$ and energy E.

$p(\bar{r},E',\bar{\Omega}',\rightarrow E,\bar{\Omega})$≡the differential scattering function, It gives the probability of a neutron of energy E' at position $\bar{r}$ with a direction $\bar{\Omega}'$ to reappear with energy E and direction $\bar{\Omega}$ at position $\bar{r}$ upon encountering a collision

and

$\Phi(\bar{r},E,\bar{\Omega}),\Phi^{*}(\bar{r},E,\bar{\Omega})$≡the forward and adjoint angular fluxes of the system at $\bar{r}$,E, and $\bar{\Omega}$.

$S(r,E,\bar{\Omega})$≡the external source per unit volume per unit time emitted at $\bar{r}$ with energy in dE about E and direction $d\bar{\Omega}$ about Ω.

$\Sigma_{r}(\bar{r},E)$≡the source for the adjoint flux equation, the response function. We note that

$$\Sigma(\bar{r},E)\ p(\bar{r},E',\bar{\Omega}'\rightarrow E,\bar{\Omega}) = \sum_{x} \Sigma_{x}(\bar{r},E)\ p_{x}(\bar{r},E',\bar{\Omega}'\rightarrow E,\bar{\Omega})\ ,$$

where the summation over "x" includes the elastic, nonelastic, and fission events and p is normalized to the appropriate number of secondary

neutrons per reaction.[3] An integrated response functional, R, is given by

$$R = \langle \Sigma_r, \Phi \rangle = \langle \Phi^*, S \rangle \tag{VI.5}$$

where the notation $\langle\ ,\ \rangle$ means integration over all the phase space $\bar{\xi} \equiv (\bar{r}, E, \bar{\Omega})$.

The operator $\hat{L}$ is divided into two parts,

$$\hat{L} = \hat{H} - \hat{F} \tag{VI.6}$$

where

$$\hat{H} = \bar{\Omega}\cdot\nabla\Phi + \sum_{j,x} \Sigma_{jx}\Phi - \sum_{j} \sum_{x\neq f} \int_{E'} dE' \int_{\bar{\Omega}'} d\bar{\Omega}'\ \Sigma_{jx}\ p_{jx}(\bar{r}, E', \bar{\Omega}' \rightarrow E, \bar{\Omega})\Phi(\bar{r}, E', \Omega') \tag{VI.7}-a$$

and

$$\hat{F} = \sum_{j=fiss} \sum_{x=f} \int_{E'} dE' \int_{\bar{\Omega}'} d\bar{\Omega}'\ \Sigma_{jx}\ p_{jx}(\bar{r}, E', \bar{\Omega} \rightarrow E, \bar{\Omega})\Phi(\bar{r}, E', \bar{\Omega}') \tag{VI.7}-b$$

The subscript j denotes the elements present in the system at $\bar{r}$, x denotes the reaction type, and f denotes fission. p_{jf} is the probability distribution for neutrons produced in fission weighted by $\nu(E)$, the number of neutrons per fission event. The subscript "fiss" denotes fissile materials.

Let Φ_1 denote the solution to the equation

$$\hat{H}\,\Phi_1 = S \tag{VI.8}$$

where S is the external fusion source. Let Φ_2 denote the solution to

the equation

$$(\hat{H} - \hat{F})\,\Phi_2 = \hat{L}\,\Phi_2 = \hat{F}\,\Phi_1 \equiv S_f \quad , \tag{VI.9}$$

where S_f is the fission source constructed from the solution of Eq. (VI.8). Adding Eqns. (VI.8) and (VI.9) gives

$$\hat{L}\,\Phi = S$$

where

$$\Phi = \Phi_1 + \Phi_2 \quad . \tag{VI.10}$$

Any liniar integral parameter, R, can be described by two parts, i.e.,

$$R = R_1 + R_2 \tag{VI.11}$$

where

$$R_1 = \langle \Sigma_r, \Phi_1 \rangle \tag{VI.11-a}$$

and

$$R_2 = \langle \Sigma_r, \Phi_2 \rangle \tag{VI.11-b}$$

VI.2.B Use of the Adjoint Flux

The adjoint flux, Φ_1^*, for the first part satisfies the equation

$$\hat{H}^*\,\Phi_1^* = \Sigma_r \quad . \tag{VI.12}$$

The corresponding adjoint equation for the second part is

$$(\hat{H}^* - \hat{F}^*)\,\Phi_2^* = \hat{L}^*\,\Phi_2^* = \hat{F}^*\,\Phi_1^* \equiv S_f^* \tag{VI.13}$$

S_f^* is the adjoint source constructed from the solution of Eq. (VI.12).

Upon adding Eqns. (VI.12) and (VI.13) we obtain Eq. (VI.2), the adjoint equation for the system. The total adjoint Φ^* is

$$\Phi^* = \Phi_1^* + \Phi_2^* \tag{VI.14}$$

An expression for R_1 can be obtained by multiplying Eq. (VI.8) by Φ_1^* and Eq. (VI.12) by Φ_1, integrating over phase space $\bar{\xi} \equiv (\bar{r},E,\bar{\Omega})$, and subtracting. The result is

$$R_1 = \langle \Phi_1^*, S \rangle = \langle \Sigma_r, \Phi_1 \rangle \quad . \tag{VI.15}$$

To obtain a similar relation for R_2, multiply Eq. (VI.9) by Φ^* and Eq. (VI.2) by Φ_2, integrate over phase space and subtract the two results.

One obtains

$$R_2 = \langle \Phi^* , \hat{F}\Phi_1 \rangle = \langle \Sigma_r, \Phi_2 \rangle \tag{VI.16}$$

With the adjoint fluxes defined as importance functions,[16] Eq. (VI.16) gives the contribution of the fission source, constructed from the solution of the first part, to the total result R. The contribution to R_2 from a particular fissile material (j=fiss) can be evaluated when the operator $\hat{F}_j$ is used in this equation.

Other expressions for R_2 can be obtained. For example, multiplying Eq. (VI.9) by Φ_1^* and Eq. (VI.12) by Φ_2, integrating over phase space and subtracting, will give

$$R_2 = \langle \Phi_1^*, \hat{F}\Phi \rangle = \langle \Sigma_r, \Phi_2 \rangle \tag{VI.16)-a}$$

where Eqns. (VI.6) and (VI.10) have been used. Similarly, when Eq.

(VI.8) is multiplied by Φ_2^* and Eq. (VI.13) is multiplied by Φ_1, integration over phase space and subtraction gives

$$R_2 = \langle \Phi_2^*, S \rangle = \langle \Phi^*, \hat{F}\Phi_1 \rangle \quad , \qquad \text{(VI.16)-b}$$

where the relation $L^* = H^* - F^*$ and Eq. (VI.14) have been used. Thus,

$$R_2 = \langle \Phi^*, \hat{F}\Phi_1 \rangle = \langle \Phi_1^*, \hat{F}\Phi \rangle = \langle \Phi_2^*, S \rangle \qquad \text{(VI.16)-c}$$

From Eqns. (VI.5) and (VI.11)

$$R = R_1 + R_2 = \langle \Phi^*, S \rangle \qquad \text{(VI.17)}$$

Using Eqns. (VI.15) and (VI.16) in Eq. (VI.17), one finds

$$\langle \Phi^*, S \rangle = \langle \Phi_1^*, S \rangle + \langle \Phi^*, \hat{F}\Phi_1 \rangle \quad . \qquad \text{(VI.17)-a}$$

Eq. (VI.17)-a establishes a relation between the adjoint flux of the first part, the total adjoint flux, and the external source. Thus, a mixed technique can be used to evaluate R where Φ_1 is used to evaluate R_1 using Eq. (VI.11)-a, and Φ^* is used to evaluate R_2 using Eq. (VI.16).

VI.2.C The Relative Sensitivity Coefficient for External Sources $S^{(1)}$

From Eqns. (VI.8) and (VI.12) for the unperturbed system we have

$$\hat{H}_u \, \Phi_1^u = S \qquad \text{(VI.18)}$$

$$\hat{H}_u^* \, \Phi_1^{*u} = \Sigma_{ru} \quad . \qquad \text{(VI.19)}$$

The corresponding equations for the perturbed system are

$$\hat{H}_p \, \Phi_1^p = S \qquad \text{(VI.20)}$$

$$\hat{H}_p^* \, \Phi_1^{*p} = \Sigma_{rp} \; . \qquad \text{(VI.21)}$$

Subtracting Eq. (VI.19) from Eq. (VI.21), subtracting $\hat{H}_p^* \Phi_1^{*u}$ from both sides, multiplying by Φ_1^p, and integrating over phase space gives

$$\delta R_1 = \langle \Phi_1^p, -\delta\hat{H}^* \, \Phi_1^{*u} \rangle + \langle \delta \, \Sigma_r, \Phi_1^p \rangle \qquad \text{(VI.22)}$$

where

$$\delta R_1 = \langle \Sigma_{rp}, \Phi_1^p \rangle - \langle \Sigma_{ru}, \Phi_1^u \rangle \qquad \text{(VI.23)}$$

and

$$\delta H^* = \hat{H}_p^* - \hat{H}_u^* \qquad \text{(VI.24)-a}$$

$$\delta \Sigma_r = \Sigma_{rp} - \Sigma_{ru} \; . \qquad \text{(VI.24)-b}$$

Assume that for any element j and cross-section type x the perturbation is proportional to the corresponding unperturbed value in all regions of phase space where the perturbation takes place,[17-24] i.e.,

$$\Sigma_{px} \, p_x \, (\bar{r}, E, \bar{\Omega} \rightarrow E', \bar{\Omega}') = c \, \Sigma_{ux} \, p_x \, (\bar{r}, E, \bar{\Omega} \rightarrow E', \bar{\Omega}') \qquad \text{(VI.25)-a}$$

with

$$\Sigma_{px}(\bar{r}, E) = c \, \Sigma_{ux}(\bar{r}, E) \; . \qquad \text{(VI.25)-b}$$

The factor c is a constant, independent of $\bar{r}$, E, E', $\bar{\Omega}$, j, and $\bar{\Omega}'$ in all regions in phase space where $c \neq 1$. The quantity δc is c-1. Therefore, Eq. (VI.22) becomes [Note in the following that $H_{u,x}^*$ (or $L_{u,x}^*$) is the

part of H_u^* (or L_u^*) corresponding to the cross section perturbed x; and x = r, the response function.]

$$\delta R_1 = \delta c \{-\langle \Phi_1^p, \hat{H}_{u,x}^* \Phi_1^{*u} \rangle + \langle \Sigma_{ru}, \Phi_1^p \rangle\} \qquad \text{(VI.26)}$$

where it is understood that integration in Eq. (VI.26) is to be performed only over the perturbed regions of phase space where $\delta c \neq 0$.

The relative sensitivity coefficient of the first part, $S^{(1)}$ (associated with the external source) is defined as the relative change in R_1 per unit change in the value of δc. If δc is small, we replace Φ^p by Φ^u. In this case, $S^{(1)}$ is given by

$$S^{(1)} = \frac{\delta R_1 / R_1}{\delta c} = \frac{1}{R_1} \{-\langle \Phi_1^u, \hat{H}_{u,x}^* \Phi_1^{*u} \rangle + \langle \Sigma_{ru}, \Phi_1^u \rangle\} \qquad \text{(VI.27)}$$

VI.2.D The Relative Sensitivity Coefficient to Fission Sources, $S^{(2)}$

The relative sensitivity coefficient for the second part, $S^{(2)}$, is more difficult to evaluate because the two separated equations, Eqns. (VI.8) and (VI.9), are coupled through the fission source, $\hat{F}\,\Phi_1$. For the perturbed and the unperturbed system, we have

$$\hat{L}_u \Phi_2^u = \hat{F}_u \Phi_1^u \qquad \text{(VI.28)}$$

$$\hat{L}_u^* \Phi_u^* = \Sigma_{ru} \qquad \text{(VI.29)}$$

and

$$\hat{L}_p \Phi_2^p = \hat{F}_p \Phi_1^p \qquad \text{(VI.30)}$$

$$\hat{L}_p^* \Phi^{*p} = \Sigma_{rp} \quad . \qquad \text{(VI.31)}$$

Subtracting Eq. (VI.29) from Eq. (VI.31), subtracting $\hat{L}_p^* \Phi^{*u}$ from both sides, transferring the term $L_u^* \Phi^{*u}$ to the right side, multiplying by

Φ_2^p, and integrating over phase space, the left side (L.H.S.) becomes

$$\begin{aligned} \text{L.H.S.} &= \langle \Phi_2^p, L_p^* \, \Phi^{*p} \rangle - \langle \Phi_2^p, L_p^* \, \Phi^{*u} \rangle \\ &= \langle \Sigma_{rp}, \Phi_2^p \rangle - \langle \Phi^{*u}, \hat{F}_p \, \Phi_1^p \rangle \end{aligned} \qquad \text{(VI.32)-a}$$

where Eqns. (VI.30) and (VI.31) have been used. However,

$$\hat{F}_p = \hat{F}_u + \delta\hat{F} \qquad \text{(VI.33)-a}$$

$$\Phi_1^p = \Phi_1^u + \delta\Phi_1 \quad , \qquad \text{(VI.33)-b}$$

so that Eq. (VI.32)-a becomes

$$\begin{aligned} \text{L.H.S.} &= \langle \Sigma_{rp}, \Phi_2^p \rangle - \langle \Phi^{*u}, \hat{F}_u \, \Phi_1^u \rangle - \delta R_c \\ &= \delta R_2 - \delta R_c \end{aligned} \qquad \text{(VI.32)-b}$$

where

$$\delta R_c = \langle \Phi^{*u}, \delta\hat{F} \; \Phi_1^u \rangle + \langle \Phi^{*u}, (\hat{F}_u + \delta\hat{F}) \delta\Phi_1 \rangle \qquad \text{(VI.34)}$$

and

$$\delta R_2 = \langle \Sigma_{rp}, \Phi_2^p \rangle - \langle \Sigma_{ru}, \Phi_2^u \rangle \qquad \text{(VI.32)-c}$$

The right side (R.H.S.) is

$$\text{R.H.S.} = \langle \Phi_2^p, -\delta\hat{L}^* \Phi^{*u} \rangle + \langle \delta\Sigma_r, \Phi_2^p \rangle \qquad \text{(VI.32)-d}$$

so that δR_2 is

$$\delta R_2 = \langle \Phi_2^p, -\delta\hat{L}^* \Phi^{*u} \rangle + \langle \delta\Sigma_r, \Phi_2^p \rangle + \delta R_c \quad . \qquad \text{(VI.35)}$$

In Eq. (VI.35), δR_c is the variation in the coupling term between the

two parts of the problem. As with Eqns. (VI.25) to (VI.27), the sensitivity coefficient of the second part associated with the fission source is

$$S^{(2)} = \frac{\delta R_2/R_2}{\delta c} = S_c^{(2)} + S_{uc}^{(2)} \tag{VI.36}$$

where $S_c^{(2)}$ and $S_{uc}^{(2)}$ are the coupled and uncoupled coefficient, respectively. Here,

$$S_c^{(2)} = \frac{1}{R_2 \delta c} \{<\Phi^{*u}, \delta\hat{F}\Phi_1^u> + <\Phi^{*u}, (\hat{F}_u + \delta\hat{F})\delta\Phi_1>\} \tag{VI.37}$$

$$S_{uc}^{(2)} = \frac{1}{R_2} \{<\Phi_2^u, -\hat{L}^*_{u,x}\Phi^{*u}> + <\Sigma_{ru}, \Phi_2^u>\} \tag{VI.38}$$

In Eqn. (VI.38), we assume $\Phi_2^p \cong \Phi_2^u$ as is the case for small perturbation. The total sensitivity coefficient of the system, S, is

$$S = \frac{R_1 S^{(1)} + R_2 S_{uc}^{(2)}}{R_1 + R_2} + \frac{R_2 S_c^{(2)}}{R_1 + R_2} \tag{VI.39}$$

Using $\delta\phi_1 = 0$ leads to an error in evaluating $S_c^{(2)}$ if Eqns. (VI.34) and (VI.37) are used. The total sensitivity coefficient, S, evaluated from Eq. (VI.39) is thus <u>not</u> equal to the corresponding value given by the once-through (no separation) calculation. Accurate evaluation of $S_c^{(2)}$ requires a direct calculation to obtain $\delta\Phi_1$.

It is possible, however, to evaluate the total sensitivity coefficient, S, without performing a direct calculation of $\delta\Phi_1$ by noting that the total variation in the integrated result, R, is given by

$$\delta R = <\Phi^{*u}, -\delta\hat{L}\Phi^p> + <\delta\Sigma_r, \Phi^p> \tag{VI.40}$$

Approximating ϕ^p by ϕ^u and using $\phi^u = \phi_1^u + \phi_2^u$ means we can rewrite Eq. (VI.40) as

$$S = \frac{\delta R/R}{\delta c} = \frac{1}{R_1+R_2}\left[<\Phi^{*u}, -\hat{L}_u \Phi_1^u> + <\Sigma_{ru}, \Phi_1^u> + R_2 S_{uc}^{(2)}\right] \qquad \text{(VI.41)}$$

where the assumptions given by Eqns. (VI.25) have been used and $S_{uc}^{(2)}$ is given by Eq. (VI.38). The use of Eq. (VI.41) avoids direct calculation of $\delta\Phi_1$ and is recommended when the separation method is used.

A useful and exact expression which relates $\delta\phi_1$ to the adjoint fluxes of the two parts can be obtained from

$$\delta R = \delta R_1 + \delta R_2. \qquad \text{(VI.42)}$$

Substituting the exact values for δR_1 and δR_2, given respectively by Eqns. (VI.22) and (VI.35), into Eq. (VI.40), using $\Phi^p = \Phi_1^p + \Phi_2^p$ and $\delta\hat{L} = \delta\hat{H} - \delta\hat{F}$, we find

$$<(\Phi^{*u} - \Phi_1^{*u}), -\delta\hat{H}\,\Phi_1^p> = <\Phi^{*u}, \hat{F}_u\,\delta\Phi_1> \qquad \text{(VI.43)}$$

which is exact. In Eq. (VI.43), the difference between the unperturbed adjoint fluxes is used as a weighting function to evaluate the coupling term required when S is evaluated from Eq. (VI.39). However, it is simpler to evaluate S from Eq. (VI.41) as we show in the application section that follows. Define the integral quantities, S_{uc} and D_c, as

$$S_{uc} = \frac{R_1 S^{(1)} + R_2 S_{uc}^{(2)}}{R_1+R_2} \qquad \text{(VI.44)}$$

and

$$D_c = \frac{R_2 S_c^{(2)}}{R_1+R_2} \cdot \qquad \text{(VI.45)}$$

For clarity, we give below the expressions used to evaluate the sensitivity coefficients $S^{(1)}_{jx}$, $S^{(2)}_{jx,uc}$ if cross-section type x is perturbed for element j.

If $x \neq f$ (fission), but x is the response function r, then, for all j, we have

$$S^{(1)}_{jx} = \frac{1}{R_1}\{\int_E dE \int_{\bar{r}} d\bar{r}\, \Sigma_{jx}(\bar{r},E)[-\phi^0_1(\bar{r},R)\phi^{*0}_1(\bar{r},E) + \sum_{\ell=0}^{\infty} \frac{2\ell+1}{4\pi} \cdot \int_{E'} dE'\, \phi^{\ell}_1(\bar{r},E)\, p^{\ell}_{jx}(\bar{r},E\to E')\, \phi^{*\ell}_1(\bar{r},E')] + \int_E dE \int_{\bar{r}} d\bar{r}\, \Sigma_r(\bar{r},E)\, \phi^0_1(\bar{r},E)\} \qquad \text{(VI.46)}$$

and

$$S^{(2)}_{jx,c} = \frac{\delta R_{jx,c}/R_2}{\delta c} = \frac{1}{R_2 \delta c} \sum_{j'=fiss} \langle \Phi^*, \hat{F}_{j'}, \delta\Phi_1 \rangle \quad . \qquad \text{(VI.47)}$$

The value of $S^{(2)}_{jx,uc}$ is given by Eq. (VI.46) if $\phi^{\ell}_2, \phi^{*\ell}$, and R_2 replace $\phi^{\ell}_1, \phi^{*\ell}_1$, and R_1 respectively. In Eq. (VI.47), $\delta R_{jx,c}$ is obtained from Eq. (VI.34) with $\delta\hat{F}=0$ since $x \neq f$. The summation over j' is taken for all fissionable materials in the fusion blanket. The coefficients $\phi^{\ell}, \phi^{*\ell}$ and p^{ℓ}_{jx} are given by[3]

$$\phi^{\ell} = \int \Phi(\bar{r},E,\bar{\Omega})\, P_{\ell}(\mu)\, d\bar{\Omega}$$

$$\phi^{*\ell} = \int \Phi^*(\bar{r},E,\bar{\Omega})\, P_{\ell}(\mu)\, d\bar{\Omega}$$

$$p^{\ell}_{jx} = \int p_{jx}(\bar{r},E,\bar{\Omega}\to E',\bar{\Omega}')\, P_{\ell}(\mu_o)\, d\mu_o \qquad \text{(VI.48)}$$

where $\mu = \hat{z}\cdot\bar{\Omega}$, $\mu_o = \bar{\Omega}\cdot\bar{\Omega}'$, P_{ℓ} is the legendre polynomial of order ℓ,

$p^{\ell}_{jx}(r,E\to E')$ is the ℓ'th legendre moment of the normalized secondary angular distribution for element j and reaction x. It is to be understood that if x=absorption, p^{ℓ}'s are zeros. If $x\neq r$, the last term in Eq. (VI.46) is eliminated. If x=f, x=r, and for j=fiss, we have

$$S^{(1)}_{jf} = \frac{1}{R_1}\{\int_E dE \int_{\bar{r}} d\bar{r}\ \Sigma_{jf}(\bar{r},E)\ [-\phi^0_1(\bar{r},E)\phi^{*0}_1(\bar{r},E)]$$

$$+ \int_E dE \int_{\bar{r}} d\bar{r}\ \Sigma_r(\bar{r},E)\ \phi^0_1(\bar{r},E)\} \qquad \text{(VI.49)}$$

$$S^{(2)}_{jf,uc} = \frac{1}{R_2}\{\int_E dE \int_{\bar{r}} d\bar{r}\ \Sigma_{jf}(\bar{r},E)[-\phi^0_2(\bar{r},E)\ \phi^{*0}(\bar{r},E)$$

$$+ \int_{E'} dE'\ \phi^0_2(\bar{r},E)\ \bar{\nu}(E)\ \chi(E')\ \phi^{*0}(\bar{r},E')]$$

$$+ \int_E dE \int_r d\bar{r}\ \Sigma_r(\bar{r},E)\ \phi^0_2(\bar{r},E)\} \qquad \text{(VI.50)}$$

$$S^{(2)}_{jf,c} = \frac{\delta R_{jf,c}/R_2}{\delta c} = \frac{1}{R_2}\langle\Phi^*,\ \hat{F}_j\ \Phi^p_1\rangle + \frac{1}{R_2\delta c}\sum_{j'=fiss}\langle\Phi^*,\hat{F}_{j'}\ \delta\Phi_1\rangle \qquad \text{(VI.51)}$$

where Eq. (VI.34) has been used to express $S^{(2)}_{jf,c}$ and we have taken $\delta\hat{F}_j=\delta c\hat{F}_j$. $\chi(E')$ is the probability that neutrons appear with energy E' following fission.

The sensitivity of the result R to the number of terms considered in the expression of the transfer probability distribution function,

p_{jx}, can be evaluated for a particular element j and a particular reaction type x by truncating the legendre expansion at ℓ=L. If scattering is highly anisotropic, as is the case with a fusion neutron source (the first part), a larger number of terms must be retained.

VI.3 Applications

VI.3.A Results for Different Separation Approximations

The method of separation has been applied to the analysis of the laser drive fusion-fission hybrid reactor, SOLASE-H,developed in Chapters IV and V. One-dimensional spherical geometry has been adopted to carry out the calculations with the neutron transport code "ANISN". The schematic describing the blanket is shown in Fig. (V.1).

For reference, we use the separation method to analyze the blanket shown on Fig. (V.1) using the same number of neutron energy groups (25) and S_N-P_L order (S_4-P_3) for both parts (Eqns. (VI.8) and (VI.9)). The results presented in the first column of table (VI.1) agree with the standard uncoupled once-through calculation, as expected. However, the separation method shows that most of the contribution to the uranium breeding ratio, UBR, and the tritium breeding ratio, TBR, is due to fusion neutrons (analyzed by the first part). This is likewise anticipated in a blanket designed explicitly to reduce the burnup of fuel bred via fissions such as in the SOLASE-H blanket. In this case, the blanket energy multiplication is likewise low.

To compare different levels of approximations in each part of the separation technique, we have analyzed the SOLASE-H blanket with a

Table (VI.1) Various Integrated Parameters for Different Separation Approximations+

Case / Parameter	Part 1 25-g (S_4-P_3)	Part 1 46-g (S_4-P_3)	Part 2 25-g (S_4-P_3)	Sum Col.2+3	Part 2 25-g (S_2-P_1)	Sum Col.2+5	Part 2 16-g (S_2-P_1)	Sum Col.2+7
	Col.#1	2	3	4	5	6	7	8
Leakage	7.6992-3	6.9206-3	2.9946-4	7.2201-3	2.6235-4	7.1829-3	3.0732-4	7.2279-3
Absorption	1.7019	1.7031	7.7091-2	1.7802	7.7052-2	1.7801	8.0453-2	1.7835
Sum (neutron population)	1.7096	1.7100	7.7390-2	1.7874	7.7314-2	1.7873	8.0760-2	1.7908
(n,2n)+(n,3n)	7.0960-1	7.0960-1	1.7866-4	7.0978-1	1.8043-4	7.0978-1	2.7582-3	7.1236-1
$(n,\nu\sigma_f)$	0	0	1.6892-3	7.8391-2	1.6144-3	7.8316-2	2.2789-3	7.8981-2
External source	1	1	7.6702-2	1	7.6702-2	1	7.6702-2	1
Source+(n,2n)+(n,3n) +$(n+\nu\sigma_f)$	1.7096	1.7096	7.8570-2	1.7882	7.8496-2	1.7881	8.1739-2	1.7913
TBR(^{6}Li): Zone 4	9.8813-2	8.8043-2	3.3683-3	9.1411-2	3.6640-3	9.1707-2	3.6551-3	9.1698-2
Zone 8	4.0139-1	4.4648-1	2.0988-2	4.6747-1	2.1419-2	4.6789-1	2.2652-2	4.6913-1
Zone 10	7.2363-2	8.3050-2	3.8282-3	8.6878-2	3.8061-3	8.6856-2	4.2487-3	8.7298-2
System	5.7257-1	6.1757-1	2.8499-2	6.4607-1	2.8889-2	6.4646-1	3.0556-2	6.4813-1
TBR(^{7}Li): Zone 4	1.2979-2	1.2957-2	4.6910-5	1.3004-8	4.8064-5	1.3005-2	1.4328-4	1.3100-2
Zone 8	1.3864-2	1.3849-2	1.0140-4	1.3950-2	1.1927-4	1.3968-2	4.2475-4	1.4274-2
Zone 10	9.1570-5	9.1695-5	1.9206-7	9.1887-5	5.2957-8	9.1747-5	4.7326-7	9.2168-5
System	2.6929-2	2.6897-2	1.4850-4	2.7046-2	1.6739-4	2.7064-2	5.6850-4	2.7466-2
Total TBR	5.9949-1	6.4447-1	2.8647-2	6.7312-1	2.9057-2	6.7353-1	3.1124-2	6.7559-1
UBR [Th(n,γ)]	8.8858-1	8.2224-1	4.0070-2	8.6231-1	3.9806-2	8.6204-1	3.9652-2	8.6189-1

+ All the results are given per D-T neutron. Calculations have been carried using the one-dimensional transport code, 'ANISN'.

46-group, S_4-P_3 approximation for the first part and several approximations (25-group, S_4-P_3; 25-group, S_2-P_1; and 16-group, S_2-P_1) for the second part related to subsequent fission neutron generations. The results are presented in Table (VI.1).

We note first that the tritium production rate from $^6Li(n,\alpha)t$ reactions has increased from 0.57 to 0.62 (~8%) when more energy groups (46) are used. This is due to a finer group structure in the low energy range where this capture reaction is large. Because of the competition between fissile fuel and tritium production, the UBR is reduced from 0.886 to 0.822 (~8%). The fission source to the second part is effectively unchanged.

In general, the results show that a slight decrease in UBR and a slight increase in TBR occurs when the second part of the problem is solved using lower S_N-P_L and a smaller number of energy groups. The maximum error in the contribution of fission produced neutrons to all reaction rates and to leakage is about 9%. However, the largest error in the total reaction rates or the leakage is less than 1%. Thus, the separation method is advantageous and a low order (or even diffusion theory) treatment of the second and subsequent neutron generations (all fission produced neutrons) lead to a computational cost reduction of a factor of 2 to 3.

VI.3.B Sensitivity Analysis

In this section, we discuss the application of sensitivity analysis by evaluating the sensitivity of the main results to scattering order and to the number of energy groups used to describe the

second and subsequent neutron generations. We also compare results for the total sensitivity coefficient obtained from once-through calculations, from direct calculations to evaluate the coupling coefficient in Eq. (VI.47), and from the expression we have developed, Eq. (VI.41), to avoid direct calculation.

To identify which elements have a large sensitivity coefficient for fissile fuel production, the sensitivity coefficient of the first part, $S_{jx}^{(1)}$, is evaluated for each element present in the SOLASE-H blanket. The one-dimensional sensitivity code, "SWANLAKE",[19] has been used to evaluate the sensitivity coefficients. The cross-section perturbed is the total cross-section. The value of R_1, as given in Table (VI.1), is 0.89 in this case. It turns out that Pb and ^{6}Li have the highest values of $S_{jx}^{(1)}$ (excluding Th).

The sensitivity coefficients for lead, $S_{jx}^{(1)}$ and $S_{jx,uc}^{(2)}$, obtained from the separation method, and S_{jx}, the total coefficient, obtained from the once-through calculation with no separation, are given in the last row of Table (VI.2). In evaluating these coefficients the relevant fluxes using 25-group, S_4-P_3, have been used. The predicted percentage change in the values of these coefficients, when only one term (ℓ=0) is considered in the expansion expressing scattering, is given in the first row. The corresponding predicted changes, when two terms (ℓ=1) and three terms (ℓ=2) are considered, are introduced in the second and third row of Table (VI.2), respectively. One notices from this table that the predicted percentage changes in the sensitivity coefficients $S_{jx}^{(1)}$ and $S_{jx,uc}^{(2)}$, from the corresponding values when ℓ=3,

Table (VI.2) The Sensitivity Coefficients of the Fissile Fuel Breeding Coefficient, UBR, and its % Changes for Pb(n,tot) Cross Section Evaluated for the Total System

Parameters \ Sensitivity Coefficient	$S_{jx}^{(1)}$ 25-g $(S_4-P_3)^+$	$S_{jx,uc}^{(2)}$ 25-g $(S_4-P_3)^*$	$\tilde{S}_{jx}$ Once-Through 25-g $(S_4-P_3)^{++}$	$S_{jx,uc}$
Percentage Changes in Sensitivity Coefficients for Different Lower Order P_L Approximations (ℓ=0)	6.96	2.20-1	5.58	6.66
(ℓ=1)	2.15	6.59-3	1.75	2.05
(ℓ=2)	-2.82-1	8.38-4	1.99-1	-2.69-1
Reference Sensitivity Coefficients Based on P_3 Calculations	2.29-1	2.49-2	1.88-1	2.19-1

\+ $R_1 = 0.89$

* $R_2 = 0.04$

++ $R = 0.93$

increase if lower number of terms are retained in the total scattering cross section-Legendre expansion. These predictions are always much less in $S^{(2)}_{jx,uc}$ than in $S^{(1)}_{jx}$. This holds true for all zones where Pb is present. That is, if lower order of scattering is used when solving for the second part, the change in the contribution R_2 to the total result R(=UBR) will not significantly change. This is consistent with the results shown in Table (VI.1). This is due to the isotropic nature of the fission neutrons source to the second part. One should notice also from Table (VI.2) that the integrated quantity $S_{jx,uc}$, given by Eq. (VI.44), is not equal to the total sensitivity coefficient, S_{jx}, evaluated from the once-through calculation. The difference between the two quantities is the contribution from the coupling between the two parts of the total solution.

To evaluate the coupling term, $D_{jx,c}$, given by Eq. (VI.45), a direct calculation of $\delta\Phi_1$ has been carried out and the result is introduced in Table (VI.3). In this calculation, 1% change in the total cross-section of Pb has been assumed in different zones. Adding $D_{jx,c}$ to $S_{jx,uc}$ gives the total sensitivity coefficient, S_{jx}. Included in Table (VI.3) is the value of S_{jx} evaluated from Eq. (41). It is the same as the value obtained from direct calculation. For comparison, we included in Table (VI.3) the value of S_{jx} evaluated from the once-through calculation.

VI.3.C. Burn-up Calculations

As shown in Chapter V, the fissile fuel production rate per D-T neutron, UBR, changes with time. The value of UBR(t) can be

Table (VI.3) The Sensitivity Coefficients of the Fissile Fuel Breeding Ratio, UBR for PB(n,tot) Cross Section Evaluated by Zone and for the System Using Direct Calculation and Eq. (41)+

Zone	$S^{(1)}_{jx}$	$S^{(2)}_{jx,uc}$	$S_{jx,uc}$	$D_{jx,c}$	$S_{jx,uc} + D_{jx,c}$	S_{jx} Eq. 41	S_{jx} Once-Through Calculation
3	2.05-1	1.97-3	1.96-1	-3.10-2	1.65-1	1.65-1	1.65-1
9	2.38-2	2.29-2	2.37-2	-1.00-4	2.36-2	2.36-2	2.36-2
The System	2.29-1	2.49-2	2.19-1	-3.10-2	1.88-1	1.88-1	1.88-1

+ 25-g (S_4-P_3) approximation is used for both parts as well as the once-through calculation

approximated using the expression

$$UBR(t) \cong UBR_1^0 + \sum_{j'=fiss} \langle \Phi^{*0}, F_{j'}(t)\, \Phi_1^0 \rangle \qquad (VI.52)$$

where

$$UBR_1^0 = \langle \Sigma_{Th}(n,\gamma), \Phi_1^0 \rangle \quad . \qquad (VI.53)$$

In the above equations, the forward flux at the beginning of life, Φ_1^0, is used to evaluate UBR_1^0, which is assumed to be constant. The adjoint flux of the system at the beginning of life, Φ^{*0}, is used to evaluate the contribution to UBR from all fissile materials present in the hybrid blanket at subsequent times. Knowledge of the variation of atomic densities of these fissionable materials is required. Eq. (VI.52) can be used to identify which fissile element contributes most to UBR as function of time.

The results of these calculations for the SOLASE-H blanket are presented in Table (VI.4). The UBR is the total uranium breeding ratio at time t, and UBR_1 and UBR_2 are the corresponding contributions to UBR from the first and second parts of the separated solutions for the neutron flux. We see that the contribution to UBR_2 is primarily from fission in ^{233}U and this increases with time as the ^{233}U builds up. However, the contribution from ^{232}Th fission to UBR_2 decreases slightly with time. In fact, as it has been shown in Chapter V using direct calculations, the fission rate in ^{232}Th is almost constant with time. The value of $^{232}Th(n,\nu\sigma_f)$ reaction rate per fusion event has been evaluated to be 0.0799, 0.0822 and 0.0848 at t=0, t=0.7 yr and t=1.4 yr,

Table (VI.4) Value of UBR Vs. Time Using the Separation Method and Eq. (52)

Time	$UBR_1^{0(*)}$	$UBR_{2j}^{(+)}$ ($j=^{233}U$)	$UBR_{2j}^{(+)}$ ($j=^{232}Th$)	Total UBR_2	Total UBR	UBR From Once-Through Calculation(**)	% Error
t=0	0.8886	0	0.0413	0.0413	0.9299	0.9299	0
t=0.7 yr	0.8886	0.0701	0.0406	0.1107	0.9993	0.9673	+3.31
t=1.4 yr	0.8886	0.1374	0.0401	0.1775	1.0661	1.0026	+6.32

(*) From Eq. (53) using 25-g (S_4-P_3) approximation.

(+) From Eq. (16) using 25-g (S_4-P_3) approximation.

(**) Using 25-g (S_4-P_3) approximations.

respectively. The corresponding values for ^{233}U $(n,\nu\sigma_f)$ fission rate per fusion event were found to be 0.0, 0.1474 and 0.3048 for t=0, 0.7 yr and 1.4 yr, respectively.

VI.4 Conclusions

The method of separation discussed in this chapter can be applied to fusion-fission hybrid systems with a substantial reduction in computational costs and small errors in the predicted integrated results. The method in discrete ordinates is similar to the procedure used by Kotov et. al.[15] where fusion neutron behavior (the first part) is treated by the Monte Carlo technique. Indeed, any transport method can be used. Here, we use high order scattering and discrete ordinates for the zeroth generation and low order P_L (or diffusion theory) for subsequent generations due to fission.

The sensitivity coefficients for both parts of the solution and for the system as a whole has been derived and applied to show that low order scattering can be used to solve for the fision neutron part in hybrid calculations. The method can also be used to identify which element in the system has the greatest impact on a total result (e.g., fissile fuel production).

The adjoint fluxes can be used to evaluate a particular reaction rate. In a hybrid, when the reation rate is the uranium breeding ratio, UBR, we have shown that variation of UBR due to fission in the bred fissile fuel can be accounted for using the beginning-of-life values of the total adjoint flux and the forward flux of the first part. A 6% error in the uranium breeding ratio after about 1.5 years of exposure

is found for the hybrid blanket used in this study.

It can be noticed that the sensitivity treatment developed in this chapter has been devoted to demonstrate the applicability of the separation method with simplifications made when treating the second part of the solution to the transport equation. In this treatment, a 1% uncertainty in the total cross-section at all neutron energies has been assumed. The design parameter of interest can have an appreciable uncertainty due to the present uncertainties associated with the nucelar data base. An elaborated sensitivity and uncertainty analysis is needed to give an estimate to the design parameter uncertainty. This has been carried out for the SOLASE-H blanket and is presented in the next chapters. In the following chapter, the treatment used and the adequacy of the present cross section evaluation are described.

References

1. Weinberg, A.M, Wigner, E.P., "The Physical Theory of Neutron Chain Reactors", University of Chicago Press (1958).

2. Davison, B., "Neutron Transport Theory", Van Nostrand Reinhold Co. (1970).

3. Bell, G.S. and Glasstone, S., "Nuclear Reactor Theory", Van Nostrand Reinhold Co. (1970).

4. Steiner, D., Nucl. Appl. Tech., 9, 83 (1970).

5. "UWMAK-1, A Wisconsin Toroidal Fusion Reactor Design", Report UWFDM-68, Fusion Research Program, The University of Wisconsin, May (1974).

6. Abdou, M.A., Maynard, C.W., "Nuclear Design of the Magnet Shield of Fusion Reactors", Report UWFDM-98, Fusion Research Program, The University of Wisconsin (1973).

7. "DCTR Fusion-Fission Energy Systems Review Meeting", ERDA-4, UC-20, Dec. 3-4, 1974, Germantown, Maryland, Energy Research and Administration (1974).

8. Proceedings of the Second Topical Meeting on the Technology of Controlled Nuclear Fusion", CONF-760935-P2, Sept. 21-23, 1976, Richland, Washington (1976). Refs. 8-10 include the recent conceptual designs of fusion-fission hybrid systems.

9. "Proceedings of US-USSR Symposium on Fusion-Fission Reactors", Hosted by Lawrence Livermore Laboratory, July 13-16 (1976), CONF-760733, July (1976).

10. "Proceedings of the Second Fusion-Fission Energy Systems Review Meeting", U.S. Department of Energy, November 2-3 (1977), Washington, D.C., Vol. I-II, CONF-771155, July (1978). Also see Proc. of the US/USSR Symposium on Fusion-Fission Hybrids, Princeton University, Jan. (1979).

11. Goertzel, G., Kalos, M.H., "Monte Carlo Methods in Transport Problems", in Prog. Nucl. Energy, Series I, Vol. II, Pergamon Press (1958).

12. Cashwell, E.D., Everett, G.J., "The Monte Carlo Method for Random Walk Problems", Pergamon Press (1959).

13. Spanier, J, Gelbard, E.M., "The Monte Carlo Principles and Neutron Transport Problems", Addison-Wesely Publishing Co. (1969).

14. Butler, M.K., Cook, J.M., "Computing Methods in Reactor Physics" (1968).

15. Kotov, V.V., Maynard, C.W., Markovskii, D.V., Shatalov, G., "Analysis of the Sensitivity of Hybrid Reactors to Nuclear Data", I.V. Kurchatove Institute of Atomic Energy, USSR, IAE-2817 (1977).

16. Lewis, J., "Importance - The Adjoint Function", Chap. 2, Pergamon Press, New York (1965).

17. Bartine, D.E., Oblow, E.M., Mynatt, F.R., "Radiation-Transport Cross-Section Senstivity Analysis - A General Approach Illustrated for a Thermonuclear Source in Air", Nucl. Sci. Eng. 55, 147-167 (1974).

18. Oblow, E.M., "General Sensitivity Theory for Radiation Transport", ORNL-TM-4110, Oak Ridge National Laboratory (1973).

19. Bartine, D.E., Mynatt, F.R., Oblow, E.M., "SWANLAKE, A Computer Code Utilizing ANISN Transport Calculations for Cross-Section Sensitivity Analysis", ORNL-TM-3809, Oak Ridge National Laboratory (1973).

20. Weisbin, C.R., Marable, J.H., Lucius, J.L., Oblow, E.M., Mynatt, F.R., Peelle, R.W., Perey, F.G., "Application of "FROSS" Sensitivity and Uncertainty Methodology to Fast Reactor Benchmark Analysis", ORNL-TM-5563, Oak Ridge National Laboratory (1976).

21. Alsmiller, R.G., Jr., Santoro, R.T., Barish, J., Gabriel, T.A., "Comparison of the Cross-Section Sensitivity of the Tritium Breeding Ratio in Various Fusion-Reactor Blankets", Nucl. Sci. & Eng., 57, 122-128 (1975).

22. Gerstl, S.A.W., Budziak, Donald J., Muir, D.W., "Cross Section Sensitivity and Uncertainty Analysis With Application to a Fusion Reactor", Nucl. Sci. & Eng., 62, 137-156 (1977).

23. Alsmiller, R.G., Jr., Barish, J., Weisbin, C.R., "Uncertainties in Calculated Heating and Radiation Damage in the Toroidal Field Coil of a Tokamak Experimental Power Reactor Due to Neutron Cross-Section Error", Nucl. Tech., 34, 376-386 (1977).

24. Arcipiani, B., Palmiotte, G., Salvatores, M., "Neutron Heating Sensitivity to Cross-Section Variations in a Controlled Thermonuclear Reactor Blanket", Nucl. Sci. & Eng., 65, 540-544 (1978).

Chapter VII

CROSS SECTIONS SENSITIVITY AND UNCERTAINTY TREATEMENTS: THE ADEQUACY OF NUCLEAR DATA

VII.1 Introduction

After extensive refinements in calculational methods[1] and computer codes, more emphasis in recent years has been directed towards improving the cross-section data base to assure accurate nuclear design calculations.

Sensitivity analysis, the procedure by which one can determine how sensitive an integrated flux design parameter is to system alterations, has been applied in the area of radiation shielding,[2-4] thermal hydraulics,[5] reactor physics,[6-16] dosimetry[17-19] and fusion blanket studies.[20-28] Two approaches are applicable, namely, direct data manipulation techniques,[22],[29-32] and the use of variational[6],[24-26] and perturbation theory.[7-13] However, the first approach is limited in the information content that can be obtained and furnishes at best the magnitude of typical errors in the calculation of a given design parameter due to errors in the cross-section data base. The second approach is characterized by the simplicity of incorporating information about the variance of the parameters perturbed (e.g. cross sections) in the frame of perturbation theory and thus establishing an estimate of the integrated result errors (variance). Furthermore, the second approach is an efficient means of surveying large amounts of data with rather simple calculations. The

two approaches, however, are basically an attempt to find the cross sections which are most important to the solution of a given problem.

It should be emphasized that the importance of a specific cross section for a specific system design (e.g. pure fusion, hybrid, ...) depends strongly on the details of that particular design. While the accuracy of an existing cross section set may be fully satisfactory for a given design parameter calculation in a particular system, it may not be so in another system. Sensitivity questions for which quantitative answers are to be provided are, therefore, strictly problem dependent and generalizations from a particular study should be applied cautiously. However, sensitivity predictions may cover a generic class of designs. Thus, these predictions will provide valuable information that can be used in guiding new cross section measurement and evaluation efforts regarding priority assignments. This will be an integral part of the present study which is applied to the SOLASE-H hybrid reactor.

In the next section, a brief review of the various variational and perturbation treatment methods to evaluate the sensitivity coefficients, is given. Although most of these methods are based on the first order perturbation theory, higher order treatment has been recently attempted.[15-16],[28] In the following methods, the perturbed (exact) system is defined as the one for which the transport equation is solved using the "true" cross section values while in the unperturbed system, the neutron cross sections used are those evaluated from the current data base such as the Evaluated Neutron Data Files[42]

(ENDF/B-III;ENDF/B-IV...).

VII.2 Various Perturbation and Variational Techniques to Evaluate The Sensitivity Coefficients

In the following methods, the result is accurate up to the second-order accuracy. As given by Eq. (VI.5), the design parameter R is assumed to be linear functional of the neutron flux, i.e.,

$$R = \langle \Sigma_r, \Phi \rangle \tag{VII.1}$$

where Σ_r is the response function. We also assumed the unperturbed (approximate) system is represented by the equations

$$\bar{L}\,\bar{\Phi} = S \tag{VII.2}$$

$$\bar{L}^*\,\bar{\Phi}^* = \Sigma_r \tag{VII.3}$$

where $\bar{\Phi}$ and $\bar{\Phi}^*$ are the unperturbed forward and adjoint fluxes, respectively. These fluxes are used as trial functions for the perturbed (exact) system represented by the equations

$$L\,\Phi = S \tag{VII.4}$$

$$L^*\,\Phi^* = \Sigma_r \tag{VII.5}$$

where

$$L = \bar{L} + \delta L \tag{VII.6}$$

$$\Phi = \bar{\Phi} + \delta\Phi \tag{VII.7}$$

$$\Phi^* = \bar{\Phi}^* + \delta\Phi^* \tag{VII.8}$$

and we are interested in evaluating the change in R, δR, due to changes in the system (e.g., cross-section changes, density changes, geometrical

change, ...).

VII.2.A The Adjoint Difference Method[33]

Equation (VII.4) is rewritten as

$$(\bar{L} + \delta L)\ (\bar{\Phi} + \delta\Phi) = S$$

i.e.

$$\bar{L}\bar{\Phi} - S + (\bar{L} + \delta L)\ \delta\Phi = -\ \delta L\bar{\Phi} \quad . \tag{VII.9}$$

The first two terms vanish by the virtue of Eq. (VII.2) and the right side of Eq. (VII.9) is considered as a known source after Eq. (VII.2) for the unperturbed system is evaluated, i.e., the equation for the difference flux, $\delta\phi$, is

$$L\delta\Phi = q, \text{ with } q = -\ \delta L\bar{\Phi} \ . \tag{VII.10}$$

Using the difference flux, $\delta\Phi$, in evaluating R in the perturbed system, we get

$$\begin{aligned} R &= \langle\Sigma_r,\Phi\rangle \\ &\quad \langle\Sigma_r,\bar{\Phi}\rangle + \langle\Sigma_r,\delta\Phi\rangle \\ &\quad \langle\Sigma_r,\bar{\Phi}\rangle + \langle L^*\Phi^*,\delta\Phi\rangle \\ &\quad \langle\Sigma_r,\bar{\Phi}\rangle + \langle\Phi^*,L\delta\Phi\rangle \\ &\quad \langle\Sigma_r,\bar{\Phi}\rangle + \langle\Phi^*,q\rangle \quad . \end{aligned} \tag{VII.11}$$

With $\bar{\Phi}^*$ approximating Φ^* in the last line of Eq. (VII.11), we get

$$R = \langle\Sigma_r,\bar{\Phi}\rangle + \langle\bar{\Phi}^*,q\rangle \ . \tag{VII.12}$$

Thus, the fluxes $\bar{\Phi}$ and $\bar{\Phi}^*$ can be used as approximate solutions in Eq. (VII.12) and there is no need to solve for $\delta\Phi$ from Eq. (VII.10) (or Φ^* from Eq. (VII.5)) to obtain exact value for R from Eq. (VII.11).

The order of error in R, denoted by E_{AD}, is the difference between Eqns. (VII.11) and (VII.12), i.e.

$$\begin{aligned} E_{AD} &= \langle(\Phi^* - \bar{\Phi}^*),\ q\rangle \\ &= -\langle\delta\Phi^*, \delta L\bar{\Phi}\rangle \\ &= -\langle\delta\Phi^*, (L-\bar{L})(\Phi-\delta\Phi)\rangle \\ &= -\langle\delta\Phi^*, (L\Phi-\bar{L}\bar{\Phi})\rangle + \langle\delta\Phi^*, L\delta\phi\rangle \\ &= \langle\delta\Phi^*, L\delta\Phi\rangle\ , \end{aligned} \tag{VII.13}$$

i.e., a second order error. From Eq. (VII.12), δR is now given by

$$\begin{aligned} \delta R &= \langle\Sigma_r, \Phi\rangle - \langle\Sigma_r, \bar{\Phi}\rangle \\ &= \langle\bar{\Phi}^*, q\rangle \end{aligned} \tag{VII.14}$$

VII.2.B The Forward Difference Method[34]

Equation (VII.5) can be rewritten as

$$(\bar{L}^* + \delta L^*)\ (\bar{\Phi}^* + \delta\Phi^*) = \Sigma_r \tag{VII.15}$$

which becomes upon using Eq. (VII.3)

$$L^*\ \delta\Phi^* = r, \text{ with } r = -\delta L^*\ \bar{\Phi}^* \quad . \tag{VII.16}$$

With $R = \langle\Sigma_r, \Phi\rangle = \langle\Phi^*, S\rangle$, we have

$$\begin{aligned} R &= \langle\Phi^*, S\rangle \\ &= \langle\bar{\Phi}^*, S\rangle + \langle\delta\Phi^*, L\Phi\rangle \\ &= \langle\bar{\Phi}^*, S\rangle + \langle L^*\ \delta\Phi^*,\ \Phi\rangle \\ &= \langle\bar{\Phi}^*, S\rangle + \langle r, \Phi\rangle\ . \end{aligned} \tag{VII.17}$$

With $\bar{\Phi}$ approximating Φ in the last line of Eq. (VII.17), we get

$$R = \langle\bar{\Phi}^*, S\rangle + \langle r, \bar{\Phi}\rangle \quad . \tag{VII.18}$$

Thus, the fluxes $\bar{\Phi}$ and $\bar{\Phi}^*$ can be used as approximate solutions in Eq. (VII.18) and there is no need to solve for $\delta\Phi^*$ from Eq. (VII.16) (or Φ from Eq. (VII.4)) to obtain exact value for R from Eq. (VII.17). The order of error in R, denoted E_{FD}, is the difference between Eqns. (VII.17) and (VII.18), i.e.,

$$\begin{aligned} E_{FD} &= \langle r,(\Phi-\bar{\Phi})\rangle \\ &= -\langle(L^* - \bar{L}^*)\,(\Phi^* - \delta\Phi^*),\delta\Phi\rangle \\ &= \langle\delta\Phi^*,\, L\delta\Phi\rangle \quad , \end{aligned} \tag{VII.19}$$

i.e., a second order error. From Eq. (VII.18), δR is now given by

$$\begin{aligned} \delta R &= \langle\Phi^*,S\rangle - \langle\bar{\Phi}^*,S\rangle \\ &= \langle r,\bar{\Phi}\rangle \end{aligned} \tag{VII.20}$$

VII.2.C Perturbation Theory[8],[34-35]

We write Eq. (VII.4) for the perturbed system as

$$(\bar{L} + \delta L)\,\Phi = S \ . \tag{VII.21}$$

Multiplying Eq. (VII.21) by $\bar{\Phi}^*$, we get

$$\langle\bar{\Phi}^*,\bar{L}\Phi\rangle + \langle\bar{\Phi}^*,\delta L\Phi\rangle = \langle\bar{\Phi}^*,S\rangle \quad . \tag{VII.22}$$

But the first term on the left side is

$$\begin{aligned} \langle\bar{\Phi}^*,\bar{L}\Phi\rangle &= \langle\bar{L}^*\,\bar{\Phi}^*,\,\Phi\rangle \\ &= \langle\Sigma_r,\Phi\rangle = R \quad . \end{aligned} \tag{VII.23}$$

Inserting Eq. (VII.23) into Eq. (VII.22) we get

$$R = \langle\bar{\Phi}^*,S\rangle - \langle\bar{\Phi}^*,\delta L\Phi\rangle \quad . \tag{VII.24}$$

Using $\bar{\Phi}$ as an approximation for Φ, and with $\langle\bar{\Phi}^*,S\rangle = \langle\Sigma_r,\bar{\Phi}\rangle$

$$R = \langle\Sigma_r,\bar{\Phi}\rangle - \langle\bar{\Phi}^*,\delta L\bar{\Phi}\rangle \quad . \tag{VII.25}$$

Eq. (VII.25) is identical to Eq. (VII.12) (with $q = -\delta L\bar{\Phi}$), thus, the order of the approximation inherent in Eq. (VII.25), E_p, is given by Eq. (VII.13). Now, δR is given by

$$\delta R = -\langle\bar{\Phi}^*, \quad \delta L \quad \bar{\Phi}\rangle \tag{VII.26}$$

VII.2.D Variational Method[24],[34],[36]

The Roussopoulos[37] variational principle

$$F_R[\Phi,\Phi^*] = \langle\Sigma_r,\Phi\rangle + \langle\Phi^*,(S-L\Phi)\rangle \tag{VII.27}$$

can be used to evaluate the design parameter R, given by Eq. (VII.1) by noticing that the last term of the right side vanishes by the variative of Eq. (VII.4). If the trial functions $\bar{\Phi}$ and $\bar{\Phi}^*$ are used in Eq. (VII.27), we get an approximate estimate of R, i.e.,

$$\begin{aligned} F_R[\bar{\Phi},\bar{\Phi}^*] &= \langle\Sigma_r,\bar{\Phi}\rangle + \langle\bar{\Phi}^*, \ [S - (\bar{L} + \delta L)\ \bar{\Phi}]\rangle \\ &= \langle\Sigma_r,\bar{\Phi}\rangle - \langle\bar{\Phi}^*, \ \delta L\ \bar{\Phi}\rangle \end{aligned} \tag{VII.28}$$

But we have,

$$\begin{aligned} F_R[\bar{\Phi},\bar{\Phi}^*] &= \langle\Sigma_r,(\Phi-\delta\Phi)\rangle + \langle(\Phi^* - \delta\Phi^*), \ [S - L(\Phi-\delta\Phi)]\rangle \\ &= F_R[\Phi,\Phi^*] - \langle\delta\Phi^*,L\delta\Phi\rangle \quad . \end{aligned} \tag{VII.29}$$

Thus,

$$F_R[\Phi,\Phi^*] = F_R[\bar{\Phi},\bar{\Phi}^*] + \langle\delta\Phi^*,L\delta\Phi\rangle \quad , \tag{VII.30}$$

i.e., the functional $F_R[\bar{\Phi},\bar{\Phi}^*]$ is accurate up to the second order and is stationary about Φ and Φ^*. Therefore, from Eq. (VII.28), we have

$$\delta R = - \langle \bar{\Phi}^*, \delta L \bar{\Phi} \rangle \quad . \tag{VII.31}$$

VII.2.E Schwinger Variational Method:[6],[38-39]

The variational principle given by Eq. (VII.27) depends on the normalization of Φ and Φ^*. To arrive at a variational principle which is independent of this normalization, we assume an arbitrary normalization, i.e.,

$$\Phi = C\,\Phi_1$$

$$\Phi^* = C^*\,\Phi_1^* \quad . \tag{VII.32}$$

Inserting Eq. (VII.32) into Eq. (VII.27) and requiring the functional $F_p\,[C\Phi_1, C^*\Phi_1^*]$ to be stationary w.r.t. arbitrary variations in the normalization factors C and C*, i.e., $\frac{\partial F_p}{\partial C} = \frac{\partial F_p}{\partial C^*} = 0$, and upon substituting the resultant values of C and C* in $F_p[C\Phi_1, C^*\Phi_1^*]$, we get

$$F_{sv}\,[\Phi_1, \Phi_1^*] = \frac{\langle \Sigma_r, \Phi_1 \rangle \langle \Phi_1^*, S \rangle}{\langle \Phi_1^*, L\Phi_1 \rangle} \tag{VII.33}$$

which is independent of the normalization of the trial functions and we can use $\bar{\Phi}$ and $\bar{\Phi}^*$ as trial functions instead of Φ_1 and Φ_1^*. This is an equivalent expression for the second-order estimate of the design parameter R.

From the above methods, one notices that the change in R due to system perturbation (e.g., cross section errors) is always given by Eq. (VII.31). As mentioned in Section VI.2.C, if the perturbation is constant over the phase space where it takes place, i.e., the pertubed (p) cross section is proportional to the unperturbed (u) value in all neutron energy groups i ($\Sigma_i^p = \delta c\ \Sigma_i^u$), we get

$$\delta R_i = \delta c \, \langle \bar{\Phi}^*, -L_\Sigma \bar{\Phi} \rangle_i \qquad \text{(VII.35)}$$

The relative sensitivity coefficient at energy group E_i is defined as

$$P_{\Sigma_i} = \frac{\delta R/R}{\delta c} = \frac{1}{R} \langle \bar{\Phi}^*, -L_\Sigma \bar{\Phi} \rangle_i \qquad \text{(VII.36)}$$

where L_Σ is the portion of the Boltzmann transport operator that contains the cross section Σ_i in group i. One should notice that in the above treatment, only the indirect effect of the perturbed cross section is accounted for. If the response function Σ_r is also perturbed, its effect (direct effect) on R should be added to the indirect part. For clarity, one can write the sensitivity coefficient, $P_{\Sigma_r}(E)$, at energy E for cross section perturbed Σ_r, as [see notations in Chapter (VI), note that we used Φ and Φ^* for $\bar{\Phi}$ and $\bar{\Phi}^*$ from now on]

$$\begin{aligned} P_{\Sigma_r}(E) = {} & \frac{1}{R} \cdot \int_{\bar{r}} d\bar{r} \, \Sigma_r(\bar{r},E)[-\phi^0(\bar{r},E)\phi^{0*}(\bar{r},E)] \\ & + \frac{1}{R} \int_{\bar{r}} d\bar{r} \, \Sigma_r(\bar{r},E) \int_{E'} dE' \phi^\ell(\bar{r},E) \, f_x^\ell(\bar{r},E\to E') \phi^{*\ell}(\bar{r},E') \\ & + \frac{1}{R} \int_{\bar{r}} d\bar{r} \, \Sigma_r(\bar{r},E) \int_{E'} dE' \, \phi^0(\bar{r},E) \, \bar{\nu}(E)\chi(E')\phi^{0*}(\bar{r},E') \\ & + \frac{1}{R} \int_{\bar{r}} d\bar{r} \, \Sigma_r(\bar{r},E) \, \phi^0(\bar{r},E). \end{aligned} \qquad \text{(VII.37)}$$

where the cross section perturbed is assumed to be the response function, i.e., $\Sigma(\bar{r},E) = \Sigma_r(\bar{r},E)$. The third term (fission term) appears in Eq. (VII.37) is eliminated if the perturbed cross section is not the fission cross section, i.e., $\Sigma(\bar{r},E) \neq \Sigma_f(\bar{r},E)$. One can identify the terms appearing in Eq. (VII.37) as follows

(a) The first term ≡ The collision loss term. It gives the loss of sensitivity (weighted by the adjoint flux) due to removing the particle from the phase space $\bar{\xi}(\bar{r},E,\bar{\Omega})$ upon encountering a collision.

(b) The second term ≡ The scattering gain term. It represents the gain in sensitivity when the particle is transfered to the phase space $\bar{\xi}(\bar{r},E',\bar{\Omega}')$ upon encountering scattering collision at $\bar{\xi}(\bar{r},E,\Omega)$.

(c) The third term ≡ when present, it is the fission gain term, i.e., the gain in the sensitivity due to neutron reappearance with energy E' upon encountering a fission event at energy E.

(d) The last term ≡ The direct effect term. It is only included if the cross section perturbed is the response function.

The collision loss term, the scattering gain term, and the fission gain term reflect the flux perturbation resulting from cross sections perturbation. Their algebraic sum gives the total indirect effect. The direct term gives the effect on the response R resulting from the cross section uncertainty itself. The net effect is the sum of the direct and indirect effects.

VII.3 Basic Covariance Formulation

VII.3.A Theory

The change in the flux-integrated design parameter, R, using first order perturbation theory, is

$$\delta R \simeq \sum_i \frac{\partial R}{\partial \Sigma_i} \delta \Sigma_i \qquad \text{(VII.38)}$$

where $\delta\Sigma_i$ represents the error in the cross section set Σ_i (particular cross section type and/or multigroup cross section for group i). However, due to the statistical nature of $\delta\Sigma_i$, we are interested in evaluating the standard deviation of R derived from the statistical population of possible cross-section values. Thus, we have

$$\Delta R = [E\{\delta R^2\}]^{1/2} = [\mathrm{var}(R)]^{1/2} = [E\{\sum_{i,j} \frac{\partial R}{\partial \Sigma_i} \frac{\partial R}{\partial \Sigma_j} \delta\Sigma_i \delta\Sigma_j\}]^{1/2}$$

$$= [\sum_{i,j} \frac{\partial R}{\partial \Sigma_i} \frac{\partial R}{\partial \Sigma_j} E\{\delta\Sigma_i \delta\Sigma_j\}]^{1/2} \qquad \text{(VII.39)}$$

where E {. . .} denotes the expectation value of a distribution, $\delta(\ldots)$ identifies the statistical variation of a variable, and Δ identifies the standard deviation. Var (...) stands for the variance of the given parameter. For a joint probability density function, $f(\Sigma_i,\Sigma_j)$, the expectation value of the product of $\delta\Sigma_i$ and $\delta\Sigma_j$ is a matrix element of the covariance matrix $\mathrm{COV}(\Sigma_i,\Sigma_j)$ given by the expression

$$\mathrm{COV}(\Sigma_i,\Sigma_j) = E\{\delta\Sigma_i \, \delta\Sigma_j\}$$

$$= \int_{-\infty}^{\infty} \int (\Sigma_i - \hat{\Sigma}_i)(\Sigma_j - \hat{\Sigma}_j) \, f(\Sigma_i,\Sigma_j) \, d\Sigma_i d\Sigma_j \qquad \text{(VII.40)}$$

where $\hat{\Sigma}_i$ and $\hat{\Sigma}_j$ are the expectation values of Σ_i and Σ_j, respectively.

As given by Eq. (VII.36) the relative sensitivity coefficient, P_{Σ_i}, for cross section type i, is given by

$$P_{\Sigma_i} = \frac{\partial R/R}{\partial \Sigma_i/\Sigma_i} , \qquad \text{(VII.41)}$$

and is called the sensitivity profile for cross section Σ_i, or briefly, the sensitivity coefficient. Thus, transforming Eq. (VII.39) into a form containing only fractional quantities, we get

$$\frac{\Delta R}{R} = \left[\sum_{i,j} P_{\Sigma_i} P_{\Sigma_j} \, RCOV(\Sigma_i,\Sigma_j) \right]^{1/2} \qquad \text{(VII.42)}$$

where

$$RCOV(\Sigma_i,\Sigma_j) = \frac{COV(\Sigma_i,\Sigma_j)}{\Sigma_i \; \Sigma_j} . \qquad \text{(VII.43)}$$

Here, $RCOV(\Sigma_i,\Sigma_i)$ is the relative covariance matrix whose off-diagonal elements represent the correlations betwen the cross-sections Σ_i and Σ_j. All cross-section uncertainty information is contained in the relative covariance matrix $RCOV(\Sigma_i, \Sigma_j)$ and all the sensitivity information is contained in the product of the profiles P_{Σ_i} and P_{Σ_j}.

It is convenient to define an integral cross-section senstivity parameter, S_Σ, as (see Eq. (VI.27))

$$S_\Sigma = \sum_i P_{\Sigma_i} \qquad \text{(VII.44)}$$

which is interpreted as the percentage change of the design parameter of interest, $\partial R/R$, resulting from a simultaneous 1% increase of the group cross-sections Σ_i in all energy groups i (assuming full correlation between Σ_i and Σ_j with a correlation coefficient of +1).

VII.3.B Simplifications to Evaluate Upper Limits for $\frac{\Delta R}{R}$

In cases where no complete covariance informations are available for different cross-sections, one can evaluate estimates of the error in a given design parameter using estimates of cross section uncertainties based on ignoring cross-section correlations and/or energy dependence. In this case certain conservative assumptions can be made to assign reasonable cross-section errors based on the information regarding measurement accuracy in different energy ranges.

If the cross sections Σ_i are assumed to be uncorrelated, their uncertainties are also uncorrelated and thus Eq. (VII.42) reduces to

$$\left(\frac{\Delta R}{R}\right)_{\text{uncorr}} = \left[\sum_i \left(P_{\Sigma_i} \frac{\Delta\Sigma_i}{\Sigma_i}\right)^2\right]^{1/2}, \qquad \text{(VII.45)}$$

since

$$\text{COV}(\Sigma_i,\Sigma_j)_{\text{uncorr}} = \text{COV}(\Sigma_i,\Sigma_j)\delta_{ij} \qquad \text{(VII.46)}$$

and we have

$$\text{COV}(\Sigma_i,\Sigma_i) = \text{var}(\Sigma_i) = E\{(\Sigma_i-\hat{\Sigma}_i)^2\} = (\Delta\Sigma_i)^2 \ . \qquad \text{(VII.47)}$$

On the other hand, if the cross-section Σ_i and Σ_j are assumed fully correlated (more conservative assumption) with a correlation coefficient +1, then we have

$$\left(\frac{\Delta R}{R}\right)_{\text{corr}(+1)} = \left| \sum_i P_{\Sigma_i} \frac{\Delta\Sigma_i}{\Sigma_i} \right| \qquad \text{(VII.48)}$$

where

$$\text{COV}(\Sigma_i,\Sigma_j)_{\text{corr}(+1)} = [\text{COV}(\Sigma_i,\Sigma_i)]^{1/2}\ [\text{COV}(\Sigma_j,\Sigma_j)]^{1/2}. \qquad \text{(VII.49)}$$

The most conservative error estimate of R can be obtained if we

assume that all uncertainties in an entire cross section set are equal to the largest uncertainty in any of the individual cross-sections which possess significant sensitivity, i.e.,

$$\frac{\Delta\Sigma_i}{\Sigma_i} = \left(\frac{\Delta\Sigma}{\Sigma}\right)_{max} = \text{const.} \qquad \text{(VII.50)}$$

Furthermore, if we assume full correlation among different group cross-sections, we get from Eq. (VII.48),

$$\left(\frac{\Delta R}{R}\right)_{max} = \bar{S}_\Sigma \cdot \left(\frac{\Delta\Sigma}{\Sigma}\right)_{max} \qquad \text{(VII.51)}$$

where

$$\bar{S}_\Sigma = \sum_i |P_{\Sigma_i}| \ . \qquad \text{(VII.52)}$$

In addition, we can assume that uncertainties in partial cross sections are fully correlated. In this case $\bar{S}_\Sigma$ in Eq. (17) will be the sum of all the S_Σ's values of the different partial cross sections, i.e., no cancellation occurs in the impact of different partial cross section on the design parameter R. Usually uncertainties in the total neutron cross section is small compared to the partial cross sections.[21-22] In this case, one may only consider the uncertainty in a particular partial cross section of significant sensitivity and modify (with a prescribed correlation) the value of another cross section to keep the total cross section unchanged. Analysis of this sort has been carried out in an attempt to investigate the expected tritium breeding values in pure fusion reactor blankets when $^6Li(n,\alpha)$ and $^7Li(n,n',\alpha)$ cross section errors are considered. While the accuracy of the $^6Li(n,\alpha)$

cross section is found to be adequate for this class of blankets, the error associated with $^{7}Li(n,n'\alpha)t$ has a more significant impact on the tritium breeding function.[22] Generalization to fission-fusion systems should not be made unless a sensitivity study is performed for these systems, as we did in the next chapters.

VII.4 Adequacy of the Present Cross Section Evaluation for Pure Fusion and Fusion- Fission Reactors

The status of available evaluated nuclear cross section data for fusion reactor calculations and their present uncertainties have been discussed either through critical reviews[43],[46] or committee meeting on national and international levels.[45] The types of data available in the ENDF/B and ENDL (on the national level) have increased to keep pace with an increase in the number of applications.[46] For our purpose, data up to 20 MeV are important. More accurate neutron cross-section and gamma-ray production cross sections are needed for transport calculation. For breeding purposes (tritium or fissile fuel breeding), accurate evaluations of breeding materials (^{6}Li, ^{7}Li, ^{232}Th, ^{238}U, ...) are required. As far as radiation damage data are concerned, evaluation of cross sections needed for gas production and displacement damage are of prime importance. We summarize in the following the cross sections and its accuracy required for several important design parameters in the pure fusion and fusion-fission reactor blanket design.

VII.4.A Tritium Production

The estimated $^{6}Li(n,\alpha)t$ cross section is known to 0.5% at

1.0E-05 eV, 1.0% at 10 keV, 2.0% at 30 keV, 3.0% at 230 keV, 4.0% at 450 keV, and 5.0% at 750 keV and above.[21],[46] For $^{7}Li(n,n')\alpha t$ cross section, they are 15% from threshold (~2.82 MeV) to 3.0% at 14.0 MeV and about 25% at 20 MeV.[46] Several studies aimed at evaluating the error associated with the tritium breeding ratio in different pure fusion reactors.[21-23] As mentioned before, it was found that $^{6}Li(n,\alpha)t$ cross-section data is adequate to determine the tritium breeding ratio to 1%.[22] Uncertainties in exess of 5% in breeding ratio results from 20% error in the $^{7}Li(n,n')\alpha t$ cross section from 3-15 MeV. As was found, uncertainties in the secondary neutron energy distribution of this reaction may lead to ~ 4% in the tritium breeding. If Be is present in the blanket for neutron multiplication, uncertainties in the Be(n,2n) and the secondary neutron energy distribution could introduce errors of the order of several percent in the tritium breeding.[46]

For fusion-fission reactors, errors associated with the reactions which compete with tritium production (e.g., $^{232}Th(n,\gamma)$ in SOLASE-H design) and its impact on tritium production rates should be evaluated.

VII.4.B Fissile Fuel Production

In general, accurate data are needed on neutron producing reactions and fissile fuel breeding reactions in fusion-fission systems from thermal energy up to 14 MeV. Information on the fission spectrum and its variation with energy and the angular and energy distribution of secondary neutrons are also needed. The sensitivity of the fissile fuel production for this information as well as tritium production

cross sections should be studied along with the uncertainties in fissionable nuclide cross sections. As examples for U-238, it is estimated[46] that the fission cross section has an error of about 9% at 0.3 MeV, 12% at 0.6 MeV, decreasing to 3% at 2.5 MeV, 2.4% at 4 MeV and about 4% at 14 MeV. The uncertainty in the capture cross section is about 9% at 20 keV, 5% at 100 keV and 1 MeV. For the (n,2n) cross sections, the uncertainties are estimated to be less than 10% near the maximum where the cross section is large; at 14 MeV the observed data spread lies outside this error band. The fission spectra and their variation with energy are not well known. The same may also be said about the energy spectrum of secondary neutrons inelastically scattered into the continuum and those due to (n,2n) and (n,3n) processes.

VII.4.C Nuclear Heating

Accuracy in the evaluation of neutron kerma factor and gamma-ray kerma factor[49] is important to the design of a reliable heat removal system in fusion and fusion-fission reactors since these factors are used to estimate the rate of heat deposition in their blankets. Neutron heating, H_n and gamma-ray heating, H_γ, are defined as $H_n = \langle K_n, \Phi_n \rangle$ and $H_\gamma = \langle K_\gamma, \Phi \rangle$, where K_n and K_γ are the neutron and γ-ray kerma factors, respectively. Although the uncertainties in γ-ray kerma factors is well known due to the well evaluated gamma-ray interaction, it is not so for neutron kerma factors. The latter requires accurate evaluation of: (i) partial reaction cross sections [e.g., n,charged particle), (n,n',charged particle), (n,γ), (n,xn'),..], (ii) energy and angular distribution of seconary neutrons, (iii) energy,

angular distribution and yields of secondary photons, (iv) energy deposition for reaction from radioactive decay, and (v) reaction Q-value. Several neutron heating sensitivity studies have been performed.[29],[47-49] In pure fusion reactor blankets, it was found that 30-50% of neutron heating is due to (n,charged particle) reactions[20]. This may reach 70% in S.S.[46] Also, heating due to (n,n' charged particle) reactions is ~ 30-50% of that due to (n,charged particle) reactions.[29] The heating due to ^{7}Li is very sensitive to the angular and energy distribution of the secondary neutrons. For fusion-fission reactors, most of the heat deposited is due to (n,fission) reaction. Accurate evaluation of this reaction and the fission spectra is of prime importance for local heat deposition calculations.

VII.4.D Radiation Damage

The primary knock-on atom (PKA) spectrum, $\psi_i(E,T)$ (barns/eV), is defined as the product of $\sigma_i(E)$ and $K_i(E,T)$ where $\sigma_i(E)$ is the energy dependent reaction cross section for reaction type; and $K_i(E,T)$ is the probability that an interacting neutron of energy E will produce a recoil of energy T through reaction i. $K_i(E,T)$ depends on the kinamatics of the particular reaction and may be calculated from the data on secondary particle angle and energy distributions. Thus, evaluation of the displacement per atom (DPA) in fusion reactors depends on accurate evaluations of the partial cross sections as well as the number of displaced atoms $\nu(T)$ for a recoil of energy T. As reported,[46] describing the inelastically scattered neutrons into the continuum by isotropic scattering models may lead to an error ~ 15% in the

DPA cross section. For gas production calculations, accurate evaluations of (n,p), (n,n',p), (n,d), (n,α), etc. are important as it is the case for nuclear heating.

References

1. Lathrop, K.D., Reactor Technology, 15, 107 (1972).

2. Bartine, D.E., Oblow, E., Mynatt, F.R., "Neutron Cross Section Sensitivity Analysis: A General Approach Illustrated for a Na-Fe System", ORNL-TM-3944, Oak Ridge National Lab. (Dec. 1972).

3. Bartine, D.E., Oblow, E.M., Mynatt, F.R., "Radiation-Transport Cross Section Sensitivity Analysis - A General Approach Illustrated for a Thermonuclear Source in Air", Nucl. Sci. Eng., 55, 147-167 (1974).

4. Oblow, E.M., "General Sensitivity Theory for Radiation Transport", ORNL-TM-4110, Oak Ridge National Lab (1973).

5. Oblow, E.M., "Sensitivity Theory for Reactor Thermal Hydraulics Problems", Nucl. Sci., Eng., 68, 322-337 (1978).

6. Stacey, W., "Variational Estimates and Generalized Perturbation Theory for the Ratios of Linear and Bilinear Functionals", FRA-TM-21, Argonne National Lab., Oct. (1971).

7. Gandini, A., Salvatories, M., and Sena, G., "Use of Generalized Perturbation Methods for Optimization of Reactor Design", J. Nucl. Energy, 23, 469-475 (1967).

8. Usachev, L.N., "Perturbation Theory for the Breeding Ratio and for Other Number Ratios Pertaining to Various Reactor Processes", J. Nucl. Energy, Parts A/B , Vol. 18, 571-583 (1964).

9. Pomraning, G.C., "The Calculation of Ratios in Critical Systems", J. Nucl. Energy, 21, 285-291 (1967).

10. Weisbin, C.R., et. al., "Application of Sensitivity and Uncertainty Methodology to Fast Reactor Integral Experiment Analysis", Nucl. Sci. Eng., 66, 307-33 (1978).

11. Weisbin, C.R., et. al., "Application of FORSS Sensitivity and Uncertainty Methodology to Fast Reactor Benchmark Analysis", ORNL/TM-5563, Oak Ridge National Lab. (Dec. 1976).

12. Greenspan, E., 'Development IN Perturbation Theory", Advances in Nucl. Sci. and Technology, Vol. 9, pg. 182, Eds. E.J. Henley and J. Lewins, Academic Press (1976).

13. Lewins, J., "Development in Perturbation Theory", Advances in Nucl. Sci. and Technology, Vol. 4, pg. 309, Eds. E.J. Henley and J. Lewins, Academic Press (1967).

14. McKnight, R.D., "Projections of ENDF/B Version V Performance for Fast and Thermal Reactors Using Sensitivity Coefficients", Nucl. Sci. Eng., 55, 79 (1974).

15. Gandini, A., "Higher Order Time-Dependent Generalized Perturbation Theory", Nucl. Sci. Eng., 67, 91-106 (1978).

16. Greenspan, E., Karni, Y., Gilai, D., "High Order Effects in Cross Section Sensitivity Analysis", ORNL/RSIC-42, pg. 231, "Review of the Theory and Application of Sensitivity and Uncertainty Analysis", Proc. of a Seminar Workshop, Oak Ridge National Lab., TN, U.S.A., Feb. (1979).

17. Broadhead, B.L., "Sensitivity and Uncertainty Analysis Applied to the NBS-ISNF", a paper in "Review of the Theory and Application of Sensitivity and Uncertainty Analysis", Proc. of a seminar workshiop ORNL/RSIC-42, Oak Ridge National Lab., TN, U.S.A., Feb. (1979).

18. Broadhead, B.L., Lucius, J.L., Perey, F.G., Weisbin, C.R., Dodds, H.L, Jr., "Calculation of Flux Covariance Matrix for the National Bureau of Standards - Intermediate Energy Standard Neutron Field (NBS-ISNF)", Trans. Am. Nucl. Soc., 30, 590, Nov. (1978).

19. Mannhart, W., "Testing of ENDF/B Cross-Section Data in the Californium-252 Neutron Benchmark Field", ORNL/RSIC-42, pg. 119, in Proc. of a seminar workshop, Oak Ridge National Lab., TN. U.S.A., Feb. (1979). Also see D.T. Ingersoll, "Sensitivity Analysis Applied to an Integral Test of Niobium Cross-sections, pg. 179, the same reference.

20. Gerstl, S.A., Dudziak, D.J., Muir, D.W., "Cross Section Sensitivity and Uncertainty Analysis With Application to a Fusion Reactor", Nucl. Sci. Eng., 62, 137-156 (1977).

21. Alsmiller, R.G., Santoro, R.T., Barish, J., Gabriel, T.A., "Comparison of the Cross Section Senstivity of the Tritium Breeding Ratio in Various Fusion-Reactor Blankets", Nucl. Sci. Eng., 57, 122-128 (1975).

22. Steiner, D., Tobias, M., "Cross Section Sensitivity of Tritium Breeding in a Fusion Reactor Blanket: Effect of Uncertainties in Cross Sections of ^{6}Li, ^{7}Li, and ^{93}Nb", Nucl. Fusion, 14, 153-163 (1974).

23. Bartine, D.E., Alsmiller, R.G., Oblow, E.M., "Cross Section Sensitivity of Breeding Ratio in a Fusion Reactor Blanket", Nucl. Sci. Eng., 53, 304-318 (1974).

24. Conn, R., Stacey, W.M., "Variational Methods for Controlled Thermonuclear Reactor Blanket Studies", Nucl Fusion, 13, 185-191 (1973).

25. Cheng, E.T., Conn, R.W., "A Multi-point Interpolation Method Based on Variational Principles for Functionals of the Solution to Linear Equations", J. Math. Phys. Vol. 17, No. 5, 683-687 (1976).

26. Cheng, E., Conn, R.W., "The Influence of Design Variations on Controlled Thermonuclear Reactor Blanket Neutronic Performance Using Variational Techniques", Nucl. Sci. Eng., 62, 601-616 (1977).

27. Wu, T., Maynard, C.W., "The Application of Uncertainty Analysis in Conceptual Fusion Reactor Design", ORNL/RSIC-42, pg. 191, in the Proc. of a seminar workshop, Oak Ridge National Lab., TN, U.S.A., Feb. (1979).

28. Greenspan, E, Gilai, D., "Second-Order Generalized Perturbation Theory for Source-Driven Systems, Nucl. Sci. Eng., 68, 1-9 (1978).

29. Abdou, M.A., Maynard, C.W., "Calculational Method for Nuclear Heating - Part II: Applications to Fusion Reactor Blankets and Shields", Nucl. Sci. Eng., 56, 381-398 (1975).

30. Tobias, M.L., Steiner, D., "Outline of Direct Methods Used in Computing the Cross Section Senstivity of Neutron Parameters in a Fusion Reactor", ORNL-TM-4184, Oak Ridge National Lab., June (1973).

31. Yasushi Seki and Hiroshi Maekawa, "Absolute Fission-Rate Distributions in Lithium and Hybrid Fusion Blanket Assemblies (II)". J. Nucl. Sci. and Tech., 14 [3], 210-225 (March 1977).

32. Straker, E.A., "Sensitivity of Secondary Gamma-Ray Dose to Angular Distribution of Gamma Rays from Neutron Inelastic Scattering", Nucl. Sci. Eng., 41, 147-148 (1970).

33. Hoffman, T.J., Robinson, J.C., and Stevens, P.N., "The Adjoint Difference Method and its Application to Deep-Penetration Radiation Transport", Nucl. Sci. Eng., 48, 179-188 (1972).

34. Gerstl, S.A., and Stacey, W.M., "A Class of Second-Order Approximate Formulations of Deep Penetration Radiation Transport Problems", Nucl. Sci. Eng., 51, 339-343 (1973).

35. Gandini, A., J. Nucl. Energy, Parts A/B, 21, 755 (1967).

36. Pomraning, G.C., "A Derivation of Variational Principles for Inhomogeneous Equations", Nucl. Sci. Eng., 29, 220-236 (1967).

37. Roussopoulos, P., C.R. Acad. Sci., 236, 1858 (1953).

38. Levine, H., Schwinger, J., Phys. Rev., 75, 1423 (1949).

39. Francis, N., et. al., "Variational Solutions of the Transport Equation", Prog. Nucl. Eng. Series I, 3, 360 (1959).

40. Seki, Y, Santoro, R.T., Oblow, E.M., Lucius, J.L, "Comparison of One- and Two-Deimensional Cross Section Senstivity Calculations for a Fusion Reactor Shielding Experiment", ORNL/TM-6667, Dist. Category UC-20d, MFE-Fusion System, Oak Ridge National Lab. (Jan. 1979).

41. Seki, Y., Santoro, R.T., Oblow, E.M., Barnes, J.M., Lucius, J.L, "Cross Section Sensitivity Analysis of a Proposed Neutron Streaming Experiment with a Two-Dimensional Model", ORNL/TM-6588, UC-20d, Oak Ridge National Lab. (Feb. 1979).

42. Perey, F.G., "The Data Covariance Files for ENDF/B-V", ORNL/TM-5938, Oak Ridge National Lab. (July 1977).

43. Steiner, D., Coordinator, "The Status of Neutron-Induced Nuclear Data for Controlled Thermonuclear Research Applications: Critical Reviews of Current Evaluations", USNDC-CTR-1, U.S. Nuclear Data Committee (1974).

44. Drischler, J.D., Weisbin, C.R., "Compilation of Multi-group Cross Section Covariance Matrices for Several Important Reactor Materials", ORNL-5318 (ENDF-235), Oak Ridge National Lab., (Oct., 1977).

45. "IAEA Advisory Group Meeting on Nuclear Data for Fusion Reactor Technology", Vienna, 11-15, Dec. 1978, a summary report, INDC(NDS)-101/LF (May 1979).

46. Bhat, M.R., "Evaluated Files of Nuclear Cross Sections for Fusion Reactor Calculations", BNL-NCS-25295, Brookhaven National Lab. (Dec. 1978).

47. Arcipiani, B., Palmiotti, G., Salvatores, M., "Neutron Heating Sensitivity to Cross Section Variations in a Controlled Thermonuclear Reactor Blanket", Nucl. Sci. Eng., 65, 540-544 (1978).

48. Alsmiller, R.G., Barish, J., Weisbin, C.R., "Uncertainties in Calculated Heating and Radiation Damage in the Toroidal Field Coil of a Tokamak Experimental Power Reactor Due to Neutron Cross Section Errors", Nucl. Technology, 34, 376-386 (1977).

49. Abdou, M.A., Maynard, C.W., "Calculational Methods for Nuclear Heating - Part I: Theoretical and Computational Algorithms",

Nucl. Sci. Eng., 56, 360-380 (1975).

Chapter VIII

THE SOLASE-H SENSITIVITY ANALYSIS

VIII. 1 Introduction

Sensitivity analysis, which partly was presented in Chapter VI, has been extended and applied to the SOLASE-H blanket. Five design parameters have been considered. These parameters are: (a) The U-233 breeding ratio, R_U; (b) the tritium production ratio from ^6Li, $R_{^6Li}$; (c) the tritium production ratio from ^7Li, $R_{^7Li}$; (d) the damage rate measured in terms of the average displacements per atom, averaged over the first three centimeters of the fuel zone, per incident neutron, $\bar{R}_D$; and (e) the heat deposited in the blanket per incident neutron due to nuclear reactions, R_H^Q.

The objective of carrying out the sensitivity and uncertainty analysis is to investigate the percentage error estimates associated with the design parameters of interest. These estimates can thus test the adequacy of the present nuclear data for breeding, radiation damage and heat deposition calculations. In the following, we discuss the results obtained from the sensitivity analysis. First, the computational procedures used are given in the next section.

VIII.2 Processing the Partial Cross Section for the Sensitivity Analysis

To perform a sensitivity analysis, the total and the partial cross sections should be available in a format usable in the sensitivity code, "SWANLAKE".[1] The data base used to generate these cross sections is the DLC-41B/VITAMIN-C Library[2] which is distribu-

ted by the Radiation Shielding Information Center(RSIC) at Oak Ridge National Laboratory and is based on the Evaluated Neutron Data File, Version V, ENDF/B-V. This library consists of: (a) Neutron interaction library, (b) Gamma production library, and (c) Gamma interaction library. The three libraries (171-neutron energy groups and 36-gamma groups) are in the AMPX-Master interface format.[3]

The AMPX processing system,[3] has been used to construct the transfer matrices for the total and the partial cross sections. A shorthand notation to identify various cross section libraries and a chart of the processing procedures performed are shown in Figs. (VIII.1) and (VIII.2), respectively. The neutron, gamma production, and gamma interaction master interface libraries have been processed to generate binary libraries using the "AIM" code, a module of the AMPX system. The BONAMI module, which assesses Bondarenko factors and allows performing the resonance self-shielding calculation based on the narrow resonance approximation, has not been used in preparing the neutron library, since the final library is intended to be used in a fast neutron spectrum such as the one encountered in the SOLASE-H blanket. The "CHOX" module has been used to prepare a coupled interface library from the neutron, neutron gamma, and gamma libraries which is then reduced by the "MALOCS" module to the 25 neutron groups-21 gamma groups structure used in the SOLASE-H calculation. The "NITAWL" module, which represents a relatively large portion of the AMPX system, is used to generate the group dependent library in the form of transfer matrices for the total and partial cross sections.

FIG. (VIII.1) SHORTHAND NOTATION USED FOR VARIOUS CROSS SECTION LIBRARIES.

- AMPX Master Interface for Neutron only in BCD (card image) format

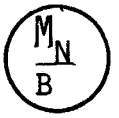

- AMPX Master Interface for Neutron only in Binary Format

- AMPX Master Interface for Gamma-Production Data in BCD format

- AMPX Master Interface for Gamma-Production Data in Binary Format

- AMPX Master Interface for Gamma-Interaction Data in BCD Format

- AMPX Master Interface for Gamma-Interaction Data in Binary Format

- Coupled AMPX Master Interface - Fine Groups (171 neutron, 36 gamma)

- Coupled AMPX Master Interface - Broad groups (25 Neutron, 21 gamma)

- ANISN Library - Group Dependent

- ANISN Library - Group Independent

- ANISN Library for Partial Cross Section - Group Dependent

- ANISN Library for Adjoint Calculation - Group Independent

Fig. (VIII.1): Shorthand Notation Used for Various Cross Section Libraries.

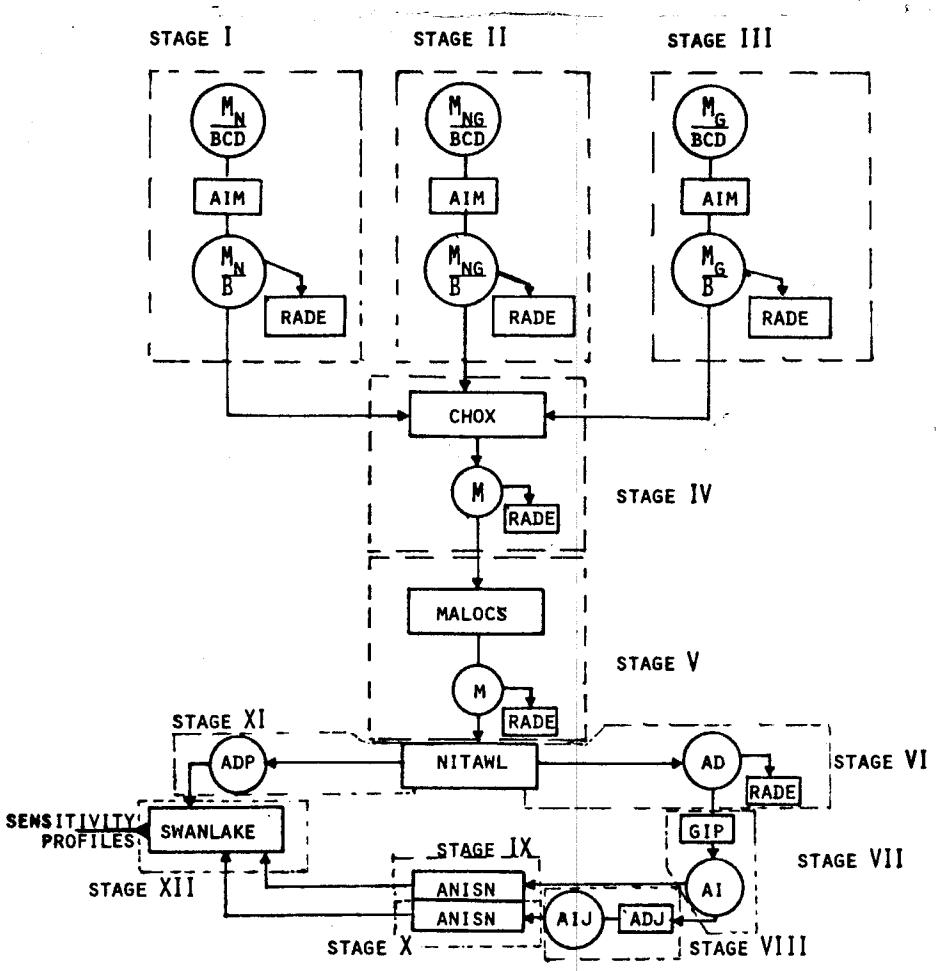

Fig. (VIII.2): Overall Calculation Scheme To Evaluate the Sensitivity Coefficients.

For transport calculations performed by the "ANISN" code, a group independent library is obtained from the group dependent library using the "GIP" module. A similar step is made when using the ANISN code for adjoint calculations. Finally, the partial cross sections library, the forward flux, and the ajoint flux for the particular design parameter considered are used to generate the sensitivity profiles. As shown in Fig. (VIII.2), these calculational procedures are performed via a sequence of various stages.

The original "SWANLAKE" code has been revised to handle and include the up-scattering effect due to fission reactions which take place in hybrid systems. This was necessary since the original code treats only down-scattering effects.[1]

VIII.3 Sensitivity Analysis Results

For each of the five design parameters (responses) considered, preliminary sensitivity calculations are first carried out to evaluate the sensitivity coefficients, S_Σ, due to a 1% increase in the total cross section of each material used. The increase is assumed to take place in each energy group and each spacial zone where the material is present in the SOLASE-H blanket.

For those materials with high sensitivity coefficients, further analysis is carried out to evaluate the sensitivity profiles, P_{Σ_i}, and the sensitivity coefficients, S_Σ, due to a 1% increase in each partial cross section. This will reveal which particular partial cross section contributes the most to the total sensitivity coefficient. As it must be, the relative sensitivity coefficient, S_Σ, for

the total cross section is the algebraic sum of the coefficients evaluated for the partial cross sections. In the following, we give the sensitivity analysis results for each design parameter considered for the SOLASE-H blanket (see Fig. IV.2).

VIII.3.A Sensitivity Analysis Results for the U-233 Breeding Ratio, R_U

The value of the U-233 breeding ratio, R_U, has been evaluated to be 0.9165 using the DLC-41B/VITAMIN-C library which is based on ENDF/B-V. This is to be compared to the beginning of life value, R_U=0.9338, obtained previously in Chapter (IV) where the DLC-2D library,[4,5] (based on ENDF/B-III) has been used. This discrepancy is due to the spectrum used in condensing the neutron groups. In the DLC-41B/VITAMIN-C library case, we have used the standard evaporation +1/E+fission+1/E+Maxwellian spectrums. In the DLC-2D library case, the 1/E weighting spectrum is used for the GAM-II group structure.[5] In the present sensitivity analysis, we have used the response values evaluated from the DLC-41B/VITAMIN-C library.

In Table (VIII.1), we give the sensitivity coefficients, $S^U_{\Sigma_{tot}}$, for uranium breeding due to the total cross section variation. As shown, the U-233 production rate is more sensitive to variation in the Th total cross section and the direct part of the total value for $S^U_{\Sigma_{tot}}$ is more dominant. The uranium breeding ratio is also sensitive to variations in Pb, ^{6}Li, ^{16}O, ^{23}Na, ^{7}Li, Zr and C total cross sections, in that order. As expected, since Pb is used as a neutron multiplier through the Pb(n,2n) reactions, $S^U_{\Sigma_{tot}}$ for Pb is larger in the front

Table (VII.1)

SENSITIVITY COEFFICIENTS, S_{Σ}, FOR THE U-233 BREEDING RATIO DUE TO A 1% INCREASE IN THE TOTAL CROSS SECTION OF DIFFERENT MATERIALS IN THE SOLASE-H BLANKET

Element	ZONE								System
	3	4	5	6	7	8	9	10	
Th				-6.08-1[+] 1.00[*]					3.92-1[**]
Pb	1.66-1						1.20-2		1.78-1
^{6}Li		-7.04-2				-9.09-2		-1.05-6	-1.61-1
^{7}Li		1.13-2				1.09-2		4.84-7	2.22-2
O				1.03-1					1.03-1
C							-2.15-2		-2.15-2
Na	7.80-3			9.75-2					8.97-2
Zr	-3.13-4			2.19-2					2.16-2
N_i	-1.31-5	-3.21-4	-2.29-3	3.25-6	-2.91-4	-6.28-4		1.30-7	-3.50-3
C_r	-8.09-6	-1.54.4	-1.22-3	7.33-6	3.72-4	7.79-6		1.37-7	-9.99-4
Fe	-1.14-5	-4.67-4	-3.65-3	1.71-5	2.15-3	-9.22-4		4.24-7	-2.89-3
Sn	-1.62-4			-4.71-6					-1.67-4

[+]Indirect Effect Part
*Direct Effect Part
**Read 3.92×10^{-1}

zone (#3) than in the reflector zone (#10). Increasing the Pb(n,tot) cross section by 1% in all zones and energy groups results in ~ 0.18% increase in R_U. The same increase in the ^{6}Li(n,tot) cross section gives a ~ 0.16% decrease in R_U, as expected. Increasing the ^{6}Li(n, tot) cross section by a 1% is equivalent to increasing the ^{6}Li atomic density by that amount which leads to decreasing the uranium breeding, R_U. The value of $S^U_{\Sigma_{tot}}$ due to a variation in the ^{6}Li(n,tot) cross section in the zone (#8) next to the fuel zone is larger than the corresponding value in the zone which proceeds it (#4) although they are comparable. No further analysis for N_i, Cr, Fe, and Sn has been performed since they have small sensitivity coefficient values.

Applying the same type of variation to the partial cross sections has been performed and the results are given in Table (VIII.2). From this table, it is clear that U-233 production is more sensitive to changes in the Th(n,γ) cross section. Positive change in this cross section enhance U-233 production. This production has also an appreciable positive sensitivity coefficient for the Pb(n,2n'), Th(n,2n'), Th(n,3n'), and Th(n,fission) cross sections, in that order. These reactions tend to increase the neutrons available for fissile fuel breeding. Except for carbon, increasing the elastic scattering cross section tends to increase the U-233 breeding ratio. This can be shown by examining the value of $S^U_{\Sigma(n,elastic)}$ for ^{16}O, Pb, Th, Zr, and ^{7}Li. While the coefficient S^U_Σ is positive for the Th(n,inelastic) cross section, it is negative for Pb(n,inelastic). This is because Th(n,inelastic) reactions reduces the neutron energy and thus

Table (VIII.2)

THE INTEGRATED RELATIVE SENSITIVITY COEFFICIENT, S_{Σ}^{U}, FOR THE U-233 BREEDING RATIO DUE TO A 1% INCREASE IN THE VARIOUS PARTIAL CROSS-SECTIONS FOR DIFFERENT MATERIALS

Cross-Section Perturbed	$S_{\Sigma}^{U} = \frac{1}{R_U}\frac{\delta R_U}{\delta C}$						
	Th	Pb	^{6}Li	^{7}Li	^{16}O	C	Zr
(n,elastic)	2.99-2[++]	4.26-2	2.99-3	2.02-2	1.17-1	-2.04-2	2.92-2
(n,inelastic)	3.33-2	-1.49-2	-5.40-5	9.13-4[+++]	-3.60-3	4.63-4	-3.81-4
(n,2n')	3.09-2	1.53-1		5.74-4			2.19-2
(n,3n')	2.16-2	8.12-3					
(n,γ)	2.46-1	-1.08-2	-5.63-6	-7.62-5	-1.75-5	-5.12-6	-2.74-2
(n,p)			-4.33-5		-2.17-3		-1.78-3
(n,d)				-3.44-4	-7.04-4		
(n,α)					-7.44-3	-1.31-3	
(n,fission)	2.07-2						
(n,α)t			-1.64-1				
(n,2n')α			1.46-4	8.60-4			
(n,absorp.)*	2.77-1	-1.08-2	-1.64-1	-4.19-4	-1.03-2	-1.31-3	-2.91-2
(n,total)**	3.92-1	1.78-1	-1.61-1	2.22-2	1.03-1	-2.15-2	2.16-2

*(n,absorp.)=(n,capture)+(n,fission)

**(n,total)=(n,absorp.)+(n,elastic)+(n,inelastic)+(n,2n')+(n,3n')+(n,2n')α + . .

++Read 2.99×10^{-2}

+++Includes ^{7}Li(n,n',α)t reaction

more Th(n,γ) reactions occur. However, the Pb(n,inelastic) reaction when increased, it will be on the expense of Pb(n,2n') reactions. This results in decreasing the available neutrons for uranium breeding.

It can be noted that all cross sections which remove neutrons from the system (e.g., (n,α), (n,p), . .) have negative sensitivity coefficients [except for Th(n,γ) cross section since the positive direct part of the sensitivity coefficient dominates the negative collision loss part]. The reactions which tend to increase neutrons in the system (e.g., (n,2n'), (n,3n'), (n,2n')α, ..) have positive sensitivity coefficients.

In Figs. (VIII.3) to (VIII.16), we give the sensitivity profiles for U-233 production, $P^{U}_{\Sigma_i}$. The ordinate in these figures give the quantity $(1/\Delta u)(1/R)\ \delta R_U/\delta C$, where Δu is the change in lethargy defined by

$$\Delta u = \ln \left(\frac{E_{i+1}}{E_i}\right) \qquad \text{(VIII.1)}$$

where E_i and E_{i+1} are the energy limits of the histogram intervals given in these figures and δC is the fractional increase in the corresponding cross section. When multiplied by Δu, each histogram value can be thoughtof as being the percent change in the breeding due to a 1% increase in the corresponding cross section perturbed at a particular neutron energy group. These profiles include valuable information since it indicates in what energy range a large change in the design parameter takes place. The dashed line represents positive sensitivity and the solide line represents negative sensi-

titivity.

In Fig. (VIII.3) to (VIII.5), the sensitivity profiles for the Th(n,γ) cross section is given where the contribution from the direct part of the sensitivity coefficient, the indirect part, and the net effect are shown. Most of the contribution is due to the direct part and is in the energy range ~ 1 keV. In Fig. (VIII.6) and (VIII.7), we show that most of the contribution to the coefficient, $S^{U}_{\Sigma(n,2n')}$ for Pb is from the front zone which faces the high energy (14.1 MeV) D-T neutrons. It can be noted from these figures that the contribution from the highest energy group is the largest. For the Th(n,2n') cross section, most of the contribution to the sensitivity coefficient comes from the scattering gain part with a monotonic increase in the sensitivity profile , as shown in Fig. (VIII.8) to (VIII.10).

The sensitivity profiles of the ^{16}O(n,total) and the ^{16}O(n,elastic) cross sections are positive and of the same order of magnitude. Their profiles are similar. This can be shown from Fig. (VIII.11) to (VIII.12). For the ^{16}O(n,tot) cross section, the profile is almost positive over all neutron energies except for the high energy range where reactions like (n,p), (n,inelastic) and (n,α) take place.

The profiles for the Th(n,fission) and Th(n,inelastic) cross sections are shown in Fig. (VIII.13) to (VIII.14), respectively. Note that the net sensitivity coefficient for the Th(n,fission) cross section is due to the fission gain part and that the highest energy group has the highest coefficient value.

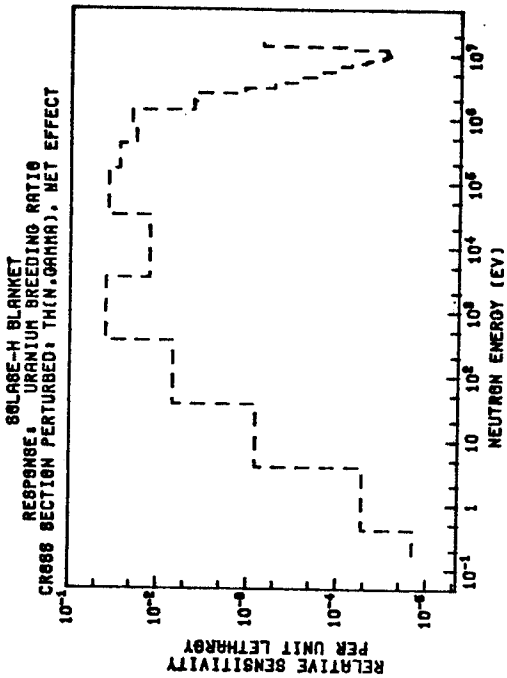

Fig. (VIII.5)

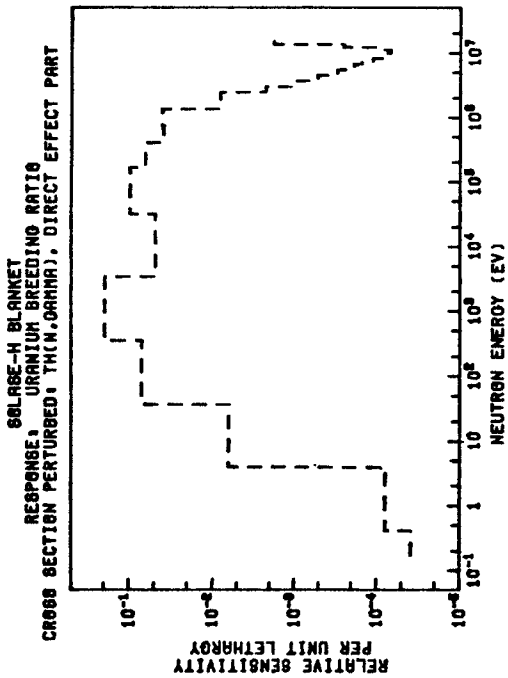

Fig. (VIII.3)

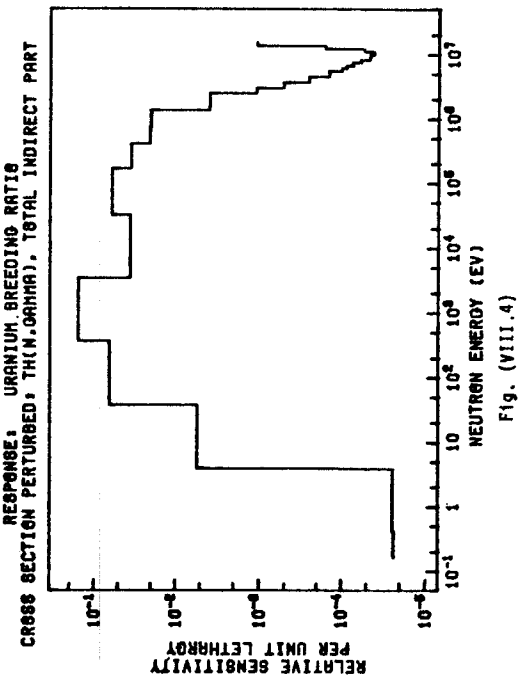

Fig. (VIII.4)

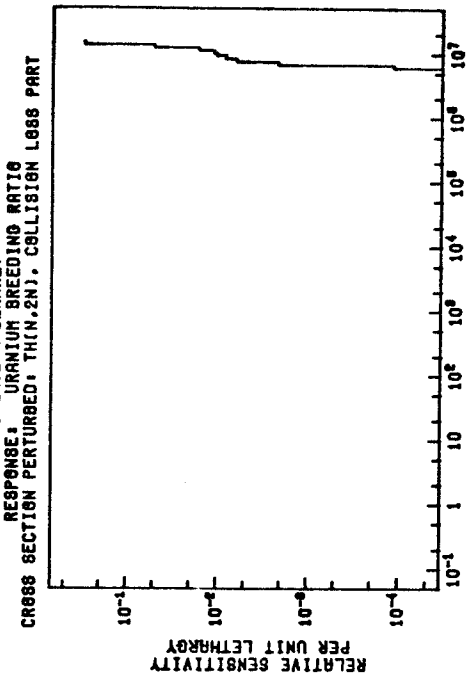

Fig. (VIII.8)

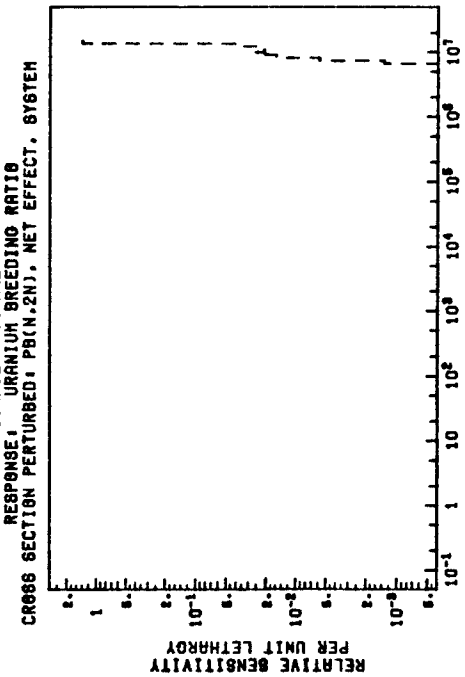

Fig. (VIII.6)

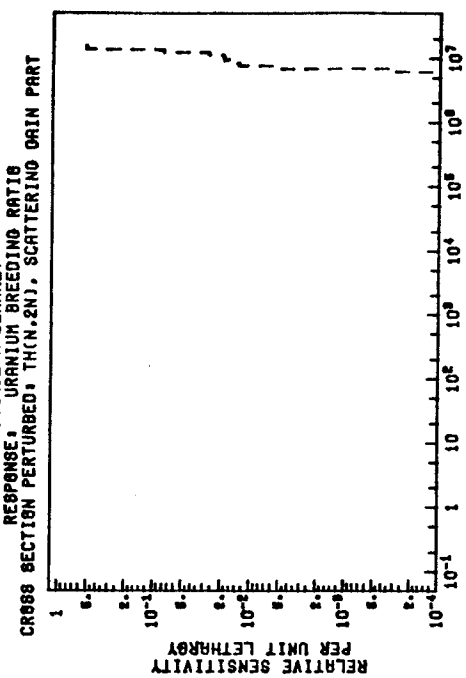

Fig. (VIII.9)

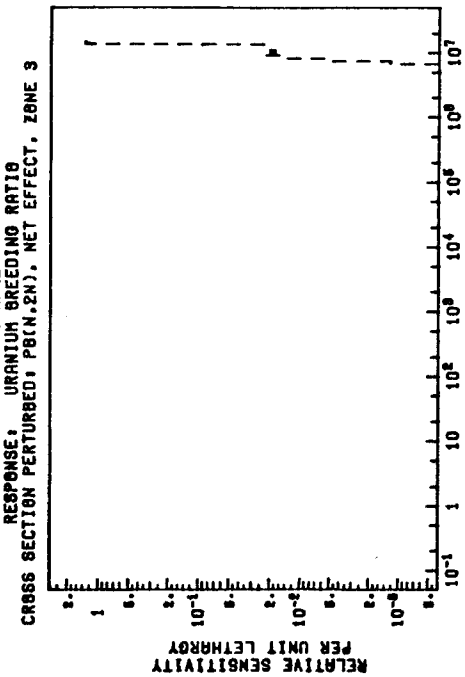

Fig. (VIII.7)

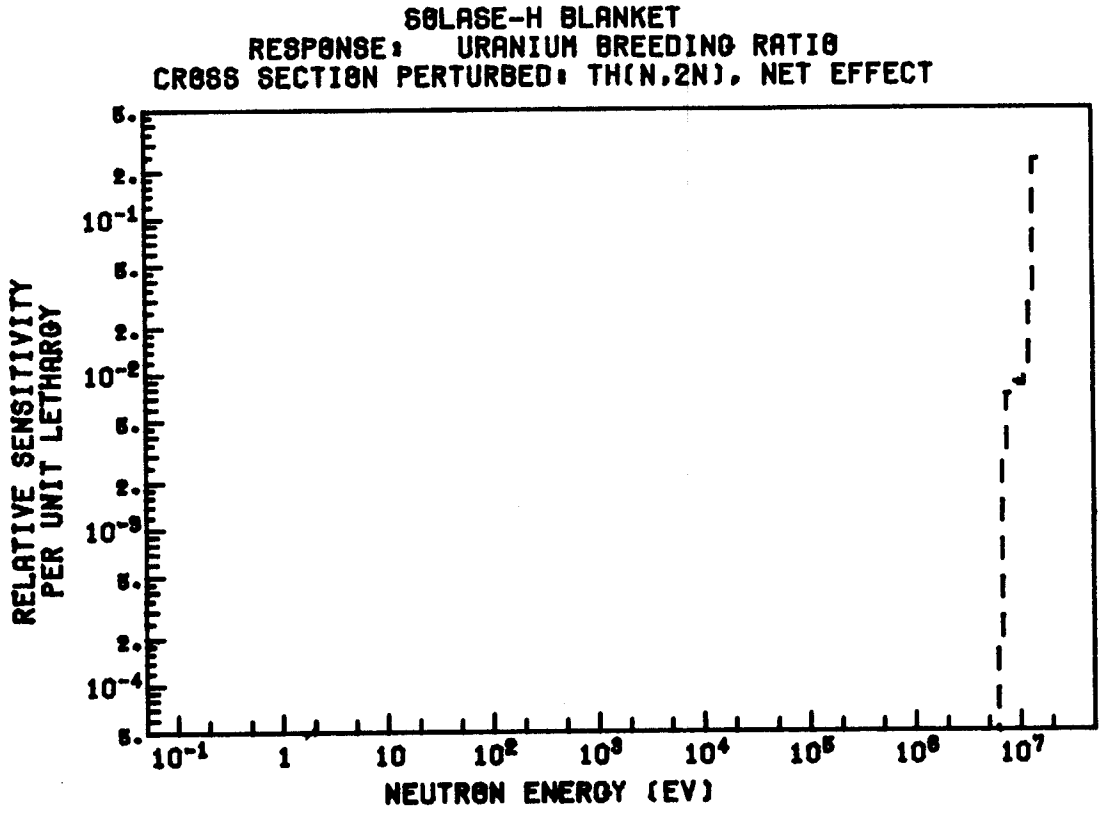
SOLASE-H BLANKET
RESPONSE: URANIUM BREEDING RATIO
CROSS SECTION PERTURBED: TH(N,2N), NET EFFECT
RELATIVE SENSITIVITY PER UNIT LETHARGY
NEUTRON ENERGY (EV)

Fig. (VIII.10)

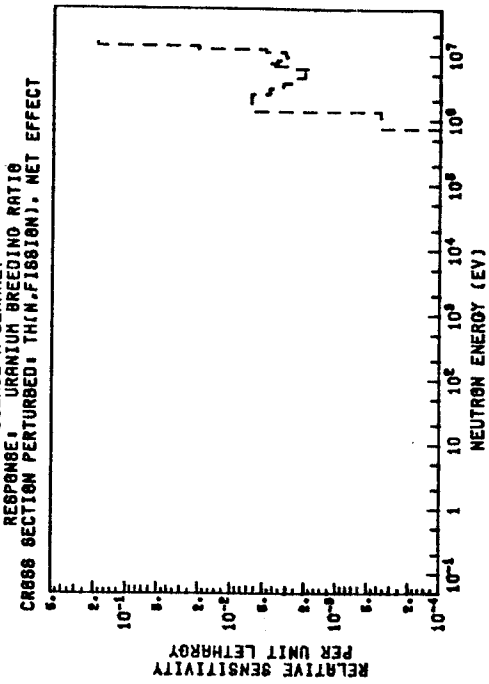

Fig. (VIII.13)

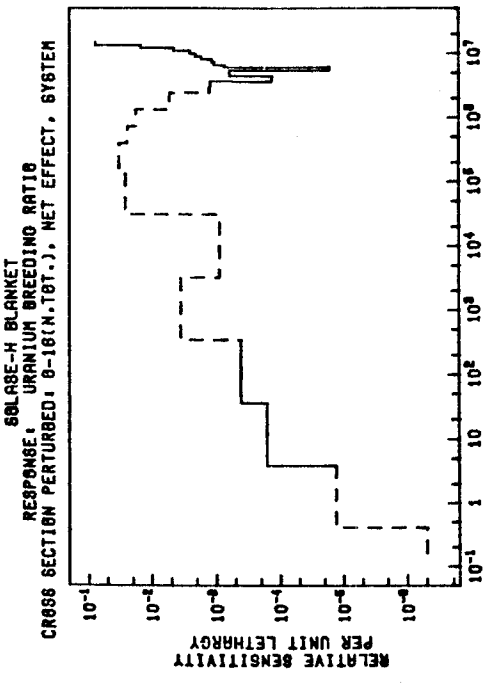

Fig. (VIII.11)

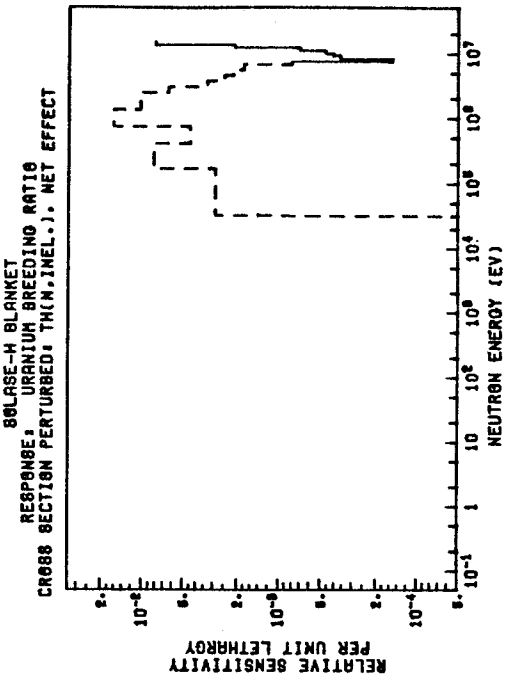

Fig. (VIII.14)

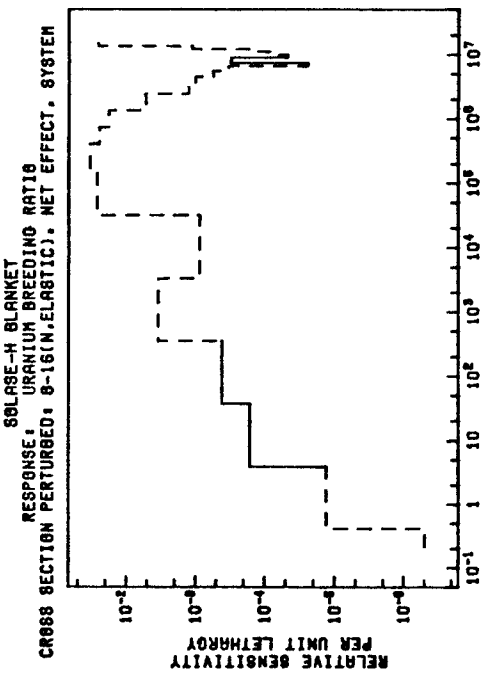

Fig. (VIII.12)

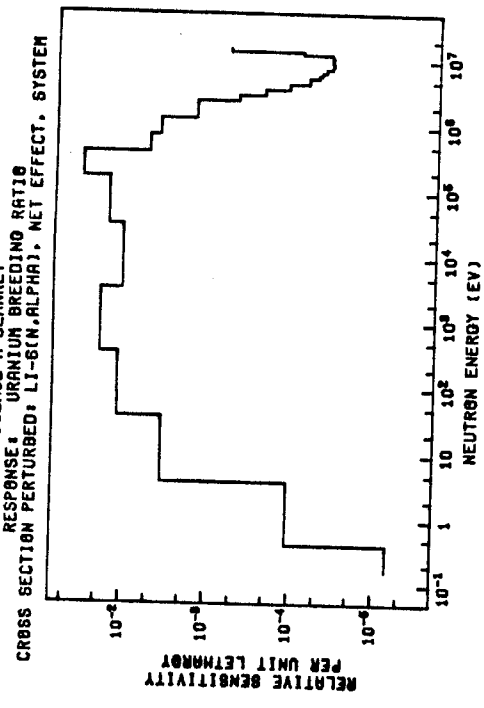

Fig. (VIII.15)

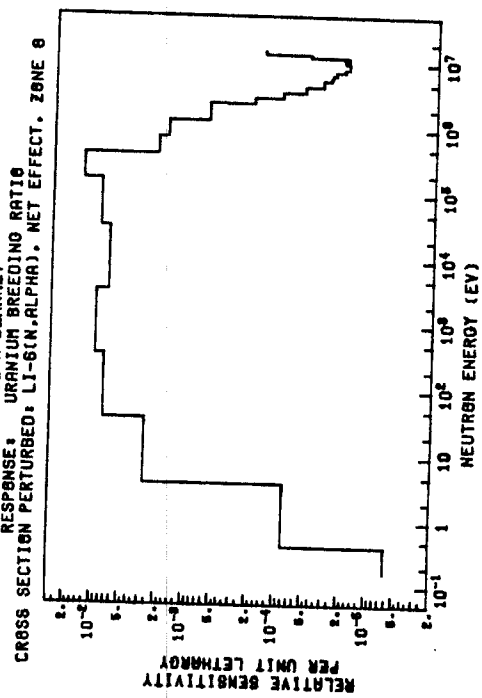

Fig. (VIII.16)

The $^{6}Li(n,\alpha)t$ cross section has an appreciable negative sensitivity coefficient and its profile in negative over all the energy range. Most of the contribution to the sensitivity coefficient comes from the low energy range where this cross section is a large (Fig. VIII.15). Shown in Fig. (VIII.16) is the sensitivity profile for this cross section in zone 8 from which an appreciable contribution to the total sensitivity coefficient is attributed. The profile in this zone follows the same pattern as the profile for the system.

VIII.3.B Sensitivity Analysis for the Tritium Breeding Ratio From ^{6}Li, $R_{^{6}Li}$

The tritium breeding ratio from ^{6}Li, $R_{^{6}Li}$, and the tritium breeding ratio from ^{7}Li, $R_{^{7}Li}$, have been evaluated to be 0.5752 and 0.0269, respectively. The values are based on the DLC-41B/VITAMIN-C library. The corresponding values when the DLC-2D library is used are 0.5983 and 0.0271, respectively. We have used the first two values in our sensitivity analysis.

The values of the integrated sensitivity coefficient, $S_{\Sigma}^{^{6}Li}$, for a 1% increase in the partial and the total cross sections is given in Table (VIII.3) for those elements of relatively large sensitivity coefficient. The total breeding ratio, R_{Li}, is 0.6021. It is found that the tritium breeding from ^{6}Li is sensitive to cross section changes in ^{6}Li, Th, Na, O, Pb, Zr, C, and ^{7}Li, in that order. Tritium breeding from ^{6}Li is most sensitive to ^{6}Li cross sections and is least sensitive to ^{7}Li cross sections. The appreciable positive sen-

Table (VIII.3)

THE INTEGRATED RELATIVE SENSITIVITY COEFFICIENT, $S_{\Sigma}^{^6Li}$, FOR TRITIUM BREEDING FROM ^6Li DUE TO A 1% INCREASE IN THE VARIOUS PARTIAL CROSS-SECTIONS FOR DIFFERENT MATERIALS*

$$S_{\Sigma}^{^6Li} = \frac{1}{R_{Li}} \cdot \frac{\delta R_{^6Li}}{\delta C}$$

Cross-Section Perturbed	Th	Pb	^6Li	^7Li	^{16}O	^{12}C	Zr	Na
(n,elastic)	-3.76-2	-5.59-2	-3.04-3	-1.16-2	-1.44-1	-3.24-2	-3.77-2	-1.43.1
(n,inelastic)	-4.79-2	-3.92-2	-5.82-4	-7.40-3	-1.21-2	-5.27-3	-1.74-2	-3.77-2
(n,2n')	1.51-2	7.77-2		4.66-4			1.25-2	1.66-4
(n,3n')	1.32-2	2.39-3						
(n,γ)	-2.72-1	-9.35-2	-4.31-5	-5.21-4	-1.24-5	-7.67-3	-1.22-2	-5.74-3
(n,p)			-6.68-5		-3.19-3		-2.05-3	-5.15-3
(n,d)				-5.55-4	-1.03-3			
(n,α)					-1.05-2	-5.45-3		-1.39-2
(n,fission)	2.80-2							
(n,α)t			3.17-1					
(n,2n')α			1.20-4	6.10-4				
(n,absorp.)	-2.44-1	-9.35-2	3.17-1	-1.08-3	-1.48-2	-1.31-2	-1.42-2	-2.48-2
(n,tot)	-3.01-1	-1.09-1	3.13-1	-2.00-2	-1.71-1	-5.07-2	-5.68-2	-2.05-1

*See footnotes of Table (VIII.2)

+$R_{^6Li} + R_{^7Li}$, $R_{^6Li} = 0.5752$, and $R_{^7Li} = 0.0269$

sitivity to $^{6}Li(n,\alpha)t$ reaction is evident since by increasing the breeding cross section, the probability that neutrons contribute to the breeding is increased and the probability that neutrons are lost from the system without contributing to the breeding is decreased.

Other cross sections of large negative sensitivity coefficients, ordered according to their absolute values are: Th(n,γ), ^{16}O(n,elastic), Na(n,elastic), Pb(n,γ), Pb(n,elastic), Th(n,inelastic), Pb(n, inelastic), Zr(n,elastic), Na(n,inelastic), Th(n,elastic), C(n,elastic), and Zr(n,inelastic). The negative sensitive coefficient for the Th(n,γ) cross section is clear since this reaction removes neutrons from the system and U-233 breeding is, in general, on the expense of tritium breeding. The elastic scattering reactions in ^{16}O (present in the ThO_2 fuel element) and ^{23}Na (a coolant) result in a negative and appreciable sensitive coefficient. This is because increasing these reactions will increase neutrons slowing down and thus decrease the energetic neutrons available for the (n,2n') and (n,fission) reactions in Pb and Th, respectively. This leads to decreasing the tritium breeding.

It can also be noted from Table (VIII.3) that the sensitivity coefficient of the Th(n,2n'), Th(n,3n'), and Zr(n,2n') cross sections is large and positive, as it must be.

The sensitivity profiles for several cross sections are shown in Fig. (VIII.17) to (VIII.27). The sensitivity to the $^{6}Li(n,\alpha)t$ cross section is positive at all energy and is appreciably large at low energy where the $^{6}Li(n,\alpha)t$ cross section is large. As shown

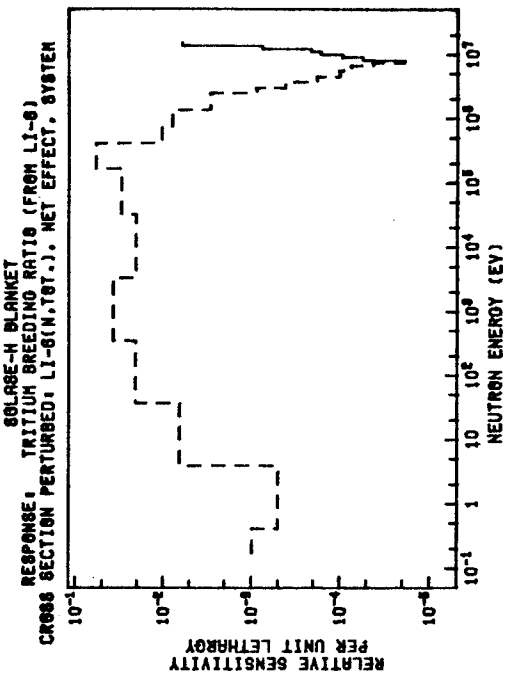

Fig. (VIII.19)

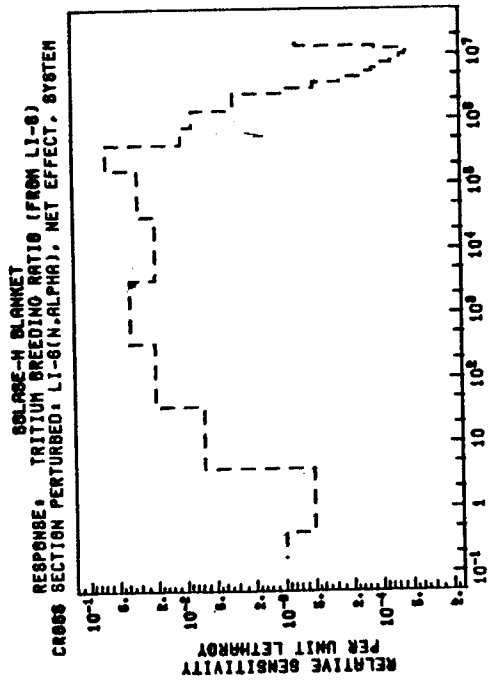

FIG. (VIII.17)

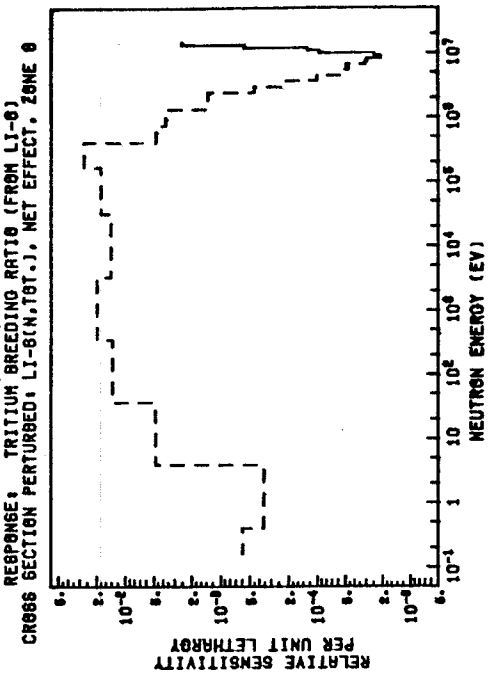

Fig. (VIII.20)

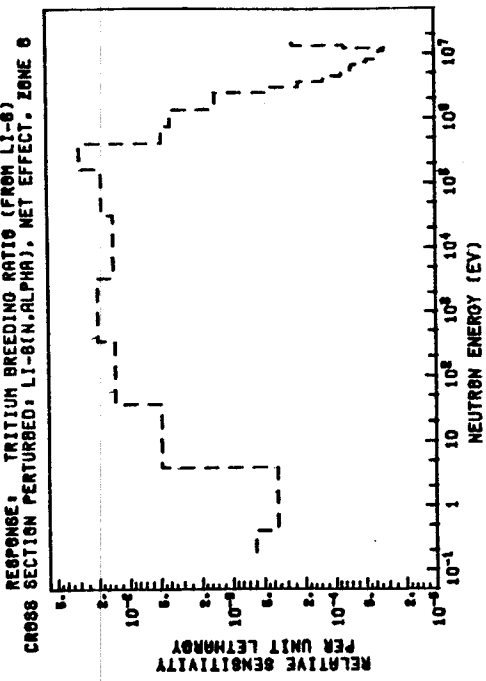

Fig. (VIII.18)

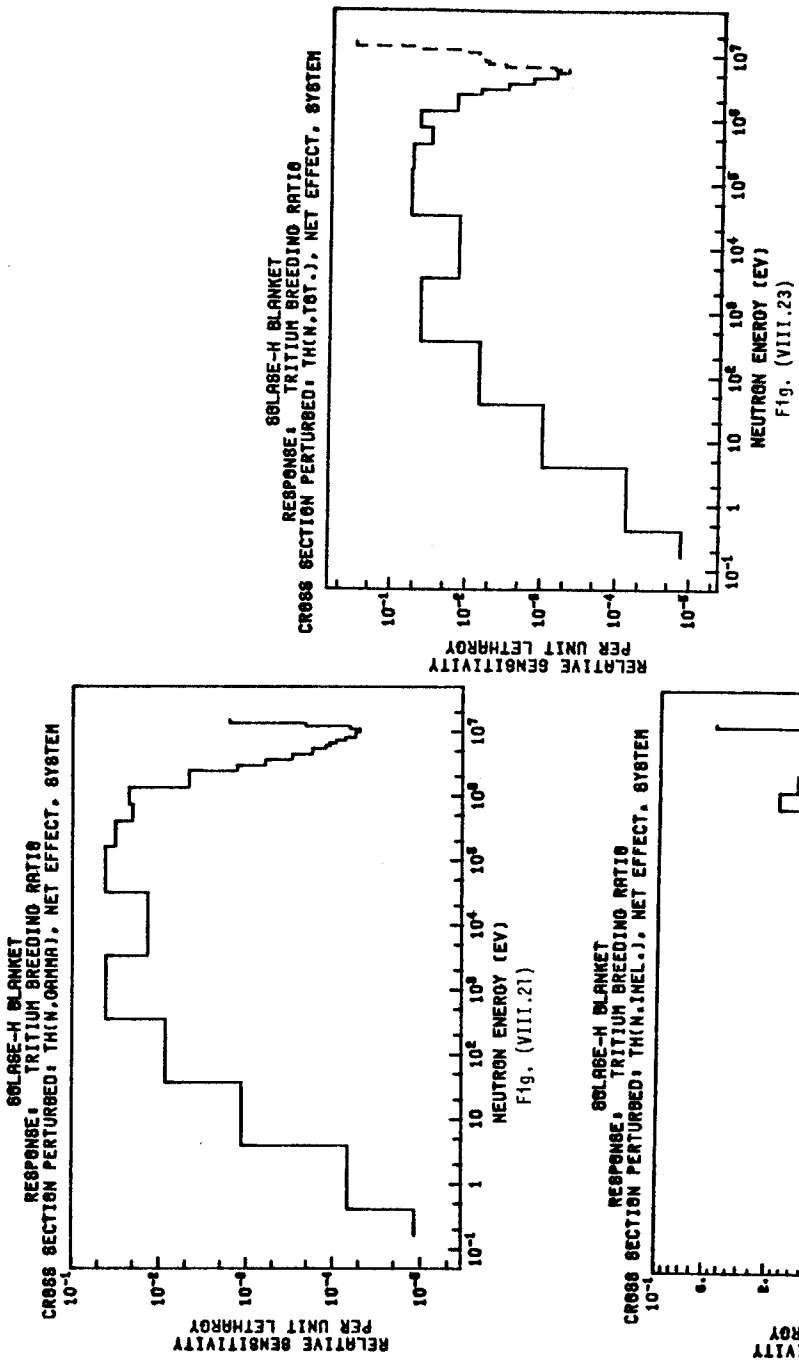

Fig. (VIII.21)

Fig. (VIII.22)

Fig. (VIII.23)

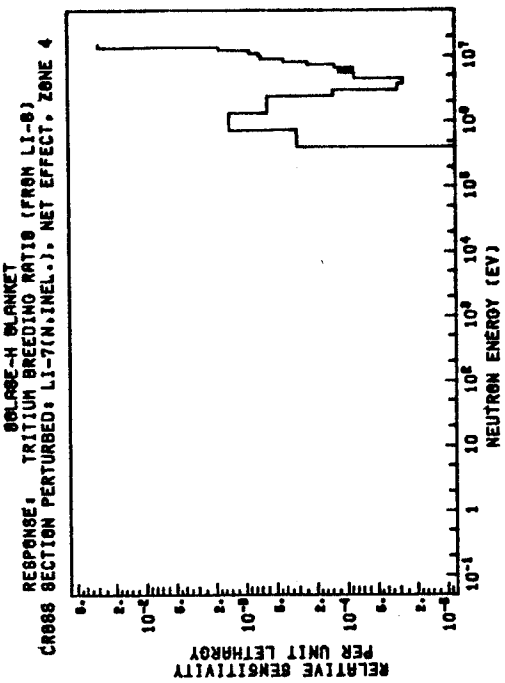

Fig. (VIII.26)

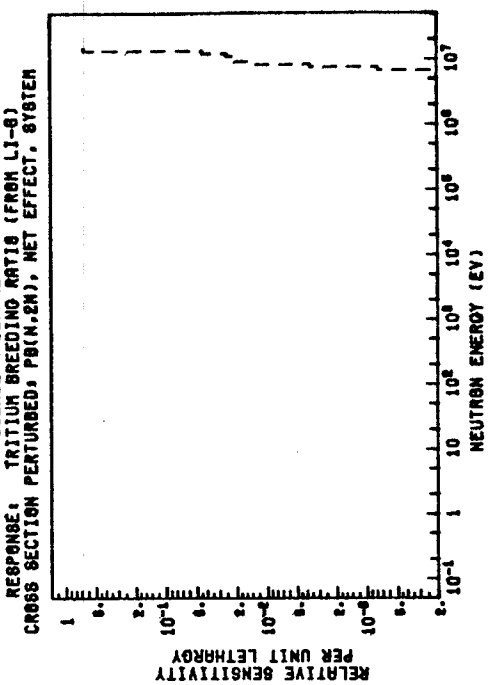

Fig. (VIII.27)

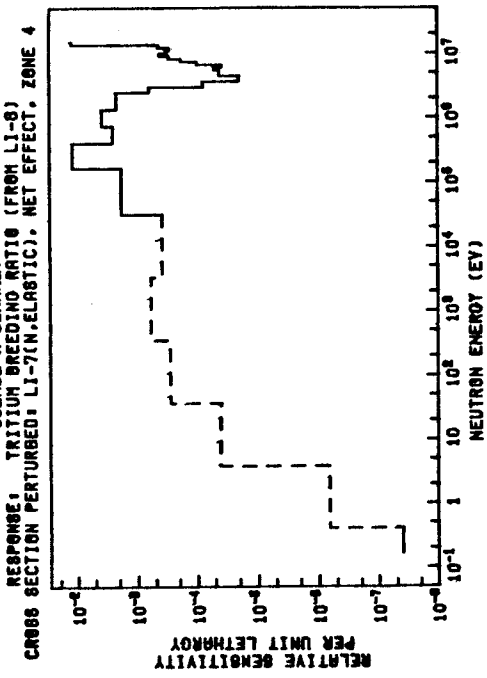

Fig. (VIII.24)

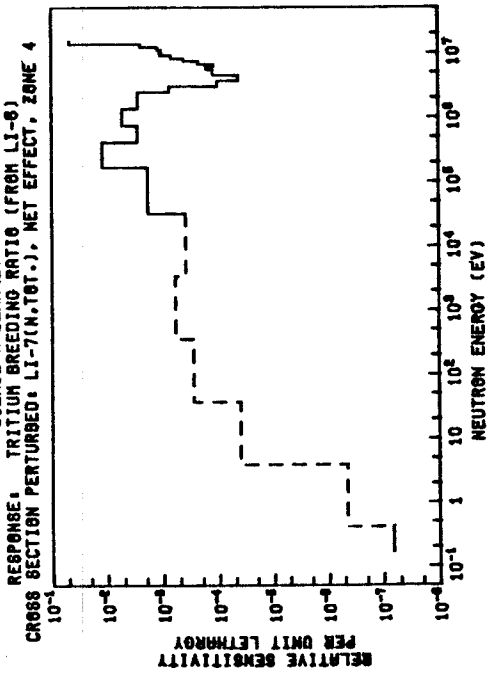

Fig. (VIII.25)

in Figs. (VIII.17) and (VIII.18), most of the contribution is from zone 8 which follows the fuel zone. The sudden depression in the sensitivity curve at ~ 0.28 MeV is due to the fact that ^{6}Li total cross section has a resonance in this energy range. This can also be shown by examining the sensitivity profile for the $^{6}Li(n,tot)$ cross section given in Fig. (VIII.19) and (VIII.20). A slight variation in the $^{6}Li(n,tot)$ cross section around 0.28 MeV results in a significant variation in the tritium breeding. Also, the sensitivity profile decreases as neutron energy exceeds 0.28 MeV due to the decrease in the contribution from the $^{6}Li(n,\alpha)t$ cross section and the increase in the contribution from the elastic scattering cross section. One notices from the profiles of the $^{6}Li(n,tot)$ cross section that at high energy it becomes negative. This is due to the fact that other neutron absorbing reactions take place (e.g., $^{6}Li(n,p)$ reactions which has a threshold around 3 MeV). It can also be noted, the similarity at low energy between the profiles for the $^{6}Li(n,\alpha)t$ and $^{6}Li(n,tot)$ cross sections. Also, note the similarity between the $^{6}Li(n,tot)$ cross section profiles in zone 8 and in the system.

The profiles for the $Th(n,\gamma)$, Th(n,inelastic), and Th(n,total) cross sections are given in Fig. (VIII.21) to (VIII.23). The $Th(n,\gamma)$ cross section profile is negative at all energies and is large in the keV energy range. The Th(n,inelastic) cross section profile exhibits negative value at all energies and is appreciable at high energy since this cross section competes with the neutron - producing cross section,e.g., Th(n,2n'), Th(n3n'), and Th(n,fission) cross

sections. Thus, an increase in the Th(n,inelastic) cross section decreases the number of the Th(n,2n') reactions at high energy and thereby decreases the number of neutrons available for $^{6}Li(n,\alpha)t$ reaction. The Th(n,total) cross section profile is similar to the $Th(n,\gamma)$ cross section profile at low energy. At high energy, it becomes positive due to the increase in the Th(n,2n'), Th(n,3n'), and Th(n,fission) cross sections.

The ^{7}Li(n,elastic), ^{7}Li(n,inelastic), and ^{7}Li(n,total) cross sections profiles are shown in Fig. (VIII.24) to (VIII.26) for zone 4 which proceeds the fuel zone. At low energies, the ^{7}Li(n,tot) cross section profile assumes the same shape as the ^{7}Li(n,elastic) cross section profile and both are positive. This is because increasing the ^{7}Li(n,elastic) cross section (which does not compete with other neutron-producing cross sections at low energy) leads to a more neutron moderation. This results in increasing the probability for the $^{6}Li(n,\alpha)t$ reactions. On the other hand, the ^{7}Li(n,elastic) and ^{7}Li (n,inelastic) cross sections, when increased at high energies will result in decreasing the number of energetic neutrons causing the (n,3n'), (n,3n'), and (n,fission) reactions. This leads to negative profiles at high energy. The depression and sudden increase in the profiles at ~ 3-5 MeV is due to the existence of thresholds for other (n,2n') and (n,3n') reactions. For example, in Fig. (VIII.27) we show the Pb(n,2n') cross section profile which has a threshold and increases monotonically with energy.

VIII.3.C Sensitivity Analysis for the Tritium Breeding Ratio From ^{7}Li, $R_{^{7}Li}$

The relative sensitivity coefficients of the tritium breeding ratio from ^{7}Li, $S_{\Sigma}^{^{7}Li}$, have been calculated for a 1% increase in the partial and the total cross sections and the results are given in Table (VIII.4).

From Table (VIII.4), we notice that the sensitivity coefficients for tritium breeding from ^{7}Li are much smaller than the corresponding values for tritium breeding from ^{6}Li although natural lithium (92.58% ^{7}Li, 7.42% ^{6}Li) is used in the SOLASE-H blanket. Tritium breeding from ^{7}Li is more sensitive to ^{7}Li, Pb, Th, Na, Zr, O, ^{6}Li, and C total cross sections, in that order. One can conclude that, in the SOLASE-H design, the tritium breeding from ^{7}Li is insensitive to ^{6}Li cross sections of any type. The sensitivity coefficients are all negative for all materials and partial cross sections (except for ^{7}Li(n,inelastic) cross section). Although increasing the neutron-producing cross sections is expected to increase neutron population in the blanket, the reactions due to these cross sections are competitive with $^{7}Li(n,n',\alpha)t$ reactions at high energy.

The sensitivity coefficient only becomes positive for the ^{7}Li(n, inelastic) cross section (which includes the $^{7}Li(n,\alpha,n')t$ cross section), as it must be, since increasing in the breeding cross section necessarily increases the breeding ratio. The cross sections of different materials can be ordered according to their importance for tritium breeding from ^{7}Li as follows: Pb(n,2n'), Th(n,2n'), Na(n,

Table (VIII.4)

THE INTEGRATED RELATIVE SENSITIVITY COEFFICIENT, $S_{\Sigma}^{^7Li}$, OF THE TRITIUM BREEDING FROM ^7Li DUE TO A 1% INCREASE IN THE VARIOUS PARTIAL CROSS-SECTIONS FOR DIFFERENT MATERIAL*

Cross-Section Pertubed	$S_{\Sigma}^{^7Li} = \frac{1}{R_{Li}} + \frac{\delta R_{^7Li}}{\delta C}$							
	Th	Pb	^6Li	^7Li	^{16}O	^{12}C	Zr	Na
(n,elastic)	-7.09-4	-3.39-3	-3.08-6	-6.04-6	-1.35-3	6.60-4	-3.98-4	-9.96-4
(n,inelastic)	-2.68-3	-4.73-3	-2.06-4	4.26-2	-3.29-3	-2.11-4	-2.67-3	-6.65-3
(n,2n')	-6.78-3	-2.99-2		-1.76-4			-4.70-3	-2.14-4
(n,3n')	-2.14-3	-4.43-4						
(n,γ)	-3.05-5	-3.34-6	-9.43-9	-1.07-7	-3.11-8	~0	-2.83-6	-2.43-6
(n,p)			-8.48-6		-3.68-4		-1.68-4	-5.41-4
(n,d)				-7.64-5	-1.19-4			
(n,α)					-1.16-3	-2.22-4		-1.48-3
(n,fission)	-1.41-3							
(n,α)t			-2.96-5					
(n,2n')α			-4.46-5	-2.45-4				
(n,absorp.)	-1.44-3	-3.34-6	-3.81-5	-7.65-5	-1.64-3	-2.22-4	-1.71-4	-2.02-3
(n,tot)	-1.37-2	-3.83-2	-2.91-4	4.21-2	-6.25-3	2.23-4	-7.94-3	-9.88-3

*See footnotes of Table (VIII.2)

+$R_{Li} = R_{^6Li} + R_{^7Li} = 0.6021$; $R_{^6Li} = 0.5752$ and $R_{^7Li} = 0.0269$

inelastic), Pb(n,inelastic), Zr(n,2n'), Pb(n,elastic), ^{16}O(n,inelastic), Th(n,inelastic), Zr(n,inelastic), Th(n,3n'), Zr(n,α), Th(n,fission), ^{16}O(n,elastic), and ^{16}O(n,α) cross section. One notices again that increasing the inelastic scattering cross sections of all materials (except ^{7}Li) leads to a negative sensitivity coefficient since inelastic scattering reactions compete with the ^{7}Li(n,n',α)t reaction.

The sensitivity profiles for the Pb(n,tot), Th(n,tot), Na(n,tot), ^{16}O(n,tot), and ^{6}Li(n,tot) cross sections are shown in Fig. (VIII.28) to (VIII.35). It can be noted that most of the contribution to the Pb(n,tot) cross section profile comes from lead presents in the front zone (#3). As stated earlier, the high energy ^{7}Li(n,n',α)t reaction is more sensitive to changes in the high energy reactions in Pb located in that zone.

Changes in the Th(n,tot) cross section necessitate a change in the Th(n,fission) cross section. The fission gain part of the sensitivity coefficient of the Th(n,tot) cross section is positive as is shown in Fig. (VIII.30). The Th(n,tot) cross section net profile is negative at most of the energy range. The system net profile for the Na(n,tot) cross section is almost the same as the profile in zone 6 where Na is used as a coolant. The sensitivity profiles for ^{16}O(n,tot) and ^{6}Li(n,tot) are shown in Fig. (VIII.36) to (VIII.37), respectively. Notice that tritium breeding ratio from ^{7}Li is more sensitive to ^{6}Li(n,tot) cross section than to ^{6}Li(n,α)t cross section (see Table (VIII.4)).

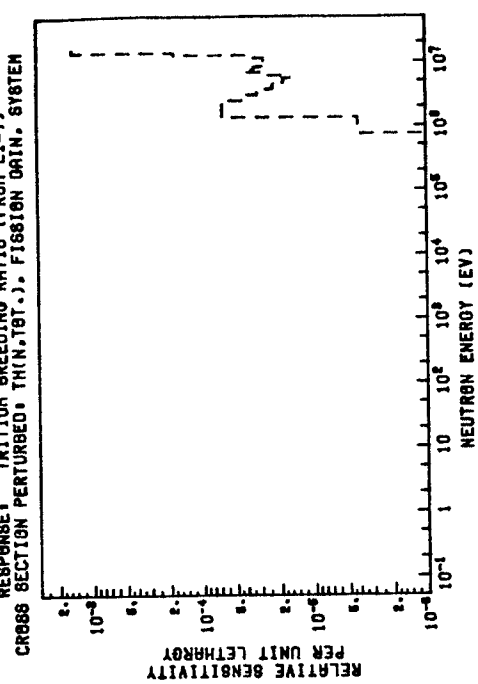

Fig. (VIII.30)

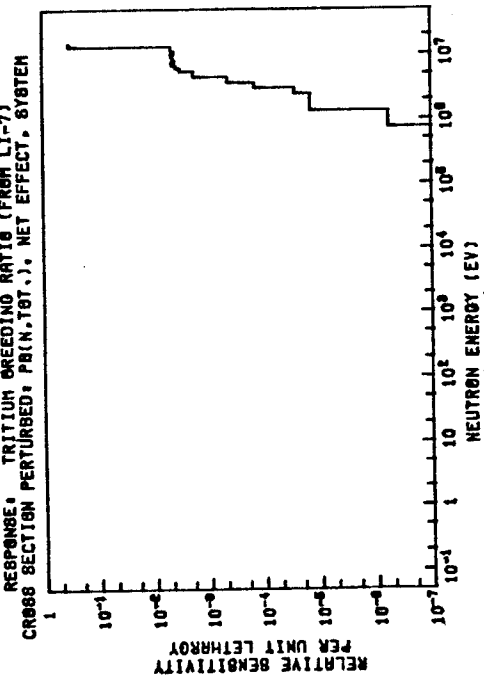

Fig. (VIII.28)

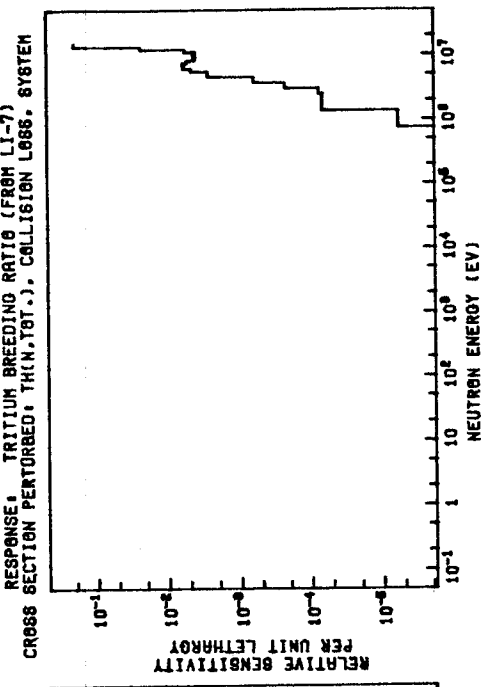

Fig. (VIII.31)

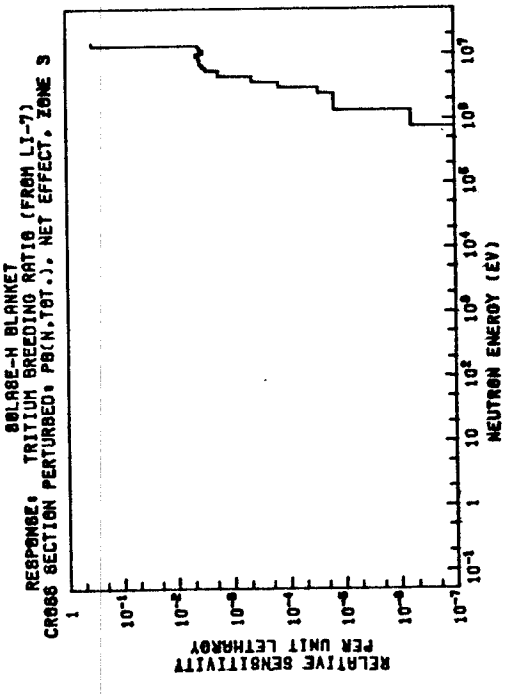

Fig. (VIII.29)

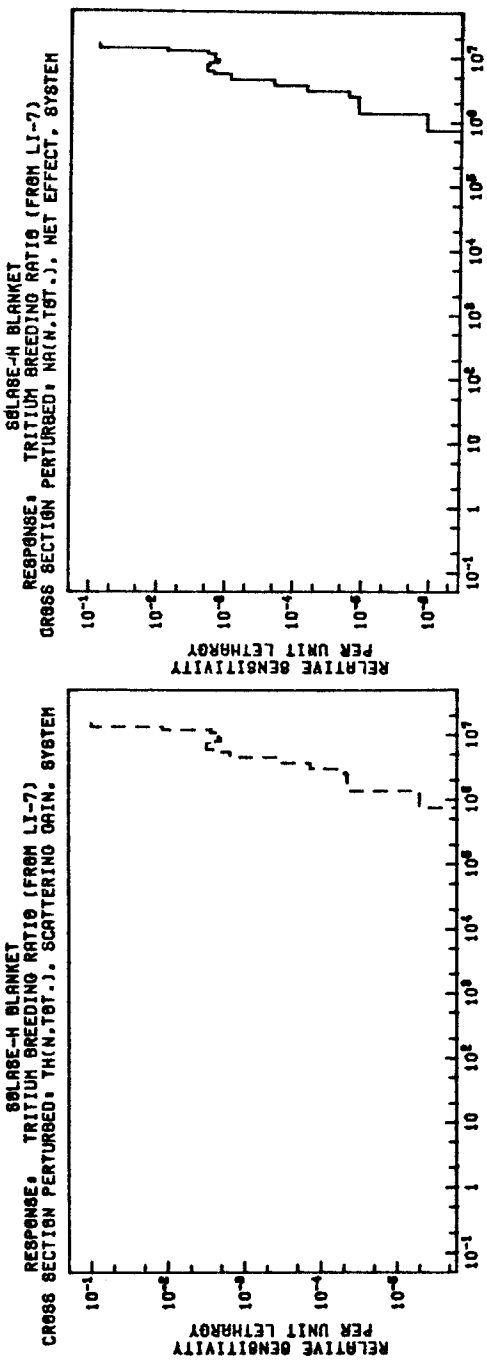

Fig. (VIII.32)

Fig. (VIII.33)

Fig. (VIII.34)

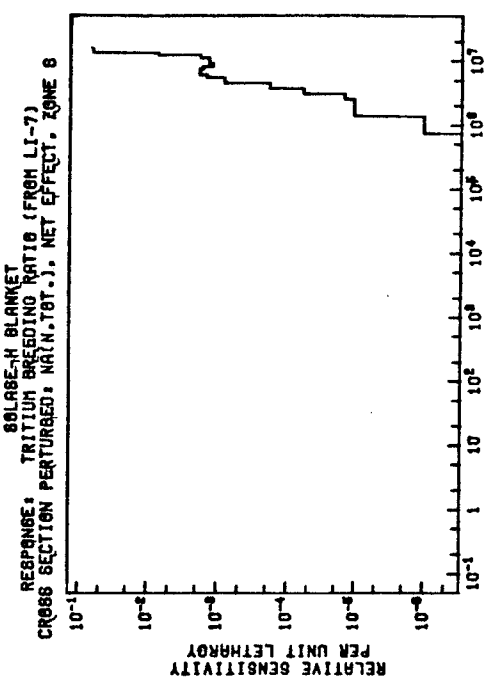

Fig. (VIII.35)

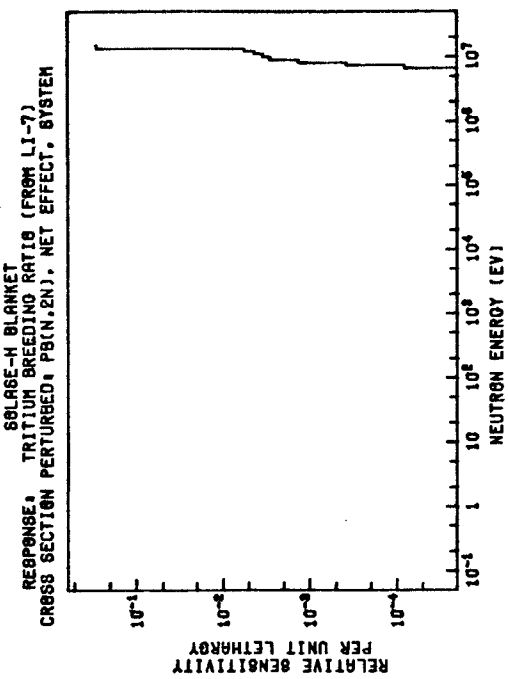

Fig. (VIII.38)

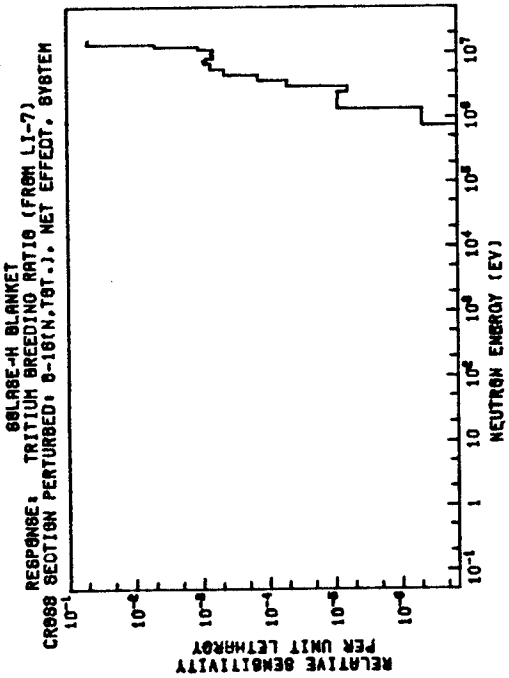

Fig. (VIII.36)

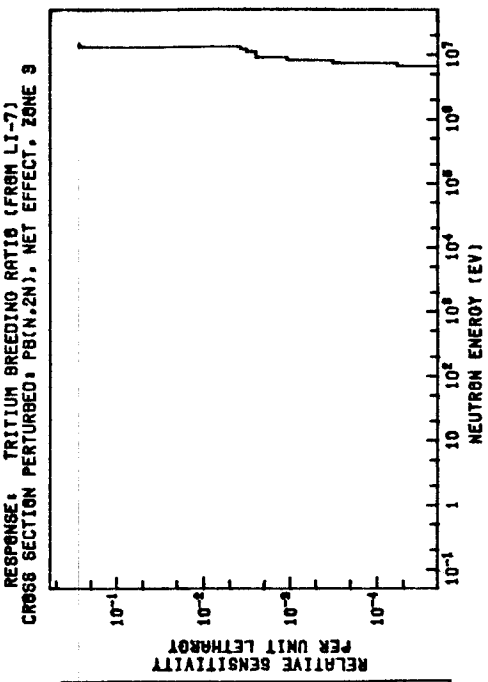

Fig. (VIII.39)

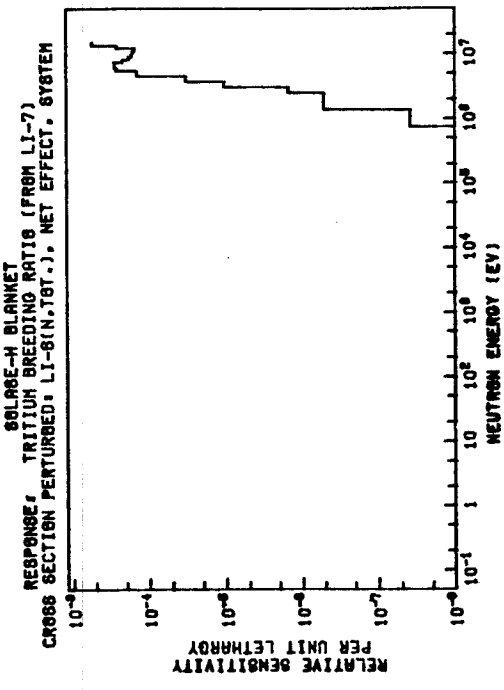

Fig. (VIII.37)

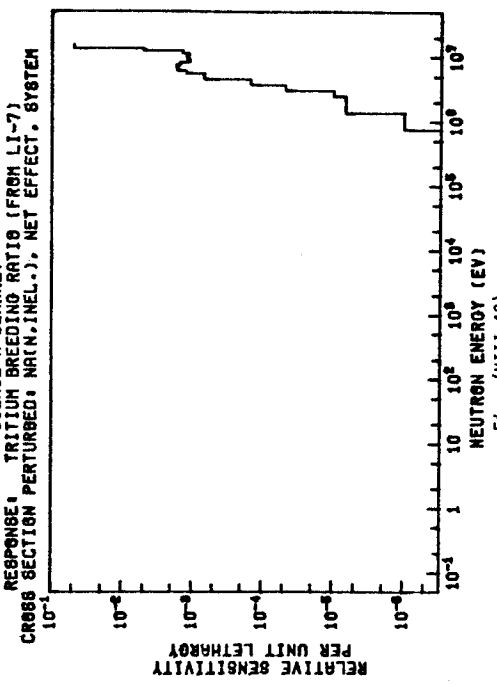

Fig. (VIII.42)

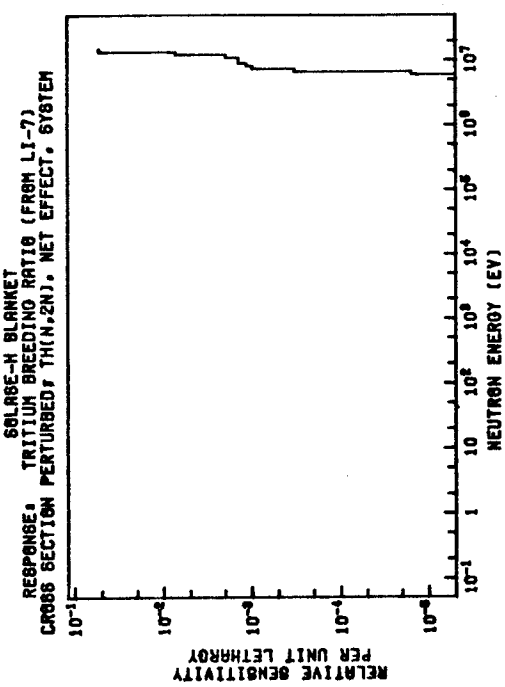

Fig. (VIII.40)

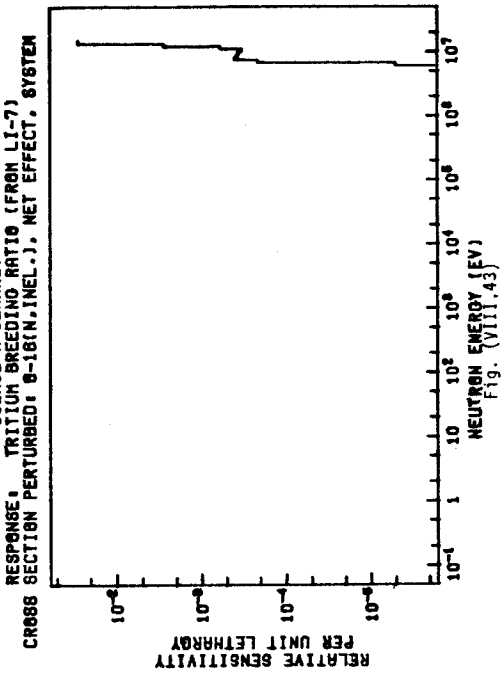

Fig. (VIII.43)

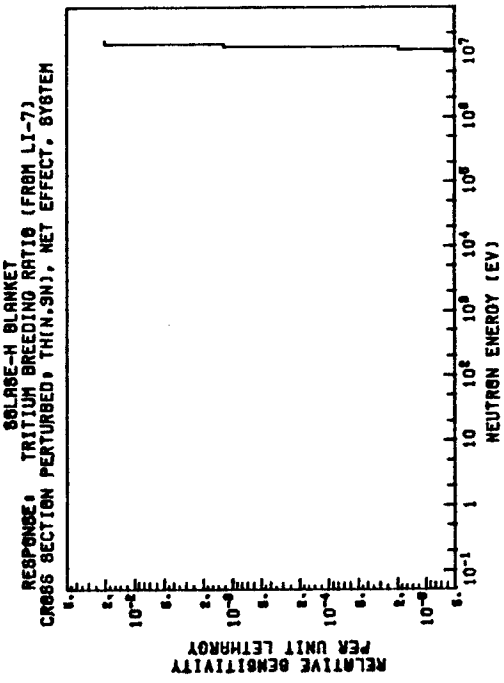

Fig. (VIII.41)

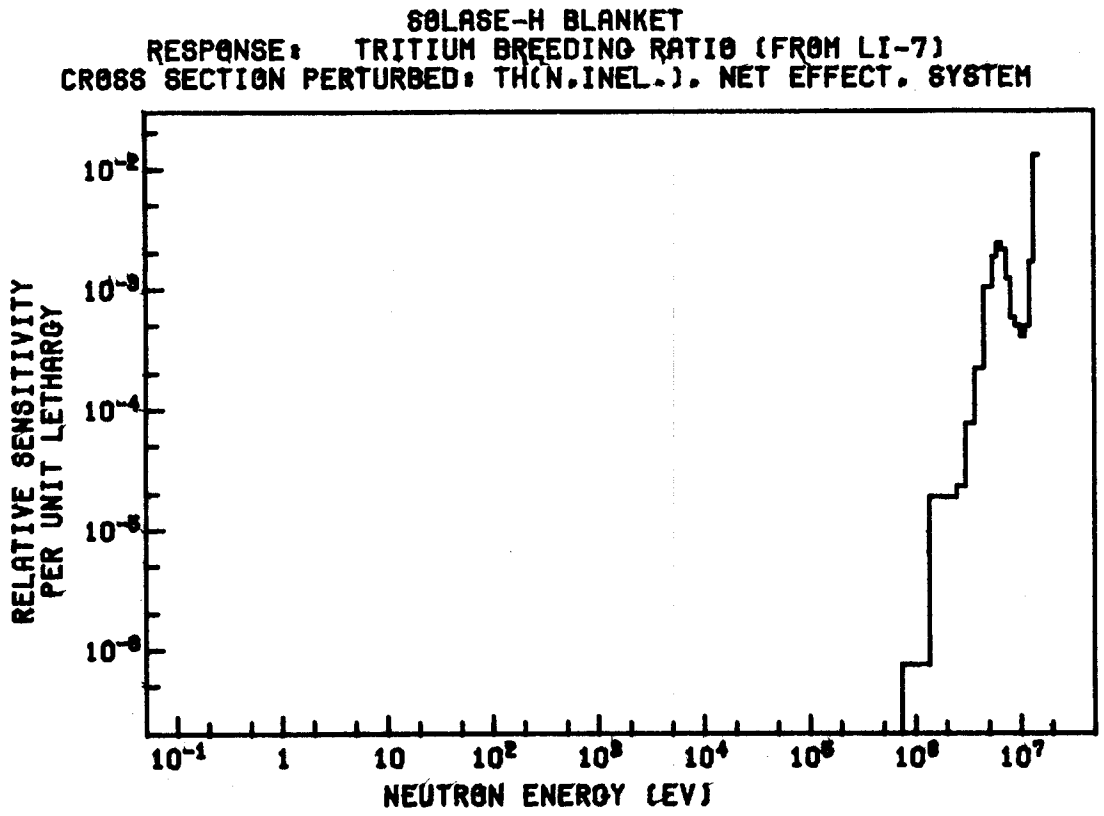
SOLASE-H BLANKET
RESPONSE: TRITIUM BREEDING RATIO (FROM LI-7)
CROSS SECTION PERTURBED: TH(N,INEL.). NET EFFECT. SYSTEM
RELATIVE SENSITIVITY PER UNIT LETHARGY
10^{-2}
10^{-3}
10^{-4}
10^{-5}
10^{-6}
10^{-1}
1
10
10^{2}
10^{3}
10^{4}
10^{5}
10^{6}
10^{7}
NEUTRON ENERGY (EV)

Fig. (VIII.44)

We give in Fig. (VIII.38) to (VIII.44) the profiles for Pb(n,2n'), Th(n,2n'), Th(n,3n'), Na(n,inelastic), ^{16}O(n,inelastic) and Th(n,inelastic) cross sections. The sensitivity coefficients for ^{16}O (n, inelastic) and Na(n,inelastic) are major contribution to the sensitivity coefficients of ^{16}O(n,tot) and Na(n,tot) cross sections, respectively,as it can be seen from Table (VIII.4). The same is true for thorium. One notices that in all the previous figures there is an increase in sensitivity coefficients in the highest energy groups because of the high-energy source used.

VIII.3.D Sensitivity Analysis for the Displacement Rate Per Atom Per Neutron in the Zircaloy Cladding, R_D

The displacement rate per atome (DPA) per neutron has been calculated in the Zircaloy-2 cladding and its constituents throughout the SOLASE-H blanket and the results are shown in Fig. (VIII.44)'. The DPA cross sections used in these calculations for Ni, Cr, Fe and Sn have been taken from Ref.(6). The DPA cross sections for Sn has been taken as the same as those for Niobium since they were not available by the time of performing the calculations. This does not affect the results obtained since Sn is ~ 1.5% of the Zircaloy-2 cladding while Zr is ~ 98.2%. The DPA cross section for Zr has been provided from Ref. (7). It has been found that the displacement rate per atom per neutron in the near edge of the front zone, in the front edge, and the back edge of the fuel zone are 3.01×10^{-27}, 1.68×10^{-27}, and 4.82×10^{-28} DPA/sec neutron, respectively. This corresponds to 8.03×10^{-7}, 4.49×10^{-7}, and 1.29×10^{-7} DPA/sec,

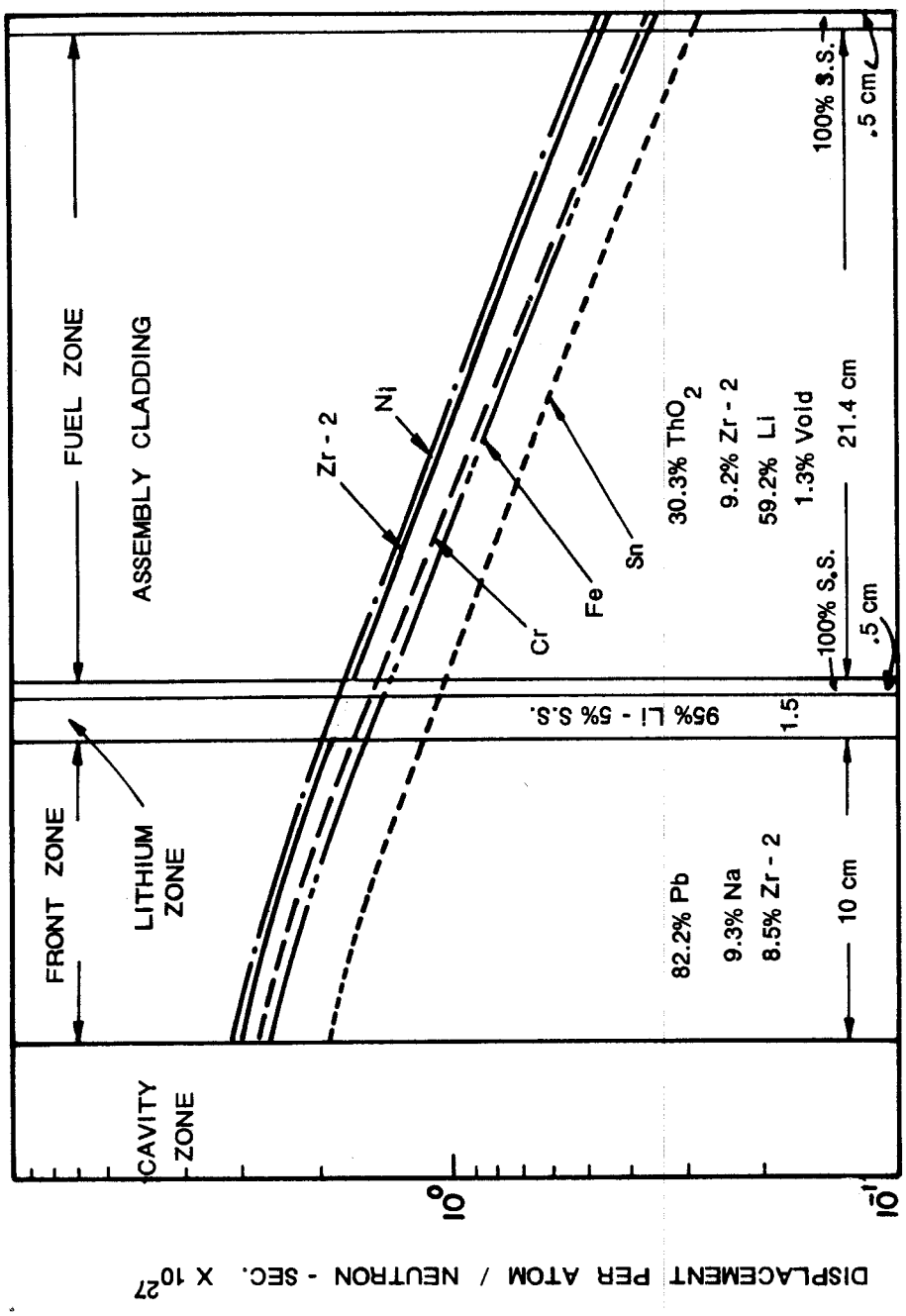

Fig. (VIII-44)[3]: DISPLACEMENT PER ATOM / D - T NEUTRON PER SEC. IN NICKEL, CROMIUM, IRON, TIN, AND ZIRCALOY - 2 CLADDING FOR THE SOLASE - H BLANKET (SPHERICAL GEOMETRY).

respectively, for a wall load ~ 1.92 Mw/m^2. After 2.72 full years of operation, the corresponding damage rate due to atoms displacements is 69, 39, and 11 DPA, respectively.

The average displacement rate per atom per neutron in the first 3 cm through the fuel zone, $\bar{R}_D$, has been estimated to be 1.59×10^{-27} DPA/sec·neutron. The sensitivity coefficients for the response $\bar{R}_D$, S_Σ^D, have been calculated for the partial and the total cross sections and the results are introduced in Table (VIII.5). When perturbing different cross sections for Ni, Cr, Fe, Zr, and Sn, only the indirect effect part was considered. Evaluating the direct effect for each partial cross section change necessitates re-evaluating the DPA cross section each time a partial cross section is perturbed. Therefore, the results given in Table (VIII.5) for these elements are not complete. However, the indirect effect part of their sensitivity coefficients gives the degree of flux perturbation due to cross sections changes. For other elements (Th,Pb,^{6}Li,^{7}Li,..), there is no direct effect from the cross section perturbation since the DPA rate is evaluated only in Zircaloy-2 cladding.

From Table (VIII.5), it can be noted that, for those elements with no direct effect, the sensitivity coefficients, S_Σ^D, are all negative for the total cross section changes and are more significant for Th, Pb, ^{6}Li, ^{7}Li, C, O, and Na. This is also true for the indirect effect part of the sensitivity coefficient for Ni, Cr, Fe, Sn, and Zr.

Table (VIII.5-A)

THE INTEGRATED RELATIVE SENSITIVITY COEFFICIENT, S_{Σ}^{D}, FOR THE AVERAGE DISPLACEMENT RATE PER ATOM PER NEUTRON IN ZIRCALOY-2 CLADDING THROUGH THE FIRST 3 CM IN THE FUEL ZONE IN THE SOLASE-H BLANKET++

Cross Section Perturbed	$S_{\Sigma}^{D} = \frac{1}{\bar{R}_D^*} \frac{\delta \bar{R}_D}{\delta C}$					
	Th	Pb	^{6}Li	^{7}Li	Ni^{+}	Cr^{+}
(n,elastic)	3.57-2	-3.69-2	-5.55-3	-4.75-2	-1.88-3	-2.48-3
(n,inelastic)	-5.04-2	-9.05-2	-5.35-4	-1.10-2	-1.83-3	-2.68-3
(n,2n')	1.87-2	-1.15-2		8.08-5	5.66-6	7.07-5
(n,3n')	8.27-3	-3.34-3				
(n,n')α						-2.51-6
(n,2n')α			2.14-5	-1.30-4		
(n,fission)	2.29-2					
(n,γ)	-3.86-2	-3.88-3	-3.73-7	-4.14-6	-2.28-4	-2.48-4
(n,p)			-4.24-5		-1.50-3	-4.52-4
(n,d)				-3.87-4		-7.14-5
(n,t)						-3.79-6
(n,^{3}He)						-5.39-9
(n,α)			-1.52-2		-5.36-4	-2.09-4
(n,n')p					-9.30-5	-5.37-5
(n,abs.)	-1.57-2	-3.88-3	-1.52-2	-3.91-4	-2.26-3	-9.85-4
(n,total)	-3.44-3	-1.46-1	-2.14-2	-5.96-2	-6.25-3	-6.25-3

*$\bar{R}_D = 1.5883 \times 10^{-27}$ DPA/sec neutron

+Direct effect is not included

++See footnotes of Table (VIII.2)

Table (VIII.5-B)

THE INTEGRATED RELATIVE SENSITIVITY COEFFICIENT, S_{Σ}^{D}, FOR THE AVERAGE DISPLACEMENT RATE PER ATOM PER NEUTRON IN ZIRCALOY-2 CLADDING THROUGH THE FIRST 3 CM IN THE FUEL ZONE IN THE SOLASE-H BLANKET++

Cross Section Perturbed	$S_{\Sigma}^{D} = \frac{1}{\bar{R}_D^*} \frac{\delta \bar{R}_D}{\delta C}$					
	Fe^+	C	O	Sn^+	Zr^+	Na
(n,elastic)	-1.21-2	-2.29-3	-2.37-2	2.29-4	1.03-2	-3.82-3
(n,inelastic)	-1.91-2	3.59-4	1.90-3	-3.54-4	-2.63-2	-3.35-2
(n,2n')	-1.31-5			9.82-5	1.39-2	-1.09-4
(n,3n')						
(n,n')α	-3.16-5					
(n,2n') α						
(n,fission)						
(n,γ)	-7.04-4	-6.84-11	-4.08-6	-1.84-4	-1.83-3	-3.96-4
(n,p)	-2.98-3		-1.58-3		-1.77-3	-3.30-3
(n,d)	-3.90-4		-5.08-4			
(n,t)	-6.12-6					
(n,^{3}He)	-5.04-6					
(n,α)	-8.89-4	-3.47-4	-5.66-3			-8.77-3
(n,n')p	-3.89-4					
(n,abs.)	-4.97-3	-3.47-4	-7.76-3	-1.84-4	-3.60-3	-1.25-2
(n,total)	-3.74-2	-2.42-3	-3.08-2	-2.10-4	-5.73-3	-5.01-2

*$\bar{R}_D = 1.5883 \times 10^{-27}$ DPA/sec neutron

+Direct effect is not included

++See footnotes of Table (VIII.2)

It can be also noted that changes in the inelastic scattering cross sections for Th,Pb,^{6}Li,^{7}Li, and Na lead to negative sensitivity coefficients and the most dominant effect is from Pb(n,inelastic) cross section. The reason is due to the fact that degrading neutron energy through (n,inelastic) reactions in these elements leads to decreasing the number of energetic neutrons which would have result in more DPA rate in Zircaloy-2 cladding. However, if the direct effect is evaluated for the (n,inelastic) cross section change in Zircaloy-2 constituents, one would expect positive coefficients in these constituents . It is clear also from Table (VIII.5) that, except for light elements (^{6}Li,^{7}Li,^{12}C,^{16}O), the (n,inelastic) cross section change is the dominant contribution to the total sensitivity coefficient. For other light elements, most of the contribution to S^{D}_{Σ} comes from the (n,elastic) cross section changes which have negative coefficients. These light elements moderate neutrons through encountering elastic scattering reations and thus reduce the number of energetic neutrons which can result in a larger DPA rate. One should notice that most of the negative value of the coefficient $S^{D}_{\Sigma(n,tot)}$ in ^{6}Li comes from the (n,α)t cross section change.

From Table (VIII.5), it can also be noted the importance of the P(n,2n'), Th(n,2n'), and Th(n,fission) cross sections changes on the DPA rate. An increase in the Pb(n,2n') cross section leads to a decrease in $\bar{R}_{D}$. The opposite is true for the Th(n,2n') cross section. This is probably due to the energy of the neutrons emitted after encountering scattering. For the Pb(n,2n') reactions, neutrons

emitted are soft compared to the corresponding neutrons from the Th(n,2n') reactions. While the two neutrons emitted from Th(n,2n') reaction are energetic enough to cause more DPA rate in Zircaloy-2 cladding, this is not true in the case of the Pb(n,2n') reaction. For Th(n,fission) reactions, the fission neutrons are also energetic enough to cause more fissions and this results in a larger DPA rate.

The sensitivity profiles, $P^{D}_{\Sigma_i}$, for the response $\bar{R}_D$ are given in Fig. (VIII.45) to (VIII.62). In Fig. (VIII.45) to (VIII.47) it can be noted that the positive profile for the Th(n,tot) cross section at high energy is mainly due to the Th(n,fission) cross section changes while the negative profile at other energies is presumably due to the Th(n,inelastic) and the Th(n,γ) cross sections changes. In Fig. (VIII.48) to (VIII.53) the profiles for Pb(n,tot), Pb(n,inelastic), and Pb(n,elastic) cross sections as shown where it is clear that most of the contribution to the profile for the Pb(n,tot) cross section comes from Pb(n,inelastic) and Pb(n,elastic) cross-sections and corresponds mainly to the front zone (#3). The shape of the Pb(n,tot) profile at low energies is due mainly to the Pb(n,elastic) cross section.

The profiles for the ^{7}Li(n,tot), and the ^{7}Li(n,elastic) cross sections are given in Fig. (VIII.54) to (VIII.57). The similarity between the profiles in the system and in zone 4, which precedes the front zone, is clear. Most of the contribution to the ^{7}Li(n,tot) cross section prfoile comes mainly from ^{7}Li(n,elastic) cross section

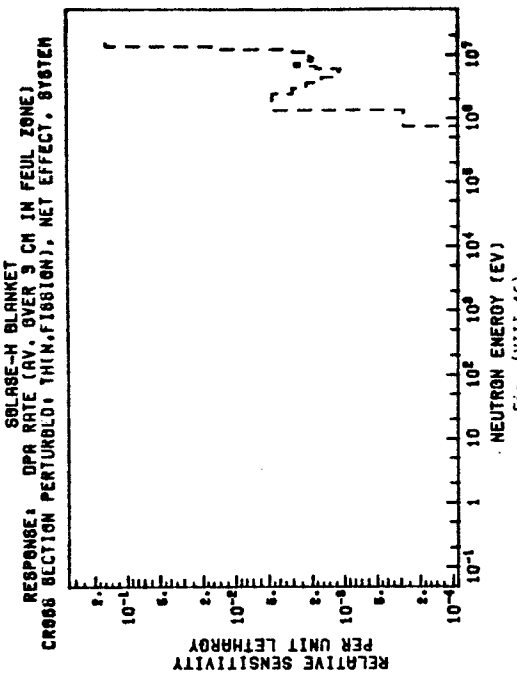

Fig. (VIII.46)

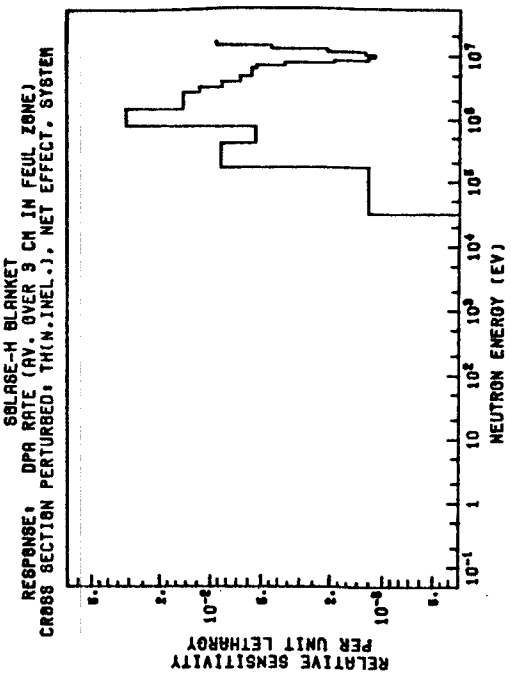

Fig. (VIII.47)

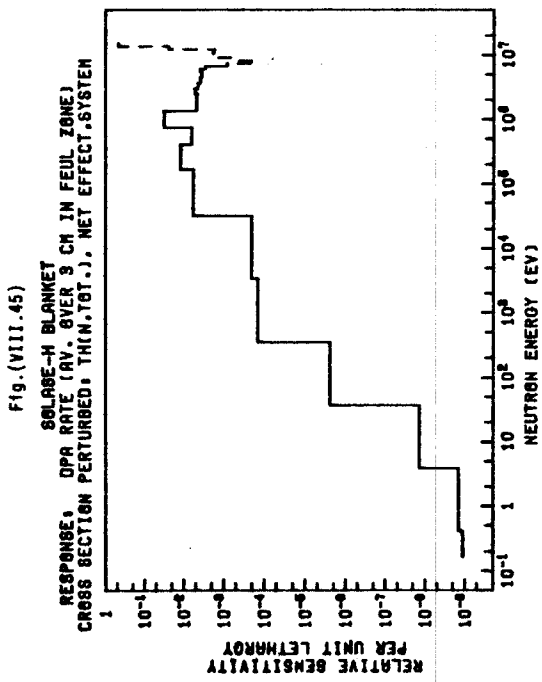

Fig.(VIII.45)

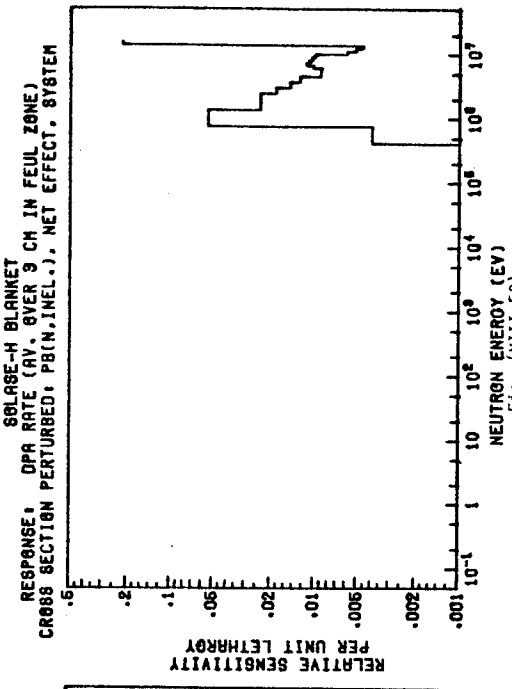

Fig. (VIII.50)

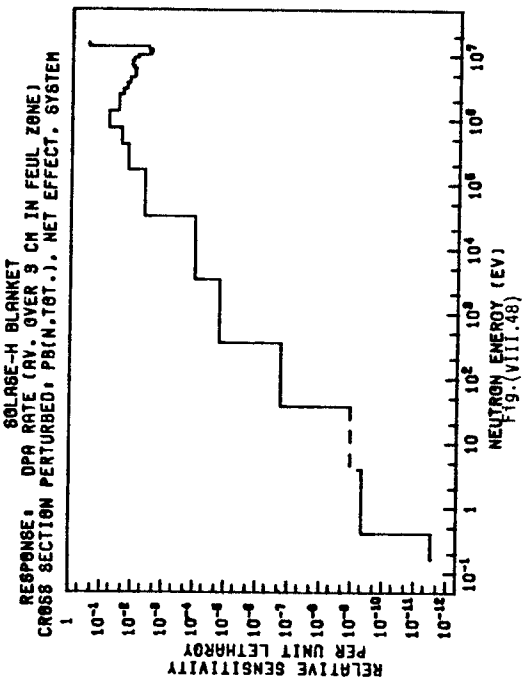

Fig.(VIII.48)

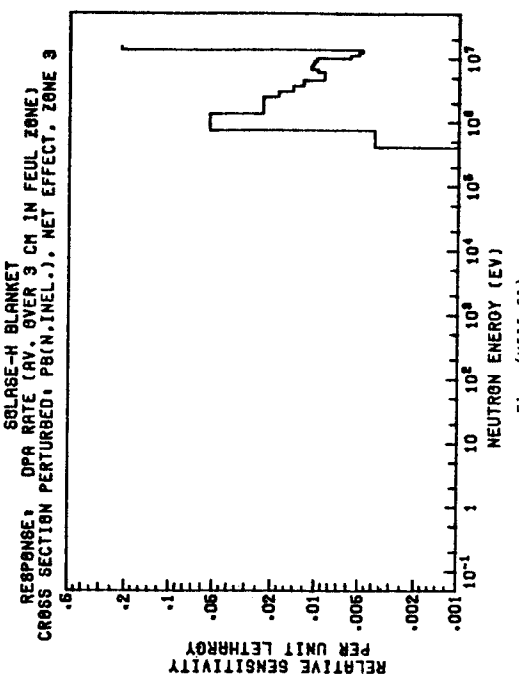

Fig. (VIII.51)

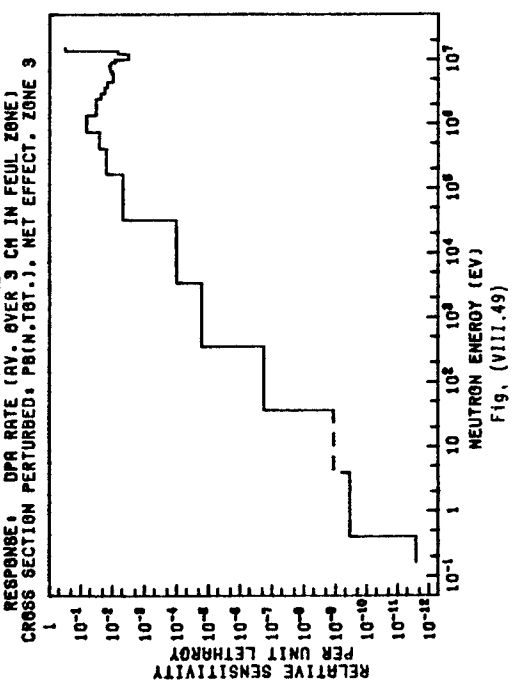

Fig. (VIII.49)

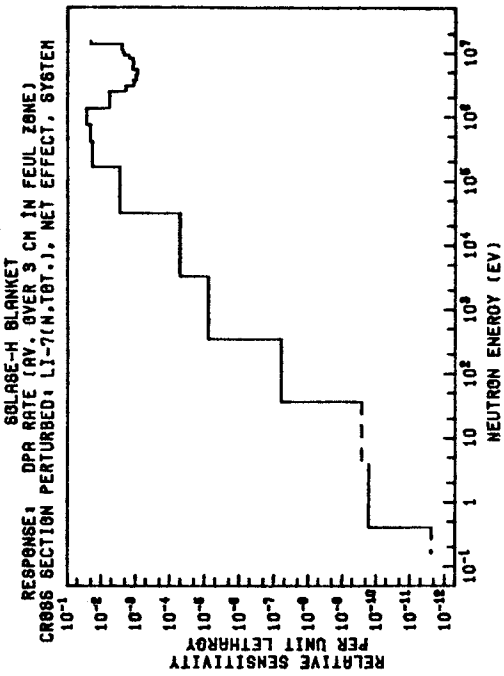

Fig. (VIII.54)

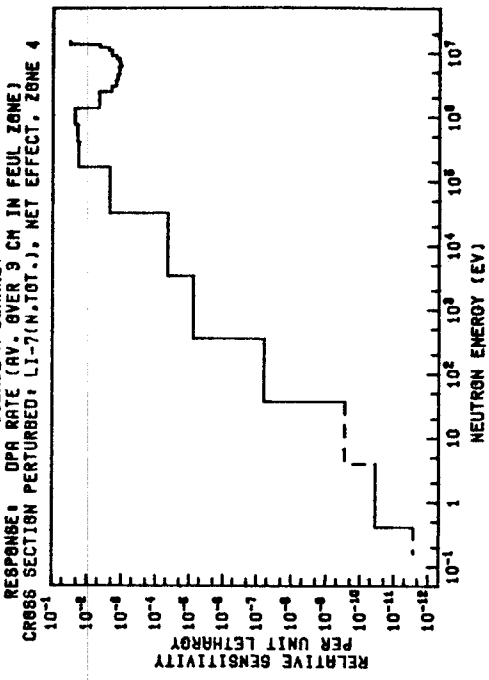

Fig. (VIII.55)

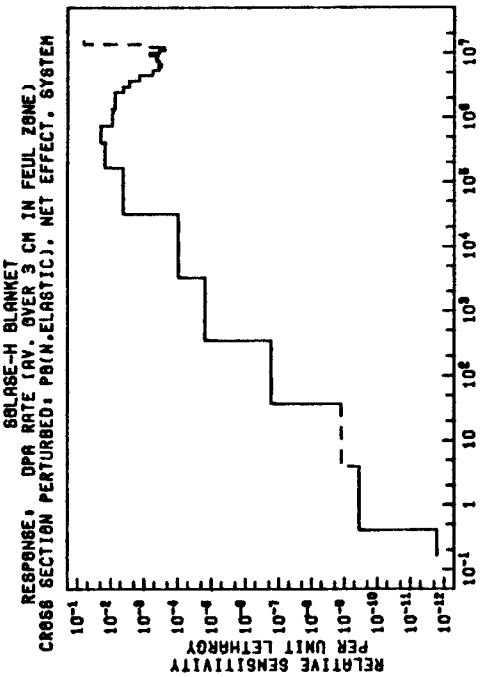

Fig. (VIII.52)

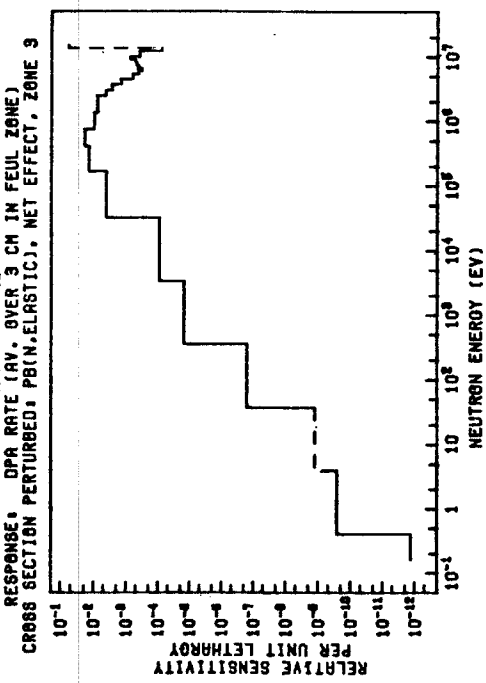

Fig. (VIII.53)

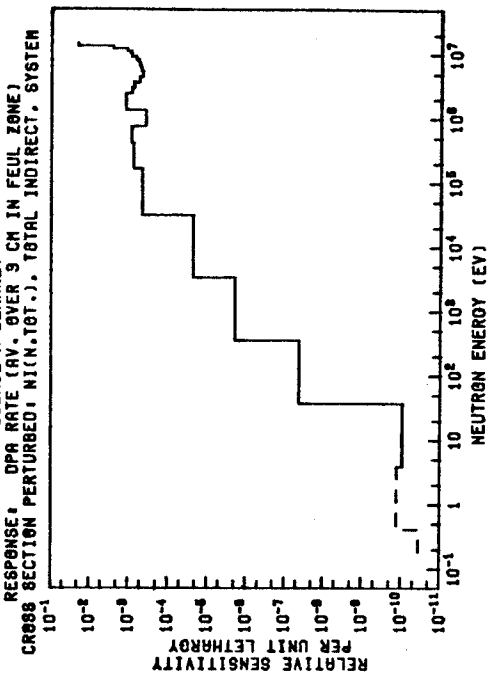

Fig. (VIII.58)

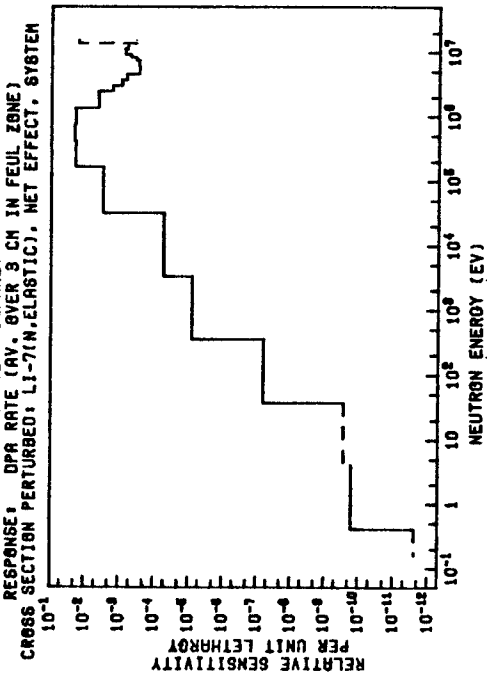

Fig. (VIII.56)

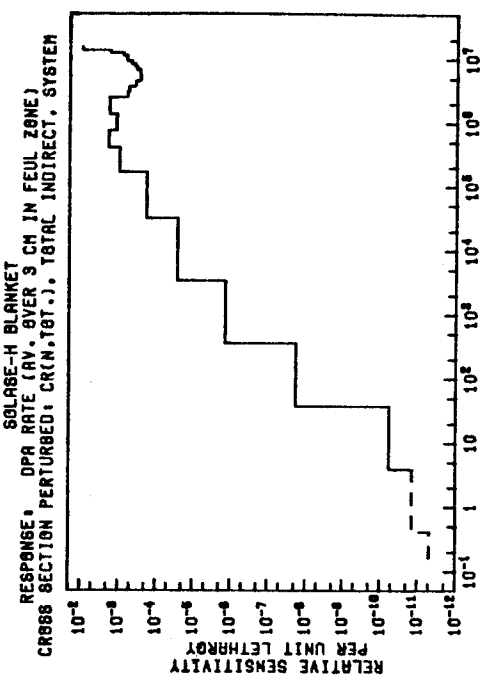

Fig. (VIII.59)

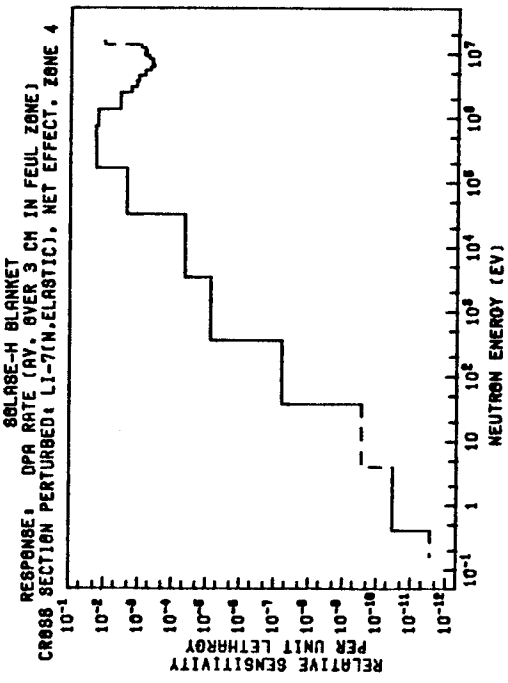

Fig. (VIII.57)

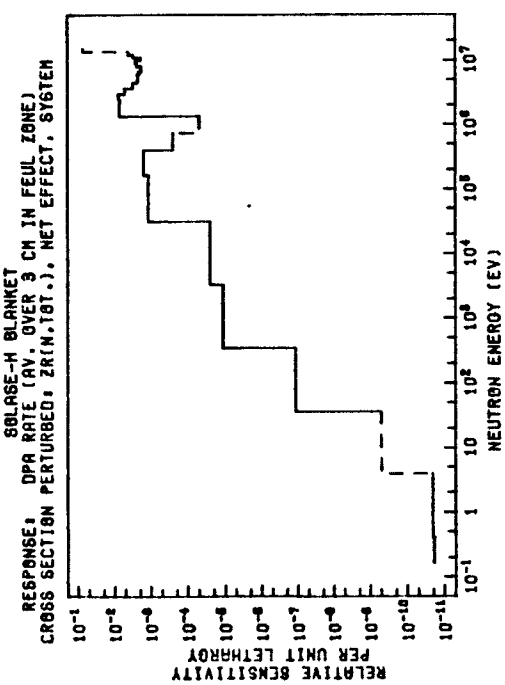

Fig.(VIII.60)

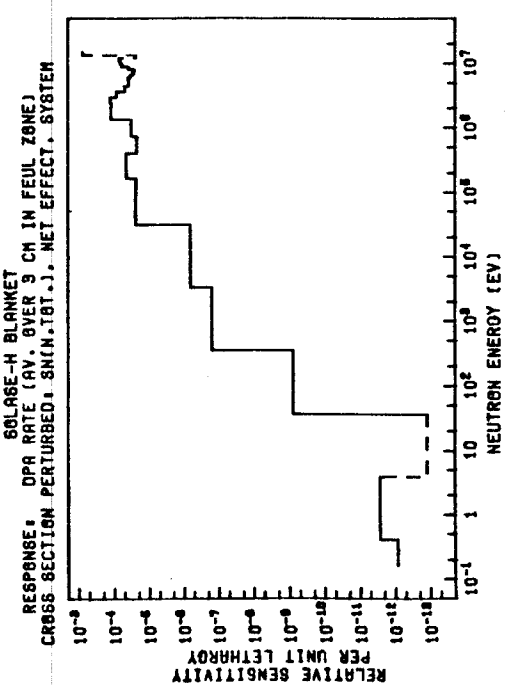

Fig. (VIII.61)

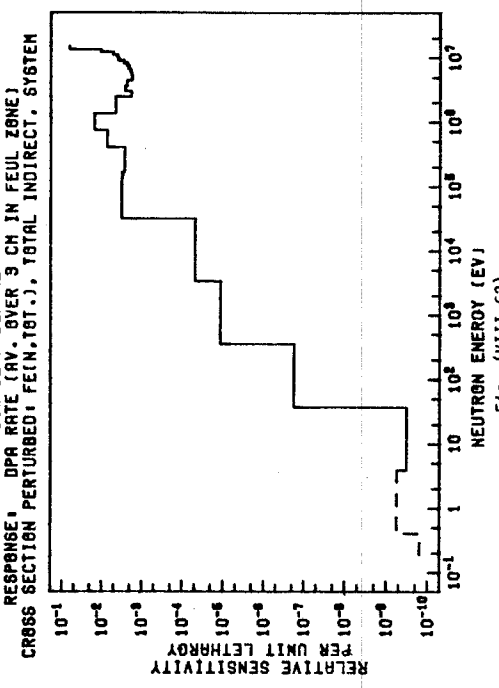

Fig. (VIII.62)

changes. The positive value at the highest group for the ^{7}Li(n, elastic) cross section profile can be expalined by noticing that increasing the ^{7}Li(n,elastic) cross section at high energy will be at the expense of reducing the ^{7}Li(n,inelastic) reaction (mainly ^{7}Li (n,n',α)t reaction) which is appreciable at high energy. Reducing ^{7}Li(n,inelastic) reactions results in increasing the available energetic neutrons which can cause further displacement in the Zircaloy-2 cladding.

The total indirect effect part of the profiles for Ni, Cr, Zr, and Sn are shown in Fig. (VIII.58) to (VIII.62). These profiles are negative over most of the energy range.

VIII.3.E Sensitivity Analysis for the Total Heat Deposited Per Neutron In the SOLASE-H Blanket From Nuclear Reaction, R_H^Q

a) Heat Deposition Calculation

The Q-Method has been used to evaluate the heat deposit rate in the SOLASE-H blanket per D-T neutron, R_H, and a computer code, 'ACTEN', was written to perform this evaluation. This code and the method used to calculate the heating rate is given in Ref. (12). The energy rate deposition in a given segment of the blanket, T_t^Q, can be evaluated from the equation

$$T_t^Q = -L_{n_E} - L_{\gamma E} + \sum_{j,i} R_{ij} Q_{ij} + \sum_{j} \sum_{i} R_{i'j} E_{D_{i'j}} + E_{ns} + E_{\gamma s} \qquad \text{(VIII.2)}$$

where

$$L_{nE} = \int_S \int_o^\infty E_n \bar{J}_n (\bar{r}_s, E_n) \cdot \bar{n} \, dE dS \qquad \text{(VIII.3)}$$

= Neutron energy leaked out the segment surface, S.

$$L_{\gamma E} = \int_S \int_o E_\gamma \bar{J}_\gamma (\bar{r}_s, E_\gamma) \cdot \bar{n} \, dE dS \qquad \text{(VIII.4)}$$

= Gamma energy leaked out the segment surface, S.

$\bar{J}_n(\bar{r}_s, E_n)$, $\bar{J}_\gamma(\bar{r}_s, E_\gamma)$ ≡ Net current at position $\bar{r}_s$ on surface S of energy E_n, and E_γ for neutron and gamma rays, respectively.

R_{ij} ≡ total reaction rate in the segment for reaction i in element j; Q_{ij} is the Q-value for that reaction.

$R_{i'j}$ ≡ total reaction rate in the segment for decay reaction type i' in element j; $E_{D_{i'j}}$ is the decay energy for this reaction.

$E_{ns}, E_{n\gamma}$ ≡ The neutron and gamma rays energy, respectively, of any external sources.

In calculating the heating rate throughout the SOLASE-H blanket, the gamma energy is assumed to be deposited locally and no gamma rays are leaked out of each spacial segment. This is particularly a reasonable assumption in a blanket utilizing heavy elements located in zones adjacent to each other. Therefore, the term $L_{\gamma E}$ is excluded from Eq. (VIII.2). Since no external neutron and gamma sources are present in the blanket, the terms E_{ns} and $E_{\gamma s}$ are also eliminated.

The total heat deposited per fusion neutron, R_H, at the begin-

ning of life in the SOLASE-H blanket has been calculated to be R_H = 20.2 MeV which corresponds to a power multiplication, M=1.43. The Q-values for different partial reactions were taken from Ref. (8). For some reactions, the Q-values are either obtained from Ref. (9) or calculated from the mass balance using Table (A-3) of Ref. (10). Decay heat informations can be found in Ref. (11). In the present calculation, decay heat contribution to the total heat deposited was ignored.

In Table (VIII.6), the energy deposited due to each nuclide is given. Except for Th, ^{6}Li, and Ni, the energy deposited for other nuclides are negative since most of the reactions taking place in these nuclides are endothermic. The (n,γ) reaction rate (has a positive Q-value) is small due to the fast and epithermal spectrum encountered in the SOLASE-H blanket. The contribution from the Th(n,fission) reactions (Q = ~ 200 MeV) is dominant. Most of the heat deposited due to reactions in ^{6}Li comes from the ^{6}Li(n,α) reaction which has a Q-value 4.79 MeV. The endothermic ^{7}Li(n,α,n')t reaction contributes the most to the heat deposited from ^{7}Li. This reaction has a Q-value -2.7 MeV.

In Table (VIII.7), we give the energy deposition rate per neutron in each zone of the SOLASE-H blanket. For each spacial zone, the difference between the energy leaked "in" and "out" the boundary is the portion of heat deposited due to the source neutron transport and is given in the third column of Table (VIII.7). This portion corresponds to the first term in Eq. (VIII.2) which is

Table (VIII.6)

ENERGY DEPOSITED IN THE SOLASE-H BLANKET PER D-T NEUTRON/SEC (BEGINNING OF LIFE)

From Reactions in:		
Ni	7.89-3*	MeV
Cr	-1.07-2	MeV
Fe	-1.78-1	MeV
Sn	-1.51-3	MeV
Zr	-3.83-1	MeV
C	-1.33-1	MeV
O	-3.86-1	MeV
Th	8.63	MeV
Li-6	2.75	MeV
Li-7	-1.08-1	MeV
Pb	-3.85	MeV
Na	-2.29-1	MeV
Sub Total	6.11	MeV
From the Source:	14.1	MeV
Total; R_H	20.21	MeV
Power Multiplication, M	1.43	

*Read 7.89×10^{-3}

Table (VIII.7)

ENERGY DEPOSITED IN THE SOLASE-H BLANKET
PER D-T NEUTRON/SEC BY ZONE
(BEGINNING OF LIFE)

Zone #	From Nuclear Reactions (MeV)	From the Source Leakage (MeV)	Sum (MeV)	% of Energy Deposited
3	-4.65	7.67	3.02	15.0
4	4.16-1*	4.16-1	8.32-1	4.0
5	-1.47-1	4.21-1	2.74-1	1.4
6	7.97	4.28	1.22+1	60.4
7	-1.26-2	9.99-2	8.73-2	0.3
8	1.87	4.38-1	2.31	11.0
9	3.35-1	9.42-1	1.28	6.3
10	3.28-1	3.24-3	3.31-1	1.6
In the system	R_H^Q = 6.11	R_H^S = 14.1	R_H = 20.2	

* Read -4.16×10^{-1}

called the source (or leakage) term. It can be noted that most of the heat is deposited in the fuel zone (#6) and is due mainly to Th(n,fission) reactions which contributes ~ 60% to the total heat deposited in the blanket. The large portion of heat deposited in the front zone is essentially due to the source term (leakage term). An appreciable amount of heat (~ 11%) is deposited in the Lithium zone (#8) following the fuel zone and is due to ^{6}Li (n,α)t reactions.

In Fig. (VIII.63), we give a histogram representing the heating rate density per neutron in the SOLASE-H blanket. Also shown, the portion of heat deposited due to the source neutron transport. It is larger than the total value in the front zone, the cladding of the fuel assembly, and in the reflector zones. This is due to the fact that reactions in these zones are endothermic. The amount of energy required for these reactions can be obtained from Fig. (VIII.63) by subtracting the dotted-line values from the solid-line values. It can be noted that the average energy desnity in the lithium zone preceding the fuel zone is larger than the corresponding value in the lithium zone following the fuel zone.

b) Sensitivity Analysis Results

Sensitivity Analysis has been carried out only for the part of heat deposited due to nuclear reactions, R_H^Q (~6.11 MeV). The Q-method used to evaluate R_H^Q enables us to evaluate easily the direct effect due to a partial cross section perturbation. If the heating rate were to be evaluated using the Kerma factors[8], then,

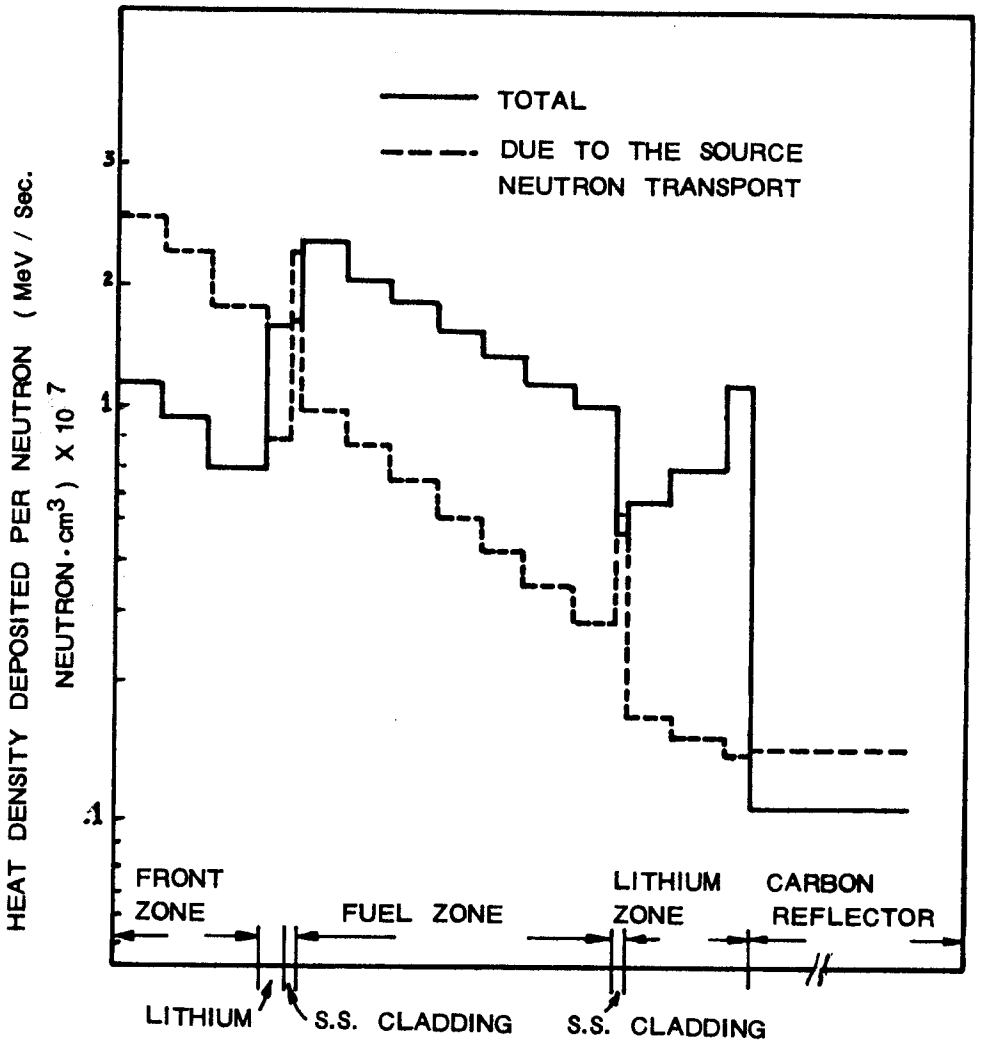

Fig. (VIII-63) THE DENSITY OF THE HEATING RATE DEPOSITED IN THE SOLASE - H BLANKET PER D - T NEUTRON

for each cross section perturbed, one should re-evaluate these factors based on the cross section new value.

The integrated sensitivity coefficients, S_{Σ}^{Q}, have been evaluated for the different cross sections and the results are presented in Table (VIII.8). The elements can be arranged according to the absolute value of their sensitivity coefficients as follows: Th, Pb, Na, O, Zr, Fe, C, ^{7}Li, ^{6}Li, Ni, and Sn. Increasing the Th(n,fission) cross section will increase the heat deposited, as it must be. The partial cross-sections for Pb which have appreciable sensitivity coefficients are Pb(n,2n'), Pb(n,inelastic), and Pb(n,γ), in that order. The first two reactions have negative sensitivity coefficients since they are threshold type reactions (all coefficients for inelastic cross sections are negative). The Pb(n,γ) reaction is exothermic and increasing its value results in increasing the heating rate. The appreciable coefficient for the ^{12}C(n,elastic) cross section is due to the fact that increasing the reaction rate due to this cross section (which degrade the neutron energy) will increase the low-energy neutrons. This leads to a larger neutron capture rate through (n,γ) reactions which have positive Q-values.

The cross sections which have negative sensitivity coefficients are ordered as follows: Pb(n,2n'), Pb(n,inelastic), Th(n,inelastic), Na(n,inelastic), Zr(n,2n'), ^{16}O(n,inelastic), Pb(n,elastic), Fe(n, inelastic), Th(n,γ), Th(n,2n'), Na(n,α), Zr(n,inelastic), ^{16}O(n,α), ^{16}O(n,elastic), ^{7}Li(n,inelastic), Th(n,3n'), Na(n,elastic), Fe(n,2n'), ^{6}Li(n,α)t, and Na(n,p) cross sections. The negative value for the

Table (VIII.8-A)

THE INTEGRATED RELATIVE SENSITIVITY COEFFICIENTS, S_{Σ}^{Q}, FOR THE HEATING RATE PER FUSION NEUTRON IN THE SOLASE-H BLANKET DUE TO NUCLEAR REACTIONS**,+

Cross Section Perturbed	$S_{\Sigma}^{Q} = \frac{1}{R_H^{Q*}} \frac{\delta R_H^Q}{\delta C}$					
	Th	Pb	^{6}Li	^{7}Li	Ni	Cr
(n,elastic)	7.32-3	-5.02-2	-5.81-4	-9.91-3	-3.41-4	-7.09-4
(n,inelastic)	-8.70-2	-2.27-1	-1.18-3	-1.90-2	-4.08-3	-6.74-3
(n,2n')	-3.55-2	-2.58-1		1.15-3	-7.42-4	-2.81-3
(n,3n')	-1.55-02	-7.59-3				
(n,n')α						-1.29-5
(n,2n')α			8.77-5	1.35-3		
(n,fission)	8.52-1					
(n,γ)	-3.99-2	3.62-2	1.27-5	-1.88-4	1.78-3	2.18-3
(n,p)			-1.17-4		-2.68-3	-9.74-4
(n,d)				-1.32-3		-2.18-4
(n,t)						-1.48-5
(n,^{3}He)						-1.89-8
(n,α)			-1.39-2		-6.29-4	-3.66-4
(n,n')p					-3.80-4	-2.86-4
(n,abs)	8.12-1	3.62-2	-1.40-2	-1.51-3	-1.52-3	6.10-4
(n,total)	6.81-1	-5.06-1	-1.60-2	-2.97-2	-7.36-3	-1.01-2

*R_H^Q = 6.11 MeV

**The Direct Part is included for each cross section perturbed

+See footnotes of Table (VIII.2)

Table (VIII.8-B)

THE INTEGRATED RELATIVE SENSITIVITY COEFFICIENTS, S_{Σ}^{Q}, FOR THE HEATING RATE PER FUSION NEUTRONS IN THE SOLASE-H BLANKET DUE TO NUCLEAR REACTIONS**,+

Cross Section Perturbed	$S_{\Sigma}^{Q} = \frac{1}{R_H^{Q*}} \frac{\delta R_H^{Q}}{\delta C}$					
	Fe	C	O	Sn	Zr	Na
(n,elastic)	-2.55-3	5.98-2	-2.05-2	-5.48-5	-3.05-3	-1.50-2
(n,inelastic)	-4.36-2	-6.96-3	-5.94-2	-4.91-4	-3.04-2	-8.74-2
(n,2n')	-1.41-2			-1.12-3	-6.28-2	-3.80-3
(n,3n')						
(n,n')α	-1.10-4					
(n,2n')α						
(n,fission)						
(n,γ)	7.26-3	-7.20-4	-4.99-6	3.55-4	1.14-2	6.27-3
(n,p)	-6.29-3		-1.03-2		-3.87-3	-1.16-2
(n,d)	-1.17-3		-3.39-3			
(n,t)	-2.27-5					
(n,^{3}He)	-1.74-5					
(n,α)	-1.35-3	-4.70-3	-2.20-2			-3.13-2
(n,n')p	-1.76-3					
(n,abs)	-1.59-3	-5.42-3	-3.57-2	3.55-4	7.55-3	-3.66-2
(n,total)	-6.38-2	4.68-2	-1.15-1	-1.31-3	-8.88-2	-1.43-1

*R_H^{Q} = 6.11 MeV

**The direct part is included for each cross section perturbed

+See footnotes of Table (VIII.2)

Th(n,γ) cross section can be explained by noticing that Th(n,γ) reactions remove neutrons from the system and thus decrease the fission rate in thorium. Although the Th(n,γ) cross section has a positive Q-value, the indirect part of the sensitivity coefficient due to flux perturbation dominates the direct part. This results in a net negative value. For other positive sensitivity coefficients for (n,γ) cross sections, the direct part (positive) dominates the indirect part (negative). It can be noted also that the ^{6}Li(n, α)t cross section has a negative coefficient. Increasing this cross section not necessarily will lead to increasing the heating rate since this increase causes a more negative and dominant contribution from flux perturbation.

VIII.4 Remarks Regarding the Angular Adjoint Flux Evaluation

We give below some remarks concerning the evaluation of the angular adjoint flux, Φ^*.

(a) The adjoint source, S^*, used in solving the adjoint equation $L^*\Phi^*=S^*$ is the response function. For the design parameters (responses) considered, we have

1. For U-233 Breeding Ratio, R_U

$$R_U = \int_{\bar{r}} \int_{E} \int_{\bar{\Omega}} N_{Th}(\bar{r})\sigma_{Th(n,\gamma)}(E) \; \Phi(\bar{r},E,\bar{\Omega}) \, d\bar{r} \, dE \, d\bar{\Omega} \qquad \text{(VIII.5)}$$

and

$$S^* = N_{Th}(\bar{r})\sigma_{Th(n,\gamma)}(E) \quad , \qquad \text{(VIII.6)}$$

2. For Tritium Breeding Ratio From ^{6}Li, $R_{^{6}Li}$

$$R_{^{6}Li} = \int_{\bar{r}} \int_{E} \int_{\bar{\Omega}} N_{^{6}Li}(\bar{r})\, \sigma_{^{6}Li\ (n,\alpha)t}(E)\, \Phi(\bar{r},E,\bar{\Omega})\, d\bar{r}\, dE\, d\bar{\Omega} \qquad \text{(VIII.7)}$$

and

$$S^{*} = N_{^{6}Li}(\bar{r})\sigma_{^{6}Li\ (n,\alpha)t}(E) \qquad \text{(VIII.8)}$$

3. For Tritium Breeding Ratio from ^{7}Li, $R_{^{7}Li}$

$$R_{^{7}Li} = \int_{\bar{r}} \int_{E} \int_{\bar{\Omega}} N_{^{7}Li}(\bar{r})\, \sigma_{^{7}Li\ (n,n',\alpha)t}(E)\, \Phi(\bar{r}, E, \bar{\Omega})\, d\bar{r}\, dE\, d\bar{\Omega} \qquad \text{(VIII.9)}$$

and

$$S^{*} = N_{^{7}Li}(\bar{r})\sigma_{^{7}Li\ (n,n',\alpha)t}(E) \qquad \text{(VIII.10)}$$

4. For the Average DPA Rate Per Fusion Neutron In Zircaloy-2 Cladding Through the First 3 cm in the Fuel Zone, $\bar{R}_{D}$

$$\bar{R}_{D} = \frac{\int_{\bar{r}} \int_{E} \int_{\bar{\Omega}} N_{Zirc}(\bar{r})\, \sigma^{DPA}_{Zirc}(E)\, \Phi(\bar{r},E,\bar{\Omega})\, d\bar{r}\, dE\, d\bar{\Omega}}{V} \qquad \text{(VIII.11)}$$

$$S^{*} = \frac{N_{Zirc}(\bar{r})\, \sigma^{DPA}_{Zirc}(E)}{V} \quad . \qquad \text{(VIII.12)}$$

where

V≡The volume of the segment whose thickness is the first 3 cm in the fuel zone. The integration over $\bar{r}$ is carried out only in this segment.

5. For The Heating Rate Per Fusion Neutron Due to Nuclear Reactions, R^{Q}_{H}

$$R_H^Q = \sum_i \sum_j \int_{\bar{r}} \int_E \int_{\bar{\Omega}} Q_{ij} N_j(\bar{r}) \sigma_{ij}(E) \Phi(\bar{r},E,\bar{\Omega}) \, d\bar{r} \, dE \, d\bar{\Omega} \qquad \text{(VIII.13)}$$

$$S^* = Q_{ij} N_j(\bar{r}) \sigma_{ij}(E) \qquad \text{(VIII.14)}$$

where

$\sigma_{ij} \equiv$ stands for reaction type i in element j; and Q_{ij} is the Q-value for this reaction.

(b) To compare the values of the responses obtained from the forward and the adjoint claculations, the forward response by spacial interval must be integrated over the domain of interest for the forward response function, and the adjoint response must be integrated over the domain of the forward source. In the SOLASE-H design, the forward source is the D-T neutron source which is assumed to be localized within a domain of 0.5 cm radius. Therefore, in evaluating the response from the adjoint flux, integration should be only performed in this domain. In Table (VIII.9) we give the response values evaluated from the forward and the adjoint fluxes. The differences in these values are less than 7%. As reported[1], experience has shown that agreement within 10% is adequate for most analytical purposes. In general, agreement is easier to obtain for slab and cylindrical geometries, and for spacially distributed source and response function. Also, refinement of the angular quadrature and spacial mesh, particularly in the domain of the external source and response function, usually gives better agreements. In the SOLASE-H calculations, spherical geometry is adopted

Table (VIII.9)

COMPARISON OF THE DESIGN PARAMETERS (RESPONSES) VALUES OBTAINED FROM THE FORWARD AND ADJOINT CALCULATIONS AND THEIR PERCENT DIFFERENCE

Response	Evaluation From:		% Difference*
	$\langle\Sigma_r,\Phi\rangle$	$\langle S,\Phi^*\rangle$	
(1) U-233 Breeding Ratio, R_U $(\frac{\text{U-233 Atoms}}{\text{D-T Neutrons}})$	0.9165	0.8879	3.1%
(2) Tritium Breeding Ratio from ^6Li, $R_{^6Li}$ $(\frac{\text{Tritium Atoms}}{\text{D-T Neutron}})$	0.5752	0.5732	0.2%
(3) Tritium Breeding Ratio from ^7Li, $R_{^7Li}$ (Tritium atom/D-T Neutron)	0.0269	0.0286	-6.3%
(4) Average DPA rate per fusion neutron in Zircaloy-2 through the first 3 cm in the fuel zone, $\bar{R}_D$ $(\frac{\text{DPA}}{\text{Sec. Neutron}})$	1.5883×10^{-27}	1.5568×10^{-27}	1.9%
(5) Heating rate per fusion neutron due to nuclear reactions, R_H^Q $(\frac{\text{MeV}}{\text{D-T neutron}})$	6.11	6.48	-6.1%

* $\frac{\langle\Sigma_r,\Phi\rangle - \langle S,\Phi^*\rangle}{\langle\Sigma_r,\Phi\rangle} \times 100$

and we judge the maximum difference obtained ($\sim$ 6.3%) as adequate for the purpose of the analysis obtained in the chapter.

VIII.5 A Remark Regarding the Sensitivity Analysis Results

In the preceding sensitivity analysis, we obtained the change in a given response due to a 1% increase in a given cross section type and for a given nuclide. Some responses were found to be more sensitive to a particular partial cross section than others. In reality, some cross sections are known more precisely than others. As mentioned before, statistical treatment for the cross section uncertainties, as they are coupled with the sensitivity profiles, will predict the actual uncertainties in a given design parameter based on the current available nuclear data. In the following chapter, the covariance matrices for different cross sections are given. Folding the uncertainty informations with the sensitivity profiles obtained in this Chapter is given in Chapter X.

References

1. Bartine, D.E., Mynatt, F.R., Oblow, E.M., "SWANLAKE-A Computer Code Utilizing ANISN Transport Calculations for Cross-Section Sensitivity Analysis", ORNL-TM-3809, Oak Ridge National Lab. (1973).

2. "VITAMIN-C: 171 Neutron, 36 Gamma Group Cross Section Library in AMPX Interface Format For Fusion Neutrons Studies," Package DLC-41, Oak Ridge National Lab.

3. Green, N.M., et. al., "AMPX: A Modular Code System for Generating Coupled Multi-group Neutron Gamma Libraries From ENDF/B", ORNL-TM-3706, Oak Ridge Nationa Lab. (1976).

4. Wright, R.Q., Rossin, R.W., "DLC-2D/100 Group Transport Cross Section Data Generated by SUPERTOG From EDNF/B-III, RSIC Data, Package DLC-2D, July (1973).

5. Wright, R.Q., et. al., "SUPERTOG: A Program to Generate Fine Group Constants and Pn Scattering Matrices From ENDF/B", ORNL-TM-2679, Oak Ridge National Lab. (1969).

6. Avci, H.I, Kulcinski, G.L, Nuclear Engineering Department , The University of Wisconsin, private communication.

7. Kulcinski, G.L, Nuclear Engineering Department, The University of Wisconsin, private communication.

8. Abdou, M.A., Maynard, C.W., Wright,R.Q., "MACK: A Computer Program to Calculate Neutron Energy Release Parameters (Fluence-to-Kerma-Factors) and Multigroup Reaction Cross Sections From Nuclear Data in ENDF Format, ORNL-TM-3994, July (1973).

9. Maphs, C., Coth, G.W., Cerny, I, "Nuclear Reaction Q-Values", A Journal Devoted to Compilations and Evaluations of Experimental and Theoretical Results in Nuclear Physics, Vol. 2, Number 5 and 6, Dec. (1966).

10. Cohen, B.L, "Concepts of Nuclear Physics", McGraw-Hill Book Company N.Y (1971).

11. Lederer, C.M., Hollander, J.M., Perlman, I., "Table of Isotopes", 6th edition, John Wiley and Sons, N.Y.

12. Youssef, M.Z., "ACTEN: A Computer Program to Calculate the Reaction Rate, the Rate of Energy Deposited and the Power Multiplication in a Fusion Blanket Using the Reaction Q Values," UWFDM-276, The Fusion Research Program, The University of Wisconsin, Dec. (1978).

CHAPTER IX

NEUTRON CROSS SECTION UNCERTAINTIES EVALUATION

IX.1 Introduction

The expected uncertainty in a design parameter, R, is obtained by coupling the sensitivity coefficients, $P_{\Sigma i}$, with the neutron cross sections uncertainties (see Eq. (VII . 39)). Therefore, it is necessary to evaluate the different cross sections covariance matrices for the nuclides present in the SOLASE-H blanket in order to have estimates of the uncertainties associated with each design parameter considered in the sensitivity analysis presented in Chapter VIII.

The Cross Section Evaluation Working Group, CSEWG, is currently in charge of providing the cross sections uncertainties information to the users. The Data Covariance Subcommittee of the CSEWG has recently released this information as a part of the Evaluated Neutron Data File, ENDF/B-V, for different elements of importance in the field of fast reactors, shielding, dosimetry, and fusion applications. File number 33 for each material in ENDF/B-V has been reserved to store this information in a format which allows processing it together with the differential data using the currently available processing codes. As stated by the Data Covariance Subcommittee of the CSEWG[1], the covariance information implemented in the ENDF/B-V should not be treated as hard facts upon which strong conclusions

can be based since some evaluations of the cross sections covariances can be improved upon having more factual basis for some assumptions used in the evaluation. However, the current covariance information will allow us to gain a better perception of the role which our present knowledge about neutron cross sections and/or parameters play in achieving certain performance in our designs.

IX.2 Formalisms for Representing Estimated Data Covariances in the ENDF/B-V

IX.2.A Covariance, Variance, and Correlation Matrices

The covariance matrix, COV (X_i, Y_i), of the multigroup cross section X_i at energy E_i and the multigroup cross section Y_j at energy group E_j is given by (see Eq. (VII.40))

$$\begin{aligned} COV\ (X_i, Y_j) &= E(\delta X_i, \delta Y_j) \\ &= \int_{-\infty}^{\infty}\int [X_i - E(X_i)]\ [Y_j - E(Y_j)]\ f(X_i, Y_j) dX_i dY_j \end{aligned} \qquad (IX.1)$$

where E(..) denotes the expectation value of a distribution, $\delta(\cdots)$ gives the statistical variation of a variable and $f(X_i, Y_j)$ denotes the joint probability density function.

The relative covariance matrix, RCOV (X_i, Y_j) is given by

$$RCOV(X_i, Y_j) = \frac{COV(X_i, Y_j)}{X_i Y_j} = \langle dX_i,\ dY_j \rangle \qquad (IX.2)$$

and the standard deviation, S.D. , and the relative standard deviation, R.S.D. , of the cross section X_i are given, respectively, by

$$S.D.(X_i) = [COV\ (X_i,X_i)]^{1/2} = [VAR\ (X_i)]^{1/2} \qquad (IX.3)$$

$$R.S.D(X_i) = \frac{S.D.(X_i)}{X_i} = \frac{[VAR(X_i)]^{1/2}}{X_i} \qquad (IX.4)$$

where the variance of X_i is

$$VAR(X_i) = \int_{-\infty}^{\infty} [X_i - E(X_i)]^2 f(X_i)dX_i . \qquad (IX.5)$$

The type and strength of the correlation between X_i and Y_j can be better represented by the correlation matrix, $CORR(X_i,Y_j)$, which is given by

$$CORR(X_i,Y_j) = \frac{COV(X_i,Y_j)}{S.D.(X_i)\ S.D.(Y_j)}$$

$$= \frac{COV(X_i,Y_j)}{[COV(X_i,X_i)COV(Y_j,Y_j)]^{1/2}} \qquad (IX.6)$$

The extreme cases are when the cross sections X_i and Y_j are totally correlated ($CORR(X_i,Y_j) = +1$) or totally anti-correlated ($CORR\ (X_i,Y_j) = -1$).

IX.2.B Procedures for Covariance Matrices Evaluation

In the ENDF/B-V, each material is assigned a MAT number and has various files. The microscopic energy dependent neutron data for MAT is introduced in file 3 and its covariance information is introduced in file 33. Each file has different sections for each reaction type which has a MT number, thus, (MAT,3,MT) and (MAT,33,MT) represent a section in file 3 for reaction MT and a section in file 33 for the same reaction MT and the same material MAT, respectively.

For material MAT, each section (MAT,33,MT) consists of several subsections (MAT, MT, MAT_1, MT_1). Each subsection is used to describe a single covariance matrix, i.e., the covariance matrix for reaction MT, material MAT; and reaction MT_1, material MAT_1. It is the covariance matrix of the energy-dependent cross section in section (MAT, 3, MT_1) and the energy-dependent cross section in section (MAT_1, 3, MT_1).

Each subsection may contain several sub-subsections and two different types of sub-subsections may be used; the "NC-type" and the "NI-type". Each sub-subsection describes an independent contribution (i.e. component) to the covariance matrix. Thus, the total covariance matrix in a subsection , (MAT, MT, MAT_1, MT_1),is made up of the sum of the contributions from the individual sub-subsections.

A. NC-Type Sub-Subsections

This type of sub-subsection may be used to describe the covariance matrices in energy ranges where the cross sections in (MAT, 3, MT) can be "derived" in terms of other "evaluated" cross

sections in the same energy range. The evaluated cross section, in a given energy range, is defined as the one for which the covariance matrix in that energy range is given entirely in terms of "NI-type" sub-subsections. Thus, if ${}^{MAT}\sigma_{MT}(E)$ is the "derived" cross section, we have

$$ {}^{MAT}\sigma_{MT}(E) = \sum_{i=1}^{NCI} C_i * {}^{MAT}\sigma_{MT_i}(E) \qquad (IX.7) $$

where C_i's are constants, (+1 or -1), over the range of energy where ${}^{MAT}\sigma_{MT}(E)$ is derived, and ${}^{MAT}\sigma_{MT_i}(E)$'s are different MT_i cross sections for the same material in the same energy range. The number of different type of cross sections, NCI, the energy range, E_1 to E_2, the reactions MT numbers, and the coefficients, C_i's are all provided in this type of sub-subsection which is designated by a flag LTY = 0. As such, the covariance matrix of the "derived" redundant cross section ${}^{MAT}\sigma_{MT}$ can be derived in terms of the covariance matrices of the other "evaluated" cross sections.

Another case of the "NC-type" sub-subsection for which the cross section ${}^{MAT}\sigma_{MT}(E)$ is evaluated through a "ratio" measurement. Evaluation of cross sections by means of "ratio" measurements is one of the main sources of information on covariances of cross sections having different values of MAT. Thus, in the energy range bounded by E_1 and E_2, ${}^{MAT}\sigma_{MT}(E)$ is given by

$$^{MAT}\sigma_{MT}(E) = R(E)\ \ ^{MATS}\sigma_{MTS}(E) \qquad (IX,8)$$

where R(E) is the ratio measurements and $^{MATS}\sigma_{MTS}(E)$ is the "standard" cross section MTS for the standard material MATS. To obtain the covariance matrices for this type of cross section, information about the covariance of R(E) and $^{MATS}\sigma_{MTS}(E)$ are needed. Within the ENDF/B-V format, information such as E_1, E_2, MATS, and MTS are introduced in subsection (MAT,MT, MAT,MT) by the "NC-type" sub-sub-section with a flag LTY = 1. In the same subsection, the covariance of R(E) is introduced by a "NI-type" sub-subsection. In this case, the sub-subsection of the "NC-type" and LTY=1 serves as an indicator that the covariance of $^{MAT}\sigma_{MTS}(E)$ should be obtained from a sub-subsection of an "NI-type" in the subsection (MATS, MTS, MATS, MTS). There are other sub-subsections of "NC-type" with LTY = 2 and 3 which should be introduced in sub-sections (MAT, MT, MATS, MTS) and (MATS, MTS, MAT, MT), respectively, and they serve the same function as the "NC-type" sub-subsection with LTY = 1 introduced in subsection (MAT, MT, MAT, MT). For more information about the "NC-type" sub-subsection reference can be made to the format and procedure of the uncertainty files described in reference (2).

B. NI-Type Sub-subsections

These types of sub-subsections give information about the covariance of measurements for a given cross section (or ratio) over the whole (or part) of the energy range of the ENDF/B-V (10^{-5}eV→20 MeV). Thus, these types of sub-subsections describe ex-

plicity the various components of the covariance matrix given in the subsection. In each NI-type sub-subsection there is a flag, the LB flag, whose numerical value indicates whether the components are "relative" or "absolute" and the kind of correlations as a function of energy represented by the components in the sub-subsection. There are six permitted values for the flag LB. In each sub-subsection of a specific LB value, there is one (or two) table, the $\{E_k, F_k\}$ table (and the $\{E_1, F_1\}$ table). Between the energy values E_k and E_{k+1} in the $\{E_k, F_k\}$ table, the value F_k is assigned to give an element of the covariance matrix considered. The covariance matrix, $COV(X_i, Y_j)$, which can be given in a subsection such as (MAT, MT, MAT_1, MT_1), where $X_i \equiv {}^{MAT}\sigma_{MT}(E_i)$ and $Y_j \equiv {}^{MAT1}\sigma_{MT1}(E_j)$, is defined as follows for the different values of LB:

LB = 0 Absolute components only correlated within each E_k interval

$$COV(X_i, Y_j) = \sum_k S_k^i S_k^j F_{XY,k} \qquad \text{(IX.10)}$$

LB = 1 Fractional components only correlated within each E_k interval

$$COV(X_i, Y_j) = \sum_k S_k^i S_k^j F_{XY,k} X_i Y_j \qquad \text{(IX.11)}$$

LB = 2 Fractional components correlated over all E_k intervals

$$COV(X_i, Y_j) = \sum_{k,k'} S_k^i S_{k'}^j F_{XY,k} F_{XY,k'} X_i Y_j \qquad \text{(IX.12)}$$

LB = 3 Fractional components correlated over E_k and E_l intervals

$$COV(X_i,Y_j) = \sum_{k,l} S_k^i S_l^j F_{X,k} F_{Y,l} X_i Y_j . \qquad (IX.13)$$

LB = 4 Fractional components correlated over all E_l intervals within each E_k interval

$$COV(X_i,Y_j) = \sum_{k,l,l'} S_k^i S_l^i S_k^j S_{l'}^j F_k F_{XY,l} F_{XY,l'} X_i Y_j . \qquad (IX.14)$$

LB = 5 Relative covariance matrix component

$$COV(X_i,Y_j) = \sum_{k,k'} S_k^i S_{k'}^j F_{XY;k,k'} X_i Y_j . \qquad (IX.15)$$

In the above definitions, the cross sections X_i and Y_j are evaluated at energies E_i and E_j respectively. The factor, $F_{XY,k}$ means that the uncertainty components for the covariance matrix is taken from one table, the $\{E_k,F_k\}$ table. The factors $F_{X,k}$ and $F_{Y,l}$ indicate that the covariance data for the reactions X and Y are taken from two independent tables, one for X, the $\{E_k,F_k\}$ table and one for Y, the $\{E_l,F_l\}$ table. The operator $S_k^i = 1$ when the energy E_i is in the interval E_k to E_{k+1} of the $\{E_k,F_k\}$ table and $S_k^i = 0$ when E_i is outside this energy range.

IX.3 Formulation of Multigroup Covariance Matrices

Since the covariance matrices informations are given over different energy ranges for various materials and reactions, which may not be the same as the user's neutron group structure, it is necessary in order to construct the covariance matrices in a multigroup form to com-

pute the cross sections and fluxes for a group structure which is the union between the user group structure and all energies used in the uncertainty files for all the reactions and materials of interest. Obviously this supergroup structure can get very large as the level of detail available in the uncertainty files expands.

For covariance matrices which can be evaluated explicitly from "NI-type" sub-subsections we have for different values of LB:

LB = 0

$$COV(X_G,Y_H) = \frac{\sum_{k\epsilon G,H} F_{XY,k}\ \phi_{G,k}\ \phi_{H,k}}{\phi_G\ \phi_H} \qquad (IX.16)$$

LB = 1

$$COV(X_G,Y_H) = \frac{\sum_{K\epsilon G,H} F_{XY,k}(\phi_{G,k}X_{G,k})\ (\phi_{H,k}\ Y_{H,k})}{\phi_G\ \phi_H} \qquad (IX.17)$$

LB = 2

$$COV(X_G,Y_H) = \frac{[\sum_{k\epsilon G} F_{XY,k}\ \phi_{G,k}\ X_{G,k}][\sum_{k'\epsilon H} F_{XY,k'}\ \phi_{H,K'}Y_{H,k'}]}{\phi_G\ \phi_H} \qquad (IX.18)$$

LB = 3

$$COV(X_G,Y_H) = \frac{[\sum_{k\epsilon G} F_{X,k}\ \phi_{G,k}\ X_{G,k}][\sum_{1\epsilon H} F_{Y,1}\ \phi_{H,1}\ Y_{H,1}]}{\phi_G\ \phi_H} \qquad (IX.19)$$

LB = 4

$$COV(X_G,Y_H) = \frac{\sum_{k\epsilon G,H} F_k[\sum_{1\epsilon G} F_{XY,1}\ \phi_{G,1}\ X_{G,1}][\sum_{1'\epsilon H} F_{XY,1'}\ \phi_{H,1'}\ Y_{H,1'}]}{\phi_G\ \phi_H} \qquad (IX.20)$$

LB = 5

$$COV(X_G,Y_H) = \frac{\sum_{k\in G}\sum_{k'\in H} F_{XY;k,k'}\,\phi_{G,k}\,X_{G,k}\,\phi_{H,k'}\,Y_{H,k'}}{\phi_G\,\phi_H} \qquad (IX.21)$$

The derivation of the above equations are described in Refs. (3) and (4). The notation used here is

$COV(X_G,Y_H)$ ≡ Multigroup covariance between reaction X, group G as it relates to reaction Y, group H.

ϕ_G ≡ Multigroup flux per user group G.

$X_{G,k}$ ≡ Multigroup cross section for reaction X for a supergroup (G,k) constructed from the union of energy bounds for interval k of the E_k table and those which were user input.

$\phi_{G,k}$ ≡ The flux for the supergroup (G,k).

Within the multigroup formulation, the relative covariance and correlation matrices are given by

$$RCOV(X_G,Y_H) = \frac{COV(X_G,Y_H)}{X_G Y_H} \equiv \langle dX_G,\, dY_H\rangle \qquad (IX.22)$$

$$CORR(X_G,Y_H) = \frac{COV(X_G,Y_H)}{S.D.(X_G)S.D.(Y_H)} \qquad (IX.23)$$

where

$$S.D.(X_G) = \sqrt{COV(X_G,X_G)}$$
$$S.D.(Y_H) = \sqrt{COV(Y_H,Y_H)} \qquad (IX.24)$$

and

$$R.S.D.(X_G) = \frac{\sqrt{COV(X_G,X_G)}}{X_G}$$

$$R.S.D.(Y_H) = \frac{\sqrt{COV(Y_H,Y_H)}}{Y_H} \qquad (IX.25)$$

The "NC-type" sub-subsections are processed using the covariance matrices processed for the "NI-type" sub-subsections. For the "NI-type" sub-subsection with LTY = 0, i.e. for cross sections "derived" from "evaluated" cross sections as

$$X_H = \sum_{n=1}^{NCI} C_i \, Y_{H,n}, \qquad (IX.26)$$

we have

$$COV(X_G,X_H) = \sum_{n=1}^{NCI} \sum_{m=1}^{NCI} C_n \, C_m \, COV(Y_{G,n}, Y_{H,m}) \qquad (IX.27)$$

and

$$COV(X_G,Y_{H,m}) = \sum_{n=1}^{NCI} C_n \, COV(Y_{G,n}, Y_{H,m}) \qquad (IX.28)$$

Here, the indices n and m stand for several reactions MT's. If the cross section X is "derived" from ratio measurement, i.e.,

$$X(E) = R(E) \, Y(E), \qquad (IX.29)$$

where R is the ratio measurement and Y is the standard cross section,

then the relative covariance matrix $RCOV(X_G,X_H) \equiv \langle dX_G, dX_H \rangle$ is given by

$$\langle dX_G, dX_H \rangle = \langle dR_G, dR_H \rangle + \langle dY_G, dY_H \rangle \qquad \text{(IX.30)}$$

and

$$\langle dX_G, dY_H \rangle = \langle dY_G, dY_H \rangle \ . \qquad \text{(IX.31)}$$

If the cross section X is "derived" indirectly from Y through two ratio measurements, i.e.,

$$X(E) = R_X(E)\ Z(E) \qquad \text{(IX.32)}$$

$$Z(E) = R_Z(E)\ Y(E) \qquad \text{(IX.33)}$$

where $R_X(E)$ is the ratio measurements of the cross section X(E) relative to the cross section Z(E) which, in turn, is measured relative to the standard cross section Y(E) through the ratio measurement $R_Z(E)$, then we have

$$\langle dX_G,dX_H \rangle = \langle dR_{X,G},dR_{X,H} \rangle + \langle dR_{Z,G},dR_{Z,H} \rangle + \langle dY_G,dY_H \rangle$$

$$\langle dX_G,dZ_H \rangle = \langle dR_{Z,G},dR_{Z,H} \rangle + \langle dY_G,dY_H \rangle$$

$$\langle dZ_G,dZ_H \rangle = \langle dR_{Z,G},dR_{Z,H} \rangle + \langle dY_G,dY_H \rangle$$

$$\langle dZ_G,dY_H \rangle = \langle dY_G,dY_H \rangle$$

$$\langle dX_G,dY_H \rangle = \langle dY_G,dY_H \rangle$$

where the ratios, R_X and R_Z, and the standard cross section, Y, are assumed to be uncorrelated.

IX.4 Processing the Covariance Matrices, Cross Section Standard Deviations and Correlation Matrices for Materials Present In the SOLASE-H Blanket

The covariance matrices, standard deviations, and correlation matrices for the various microscopic neutron cross sections of most of the material present in the SOLASE-H blanket have been processed using the "UNCER" code[5], which is the University of Wisconsin modified version of the "PUFF" code[3]. As reported by T. Wu[5], this modification has been carried out to accomodate for the new format of the uncertainty files in the ENDF/B-V[1] as compared to the format in ENDF/B-IV for which the "PUFF" code was originally written.

The materials for which the covariance matrices, neutron cross sections, standard deviations, and the correlation matrices have been processed are: Lead, Thorium, Lithium-6, Sodium, Carbon, Nickel, Iron, and Oxygen. For other materials present in the SOLASE-H blanket (e.g., Zirconium, Lithium-7 and Tin) no uncertainty files have been given yet in the last release of the ENDF/B-V file.

The neutron cross section library DLC-41B/VITAMIN-C (171 neutron groups, 36 gamma groups) has been used to evaluate the various neutron cross sections of the supergroup structure which is the union between the 25-neutron group structure used in the SOLASE-H calculations and all the energy ranges introduced in the uncertainty files for a given material. A separate run is carried out for each element to overcome the very large computer core size requirement.

The calculation procedures and the auxiliary programs used are shown in Fig. (IX.1). Note that the parts designated A,B,C and D are performed separately.

IX.5 Uncertainty Files Contents for Materials Used in The SOLASE-H Blanket

Part A of the calculational procedures shown on Fig. (IX.1) has been carried out for Pb, Th, ^{6}Li, Na, Ni, Fe, C, and ^{16}O. The MT number designated for different cross section type is given in Table (IX.1). Tables (IX.2) to (IX.5) give a summary of the informations introduced in the uncertainty files of some materials. These informations include the cross section type, MT; the energy range over which the cross section covariance information is given (if the cross section is "evaluated"), and the method used if the cross section is derived (a linear combination or a ratio measurement) in a given energy range.

As an example, in Table (IX.2), the total cross section for Pb, MT = 1, is derived from the sum of Pb(n,elastic), MT = 2, and Pb(n,γ), MT = 102, cross sections over the energy range 1×10^{-5} - 1000 eV. Therefore, to evaluate the covariance matrices $COV(\sigma_G^{tot}, \sigma_H^{tot})$, $COV(\sigma_G^{tot}, \sigma_H^{elastic})$, and $COV(\sigma_G^{tot}, \sigma_H^{\gamma})$, the covariance matrices $COV(\sigma_G^{elastic}, \sigma_H^{elastic})$ and $COV(\sigma_G^{\gamma}, \sigma_H^{\gamma})$ should be first evaluated in this energy range. For the rest of the energy range, 1000 eV - 20 MeV, the cross section Pb(n,tot) is evaluated (measured) and the covariance matrix $COV(\sigma_G^{tot}, \sigma_G^{tot})$ is calculated directly from the uncertainty information given in this range for the Pb(n,tot) cross section. The

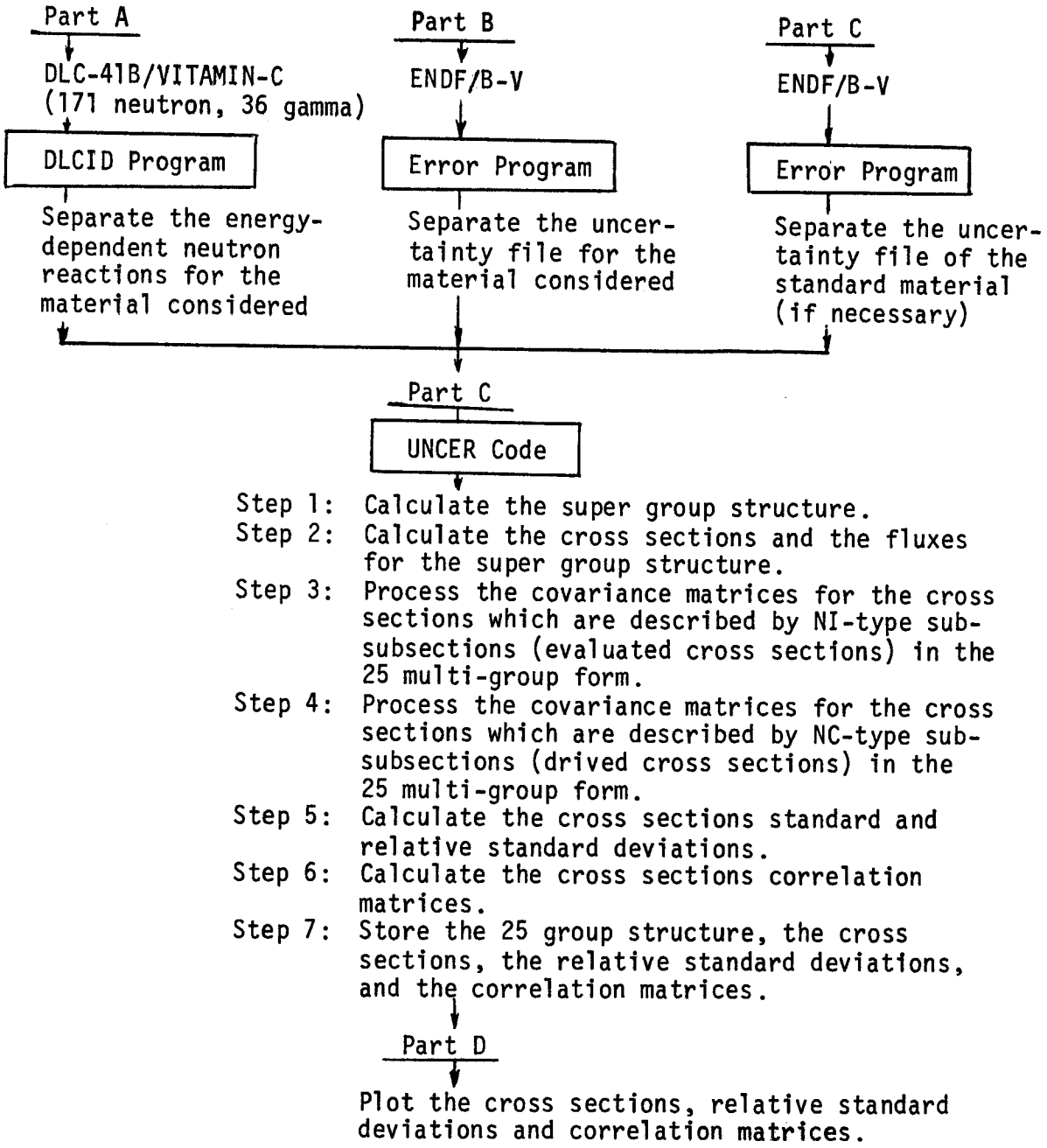

Fig. (IX.1): Computational Procedures Followed to Evaluate the Cross SEctions Correlation Matrices.

Table (IX.1)

THE MT NUMBER DESIGNATED FOR DIFFERENT CROSS SECTION TYPE

Cross Section Type	MT Number
(n,tot)	1
(n,elastic)	2
(n,nonelastic)*	3
(n,inelastic)+	4
(n,2n')	16
(n,3n')	17
(n,fission)	18
(n,n')α	22
(n,2n')α	24
(n,absorp.)	27
(n,n')p	28
(n,n') 1st Level	51
(n,n') 2nd Level	52
:	:
(n,n') 40th Level	90
(n,n') continuum	91
(n,γ)	102
(n,p)	103
(n,d)	104
(n,t)	105
(n,^{3}He)	106
(n,α)	107

*(n,nonelastic)=(n,inelastic)+(n,γ)+(n,p)+(n,α)+ . . .

+ $(n,\text{inelastic}) = \sum_{i=51}^{91} (n,\text{inelastic})_{MT_i}$

Table (IX.2) : Summary of the Uncertainty File for Pb, MAT=1382, as Given in ENDFIB-V

Reaction Type	MT #	Energy Range (MeV)								
		$1x10^{-11}$ -0.001	0.001 -0.73	0.73 -0.81	0.81 -2.63	2.63 -5.0	5.0 -6.76	6.76 -9.0	9.0-14	14-20
(n,total)	1	2+102[a]	E[b]	E	E	E	E	E	E	E
(n,elastic)	2	E	1-3	1-3	1-3	1-3	1-3	1-3	1-3	1-3
(n,non-elastic)	3	102	102	E	E	E	E	E	E	E
(n,inelastic)	4	0[c]	0	E	E	E	E	E	E	(d) 3-16-102
(n,2n')	16	0	0	0	0	0	0	E	E	E
(n,3n')	17	0	0	0	0	0	0	0	0	3-4-16-102
(n,n')1st	51	0	0	E	E	E	E	E	E	E
(n,n')2nd	52	0	0	0	E	E	E	E	E	E
(n,n')14th	64	0	0	0	0	E	E	E	E	E
(n,γ)	102	E	E	E	E	E	E	E	E	E

(a) Means: (n,total)=(n,elastic)+(n,γ) in this energy range.
(b) The letter E indicates that the covariance matrix for the corresponding cross section, MT, is evaluated directly from NI-type sub-subsections.
(c) The zero means that the corresponding cross section, MT, is zero in this range.
(d) Means: (n, inel.) = (n,nonelastic) - (n,2n) - (n,γ) in this energy range.

Table (IX.3)
Summary of the Uncertainty File for ^{6}Li, MAT 1303,
as Given in ENDF/B-V

Reaction Type	MT #	Energy Range (MeV)
		1×10^{11} - 20.0
(n,total)	1	2 + 105[a]
(n,elastic)[c]	2	E[b]
(n,α)t[c]	105	E[b]

(a) Means: (n,total) = (n,elastic) + (n,α)t.

(b) The letter E indicates that the covariance matrix for the corresponding cross section, MT, is evaluated directly from NI-type sub-subsections.

(c) The covariance matrix information between the cross sections (n,elastic) and (n,α)t is also given.

Table (IX.4): Summary of the Uncertainty File for Na, MAT=1311, as Given in ENDF/B-V
(a) For cross sections other than inelastic scattering to a level and to continuum

Reaction Type	MT #	Energy Range (MeV)			
		1×10^{-11}-3.75	3.75-4.04	4.04-12.9	12.9-20
(n,total)	1	E^+	E	E	E
(n,elastic)	2	← 1-16-102-103-107- $\sum_{i=51}^{91}$ $(n,n')_{MT_i}$ →			
(n,nonelastic)	3	← 16+102+103+107+ $\sum_{i=51}^{91}$ $(n,n')_{MT_i}$ →			
(n,inelastic)	4	← $\sum_{i=51}^{91}$ $(n,n')_{MT_i}$ →			
(n,2n')	16	0^+	0	0	E
(n,γ)	102	E	E	E	E
(n,p)	103	0	E	E	E
(n,α)	107	0	0	E	E

(b) For inelastic scattering cross section to a level and for a continuum*

Reaction Type	MT #	Energy Range++(MeV)	Reaction Type	MT #	Energy Range++(MeV)
(n,n')1st level	51	0.459-20	(n,n')11th level	61	5.62-12
(n,n')2nd "	52	2.169-20	(n,n')12th "	62	5.77-11.5
(n,n')3rd "	53	2.498-10	(n,n')13th "	63	6.01-12
(n,n')4th "	54	2.755-10	(n,n')14th "	64	6.22-11
(n,n')5th "	55	2.82-10	(n,n')15th "	65	6.35-11
(n,n')6th "	56	3.11-10.5	(n,n')16th "	66	6.55-11
(n,n')7th "	57	3.84-10	(n,n')17th "	67	7.42-12
(n,n')8th "	58	4.05-10.5	(n,n')18th "	68	8.13-12.5
(n,n')9th "	59	4.62-10.	(n,n')cont. "	91	6.1-20
(n,n')10th "	60	4.98-9.6			

+ See footnotes of Table (IX.2). ++ The cross section is zero elsewhere.
* The covariance matrices for these reactions are evaluated directly from NI-type sub-subsections.

Table (IX.5) : Summary of the Uncertainty File of ^{12}C, MAT=1306, as Given ENDF/B-V[+]

(a) For Cross Sections Other Than Inelastic Scattering to a Level and to Continuum

Reaction Type	MT #	Energy Range (MeV)					
		$1x10^{-11}$-2.0	2.0-4.81	4.81-6.32	6.32-7.89	7.89-8.29	8.29-20
(n,total)	1	2+102[+]	E[+]	E	E	E	E
(n,elastic)	2	E	E	E	E	E	E
(n,nonelastic)	3	102	102	1-2	1-2	1-2	1-2
(n,inelastic)	4	0	0	← 1-2-102-103-104-107 →			
(n,n')1st	51	0	0	1-2-102	← 1-2-102-107 →		E
(n,n')cont.	91	0	0	0	0	1-2-102-103-104-107-	$\Sigma_{i=1}^{68}\sigma MT_i$
(n,γ)	102	E	E	E	E	E	E

(b) For inelastic scattering to a level and to continuum

Reaction Type	MT #	Energy Range++(MeV)	Reaction Type	MT #	Energy Range (MeV)
(n,p)	103	13.65-20	(n,n')11th	61	14.9-20
(n,d)	104	14.88-20	(n,n')12th	62	15.4-20
(n,α)	107	6.32-20	(n,n')13th	63	15.9-20
(n,n')2nd	52	8.29-20	(n,n')14th	64	16.5-20
(n,n')3rd	53	10.4-20	(n,n')15th	65	17.1-20
(n,n')4th	54	11.2-20	(n,n')16th	66	17.6-20
(n,n')5th	55	11.7-20	(n,n')17th	67	18.15-20
(n,n')6th	56	12.2-20	(n,n')18th	68	18.7-20
(n,n')7th	57	12.7-20			
(n,n')8th	58	13.3-20			
(n,n')9th	59	13.8-20			
(n,n')10th	60	14.4-20			

+ See footnotes of Table (IX.2). *See footnote * Table .

++ The cross section is zero elsewhere.

covariance matrices $COV(\sigma_G^{tot}, \sigma_H^{elastic})$ and $COV(\sigma_G^{tot}, \sigma_H^{\gamma})$ have zero elements since the Pb(n,tot) cross section is not correlated to the Pb(n,γ) and Pb(n, elastic) cross sections in this energy range.

IX.6 Covariance Matrices for Materials Used in the SOLASE-H Blanket

Parts B and C of the calculational procedures shown in Fig. (IX.1) have been carried out for Pb, Th, ^{6}Li, Na, C, Ni, Fe, and ^{16}O and the covariance matrices for these elements have been generated. For each of these elements, we give in Fig. (IX.2) to (IX.8) information about the type of cross section for which the covariance matrices are generated, the cross sections which are "derived" from the "evaluated" cross sections, and the covariance matrices processed for these derived cross sections.

In Fig. (IX.2), we show a large square matrix for Pb including all reactions (MT's) for which uncertainty information was processed in the 25-neutron group structure. Each individual box is itself a square matrix with 25-energy group on a side. Thus, in Fig. (IX.2), the total number of elements in the full matrix is 25 x 25 x 10 = 6250. However, most of these elements are null indicating no correlation. The boxes along the major diagonal refer to the covariance of a specific reaction as a function of energy (neutron group). The off-diagonal boxes reflect correlation between reaction types. The dot mark indicates that the marked boxes (matrices) are "evaluated" directly from the uncertainty files. Thus, the different reaction types for which these matrices are evaluated are not correlated. The boxes marked with a cross mark indicate that the corresponding matrices

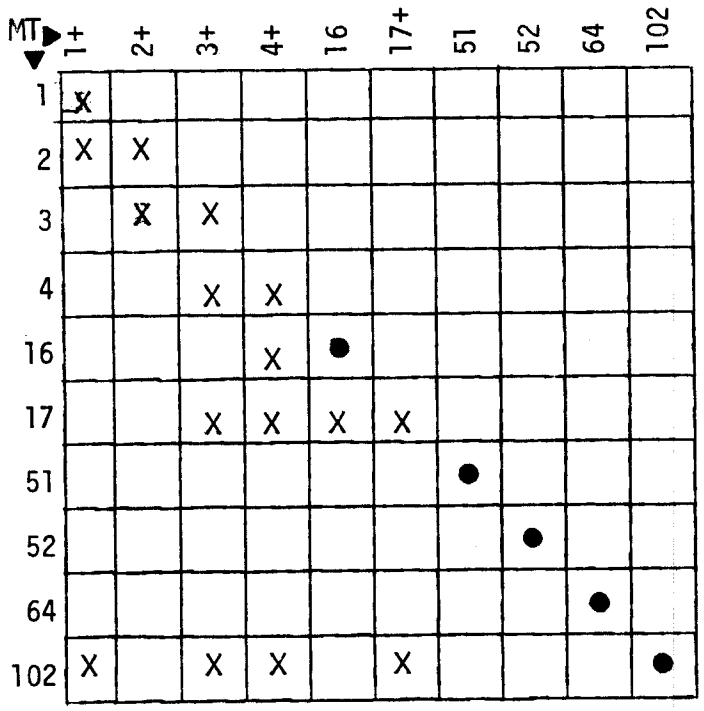

FIG. (IX.2) - THE COVARIANCE MATRICES PROCESSED FOR P_B, MAT 1382*

● THE COVARIANCE MATRIX INDICATED IS EVALUATED.

X THE COVARIANCE MATRIX INDICATED IS DERIVED.

* AFTER MAKING REFLECTION ALONG THE MAJOR DIAGONAL, THE UNFILLED BOXES (MATRICES) ARE NULL.

+ THESE CROSS SECTIONS ARE 'DERIVED' FROM OTHER 'EVALUATED' CROSS SECTIONS AT A GIVEN ENERGY RANGE.

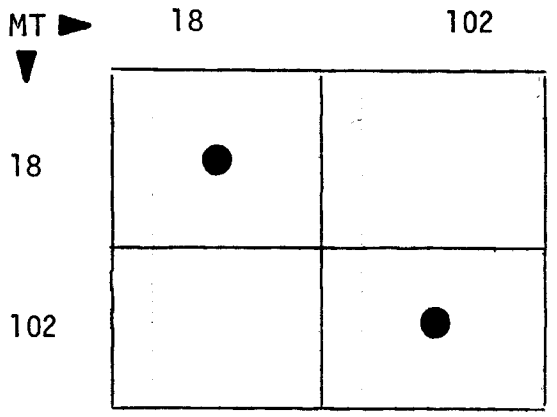

FIG. (IX,3) - THE COVARIANCE MATRICES PROCESSED FOR TH, MAT 1390*

* SEE FOOTNOTES OF FIG. (IX.2)

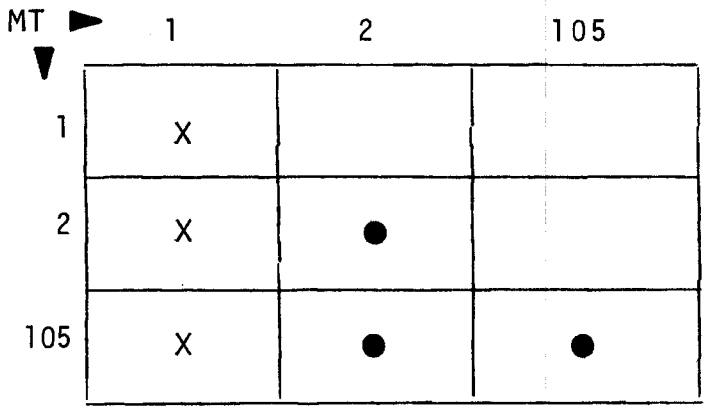

FIG. (IX.4) - THE COVARIANCE MATRICES PROCESSED FOR ^{6}Li, MAT 1303*

* SEE FOOTNOTES OF FIG. (IX.2)

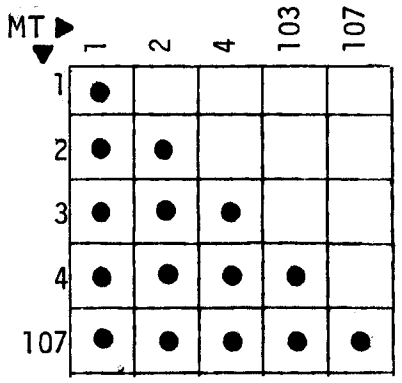

FIG. (IX.5) - THE COVARIANCE MATRICES PROCESSED FOR ^{16}O, MAT 1276*

* SEE FOOTNOTES OF FIG. (IX.2)

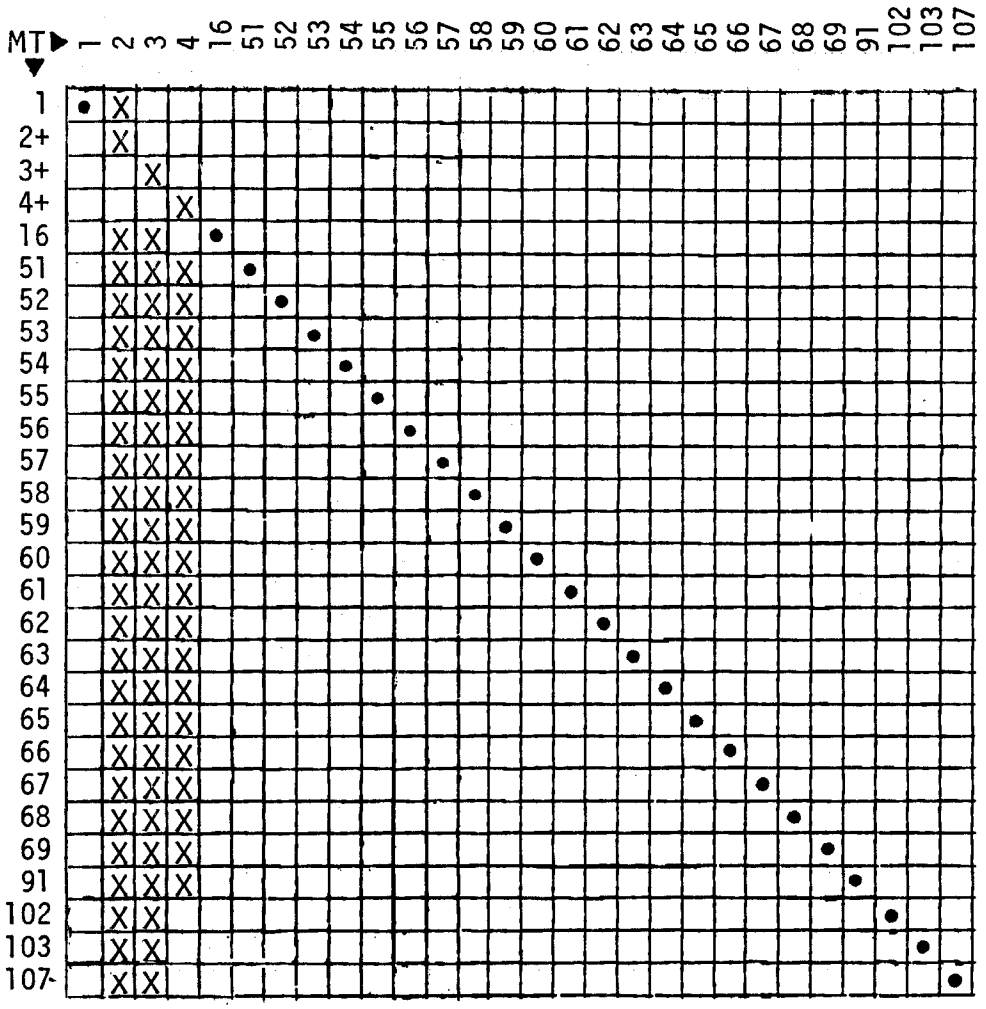

FIG. (IX.6) - THE COVARIANCE MATRICES PROCESSED FOR Na, MAT 1311*

* SEE FOOTNOTES OF FIG. (IX.2)

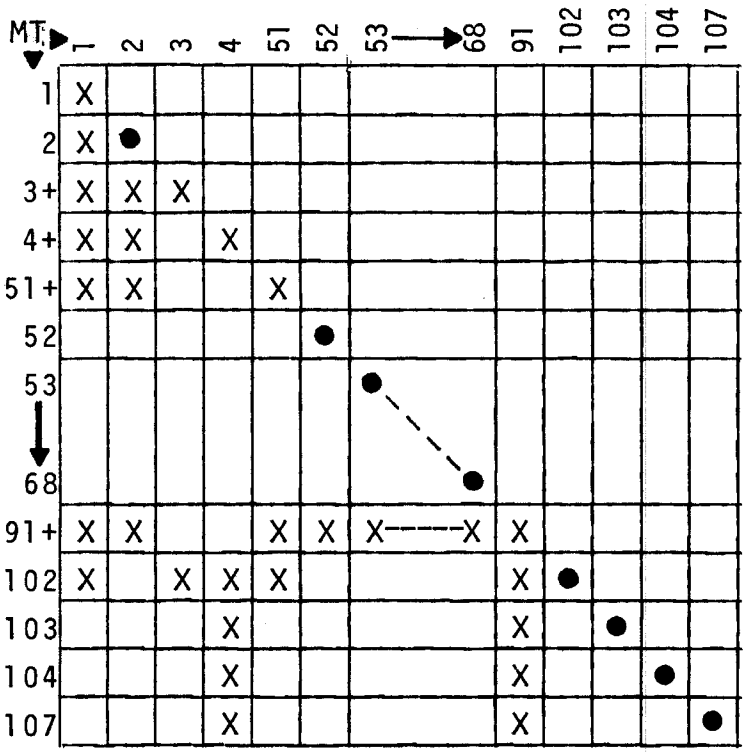

FIG. (IX.7) - THE COVARIANCE MATRICES PROCESSED FOR ^{12}C, MAT 1306*

* SEE FOOTNOTES OF FIG. (IX.2)

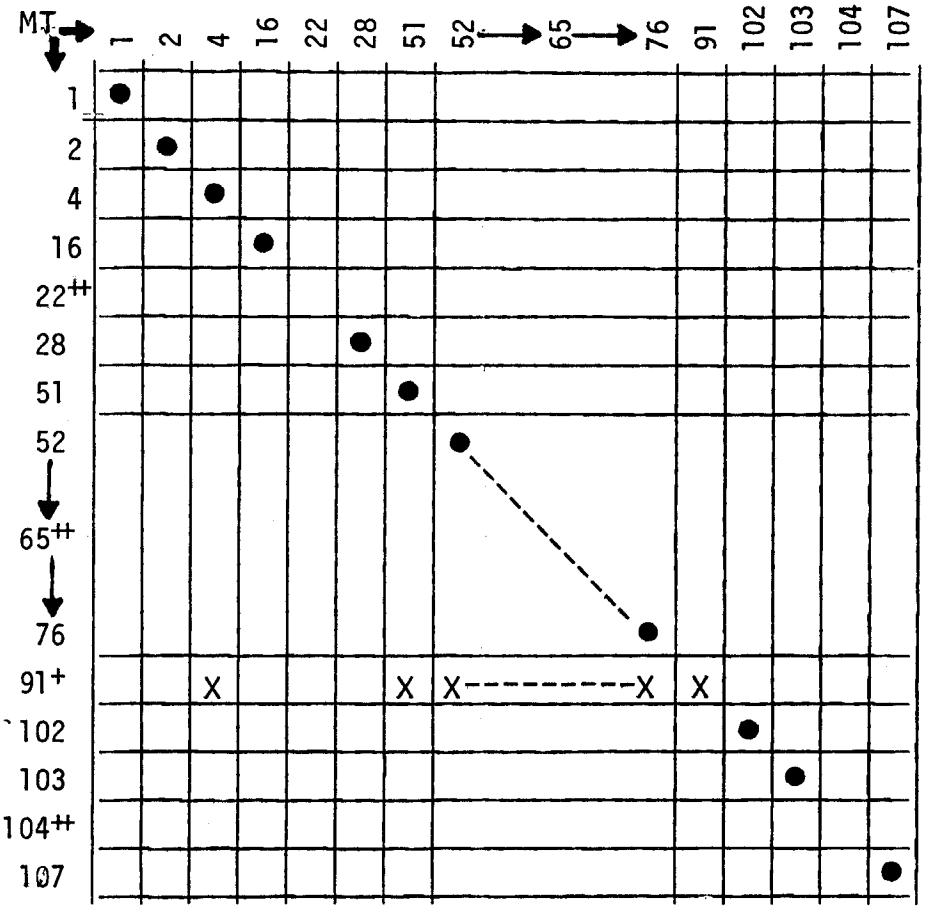

FIG. (IX.8) - THE COVARIANCE MATRICES FOR Ni, MAT 1328*

* SEE FOOTNOTES OF FIG. (IX.2)

++ THE CROSS SECTION FOR THIS REACTION IS NOT FOUND IN THE DLC-41B/VITAMIN-C LIBRARY.

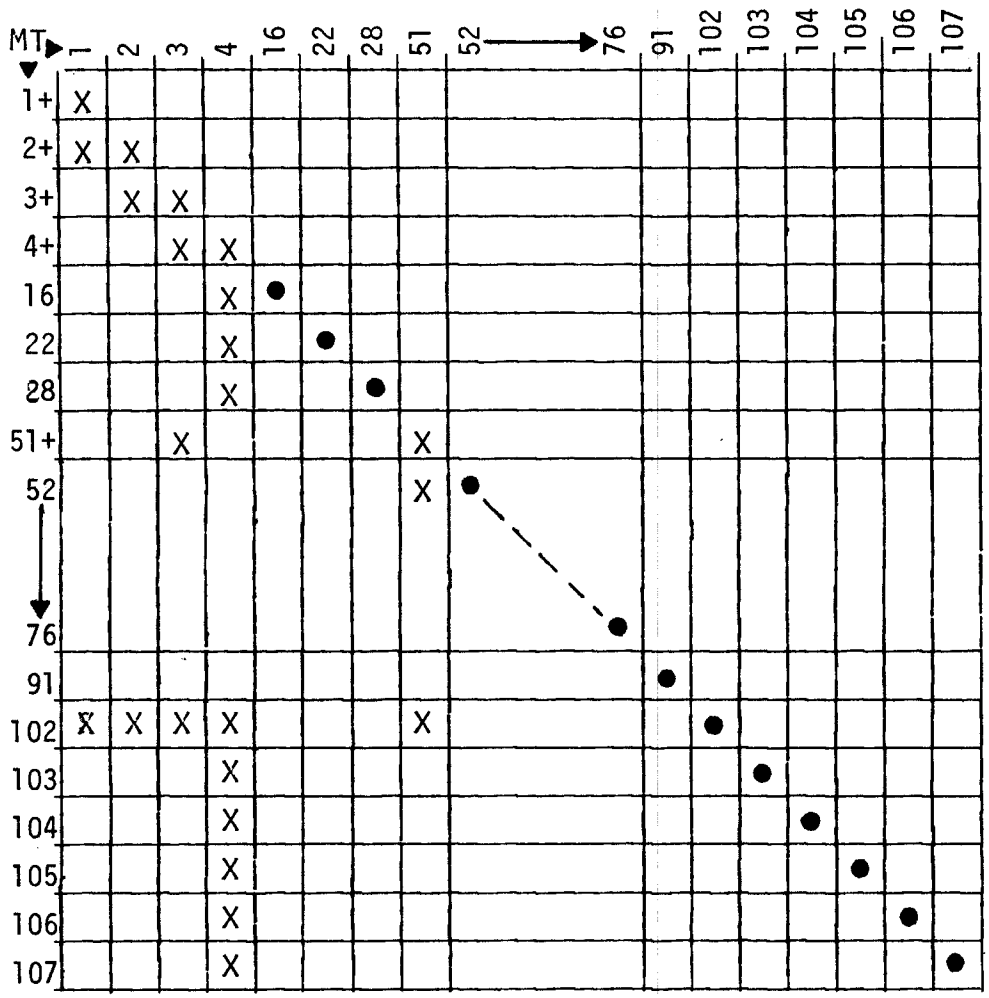

FIG. (IX.9) - THE COVARIANCE MATRICES PROCESSED FOR Fe, MAT 1326*

* SEE FOOTNOTES OF FIG. (IX.2)

are derived from the already evaluated matrices. Not all the filled boxes are shown and reflection about the major diagonal will indicate the filled and the mull matrices.

A display of the correlation matrices, the relative standard deviations and the reaction cross sections, are plotted for some materials and are shown in Fig. (IX.10) to (IX.18). The degree of correlation between the cross section MT_1 for material MAT_1 and cross section MT_2 for material MT_2 can be visualized from these figures. One can also identify the energy range of a large relative standard deviation in a particular cross section.

In Fig. (IX.10) to (IX.13), the correlation matrices of Pb (MAT 1382) for the (n, total), (n, elastic), (n,2n'), (n,3n'), and (n,γ) cross sections are shown. It can be noted from these figures that the correlation matrices are almost diagonal with a strong correlation between cross section uncertainties in adjacent neutron energy groups. This is also shown in Figs.(IX.14), (IX.15), and Fig. (IX.16) to Fig. (IX.18) for Thorium (MAT 1390), Lithium-6 (MAT 1303), and Sodium (MAT 1311), respectively. The Pb(n,2n') cross section has a large relative standard deviation (~200%) around MeV. The relative standard deviation for the Pb(n,3n') cross section in the first energy group (13.5 - 14.9 MeV) is significant (~430%). Although this cross section is small in this energy range (~0.07 barn), as will be shown in the next chapter, the large uncertainty associated with it gives rise to a large uncertainty in the uranium breeding ratio. This cross section is partly derived from the Pb(n,2n') cross section

and their uncertainties are anti-correlated as it is shown in Fig. (IX.13b).

The largest relative standard deviation in the Th(n, fission) cross section is ~16% and is in the first energy group (13.5 - 14.9 MeV), as it is shown in Fig. (IX.14a). The uncertainties associated with the Th(n,γ) cross section at higher energies are strongly correlated (see Fig. (IX.14b)) and the largest relative standard deviation for this cross section is ~20%. The Th(n,γ) cross section is an "evaluated" (measured) cross section and its uncertainties have an appreciable contribution to the uncertainty in the uranium breeding ratio, as it is discussed in the next chapter.

The correlation between the ^{6}Li(n,α)t cross section uncertainties is large, particularily at low energy, as shown in Fig. (IX.15a). The largest relative standard deviation for this cross section is ~3.5% in the energy range around 0.28 MeV where there is a resonance.

In Fig. (IX.16) to (IX.18), we give the correlation matrices for the Na(n,tot), Na(n,2n'), Na(n,elastic), Na(n, inelastic), Na(n,p), and Na(n,α) cross sections. There is a large uncertainty at the threshold for the Na (n,α) cross section (~50% relative standard deviation), as it is shown in Fig. (IX.18b). This is also true for the Na(n,2n') cross section where a relative standard deviation of ~35% is obtained.

In the next chapter we present the results of incorporating the uncertainty informations obtained in this chapter with the sensitivity coefficients for each design parameter considered.

Fig. (IX.10)

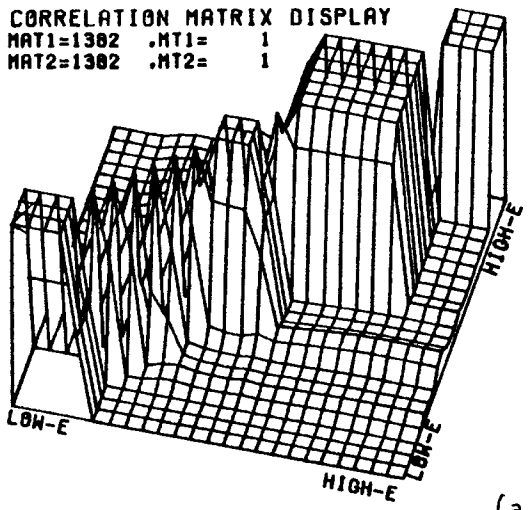
CORRELATION MATRIX DISPLAY
MAT1=1382 ,MT1= 1
MAT2=1382 ,MT2= 1
LOW-E
HIGH-E
LOW-E
HIGH-E

(a)

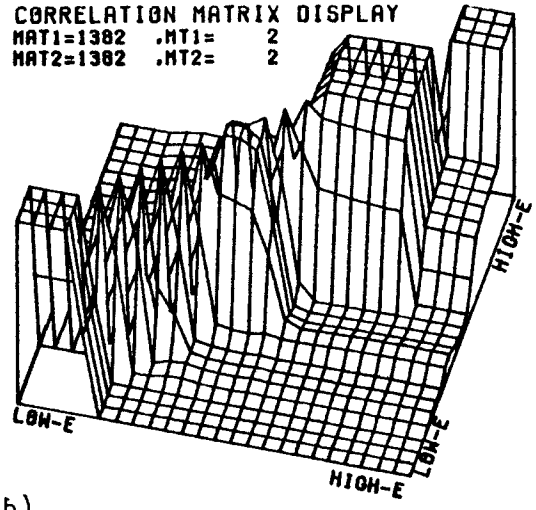
CORRELATION MATRIX DISPLAY
MAT1=1382 ,MT1= 2
MAT2=1382 ,MT2= 2
LOW-E
HIGH-E
LOW-E
HIGH-E

(b)

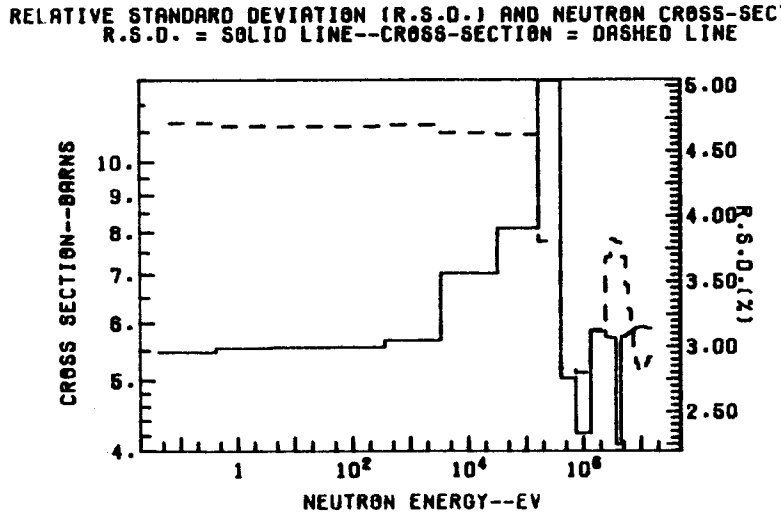
RELATIVE STANDARD DEVIATION (R.S.D.) AND NEUTRON CROSS-SECTION
R.S.D. = SOLID LINE--CROSS-SECTION = DASHED LINE
CROSS SECTION--BARNS
R.S.D.(%)
NEUTRON ENERGY--EV

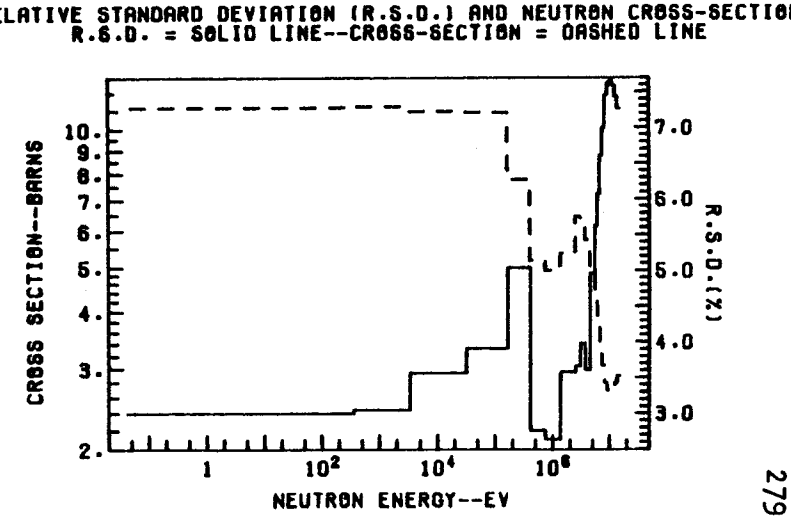
RELATIVE STANDARD DEVIATION (R.S.D.) AND NEUTRON CROSS-SECTION
R.S.D. = SOLID LINE--CROSS-SECTION = DASHED LINE
CROSS SECTION--BARNS
R.S.D.(%)
NEUTRON ENERGY--EV

Fig. (IX.11)

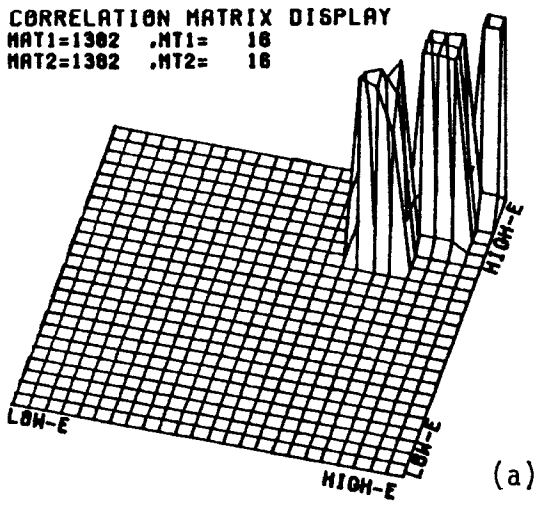
CORRELATION MATRIX DISPLAY
MAT1=1382 ,MT1= 16
MAT2=1382 ,MT2= 16
LOW-E
HIGH-E
LOW-E
HIGH-E

(a)

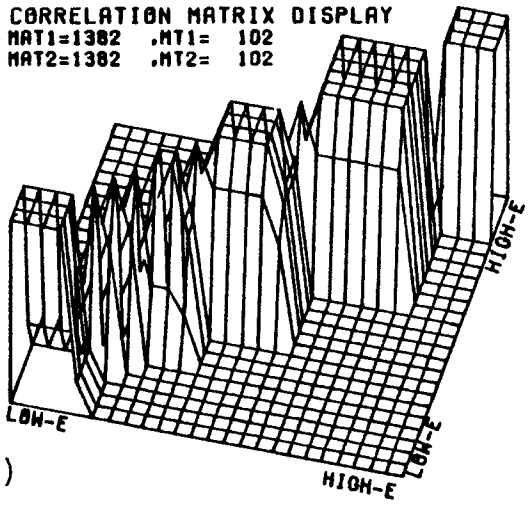
CORRELATION MATRIX DISPLAY
MAT1=1382 ,MT1= 102
MAT2=1382 ,MT2= 102
LOW-E
HIGH-E
LOW-E
HIGH-E

(b)

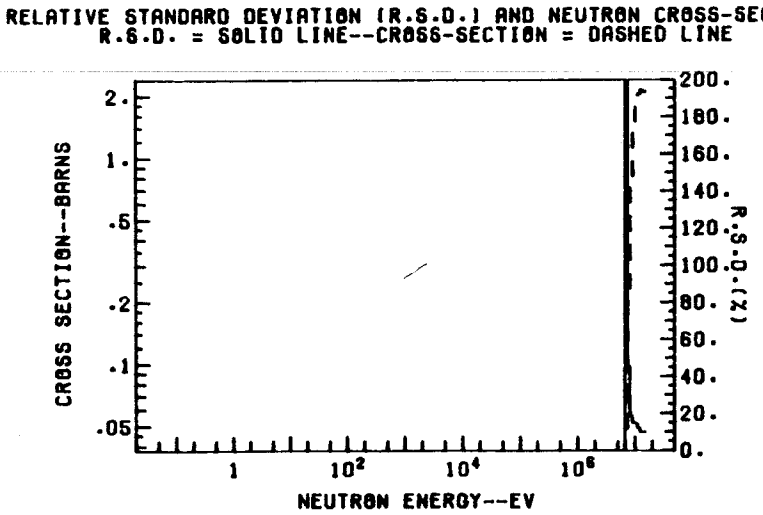
RELATIVE STANDARD DEVIATION (R.S.D.) AND NEUTRON CROSS-SECTION
R.S.D. = SOLID LINE--CROSS-SECTION = DASHED LINE
CROSS SECTION--BARNS
2.
1.
.5
.2
.1
.05
200.
180.
160.
140.
120.
100.
80.
60.
40.
20.
0.
R.S.D.(%)
1
10²
10⁴
10⁶
NEUTRON ENERGY--EV

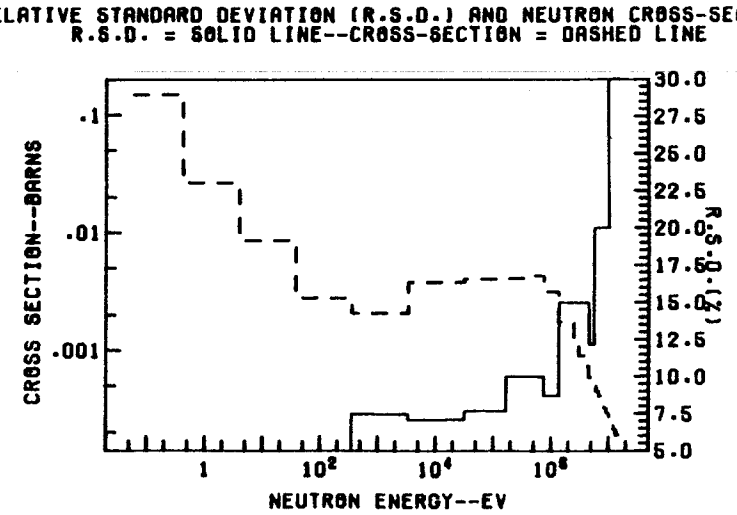
RELATIVE STANDARD DEVIATION (R.S.D.) AND NEUTRON CROSS-SECTION
R.S.D. = SOLID LINE--CROSS-SECTION = DASHED LINE
CROSS SECTION--BARNS
.1
.01
.001
30.0
27.5
25.0
22.5
20.0
17.5
15.0
12.5
10.0
7.5
5.0
R.S.D.(%)
1
10²
10⁴
10⁶
NEUTRON ENERGY--EV

Fig. (IX.12)

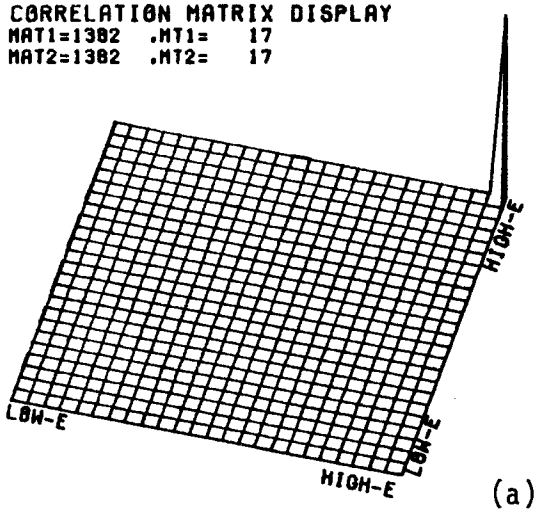
CORRELATION MATRIX DISPLAY
MAT1=1382 .MT1= 17
MAT2=1382 .MT2= 17
LOW-E
HIGH-E
LOW-E
HIGH-E

(a)

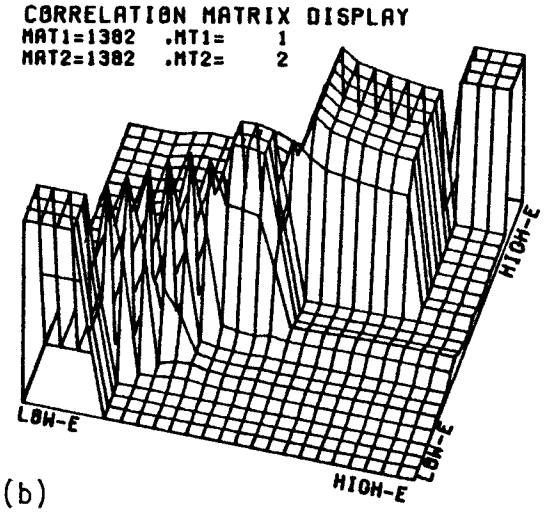
CORRELATION MATRIX DISPLAY
MAT1=1382 .MT1= 1
MAT2=1382 .MT2= 2
LOW-E
HIGH-E
LOW-E
HIGH-E

(b)

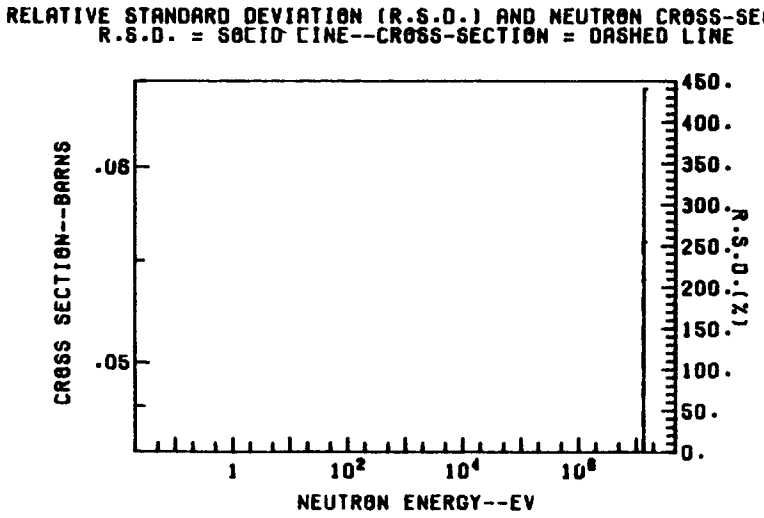
RELATIVE STANDARD DEVIATION (R.S.D.) AND NEUTRON CROSS-SECTION
R.S.D. = SOLID LINE--CROSS-SECTION = DASHED LINE
CROSS SECTION--BARNS
.06
.05
R.S.D.(%)
450.
400.
350.
300.
250.
200.
150.
100.
50.
0.
1
10²
10⁴
10⁶
NEUTRON ENERGY--EV

Fig. (IX.13)

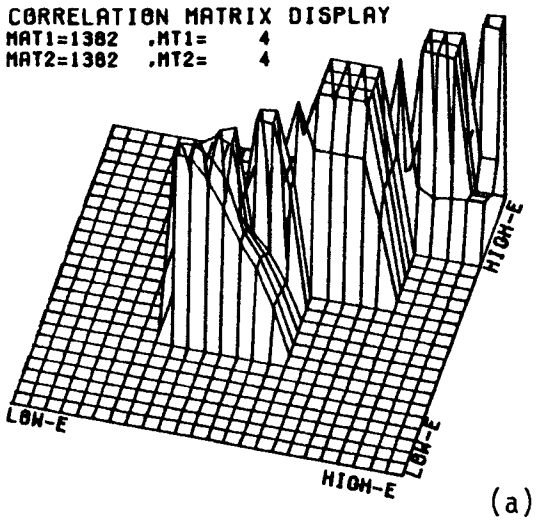
CORRELATION MATRIX DISPLAY
MAT1=1382 ,MT1= 4
MAT2=1382 ,MT2= 4
LOW-E
HIGH-E
LOW-E
HIGH-E

(a)

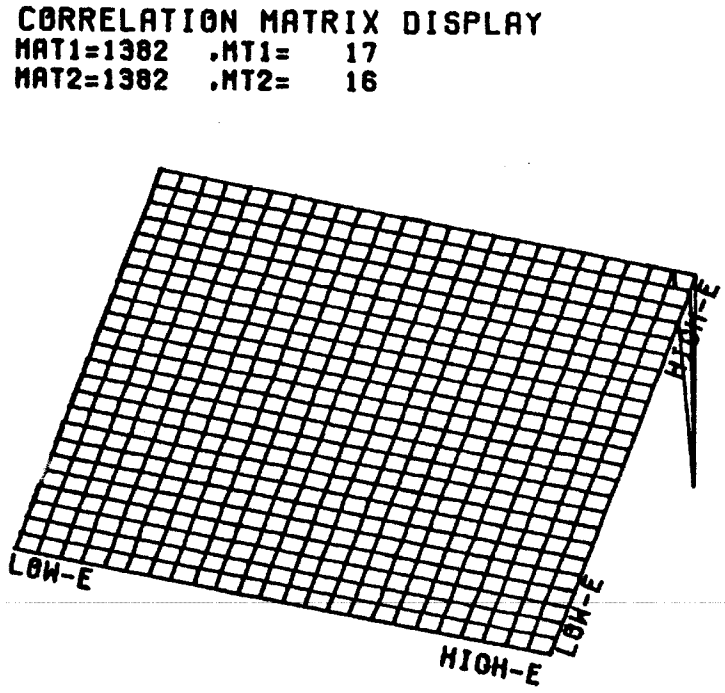
CORRELATION MATRIX DISPLAY
MAT1=1382 ,MT1= 17
MAT2=1382 ,MT2= 16
LOW-E
HIGH-E
LOW-E
HIGH-E

(b)

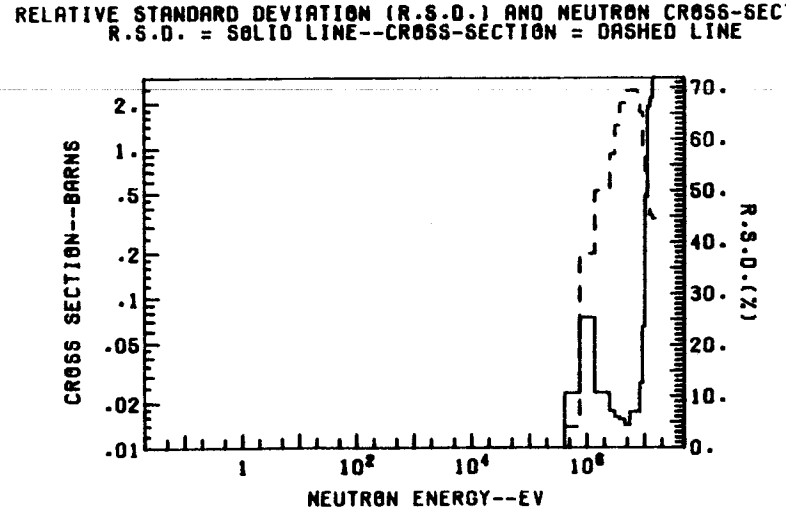
RELATIVE STANDARD DEVIATION (R.S.D.) AND NEUTRON CROSS-SECTION
R.S.D. = SOLID LINE--CROSS-SECTION = DASHED LINE
CROSS SECTION--BARNS
2.
1.
.5
.2
.1
.05
.02
.01
70.
60.
50.
40.
30.
20.
10.
0.
R.S.D.(%)
1
10²
10⁴
10⁶
NEUTRON ENERGY--EV

Fig. (IX.14)

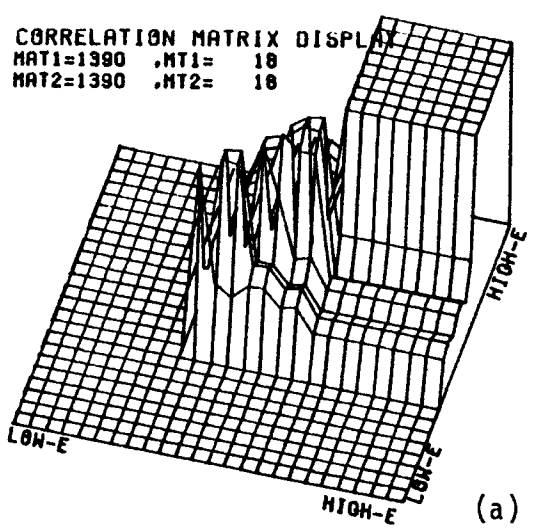
CORRELATION MATRIX DISPLAY
MAT1=1390 ,MT1= 18
MAT2=1390 ,MT2= 18
LOW-E
HIGH-E
LOW-E
HIGH-E

(a)

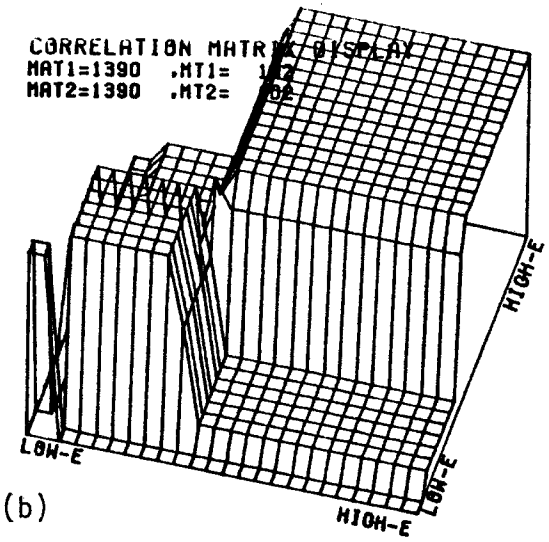
CORRELATION MATRIX DISPLAY
MAT1=1390 ,MT1=
MAT2=1390 ,MT2=
LOW-E
HIGH-E
LOW-E
HIGH-E

(b)

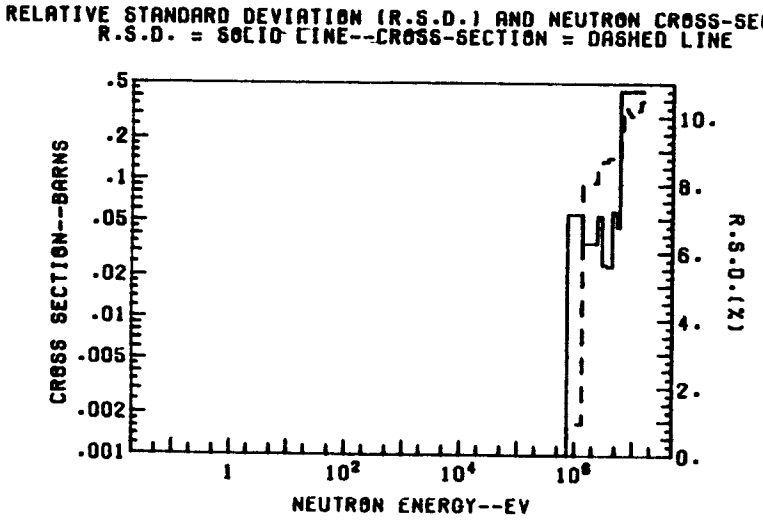
RELATIVE STANDARD DEVIATION (R.S.D.) AND NEUTRON CROSS-SECTION
R.S.D. = SOLID LINE--CROSS-SECTION = DASHED LINE
CROSS SECTION--BARNS
.5
.2
.1
.05
.02
.01
.005
.002
.001
10.
8.
6.
4.
2.
0.
R.S.D.(%)
1
10²
10⁴
10⁶
NEUTRON ENERGY--EV

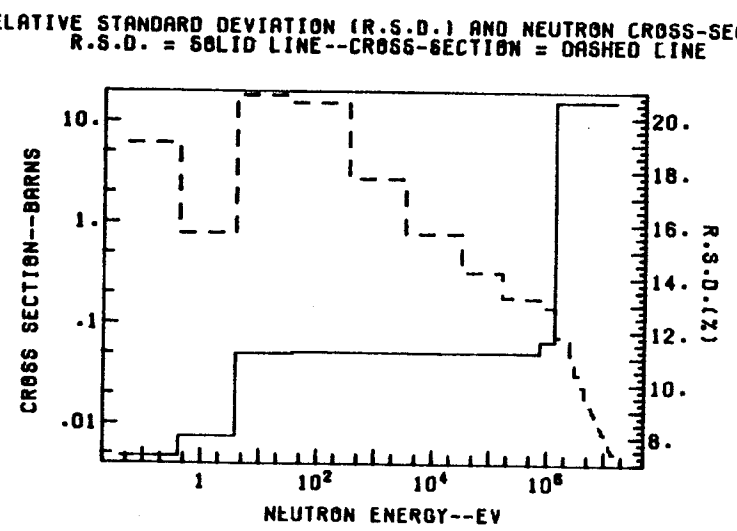
RELATIVE STANDARD DEVIATION (R.S.D.) AND NEUTRON CROSS-SECTION
R.S.D. = SOLID LINE--CROSS-SECTION = DASHED LINE
CROSS SECTION--BARNS
10.
1.
.1
.01
20.
18.
16.
14.
12.
10.
8.
R.S.D.(%)
1
10²
10⁴
10⁶
NEUTRON ENERGY--EV

Fig. (IX.15)

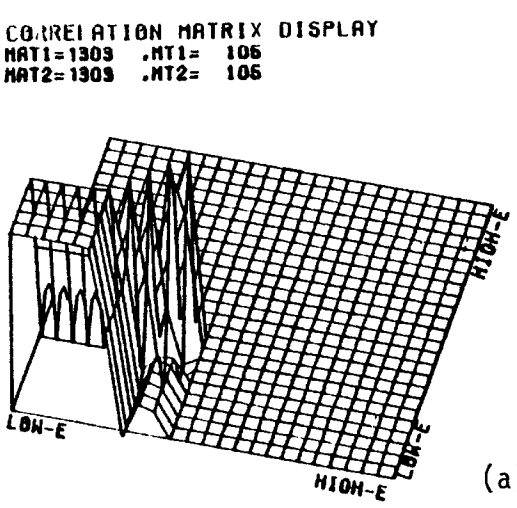
CORRELATION MATRIX DISPLAY
MAT1=1303 .MT1= 105
MAT2=1303 .MT2= 105
LOW-E
HIGH-E
LOW-E
HIGH-E

(a)

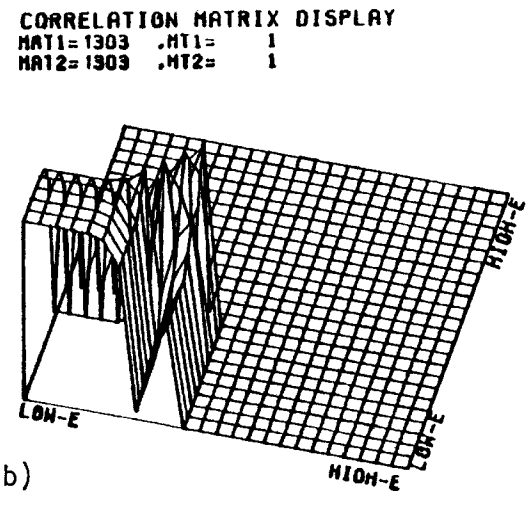
CORRELATION MATRIX DISPLAY
MAT1=1303 .MT1= 1
MAT2=1303 .MT2= 1
LOW-E
HIGH-E
LOW-E
HIGH-E

(b)

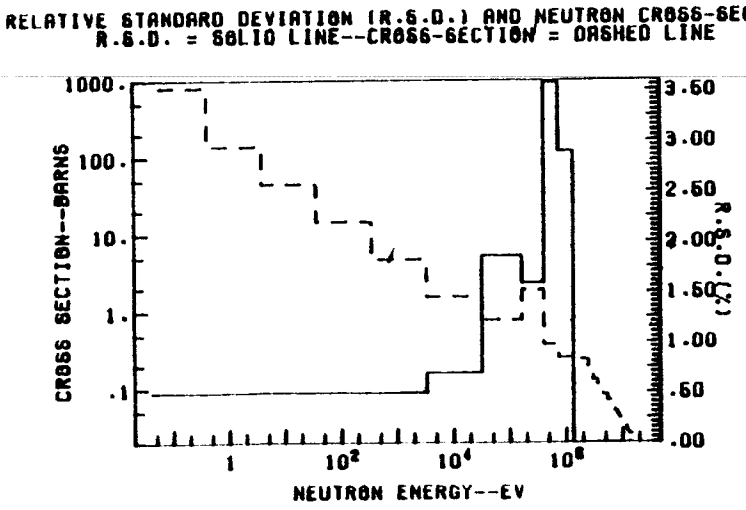
RELATIVE STANDARD DEVIATION (R.S.D.) AND NEUTRON CROSS-SECTION
R.S.D. = SOLID LINE--CROSS-SECTION = DASHED LINE
CROSS SECTION--BARNS
1000.
100.
10.
1.
.1
3.60
3.00
2.50
2.00
1.50
1.00
.50
.00
R.S.D.(%)
1
10²
10⁴
10⁶
NEUTRON ENERGY--EV

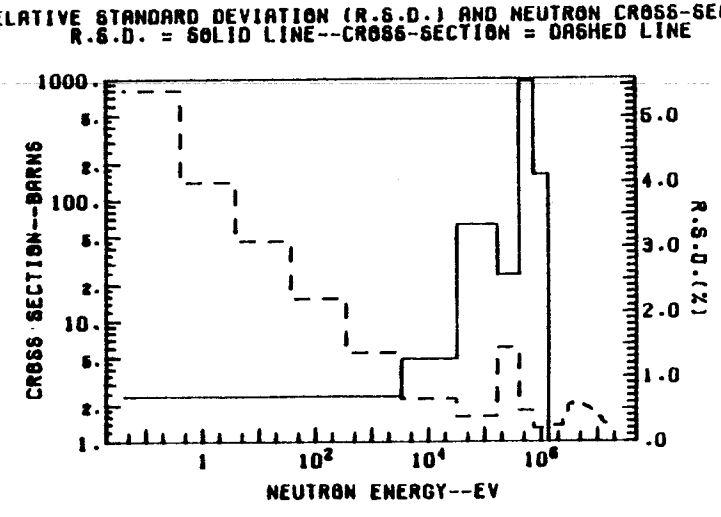
RELATIVE STANDARD DEVIATION (R.S.D.) AND NEUTRON CROSS-SECTION
R.S.D. = SOLID LINE--CROSS-SECTION = DASHED LINE
CROSS SECTION--BARNS
1000.
5.
2.
100.
5.
2.
10.
5.
2.
1.
6.0
4.0
3.0
2.0
1.0
.0
R.S.D.(%)
1
10²
10⁴
10⁶
NEUTRON ENERGY--EV

Fig. (IX.16)

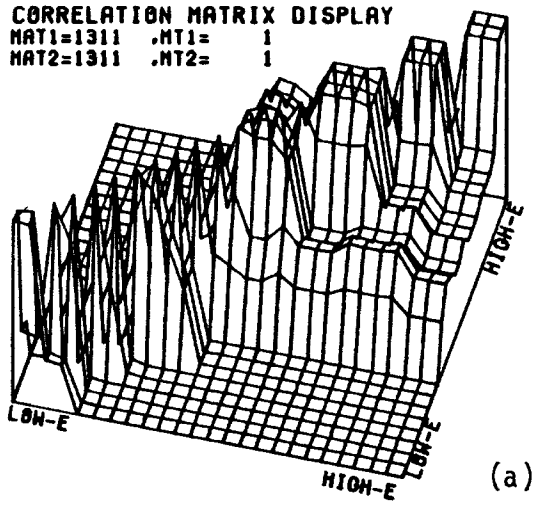
CORRELATION MATRIX DISPLAY
MAT1=1311 .MT1= 1
MAT2=1311 .MT2= 1
LOW-E
HIGH-E
LOW-E
HIGH-E

(a)

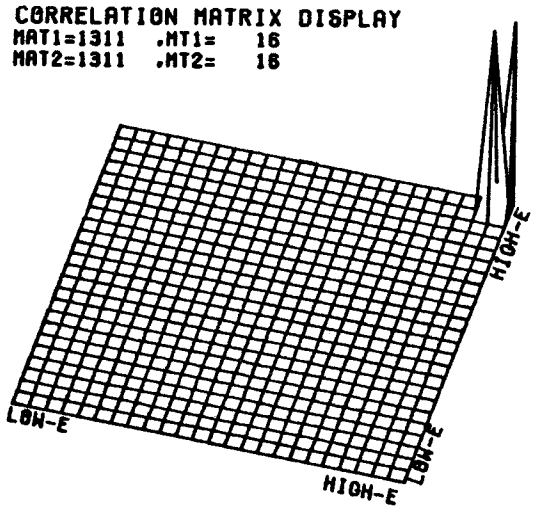
CORRELATION MATRIX DISPLAY
MAT1=1311 .MT1= 16
MAT2=1311 .MT2= 16
LOW-E
HIGH-E
LOW-E
HIGH-E

(b)

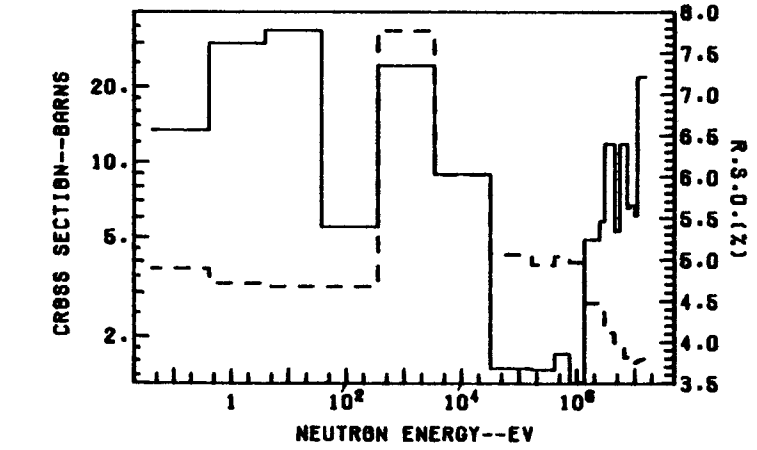
RELATIVE STANDARD DEVIATION (R.S.D.) AND NEUTRON CROSS-SECTION
R.S.D. = SOLID LINE--CROSS-SECTION = DASHED LINE
CROSS SECTION--BARNS
20.
10.
5.
2.
1
10²
10⁴
10⁶
NEUTRON ENERGY--EV
8.0
7.5
7.0
6.5
6.0
5.5
5.0
4.5
4.0
3.5
R.S.D.(%)

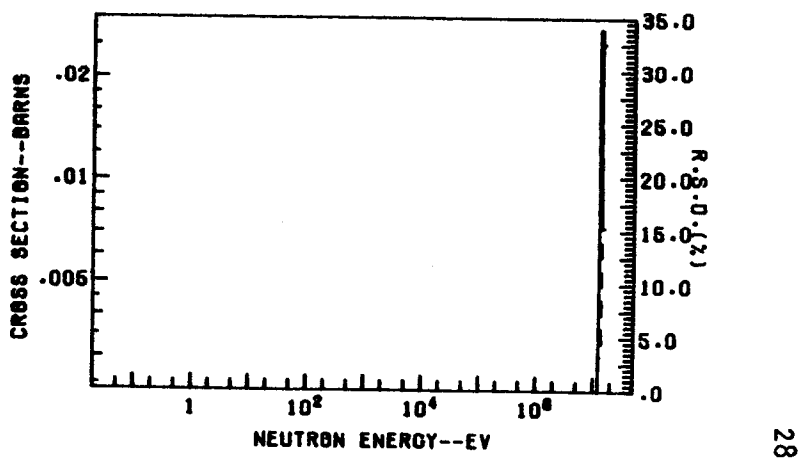
RELATIVE STANDARD DEVIATION (R.S.D.) AND NEUTRON CROSS-SECTION
R.S.D. = SOLID LINE--CROSS-SECTION = DASHED LINE
CROSS SECTION--BARNS
.02
.01
.005
1
10²
10⁴
10⁶
NEUTRON ENERGY--EV
35.0
30.0
25.0
20.0
15.0
10.0
5.0
.0
R.S.D.(%)

Fig. (IX.17)

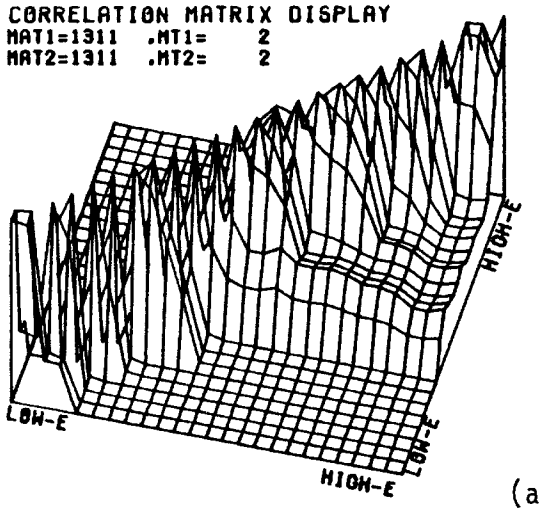
CORRELATION MATRIX DISPLAY
MAT1=1311 ,MT1= 2
MAT2=1311 ,MT2= 2
LOW-E
HIGH-E
LOW-E
HIGH-E

(a)

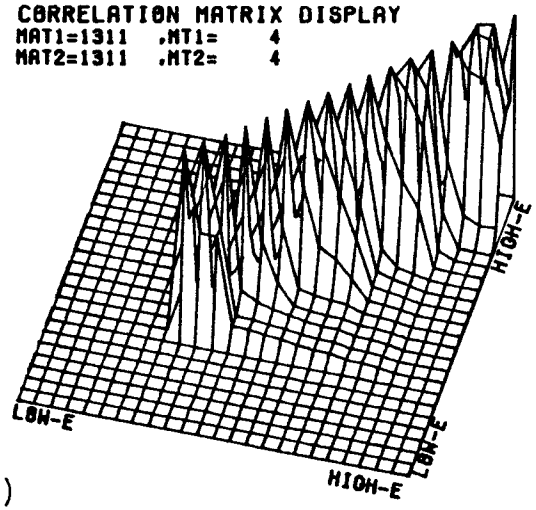
CORRELATION MATRIX DISPLAY
MAT1=1311 ,MT1= 4
MAT2=1311 ,MT2= 4
LOW-E
HIGH-E
LOW-E
HIGH-E

(b)

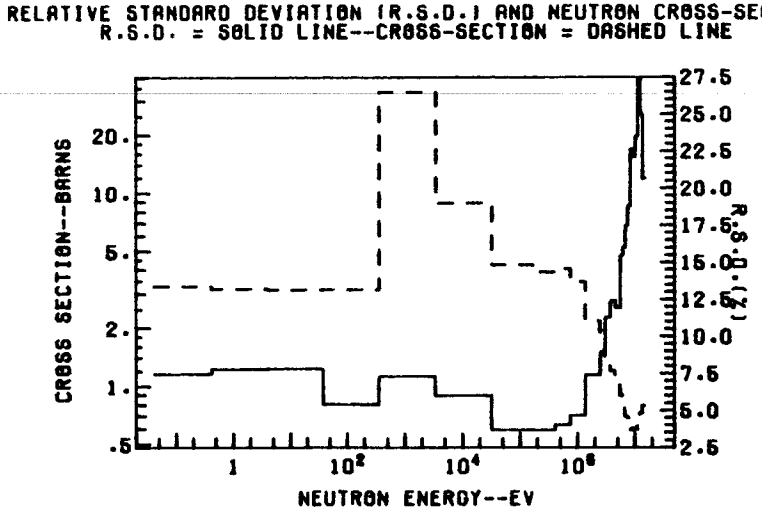
RELATIVE STANDARD DEVIATION (R.S.D.) AND NEUTRON CROSS-SECTION
R.S.D. = SOLID LINE--CROSS-SECTION = DASHED LINE
CROSS SECTION--BARNS
R.S.D.(%)
NEUTRON ENERGY--EV

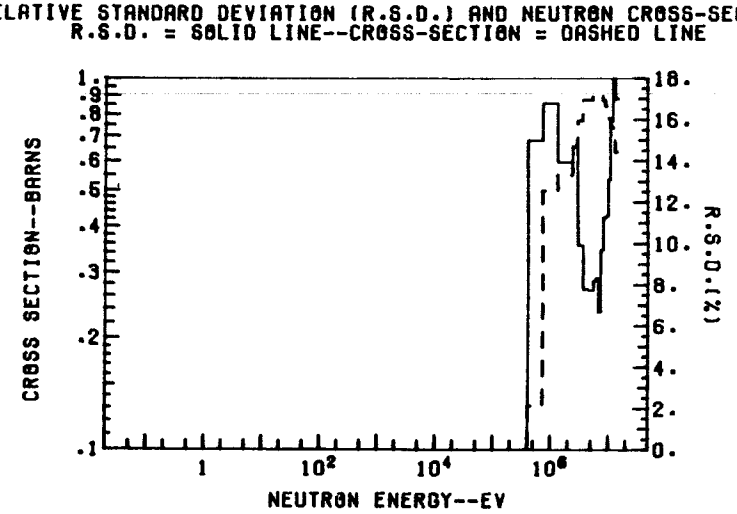
RELATIVE STANDARD DEVIATION (R.S.D.) AND NEUTRON CROSS-SECTION
R.S.D. = SOLID LINE--CROSS-SECTION = DASHED LINE
CROSS SECTION--BARNS
R.S.D.(%)
NEUTRON ENERGY--EV

Fig. (IX.18)

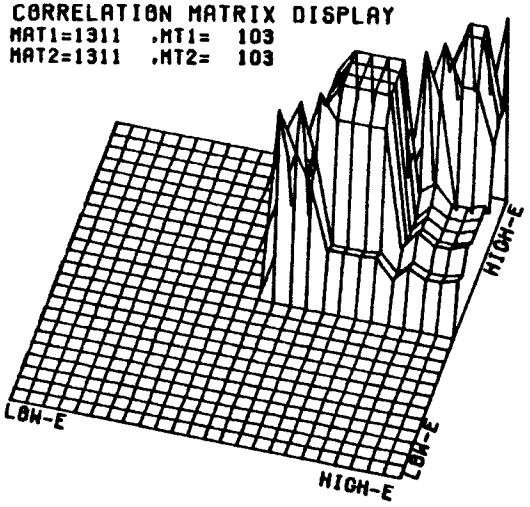
CORRELATION MATRIX DISPLAY
MAT1=1311 ,MT1= 103
MAT2=1311 ,MT2= 103
LOW-E
HIGH-E
LOW-E
HIGH-E

(a)

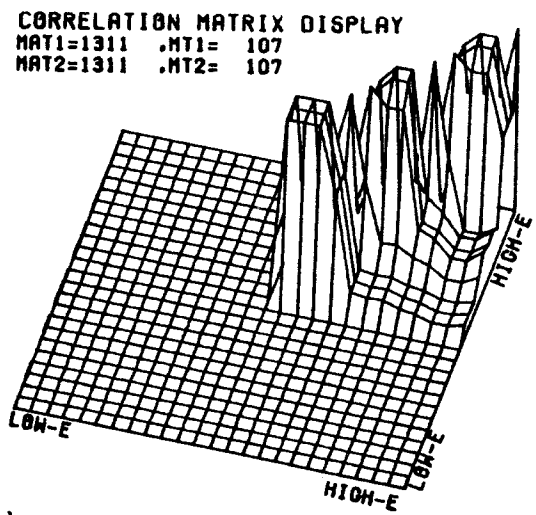
CORRELATION MATRIX DISPLAY
MAT1=1311 ,MT1= 107
MAT2=1311 ,MT2= 107
LOW-E
HIGH-E
LOW-E
HIGH-E

(b)

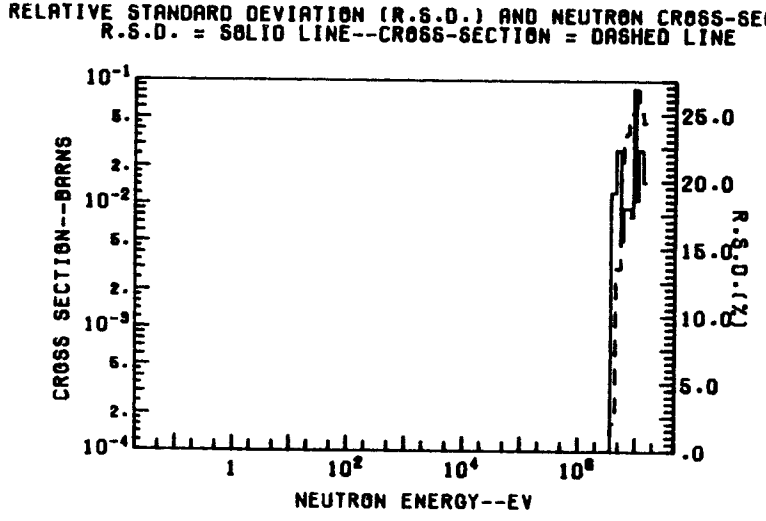
RELATIVE STANDARD DEVIATION (R.S.D.) AND NEUTRON CROSS-SECTION
R.S.D. = SOLID LINE--CROSS-SECTION = DASHED LINE
CROSS SECTION--BARNS
NEUTRON ENERGY--EV
R.S.D.(%)

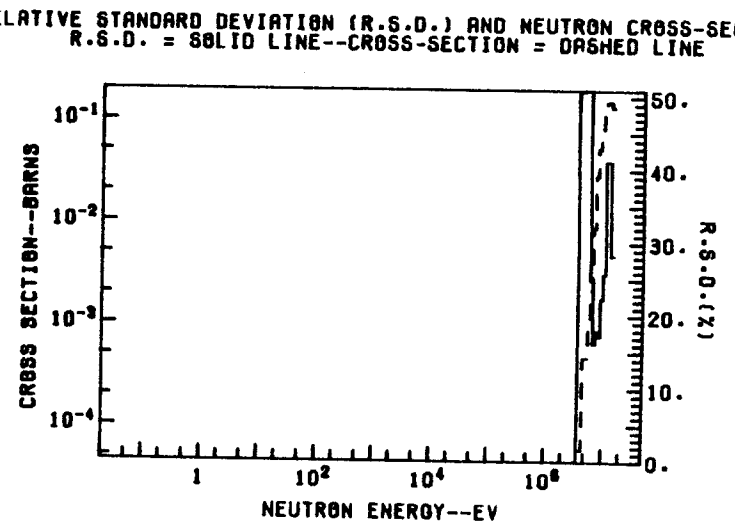
RELATIVE STANDARD DEVIATION (R.S.D.) AND NEUTRON CROSS-SECTION
R.S.D. = SOLID LINE--CROSS-SECTION = DASHED LINE
CROSS SECTION--BARNS
NEUTRON ENERGY--EV
R.S.D.(%)

REFERENCES

1. F.G. Perey, "Expectations for ENDF/B-V Covariance Files: Coverage, Strength and Limitation", in "Review of The Theory and Application of Sensitivity and Uncertainty Analysis", Proceedings of a Semiar Workshop, Oak Ridge Laboratory, TN, U.S.A., Feb. (1979). ORNL/RSIC-42.

2. F.G. Perey, "The Data Covariance Files for ENDF/B-V", ORNL/TM-5938 (ENDF-249) July 1977.

3. C.R. Weisbin and et.al., "Cross Section and Method Uncertainties: The Application of Sensitivity Analysis to Study Their Relationship in Radiation Transport Beuchmark Problems", ORNL-TM-4847 (ENDF-218), Oak Ridge National Laboratory, (August 1975).

4. F.G. Perey, "Format Modification 73-7", Minutes of the CSEWG Meeting, Dec. 1973 (enclosure 6 and 12).

5. T. Wu and C.W. Maynard, "UNCER": A University of Wisconsin Version of Uncertainty File Processor For ENDF/B-V", UWFDM-291, Fusion Research Program, University of Wisconsin, Nov. (1978).

Chapter X

UNCERTAINTY ANALYSIS FOR THE SOLASE-H BLANKET

X.I Introduction

The sensitivity analysis results obtained in Chapter VIII for the five design parameters (responses) considered have been folded with the covariance matrices obtained in Chapter IX and the uncertainties in these parameters have been evaluated.

Although some responses show high sensitivity to a particular cross section change, when the uncertainty analysis is performed, different conclusions can be drawn. This is due to the fact that some cross sections have large uncertainties which, when coupled with their sensitivity profiles, lead to a large uncertainty in the design parameter. In the following, we give the results of the uncertainty analysis performed. The conclusions from this study will follow.

X.2 Expressions Used to Evaluate the Response Uncertainty

The relative variance $(\frac{\Delta R}{R})^2$ of the response R due to the covariance between cross section X_G, at energy group G, and cross section Y_H at energy group H is given by

$$(\frac{\Delta R}{R})^2 = \sum_G \sum_H P_{X_G} P_{Y_H} RCOV(X_G, Y_H) \quad , \tag{X.1}$$

where $RCOV(X_G, Y_H)$ is the relative covariance matrix of the cross section X_G and Y_H and the coefficients P_{X_G} and P_{Y_H} are the sensitivity profiles for these cross sections, respectively. Eq. (X.1)

can be written in terms of the correlation matrix $CORR(X_G,Y_H)$ and the relative standard deviations $R.S.D.(X_G)$ and $R.S.D.(Y_H)$ as (see Eqs.(IX.22) to (IX.25))

$$\left(\frac{\Delta R}{R}\right)^2 = \sum_G \sum_H P_{X_G} P_{Y_H} CORR(X_G,Y_H)\, R\cdot S\cdot D(X_G) R\cdot S\cdot D(Y_H) \qquad (X.2)$$

Three expressions can be used to evaluate the relative covariance, $\left(\frac{\Delta R}{R}\right)^2$ and they are distinguished by the way the correlation between the cross sections X_G and Y_G is represented. These expressions are

(a) For a particular material, the correlation matrices between different cross sections and their relative standard deviations are obtained from the procedures and results given in Chapter IX, i.e., from the uncertainty information implemented in the ENDF/B-V. For each material, Eq. (IX.2) is applied for each pair of cross sections X_G and Y_H. The value of $(\Delta R/R)^2$ is made up of contributions from all pairs considered.

(b) For a particular material, and over the energy range specified in the ENDF/B-V over which correlation between the pair X and Y exists, the relative variance, $\left(\frac{\Delta R}{R}\right)^2$, is assumed to be evaluated from the expression

$$\left(\frac{\Delta R}{R}\right)^2 = \sum_G \sum_H P_{X_G} P_{Y_H} CORR(X_G,Y_H) R\cdot S\cdot D(X_G) R\cdot S\cdot D(Y_H) \delta_{GH} \qquad (X.3)$$

where δ_{GH}=1 when G=H and zero otherwise. In this formulation, it is assumed that the correlation matrix for the cross sections X_G and Y_G is filled only through its diagonal, i.e., the uncertainties are assumed to be uncorrelated between different energy

groups. This is assumed to apply for all the cross section pairs considered.

(c) For a particular material, and over the energy range specified in the ENDF/B-V over which correlation between the pair X_G and Y_H exists, the relative variance, $(\Delta R/R)^2$, is assumed to be evaluated from the expression

$$(\frac{\Delta R}{R})^2 = \sum_G \sum_H P_{X_G} P_{Y_H} R\cdot S\cdot D(X_G) R\cdot S\cdot D(Y_H) \quad . \qquad (X.4)$$

In Eq. (X.4), we assumed that the uncertainties in the cross sections X_G and Y_H are fully correlated, i.e., $CORR(X_G, Y_H) = \pm 1$ (depending on whether X_G and Y_H are correlated or anticorrelated) over the energy range specified in the ENDF/B-V. The last two expressions are used to investigate the degree of correlations between different cross sections and its impact on the response uncertainty.

X.3 Uncertainty Analysis Results

The partial cross sections considered in the uncertainty analysis for each material are summarized in Table IX.1). The choice of these cross sections, among others, is based on the availability of their uncertainty informations and on their importance in the transport and activity (reaction rate) calculations. Equations (X.2), (X.3), and (X.4) have been used to evaluate the uncertainty (relative variance) in each response due to uncertainties associated with the cross sections considered for each material. We introduced in Tables (X.2) and (X.3) the results of these evaluations based

Table(X.1)

THE CROSS SECTIONS CONSIDERED IN THE UNCERTAINTY ANALYSIS FOR EACH MATERIAL PRESENT IN THE SOLASE-H BLANKET

Material	Cross Sections Considered in the Uncertainty Analysis
Thorium	(n,fission), (n,γ)
Lead	(n,elastic),(n,inelastic), (n,2n'),(n,3'n),(n,γ),(n,tot)
Li-6	(n,elastic),(n,α)t,(n,tot)
Li-7*	
Oxygen	(n,elastic),(n,p),(n,α),(n,tot)
Sodium	(n,elastic),(n,inelastic),(n,2n'),(n,γ),(n,p),(n,α),(n,tot)
Carbon	(n,elastic),(n,n')cont.,(n,γ),(n,α),(n,tot)
Nickel	(n,elastic),(n,inelastic),(n,2n'),(n,n')p,(n,γ),(n,p),(n,α),(n,tot)
Iron	(n,elastic),(n,inelastic),(n,2n'),(n,n')α,(n,n')p,(n,γ),(n,p),(n,d),(n,t),(n,^{3}He),(n,α),(n,tot)
Cromium+	
Zirconium*	
Tin*	

*No uncertainty information is found in the ENDF/B-V for this element
+Uncertainty information found in the ENDF/B-V for this element but have not been considered in the uncertainty analysis

on Eq. (X.2). For comparison, we also introduced in these tables the uncertainty analysis results based on Eq. (X.3) where the cross sections uncertainties are assumed uncorrelated. Note that the total variance in the response R is the algebraic sum of the contributions from each material considered since the cross sections uncertainties for the materials considered are uncorrelated (see Tables (IX.2) to (IX.5)). From Tables (X.2) and (X.3), one can identify the material which contributes the most to the total relative variance in the response R. For a particular material, one can also identify the cross section type which contributes the most to the relative variance in R due to the cross sections uncertainties of this material. These procedures have been carried out for each response and the results are presented in Table (X.4). For each response, the materials are introduced in this table according to their contributions to the total relative variance in R. We also give in this table the neutron energy group in which large contribution to the relative variance in R is attributed. Introduced in Table (X.4) is the relevant information obtained from the sensitivity analysis presented in Chapter VIII.

X.4 Conclusions Drawn From the Uncertainty Analysis Results

From the uncertainty analysis results shown in Tables (X.2), (X.3), and (X.4) we can draw the following conclusions for each response considered.

X.4.A The Uranium Breeding Ratio, R_U

Table (X.2)

THE RELATIVE VARIANCE AND THE RELATIVE STANDARD DEVIATION IN THE URANIUM BREEDING RATIO, R_U; TRITIUM BREEDING FROM ^6Li, $R_{^6Li}$; AND TRITIUM BREEDING FROM ^7Li, $R_{^7Li}$, DUE TO CROSS SECTIONS UNCERTAINTIES OF DIFFERENT MATERIALS PRESENT IN THE SOLASE-H BLANKET

Material	$(\frac{\Delta R_U}{R_U})^2$		$(\frac{\Delta R_{^6Li}}{R^+_{Li}})^2$		$(\frac{\Delta R_{^7Li}}{R^+_{Li}})^2$	
	Uncertainties Are Correlated	Uncorrelated	Uncertainties Are Correlated	Uncorrelated	Uncertainties Are Correlated	Uncorrelated
Thorium	7.24	1.72	8.82	1.99	2.42-4	1.63-4
Lead	9.77	9.34	4.55	4.00	6.11-3	0.11
Lithium-6	0.06	0.02	0.24	0.09	2.75-14	2.75-14
Lithium-7*	∿0.15	∿0.15	∿0.01	∿0.01	∿0.72	∿0.72
Oxygen	0.09	0.05	0.18	0.09	2.00-3	2.00-3
Sodium++			1.72	0.69	0.16	0.13
Carbon	1.00-3	1.00-3	0.29	0.22	5.39-3	3.29-3
Total	17.31	11.28	15.81	7.09	0.89	0.97
Relative Standard % Deviation	4.16	3.36	3.98	2.66	0.94	0.98

$^+R_{Li}=R_{^6Li}+R_{^7Li}$; $R_{^6Li}=0.5752$, $R_{^7Li}=0.0269$, $R_U=0.9165$

*Error estimates for ^7Li cross sections are taken from Ref.(1).

++Uncertainties for Na is not considered in the uranium breeding ratio uncertainty analysis.

Table (X.3)

THE RELATIVE VARIANCE AND THE RELATIVE STANDARD DEVIATION IN THE AVERAGE DISPLACEMENTS PER ATOM PER FUSION NEUTRON IN ZIRCALOY-2 THROUGH THE FIRST 3 CM IN THE FUEL ZONE, R_D, AND IN THE HEAT DEPOSITED PER NEUTRON FROM NUCLEAR REACTIONS, R_H^Q DUE TO CROSS SECTIONS UNCERTAINTIES OF DIFFERENT MATERIALS IN THE SOLASE-H BLANKET

Material	$(\frac{\Delta \bar{R}_D}{\bar{R}_D})^2$		$(\frac{\Delta R_H^Q}{R_H^Q})^2$	
	Uncertainties Are Correlated	Uncorrelated	Uncertainties Are Correlated	Uncorrelated
Thorium	0.20	0.07	42.10	22.00
Lead	5.36	4.72	18.70	16.10
Lithium-6	7.10-3	3.08-3	5.34-4	2.80-4
Lithium-7*	∿0.53	∿0.53	∿ 3.30-2	∿ 3.30-2
Oxygen	0.05	0.05	0.79	0.74
Sodium	0.33	0.25	1.71	1.05
Carbon	2.92-4	2.84-4	0.37	0.34
Nickel+	1.22-3	6.21-4	5.10-3	2.21-3
Iron+	2.62-2	1.22-2	9.98-2	4.97-2
Total	6.51	5.64	63.81	40.32
Relative Standard Deviation	2.55	2.37	7.99	6.35

*Error estimates for ^{7}Li cross sections are taken from Ref.(1).

+Indirect effect only is considered in the Uncertainty Analysis

Table (X.4)

ASSIGNMENT BY MATERIAL, CROSS SECTION TYPE, AND ENERGY GROUP AS OBTAINED FROM THE SENSITIVITY AND UNCERTAINTY ANALYSIS FOR THE SOLASE-H BLANKET

Response	From Sensitivity Analysis			From Uncertainty Analysis		
	Element	Reaction Type	Energy Group	Element	Reaction Type	Energy Group
Uranium Breeding Ratio	Th	(n,γ)	21	Pb	(n,3n')	1
	Pb	(n,2n')	1	Th	(n,γ)	21
	^{6}Li	(n,α)t	21	^{7}Li	(n,elastic)	18
	^{16}O	(n,elastic)	21	^{16}O	(n,elastic)	19
	^{7}Li	(n,elastic)	18	^{6}Li	(n,α)t	19
	^{12}C	(n,elastic)	20	^{12}C	(n,n')cont.	1
Tritium Breeding Ratio from ^{6}Li	^{6}Li	(n,α)t	21	Th	(n,γ)	21
	Th	(n,γ)	21	Pb	(n,inelastic)	1
	Na	(n,elastic)	19	Na	(n,total)	20
	^{16}O	(n,elastic)	19	^{12}C	(n,n')cont.	1
	Pb	(n,γ)	25	^{6}Li	(n,total)	19
	^{16}C	(n,elastic)	25	^{16}O	(n,total)	19
	^{7}Li	(n,elastic)	18	^{7}Li	(n,elastic)	18
Tritium Breeding from ^{7}Li	^{7}Li	(n,elastic)	1	^{7}Li	(n,inelastic)	1
	Pb	(n,2n')	1	Na	(n,inelastic)	1
	Th	(n,2n')	1	Pb	(n,2n')	1
	Na	(n,inelastic)	1	^{12}C	(n,n')cont.	1
	^{16}O	(n,inelastic)	1	^{16}O	(n,inelastic)	1
	^{6}Li	(n,inelastic)	1	Th	(n,fission)	1
	C	(n,elastic)	1	^{6}Li	(n,elastic)	16
Displacement per atom averaged over the first 3 cm of the fuel zone	Pb	(n,inelastic)	16	Pb	(n,inelastic)	1
	^{7}Li	(n,elastic)	18	^{7}Li	(n,elastic)	18
	Na	(n,inelastic)	16	Na	(n,inelastic)	16
	^{16}Fe+	(n,inelastic)	16	Th	(n,γ)	19
	^{16}O	(n,elastic)	17	^{16}O	(n,elastic)	17
	^{6}Li	(n,α)t	18	Fe+	(n,inelastic)	16
	Ni+	(n,inelastic)	1	^{6}Li	(n,total)	18
	Th	(n,inelastic)	16	Ni+	(n,inelastic)	1
	^{12}C	(n,elastic)	19	^{12}C	(n,n')cont.	1
Heat Deposited in the Blanket per D-T neutron	Th	(n,fission)	1	Th	(n,fission)	1
	Pb	(n,2n')	1	Pb	(n,inelastic)	1
	Na	(n,inelastic)	15	Na	(n,α)	1
	^{16}O	(n,inelastic)	1	^{16}O	(n,inelastic)	1
	Fe+	(n,inelastic)	1	^{12}C	(n,n')cont.	1
	^{12}C	(n,elastic)	25	Fe+	(n,inelastic)	1
	^{7}Li	(n,inelastic)	1	^{7}Li	(n,inelastic)	1
	^{6}Li	(n,α)t	21	Ni+	(n,inelastic)	15
	Ni+	(n,inelastic)	15	^{6}Li	(n,tot)	19

+Direct effect not included

(1) The relative variance in the uranium breeding ratio, $(\Delta R_U/R)^2$, is mostly attributed to the uncertainties associated with the lead cross sections which contributes ~ 56% to the total relative variance $(\Delta R_U/R)^2$. In Table (X.5) we give the total relative variance in R due to the uncertainties associated with the partial and the total cross sections of lead evaluated from Eqs. (X.2), (X.3), and (X.4). In this table, the three vertical entries that follow each partial cross section, Σ, are: (a) the relative variance in R due to uncertainties in Σ, (b) the relative variance in R due to correlation between the uncertainties in the cross section Σ and other cross sections, and (c) the relative variance in R due to uncertainties in all other cross sections considered except the cross section Σ, respectively. The relative variance in R due to uncertainties in all partial cross sections considered is the summation of these three contributions. This sum (shown in the tables as the relative variance due to partial cross sections uncertainties) is the same when adding the three contributions (the three vertical entries) which follow any partial cross section. Also shown in this table is the relative variance in R due to uncertainties in the (n,total) cross section and due to its correlation with other cross sections. These two contributions are given by the two vertical entries which follow the (n,total) cross section. The sum of these two contributions is the relative variance in R due to uncertainties in the total cross section and its correlation with others. Note that the (n,total) cross section

Table (X.5)

THE RELATIVE VARIANCE, $[\frac{\Delta R}{R}]^2$ IN THE URANIUM BREEDING RATIO, R_U, AND THE CONTRIBUTION FROM EACH PARTIAL CROSS SECTION DUE TO THE UNCERTAINTIES ASSOCIATED WITH LEAD* NEUTRON CROSS SECTIONS

Cross-Section Type	Ucertainties are Correlated	Uncertainties are Uncorrelated	Uncertainties Are Fully Correlated
(n,elastic)	2.46-2	2.07-2	5.86-2
	0.	0.	0.
	9.35	8.98	1.43+1
(n,(inelastic)	8.16-1	7.03-1	9.36-1
	2.21	2.07	8.46
	6.35	6.23	4.99
(n,2n')	2.09	1.97	2.17
	-6.42	-6.56	-7.42
	1.37+1	1.36+1	1.96+1
(n,3n')	1.28+1	1.28+1	1.28+1
	-8.43	-8.43	-4.15
	5.04	4.66	5.77
(n,γ)	4.24-3	1.69-3	6.39-3
	1.36-6	1.45-6	5.90-3
	9.37	9.00	1.44+1
Relative Variance Due To Partial Cross Sections Uncertainties	9.38	9.00	1.44+1
(n,tot)	2.67-1	2.37-1	3.85-1
	1.23-1	1.06-1	3.00-1
Relative Variance Due To Total Cross Section Uncertainties	3.90-1	3.43-1	6.85-1
Relative Variance (Total)+	9.77	9.34	1.51+1

*This element contributes the most to the relative variance in the uranium breeding ratio.

+Sum of the relative variance due to the partial cross section uncertainties and the total cross section uncertainties.

is treated as an independent cross section. The total relative variance in R due to the partial and total cross sections uncertainties of Pb is given in the last entry of Table (X.5). From this table, it can be noticed that significant contribution to the total relative variance in R is due to the uncertainty in the Pb(n,3') cross section. The contribution to the total $(\Delta R_U/R)^2$ from the Pb(n,3n') cross section and its correlation with other cross sections is ~45%. The corresponding value for the (n,2n') cross sections and its correlation with other cross sections is ~ -45%. As shown in Table (IX.2), the Pb(n,3n') cross section is "derived" from the (n,nonelastic), (n,2n'), and (n,γ) in the energy range 14-20 MeV, and has a relative standard deviation ~430% (see Fig. (IX.12)-a). As shown in Fig. (IX.13)-b, the Pb(n,3n') cross section uncertainties is anti-correlated with the Pb(n,2n') cross section uncertainties. Appreciable reduction in the relative variance of the uranium breeding ratio can be achieved upon having better evaluation for the Pb(n,3n'), Pb(n,nonelastic), and Pb(n,2n') in the energy range 14-20 MeV. (2) Although the sensitivity analysis revealed that the Th(n,γ) cross section has the largest sensitivity coefficient for uranium breeding, this cross section comes next to the Pb(n,3n') cross section, as shown in Table (X.4), and contributes ~ 41% to the total relative variance $(\Delta R_U/R)^2$ particularly in group 21 (0.35-3.35 keV, see Table (IV.1)). The Th(n,γ) cross section is an "evaluated" cross section and has a relative standard deviation of ~ 20% for neutrons of energy >10 MeV and ~ 12% in the keV

range as shown in Fig. (IX.14)-b. Noticeable reduction in the variance $(\Delta R_U/R)^2$ can be obtained upon reducing these uncertainties. (3) The present uncertainties in the $^6Li(n,\alpha)t$ cross section are adequate for calculating the uranium breeding ratio in the SOLASE-H blanket since it contributes only ~0.3% to the relative variance $(\frac{\Delta R_U}{R})^2$. Therefore, more accurate evaluations for this cross section are not necessary. Although this conclusion applies to the SOLASE-H hybrid, it is expected to apply for other fusion-fission hybrids which have non-fissioning blankets. (4) The present uncertainties in the ^7Li cross sections contributes ~0.8% to the relative variance in R_U. The corresponding value for ^{16}O is ~0.5%. Among other partial cross sections, the ^7Li (n,elastic) and the ^{16}O (n, elastic) cross sections exhibit moderate contributions to the relative variance in R_U due to errors in the cross sections of these materials, particularly in the energy range 30-400 keV. (5) The present uncertainties in the Th(n,fission) cross section is adequate for U-233 breeding. As it is shown in Table (X.4), this is true for all the responses considered, except for the heating rate response.

X.4.B Tritium Breeding Ratio From ^6Li, $R_{^6Li}$

(1) Although the sensitivity analysis reveals the importance of the $^6Li(n,\alpha)t$ cross sections for tritium breeding, the uncertainty analysis showed that the present uncertainties in this cross section is adequate for tritium breeding from ^6Li. In fact, the Th(n,γ) cross section uncertainties have more impact on the

relative variance in the tritium breeding ratio from ^{6}Li, particularly in the energy range 0.35-3.35 keV. The errors associated with the Th cross sections amount to ~56% in the relative variance in $R_{^{6}Li}$ and is due mainly to the Th(n,γ) cross sections (~99%) as it is shown in Table (X.6). The errors in the ^{6}Li cross sections contributes only ~ 1.5% to the relative variance in $R_{^{6}Li}$. Therefore, efforts should be devoted to reduce the Th(n,γ) cross section uncertainties which have strong correlations among different neutron energy groups, as it is shown in Fig. (IX.14)-b. These correlations can also be noticed by comparing the results obtained in Table (X.6) using Eqs. (X.2) and (X.3).

(2) The lead cross sections uncertainties contribute appreciably to the relative variance in $R_{^{6}Li}$ (~29%) and due mostly to the Pb(n,inelastic) cross section. The uncertainty in this cross section and its correlation with other partial cross sections contributes ~80% to the total variance in $R_{^{6}Li}$ due to errors in the Pb cross sections (not shown). As it is given in Table (IX.2), the Pb(n,inelastic) cross section is "evaluated" over the energy range 0.73-14 MeV and is derived from the (n,nonelastic),(n,2n'), and (n,γ) cross sections in the energy range 14-20 MeV. Improved measurements for these cross sections in this energy range and better evaluations for the Pb(n,inelastic) cross section in the energy range 0.73-14 MeV will reduce the relative variance in $R_{^{6}Li}$.

(3) The present error estimates for ^{7}Li cross sections are acceptable for predicting the tritium breeding ratio from ^{6}Li. In

Table (X.6)

THE RELATIVE VARIANCE, $[\frac{\Delta R}{R}]^2$, IN THE TRITIUM BREEDING RATIO FROM ^6Li, $R_{^6Li}$, AND THE CONTRIBUTIONS FROM EACH PARTIAL CROSS SECTION DUE TO THE UNCERTAINTIES ASSOCIATED WITH THORIUM* NEUTRON CROSS SECTIONS

Cross-Section Type	$(\Delta R/R)^2$ Uncertainties Are Correlated	Uncertainties Are Uncorrelated	Uncertainties Are Fully Correlated
(n,fission)	5.92-2	3.43-2	7.45-2
	0.	0.	0.
	8.76	1.97	9.48
(n,γ)	8.76	1.97	9.48
	0.	0.	0.
	5.92-2	3.43-2	7.45-2
Relative Variance Due to Partial Cross Section Uncertainties+	8.82	1.99	9.56

*This element contributes the most to the tritium breeding ratio, $R_{^6Li}$

+The uncertainty informations for the total cross section is not implemented in the ENDF/B-V.

fact, the least contribution to the relative variance in $R_{^6Li}$ is due to the ^7Li cross sections uncertainties (~0.06%).

(4) Appreciable contribution (~10%) to the relative variance in $R_{^6Li}$ comes from the Na cross sections uncertainties particularly the Na(n,total), and Na(n,elastic) cross sections. The contribution from the Na(n,total) and Na(n,elastic) cross sections to the total relative variance in $R_{^6Li}$ due to uncertainties in the Na cross sections is ~40% and 9%, respectively (not shown). The Na(n,tot) cross section has a relative standard deviation of ~7.5% in the energy range 3.3-31 keV (there are resonances in this energy range), as shown in Fig. (IX.16)-a. The Na(n,elastic) cross section has ~27% relative standard deviation at ≥10 MeV and the correlation exist over all neutron energies (see Fig. (IX.17)-a). Reducing the uncertainties associated with these cross sections will reduce the variand in the tritium breeding ratio from ^6Li.

X.4.C Tritium Breeding Ratio from ^7Li, $R_{^7Li}$

(1) The uncertainties associated with ^6Li cross sections have practically no impact on tritium breeding from ^7Li. One can extend this remark to other materials shown in Table (X.2). The total relative variance in $R_{^7Li}$ is ~0.89 and due mainly to the ^7Li (n,inelastic) cross section uncertainties. (This cross section includes the $^7Li(n,n',\alpha)t$ cross section).

(2) The relative variance in $R_{^7Li}$ is due mainly to uncertainties associated with the different materials cross sections in the

first energy group (13.5-14.9 MeV).

X.4.D The Average Displacements per Atom per Neutron in Zircaloy-2, $\bar{R}_D$

(1) Both from the sensitivity and uncertainty analysis, the uncertainties associated with the Pb(n,inelastic), ^{7}Li(n,elastic), and Na(n,inelastic) cross sections have the dominant impact on the uncertainty associated with the response $\bar{R}_D$. The Pb cross section uncertainties contributes ~83% to the total relative variance in $\bar{R}_D$. The corresponding values due to uncertainties in the ^{7}Li and Na cross sections are: ~8% and 5%, respectively. The contribution from the Pb(n,inelastic) cross section uncertainties to the relative variance in $\bar{R}_D$ due to the Pb cross section uncertainties is 63% as shown in Table (X.7). Minimizing the uncertainties in the Pb(n, inelastic) cross section will reduce the uncertainty in the displacements per atom. As stated earlier, more accurate evaluation of the Pb(n,inelastic) cross section in the energy range 0.73-14 MeV is required along with better measurements for the Pb(n,2n') and Pb(n,γ) cross sections in the energy range 14-20 MeV.

(2) The uncertainties in the ^{7}Li cross sections contribute ~8% to the total uncertainty in the response $\bar{R}_D$ and is due mainly to the ^{7}Li(n,elastic) cross section uncertainties.

(3) A contribution of ~3% to the uncertainties in $\bar{R}_D$ is due to the errors in the thorium cross sections, particularly from the errors associated with the Th(n,γ) cross section which contributes ~79% to the relative variance in $\bar{R}_D$ due to the Th cross sections un-

Table (X.7)

THE RELATIVE VARIANCE, $[\frac{\Delta R}{R}]^2$, IN THE AVERAGE DISPLACMENTS PER ATOM IN ZIRCALOY-2, $\bar{R}_D$, AND THE CONTRIBUTION FROM EACH PARTIAL CROSS SECTION DUE TO THE UNCERTAINTIES ASSOCIATED WITH LEAD NEUTRON CROSS SECTIONS

Cross Section Type	$(\Delta R/R)^2$		
	Uncertainties Are Correlated	Uncertainties Are Uncorrelated	Uncertainties Are Fully Correlated
(n,elastic)	1.36-2 0. 5.24	8.61-3 0. 4.67	1.35-2 0. 8.93-1
(n,inelastic)	3.78 -4.11-1 1.88	3.21 -4.07-1 1.88	4.09 -5.02 1.83
(n,2n')	1.51-2 -6.37-1 5.88	1.51-2 -6.33-1 5.30	1.44-2 -7.46-1 1.64
(n,3n')	2.16 -3.86-1 3.48	2.16 -3.86-1 2.91	2.16 -4.99 3.73
(n,γ)	8.56-4 -1.92-6 5.26	3.01-4 -1.80-6 4.68	1.15-3 -8.25-3 9.14-1
Relative Variance Due to Partial Cross Sections Uncertainties	5.26	4.68	9.06-1
(n,tot)	6.56-2 3.32-2	2.92-2 1.04-2	2.01-1 1.04-1
Relative Variance Due to Total Cross Sections Uncertainties	9.88-2	3.95-2	3.06-1
Relative Variance (total)+	5.36	4.72	1.21

+See Footnotes of Table (X.2).

certainties.

(3) The contributions to the uncertainty in $\bar{R}_D$ from uncertainties in the ^6Li cross sections is negligibly small.

(4) Although only the indirect effect (flux perturbation) was considered for Fe and Ni in the uncertainty analysis (Zr and Sn have no uncertainty information in the ENDF/B-V), however, one can conclude from Table (X.3) that their cross sections uncertainties have small contributions to the uncertainty in $\bar{R}_D$.

X.4.E The Heat Deposited Per Neutron from Nuclear Reactions, R_H^Q

As shown in Table (X.3), the relative variance in the heating rate from nuclear reactions is ~64. This corresponds to ~8% relative standard deviation in the value of R_H^Q. Almost all the contribution is due to the uncertainties in the thorium cross sections (~66%). The uncertainties in the Th(n,fission) cross sections amount to ~99.5% to the relative variance in R_H^Q due to Th cross sections uncertainties (see Table (X.8)) particularly from the highest energy group, 13.5-14.9 MeV. In this energy range, the Th(n,fission) cross section has a relative standard deviation of ~ 15%, as shown in Fig. (IX.14)-a. Appreciable reduction in the uncertainty associated with the heating rate calculations in the SOLASE-H blanket can be achieved upon having improved measurements for the Th(n,fission) cross section and its correlation matrix (this matrix has large correlation elements). It can be concluded from Tables (X.3) and (X.4) the following:

(1) The uncertainties in the Pb cross sections contributes

Table (X.8)

THE RELATIVE VARIANCE, $[\frac{\Delta R}{R}]^2$, IN THE HEAT DEPOSITED PER NEUTRON DUE TO NUCLEAR REACTIONS, R_H^Q, AND THE CONTRIBUTION FROM EACH PARTIAL CROSS SECTION DUE TO THE UNCERTAINTIES ASSOCIATED WITH THORIUM* NEUTRON CROSS SECTIONS

Cross-Section Type	$(\Delta R/R)^2$		
	Uncertainties Are Correlated	Uncertainties Are Uncorrelated	Uncertainties Are Fully Correlated
(n,fission)	4.19+1	2.19+1	6.06+1
	0.	0.	0.
	1.78-1	5.06-2	2.22-1
(n,γ)	1.78-1	5.06-2	2.22-1
	0.	0.	0.
	4.19+1	2.19+1	6.06+1
Relative Variance Due to Partial Cross Section Uncertainties+	4.21+1	2.20+1	6.09+1

*This element contributes the most to the heat deposited per neutron due to nuclear reactions.

+See footnotes of Table (X.3).

~30% to the relative variance in R_H^Q. This is attributed mostly to the Pb(n,inelastic) cross section uncertainties, particularly in the first energy group (13.5-14.9 MeV).

(2) The uncertainties in the ^6Li cross section have the least impact on the relative variance in R_H^Q. Although ~45% of the heating from nuclear reactions is due to the $^6Li(n,\alpha)t$ reactions as shown in Chapter VIII, the changes in the $^6Li(n,\alpha)t$ cross section will not lead to large changes in the heat deposited in the blanket. In fact, the heating rate has a negative senstivity coefficient to the $^6Li(n,\alpha)t$ cross section as shown in Table (VIII.8). This remark has been explained in Chapter VIII.

(3) The uncertainties associated with the Na cross section co-tribute ~3% to the relative variance of the heat deposited. This is mainly due to the Na(n,α) cross section uncertainties which contribute ~44% to the relative variance in R_H^Q due to uncertainties in the Na cross sections. The Na(n,α) cross section has a ~30% relative standard deviation in the first group (13.5-14.9 MeV) as shown in Fig. (IX.18)-b. Reducing this deviation will reduce the relative variance in R_H^Q.

As a general remark, it can be noted from the previous tables that if the cross sections uncertainties are considered uncorrelated this will under estimate the relative variance in the response R. Also, assuming full correlation between these uncertainties will not necessarily lead to large variance in R. Therefore, realistic results can be obtained only by considering the actual correlation

between the cross section uncertainties.

X.5 Comparison Between Uncertainty Results Obtained from the ENDF/B-V Uncertainty Files and Those Obtained From the Published Cross Sections Error Estimates

Other uncertainty analyses have been carried out and applied to pure fusion reactor designs in several studies.[1-6] The error estimate for neutron cross sections used in these studies are presented in Table (X.9) for different elements. The first four columns in Table (X.9) specify the fractional increases assumed in a particular partial cross section, and the fifth column specifies the cross section type changes to compensate for the assumed variations in the first four columns. As stated in these studies, the total cross section is generally known to a higher accuracy than are the various partial cross sections. Therefore, it is often more realistic in specifying cross section errors in a given energy range to vary at least two partial cross sections in such a manner that the total cross section remains constant. When a total cross section is specified in column five of Table (X.9), it is increased by the same percentage given in column four. When a partial cross-section is specified, it is decreased in such a manner that, in accordance with increases in columns one to four, the total cross section remains constant. When no cross section is specified in column five, no compensating effect is considered and the cross sections varied are those specified in column two.

The error estimates given in Table (X.9) have been used to

Table (X.9)

ERROR ESTIMATES FOR VARIOUS PARTIAL CROSS-SECTIONS
(as obtained from literature)

Element	Cross-Section Type-Varied	Energy Range (MeV)	Percent Increase In Varied Cross-Section (δc)	Cross-Section Type Varied To Compensate
^{6}Li*	(n,α)t	$<1\times10^{-7}$	0.5	(n,total)
		10^{-7}-10^{-2}	1.0	
		10^{-2}-10^{-1}	1.0-2.0	
		10^{-1}-3×10^{-1}	5.0	
		3×10^{-1}-5×10^{-1}	5.0-10	(n,elastic)
		5×10^{-1}-7×10^{-1}	10-15	
		7×10^{-1}-1	15	
		1-1.7	15-10	
		1.7-$1.4\times10^{+1}$	10	
^{7}Li*	(n,n')αt	All Energies	20	(n,elastic)
Th+	(n,fission)	<0.6	9.0	
		0.6-2.5	12.0	
		2.5-4	3.0	
		4-14	2.4	
		>14	4.0	
	(n,γ)	<0.1	9.0	
		>0.1	5.0	
Pb**	(n,2n)	All Energies	20	(n,inelastic)
C*	(n,elastic)	<4.8	3.0	(n,total)
		4.8-9.0	5.0	(n,elastic)
		9.0-15	15	
Na**	(n,γ)	All Energies	20	
	(n,inelastic)	4.59×10^{-1}-15	20	(n,elastic)
	(n,p)	3.75-15	20	
	(n,α)	4.04-15	20	

*Error estimates are taken from Refs (1,5).

+Error estimates are considered as those in Ref (2,3)

**Errors estimates are assumed

Table (X.9 cont'd)

Element	Cross-Section Type-Varied	Energy Range (MeV)	Percent Increase In Varied Cross-Section (δc)	Cross-Section Type Varied To Compensate
Fe,*** Ni++	(n,inelastic)	8-15	25	(n,elastic)
	(n,2n')	8-15	25	
	(n,n')p	8-15	50	
	(n,n')α	8-15	50	
	(n,absorption)	8-15	25	
^{16}O+++	(n,total)	<0.5	4.0	
		0.5-15	1.0	
	(n,elastic)	<0.5	4.0	
		0.5-4.0	1.0	
		4.0-6.5	3.0	
		6.5-9.5	6.0	
		9.5-12.5	15	
		12.5-15	10	
	(n,inelastic)	6.5-15	30	
	(n,γ)	All Energies	14.0	
	(n,p)	9.5-15	20.0	
	(n,d)	9.5-12.5	50	
		12.5-15	30	
	(n,α)	2-15	20.0	

***Error estimates are taken from Ref. (4).

++Errors estimates for Ni are assumed that same as for Fe

+++Error estimates are taken from Ref. (6).

evaluate the uncertainties, $\frac{\delta R}{R}$, in the response R. These uncertainties, given in Table (X.10) as Case II, are based on non-statistical treatment for errors. However, and for comparison purposes, we introduce in Table (X.10), the relative standard deviation in R due to the cross sections uncertainties in various materials (Case I). The deviations in R are obtained from Tables (X.2) and (X.3) for the case where the cross sections uncertainties are assumed uncorrelated between different energy groups (note that in this case, the uncertainties are correlated by reaction-type).

From Table (X.10), it can be noted that, except for the uranium breeding ratio, the relative variance in the response R (Case I) is larger than its uncertainty obtained from the cross sections error estimates published in literature. In Case I, larger values, with a factor of ~9, can be obtained as compared to Case II (comparisons are made on absolute value basis). However, the dominant materials which have large contributions to the response uncertainty are almost the same in both cases. One can also conclude from Case II the importance of the Th(n,fission),Th(n,γ),Pb(n,2n') and Pb(n,inelastic) cross sections for evaluating the different responses considered in this study.

X.6 Conclusions

The uncertainty analysis results discussed above for the SOLASE-H hybrid design showed that the uncertainty (relative standard deviation) in the U-233 breeding ratio, R_U is ~4% and is

Table (X.10)

THE UNCERTAINTIES, $\delta R/R$, IN THE URANIUM BREEDING RATIO, R_U, THE TRITIUM BREEDING RATIO FROM ^6Li, $R_{^6Li}$, THE TRITIUM BREEDING RATIO FROM ^7Li, THE AVERAGE DPA RATER PER FUSION NEUTRON IN ZIRCALOY-2, $\bar{R}_D$, AND THE HEAT DEPOSITED PER NEUTRON DUE TO NUCLEAR REACTIONS, R_H^Q, USING TWO DIFFERENT CROSS SECTION ERROR ESTIMATES

Material	$\frac{\delta R_U}{R_U}$		$\frac{\delta R_{^6Li}}{R_{Li}}$		$\frac{\delta R_{^7Li}}{R_{Li}}$		$\frac{\delta \bar{R}_D}{\bar{R}_D}$		$\frac{\delta R_H^Q}{R_H^Q}$	
	Case+ I	Case++ II	Case+ I	Case++ II	Case+ I	Case++ II	Case+ I	Case++ II	Case+ I	Case++ II
Thorium	1.31	2.16	1.41	-2.07	1.28-2	-4.93-3	2.65-1	-1.27-1	4.69	4.78
Lead	3.06	3.09	2.00	2.34		-5.04-1	2.17	1.58	4.01	-6.09-1
Li-6	1.52-1	-2.79-1	2.97-1	5.29-1	1.66-7	-2.64-4	5.55-2	-5.68-2	1.67-2	-2.44-2
Li-7		-3.86-1		8.33-2		8.51-1		7.29-1		-1.82-1
Oxygen	2.21-1	5.07-1	3.05-1	-1.74	4.47-2	-1.50-1	2.25-1	-3.01-1	8.61-1	-2.64
Sodium			8.33-1	2.13	1.12-1	-9.51-2	4.96-1	-1.57	1.02	-2.11
Carbon	3.16-2	1.29-2	4.65-1	8.51-2	5.74-2	1.20-2	1.69-2	6.74-3	4.86-1	1.67-1
Nickel							2.49-2	-9.90-2	4.70-2	-1.09-1
Iron							1.10-1	-4.72-1	2.22-1	-1.02
Total	3.36*	5.10	2.66*	1.36	0.98	0.11	2.37*	-0.31	6.35*	-1.75

+Cross sections uncertainties are treated statistically and assumed to be uncorrelated between energy groups.
++Uncertainties in the Response R is evaluated using the error estimates shown in Table (X.9).
*The total uncertainty in R for Case I is the relative standard deviation in R given in the last row in Table (X.2) and (X.3), for the uncorrelated-uncertainties case.

mostly to errors in the Pb cross sections which amount to a ~56% contribution. Reducing the uncertainty in the Pb(n,2n'),Pb(n,3n'), and Pb(n,nonelastic) cross sections, particularly in the energy range 14-20 MeV, will significantly reduce the uncertainty in the ratio R_U. Improving the Th(n,γ) cross section evaluation in the energy range 0.35-3.35 keV can lead to a 40% reduction in the uncertainty in the U-233 breeding ratio. This was found to be true for the tritium breeding ratio from ^{6}Li which has a ~3.4% uncertainty. It has been found that more accurate evaluation for the Pb(n,inelastic) cross section in the energy range 0.73-14 MeV can reduce (~25%) the uncertainty in the tritium breeding from ^{6}Li. Uncertainty in the order of 1% is the tritium breeding ratio from ^{7}Li, $R_{^7Li}$, was found which shows that the present nuclear data uncertainties are adequate for predicting tritium breeding from ^{7}Li.

Most of the uncertainty (~3%) in the displacements per atom rate in the Zircaloy-2 cladding, $\bar{R}_D$, is due to the uncertainties in the Pb(n,inelastic) cross section. The uncertainty analysis reveals also the importance of reducing the present uncertainties in the Th(n,fission) cross section in order to minimize the uncertainty (8%) in the heating rate from nuclear reactions, R_H^Q. The uncertainty in the thorium cross sections contribute ~66% to the uncertainty in the response R_H^Q for which a ~99.5% is attributed to the Th(n,fission) cross section uncertainties. It has also been found that the uncertainties in the ^{6}Li cross sections are adequate for predicting the U-233 breeding, the tritium breeding,

the displacements per atom, and the heat deposition in the SOLASE-H hybrid reactor. It has also been shown that using the published estimates for the neutron cross section errors gives lower uncertainty estimates for the design parameters considered. Although the results obtained is for the SOLASE-H blanket design, it may not be appreciably different for other hybrid designs which utilize a non-fissioning blanket to breed U-233 fuel.

References

1. Alsmiller, R.G., Jr., Santoro, R.T., Barish, J, Gabriel, T.A., "Comparison of the Cross-Section Sensitivity of the Tritium Breeding Ratio in Various Fusion Reactor Blanket", Nucl. Sci. & Eng., 57, (1975).

2. Baht, M.R., "Evaluated Files of Nuclear Cross Sections for Fusion Reactor Calculations", BNL-NCS-2529 5, Brookhaven National Lab. (1978).

3. Youssef, M.Z., Maynard, C.W., Conn, R.W., "Error Estimates of Fissile Fuel and Tritium Production in the SOLASE-H Hybrid Reactor", ANS Annual Meeting at Las Vegas, 8-12, June (1980).

4. Alsmiller, R.G., Jr., Barish, J., Weisbin, C.R., "Uncertainties In Calculated Heating and Radiation Damage in the Toroidal Field Coils of A Tokamak Experimental Power Reactor Due to Neutron Cross Section Errors", Nucl. Technology, 34, 376 (1977).

5. Steiner, D., Tobias, M., "Cross-Section Sensitivity of Tritium Breeding in A Fusion Reactor Blanket; Effect of Uncertainties in Cross-Sections of ^{6}Li, ^{7}Li, and ^{93}Nb", Nucl Fusion, K1, 153 (1974).

6. Bartine, D.E., Oblow, E.M., Mynatt, F.R., "Radiation Transport Cross Section Sensitivity Analysis: A General Approach Illustrated for a Thermonuclear Source in Air", Nucl. Sci. & Eng., 55, 147-167 (1974).